Observation and Measurement of Fuel Distribution Within a Spark-Ignition Engine

by

Kathleen Bernadette Queenan

Submitted for the Degree of Doctor of Philosophy

University College London

Department of Mechanical Engineering

1998

ProQuest Number: U641848

All rights reserved

INFORMATION TO ALL USERS
The quality of this reproduction is dependent upon the quality of the copy submitted.

In the unlikely event that the author did not send a complete manuscript
and there are missing pages, these will be noted. Also, if material had to be removed,
a note will indicate the deletion.

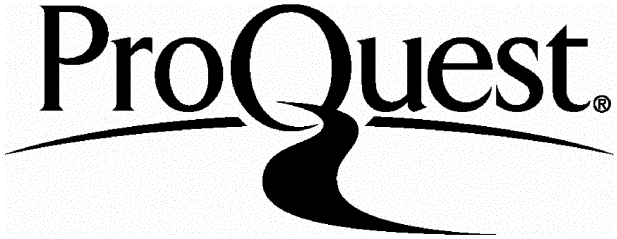

ProQuest U641848

Published by ProQuest LLC(2015). Copyright of the Dissertation is held by the Author.

All rights reserved.
This work is protected against unauthorized copying under Title 17, United States Code.
Microform Edition © ProQuest LLC.

ProQuest LLC
789 East Eisenhower Parkway
P.O. Box 1346
Ann Arbor, MI 48106-1346

Abstract

The thesis describes the work carried out to identify the behaviour of liquid fuel within the cylinder of a particular design of current spark ignition 4-valve engine for several different designs of fuel injector including an air-assisted version. A combination of techniques was used to study fuel behaviour, namely high-speed cine photography, image capture with CCD cameras, and a cylinder wall liquid skimming technique. It was concluded that the majority of the liquid fuel entering the cylinder travelled down the cylinder bore and impacted on the piston crown, regardless of what type of injector was employed.

The work changed to a study how the fuelling arrangements might be changed to satisfy the even tighter emission legislation that was being implemented. The method chosen was to develop a stratified charge engine by repositioning the injector such that its fuel spray would be deflected off an open inlet valve in the direction of the spark plug. One of the two inlet ports would be de-activated at part load to create axial swirl to stabilise the air/fuel mixture during the compression stroke.

Initial development work of this concept was carried out to enable an injector mounting block to be designed that would position the injector at the 'optimum' location when mounted onto a single cylinder research engine. Testing of the concept revolved around high-speed cine tests and the use of a Cambustion HFR400 fast flame ionisation detector to measure real-time in-cylinder HC concentrations at various locations around the combustion chamber.

The cine results indicated that the liquid fuel was mainly being deflected in the direction of the spark plug. The gas sampling measurements showed that a mixture of approximately 3 air fuel ratios richer around the spark plug at idle for the optimum -valve injection timing of 135° ATDC and 6 air fuel ratios at 1500 rpm road load condition.

Acknowledgements

The author would like to acknowledge the enthusiasm and unfailing support and supervision of Chris Nightingale, without whom this research would not have been possible. Thanks are also given to Paul Williams for his interest and help.

The UCL IC engine research group and in particular Mark Guerrier for help given in the final stages of the thesis writing-up period.

The UCL technical staff, especially Dave Hurley, who machined most of the engine components and also for his original thoughts on some of the designs.

John Bennett from the Ford Motor Company

Mark Peckham from Cambustion Ltd for his useful insights into some of the more unusual FFID traces.

Barry Morley and the Oxford Lasers team for help given in the high-speed cine visualisation tests.

The research was funded by the EPSRC and the Ford Motor Company, to whom I am grateful.

Thanks are also given to Joseph Silver for the encouragement given to undertake the research and for unfailing belief and confidence that I would finish.

Table of Contents

Chapter 1

FIGURES

Chapter 1

Chapter 2

Chapter 3

Chapter 4

Chapter 5

Chapter 6

Chapter 7

Chapter 8

Chapter 9

TABLES

Chapter 1

Chapter 2

Chapter 3

Chapter 4

Chapter 6

PLATES

Chapter 2

Chapter 3

Chapter 4

Chapter 5

Chapter 7

Chapter 9

PRINTS

Chapter 4

NOMENCLATURE

General Abbreviations

AFR	air fuel ratio
ATDC	after top dead centre
BDC	bottom dead centre
bmep	brake mean effective pressure
bsfc	brake specific fuel consumption
BTDC	before top dead centre
CA	crank angle
CAFE	Corporate Average Fuel Economy
CARB	Californian Air Resources Board
CCVS	Combustion Control through Vortex Stratification
CI	compression ignition
CVS	constant volume sampling
DF	deterioration factor
DI	direct injection
DoT	Department of Transport
ECE	Economic Commission for Europe
EEC	European Economic Community
EGR	exhaust gas recirculation
EPA	Environmental Protection Agency
EUDC	extra urban drive cycle
EVC	exhaust valve closure
EVO	exhaust valve opening
EVT	exhaust valve timing
Exh.	exhaust
FFID	fast flame ionisation detector
FTP	Federal Test Procedure
GVM	gross vehicle mass
HC	hydrocarbon
HWA	hot wire anemometry
IC	internal combustion
imep	indicated mean effective pressure
IVC	inlet valve closure
IVO	inlet valve opening
IVT	inlet valve timing
LDA/V	laser doppler anemometry/velocimetry
LEV	low emission vehicle

LML	lean misfire limit
MBT	minimum (ignition) advance for best torque
MVV	Mitsubishi Vertical Vortex
MY	model year
NDIR	non-dispersive infra-red
NMHC	non-methane hydrocarbons
NMOG	non-methane organic gases
NOx	oxides of nitrogen
PEEK	polyetheretherketone
PI	port injection
SC	stratified charge
SI	spark ignition
SR	swirl ratio
std.d.	standard deviation
TA	type approval
TDC	top dead centre
THC	total hydrocarbons
TLEV	transitional low emissions vehicle
TWC	three-way catalyst
ULEV	ultra low emission vehicle
UHC	unburnt hydrocarbon
VVT	variable valve timing
WOT	wide open throttle
ZEV	zero emission vehicle

Symbols

A	area
B	bore diameter
C_s	swirl coefficient
c_p	specific heat at constant pressure
c_v	specific heat at constant volume
d	fuel jet diameter
m	mass flow rate
mpg	miles per gallon
N	rotational speed
p	pressure
Q	quantity of heat
R_s	swirl ratio

r_v	compression ratio (volume)
t	thickness
T	temperature
u_r	relative velocity
V	volume
v_o	characteristic velocity
W	gross work output
W_e	Weber number
W_u	load to collapse
β	constant
ω_s	angular velocity of a solid body rotating flow
η_{Otto}	Otto cycle efficiency
γ	ratio of principal specific heats
σ_y	yield point
σ_t	surface tension
τ	torque
ρ_g	gas density
η	cycle efficiency
ϕ	equivalence ratio

Chemical Formulae

CO	carbon monoxide
CO_2	carbon dioxide
H	hydrogen (atomic)
H_2	hydrogen (molecular)
H_2O	water
N	nitrogen (atomic)
N_2	nitrogen (molecular)
NH_3	ammonia
NO	nitric oxide
NOx	oxides of nitrogen
O	oxygen (atomic)
O_2	oxygen (molecular)
OH	hydroxyl radical

Chapter 1

A Literature Survey

Internal Combustion Engines

The internal combustion (IC) engine uses the chemical energy contained in fuel (gasoline or diesel) to produce useful mechanical work. The means by which the fuel is ignited divides the IC engine group into two broad classes: the spark ignition (SI) engine where the fuel is ignited by a spark, and the compression ignition (CI) engine where the fuel spontaneously ignites by virtue of an adequate increase in temperature and pressure. The main part of this literature survey is concerned with the SI engine (with particular reference to exhaust pollutants and lean burn engines), however where applicable, reference will also be made to the CI engine.

1.1 Mechanical and Thermodynamic Cycles

1.1.1 The Ideal Air Standard Cycle

Several ideal air standard cycles exist, differing in complexity but all providing an illustrative guide to the thermodynamic aspects of engine operation (Heywood (1988)). In addition they indicate trends as engine operating or design parameters are varied. The simplest of these ideal air standard cycles is the Otto cycle (figure 1.1) which acts as a basic standard for the SI engine. The processes occurring in the Otto cycle are summarised beside the figure.

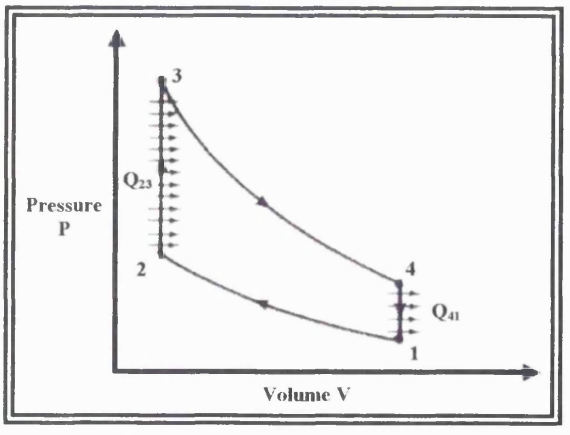

Figure 1.1: Ideal air standard Otto cycle [Stone (1994)]

1-2: Isentropic compression of air

2-3: Addition of heat Q_{23} at constant volume

3-4: Isentropic expansion of air to the original volume

4-1: Rejection of heat Q_{41} at constant volume to complete the cycle

The Otto cycle thermal efficiency is defined as:

$$\eta_{Otto} = \frac{W}{Q_{23}} = 1 - \left(\frac{Q_{41}}{Q_{23}}\right) \qquad (1.1)$$

where: W = gross work output (equivalent to the area enclosed by the pV diagram)

Assuming the working fluid to be an ideal gas, equation 1.1 reduces to:

$$\eta_{Otto} = 1 - \left(\frac{1}{r_v^{(\gamma-1)}}\right) \qquad (1.2)$$

where: r_v = compression ratio (V_1/V_2)

γ = ratio of principal specific heats (c_p / c_v)

Hence the thermal efficiency of the Otto cycle is dependent upon the compression ratio (r_v) and the ratio of specific heats (γ). The relationship between η_{Otto} and r_v for different values of γ is shown in figure 1.2.

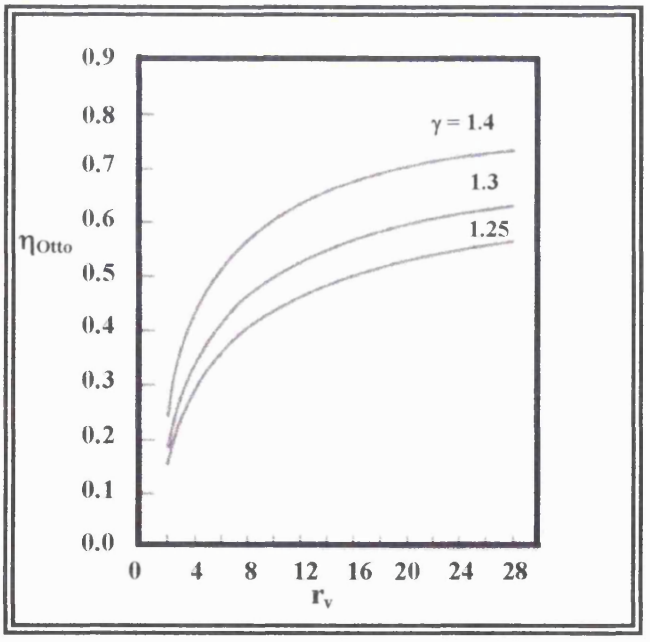

Figure 1.2: Variation of Otto cycle thermal efficiency with r_v and γ [Heywood (1988)]

1.1.2 Engine Indicator Diagram

The engine indicator diagram for a real SI engine (figure 1.3) is based on a mechanical cycle (as opposed to the Otto cycle which is based on a thermodynamic cycle), and although several differences exist between this cycle and the Otto cycle, a comparison between both is possible due to the similarity in the shape of the pV diagrams (figures 1.1 and 1.3). The idealised form of the engine indicator diagram is shown in figure 1.4.

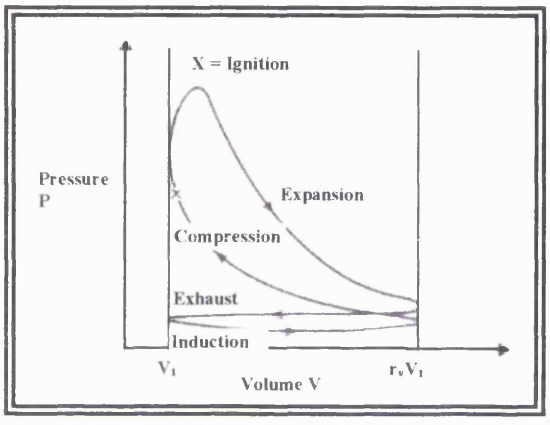

Figure 1.3: Indicator diagram for a 4-stroke engine [Stone (1994)]

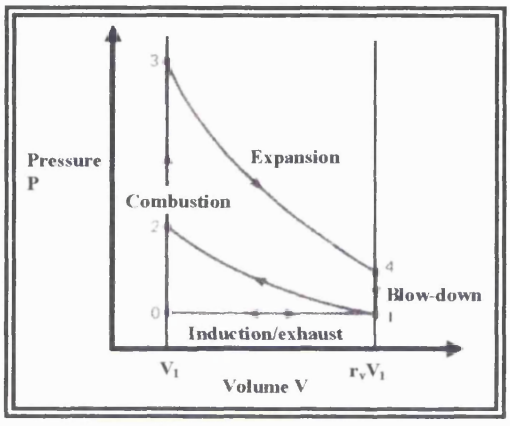

Figure 1.4: Idealised indicator diagram for a 4-stroke engine, constant volume combustion, no throttling [Stone (1994)]

In considering the differences between the Otto cycle and the engine indicator diagram, let us first allude to the Otto cycle. In the Otto cycle the working fluid is assumed to be an ideal gas (air) contained within a single closed volume. The addition of heat (figure 1.1, process 2-3) is from an external source (rather than through a combustion process), and the rejection of heat (figure 1.1, process 4-1) is to the environment (as opposed to the processes of blowdown and exhaust). Both of these processes are assumed to occur instantaneously and all processes are assumed to be fully reversible.

As the indicator diagram shows (figure 1.3) the processes occurring in an engine are not so clearly defined in reality. A finite time is required to open and close the inlet and exhaust valves, to allow the working fluid to enter and leave the system. A pressure drop occurs across the valves. Heat addition through combustion takes place neither instantaneously nor at constant volume, with combustion being initiated some 10°- 40° before top dead centre (BTDC) and completed 10°- 40° after top dead centre (ATDC)

(Heywood (1988)). Heat is rejected through gas exchange losses during blowdown and the exhaust stroke, in addition to heat transfer from the gases to the combustion chamber surfaces during the expansion stroke.

In a working engine the fluid is not an ideal gas but a mixture of air, fuel and residuals (burnt and unburnt charge which have not been exhausted from the previous cycle). The principal specific heats, c_p and c_v, do not remain constant therefore, but vary with the temperature and the composition of the working fluid at any point in the cycle.

The individual areas enclosed by a pV diagram are defined as being positive or negative, depending upon whether work is produced by processes or required for processes. The area enclosed by the induction and exhaust strokes usually represents the amount of *negative* work required to overcome the losses associated with the induction and exhaust processes, although it is possible that these two processes combine to give positive work. An example of this is a turbocharged engine where the induction stroke pressure is greater than the exhaust stroke pressure. The summation of the individual areas on a pV diagram represents the net indicated work output per cycle. Considering the differences between the Otto cycle and the engine indicator diagram, it is not surprising to find that the efficiency of a real engine is approximately 50 % less than that of the Otto cycle (Stone (1992)), partly due to the pumping losses described above and partly due to other losses such as mechanical friction.

1.2 Combustion

In a conventional SI engine under normal operating conditions, a mixture of air and fuel (homogeneous or otherwise) is drawn into the cylinder as the piston moves from top dead centre (TDC) to bottom dead centre (BDC) during the intake stroke. The fuel/air mixture must be quite close to stoichiometric (14.7:1) for reliable combustion. The mixture is then compressed to a pressure in the region of 15-25 bar (when unthrottled) resulting in a compression temperature of 400-600°C. Prior to reaching TDC on the compression stroke, (approximately 10°- 40° BTDC (Heywood (1988)) combustion is

initiated by applying a potential difference across the electrodes of the spark plug, sufficiently high to cause the air/fuel mixture in this region to ionise. The impedance between the electrodes significantly reduces, thus allowing a spark discharge to cross the gap. Burning of the fuel vapour and air mixture begins.

The energy released from this spark discharge is small and so the initial stages of combustion are slow. The time taken from spark discharge to the moment when a significant proportion of the flame front develops (usually taken as 10 % of complete combustion) is known as the ignition delay and is of the order of 2 ms (Rogers and Mayhew (1980)). The ignition delay period is shown in figure 1.5, points a-b. Schlieren techniques have been used to visualise the growth of the flame front and combustion events (Ereaut (1988), Namazian *et al* (1980)) and a developing flame recorded 5° after spark discharge is shown in figure 1.6. Within the flame kernel exothermic reactions occur that are capable of sustaining flame propagation and the flame kernel grows and radiates outwards in a spherical manner, interacting with the turbulent air motion which causes its boundaries to wrinkle and distort. The size of the reaction zone is thus increased. At an engine speed of 1000-2000 rpm, these wrinkles are approximately 2 mm in size (Heywood (1988)). The combustion rate also begins to increase and the cylinder pressure and temperature rise significantly (figure 1.5, points b-c). On reaching the cylinder walls the flame front is extinguished. For a particular engine and fuel, the time taken for flame propagation in the second phase (i.e. after the ignition delay), decreases at approximately the same rate at which the engine speed increases ((Milton (1995)). This is because the turbulence generated by the intake flow processes and modified by the compression stroke is more or less related to engine speed (Milton (1995)).

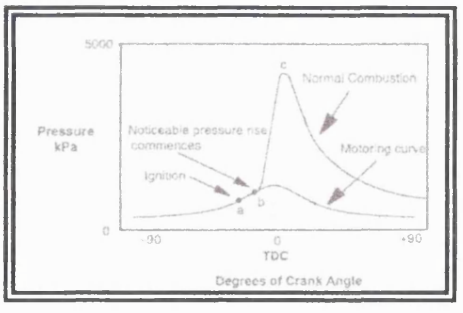

Figure 1.5: Cylinder pressure over a single engine cycle [Milton (1995)]

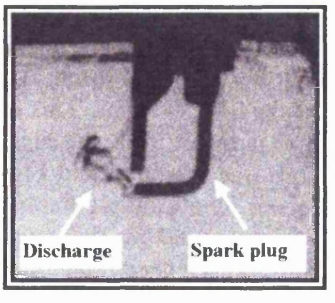

Figure 1.6: Schlieren photograph of developing flame 5°, after spark discharge [Heywood (1988)]

1.3 Exhaust Gas Composition

The exhaust gas of a SI engine usually contains less than 1% by volume of pollutants which are known to be harmful to the environment, and to plant and animal life. These pollutants comprise oxides of nitrogen, (NOx), carbon monoxide (CO) and partially burnt or unburnt hydrocarbons (UHC). The variation of each pollutant with air/fuel ratio (AFR) is shown in figure 1.7 and the mechanisms responsible for the production of each pollutant shall be considered in turn.

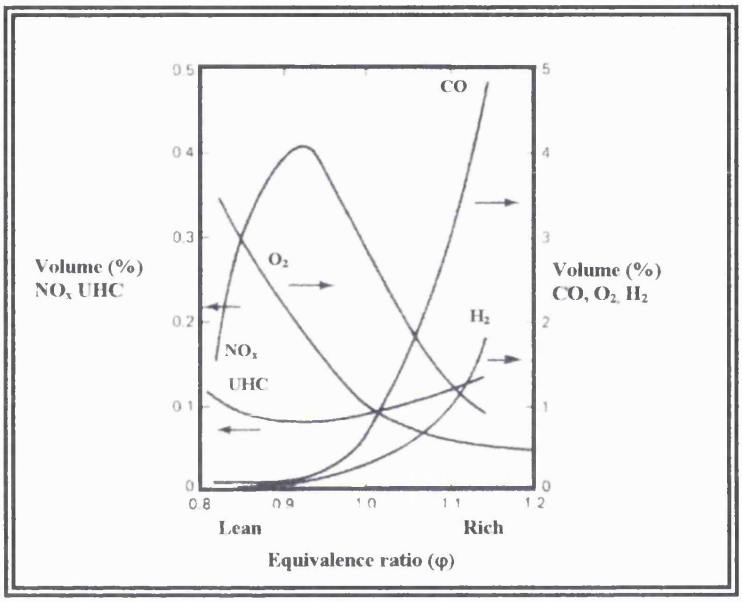

Figure 1.7: Variation of UHC, NOx and CO with air fuel ratio [Stone (1994)]

1.4 Formation of UHCs in a SI Engine

Several mechanisms are responsible for the production of UHCs in a SI engine and these are listed by Min *et al* (1994) as:

1) The existence of crevices in the combustion chamber where fuel can 'hide' during combustion.
2) The absorption and desorption of fuel vapour in the oil layers.
3) The absorption and desorption of fuel in deposits.
4) Flame quenching (e.g. wall quenching and bulk quenching).
5) The presence of liquid fuel in the cylinder.

6) Exhaust valve leakage.

1.4.1 The Crevice Effect

Several crevices exist within the combustion chamber (figure 1.8). The relative size of each crevice expressed as a percentage of the clearance volume for a modern design of engine is given in table 1.1. Although the volumes are relatively small, it has been shown both experimentally (Min *et al* (1994) and Boam *et al* (1992)) and theoretically (Namazian *et al* (1982)) that these crevices are the major cause of UHCs in the exhaust. The combination of these crevices accounts for 38 % of the total engine-out UHCs for a current production, 4 cylinder, 2-litre engine, in steady-state cruise conditions (Min *et al* (1994)), where engine-out UHCs refer to those UHCs measured in the exhaust port prior to the catalyst.

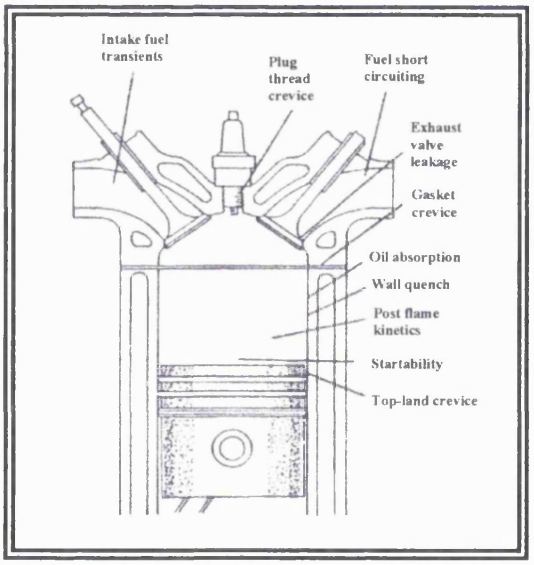

Figure 1.8: Crevices and their relative sizes in a SI engine [Heywood (1988)]

	cm^3	%
Displaced volume for cylinder	632	-
Clearance volume for cylinder	89	100
Volume above first ring	0.93	1.05
Volume behind first ring	0.47	0.52
Volume between rings	0.68	0.77
Volume behind second ring	0.47	0.52
Total ring crevice volume	2.55	2.9
Spark plug thread crevice	0.25	0.28
Head gasket crevice	0.3	0.34
Total crevice volume	3.1	3.5

Determined for cold engine

Table 1.1: V-6 engine crevice data [Heywood (1988)]

The most significant crevice (in terms of size and UHC emissions) is the region between the piston, the piston top ring and the cylinder bore, otherwise known as the top-land crevice. The piston crevices at peak cylinder pressure trap some 5%-10% of the total cylinder charge. The portion of this charge that will return to the cylinder to be burnt at a condition of 2000 rpm WOT is given in table 1.2. Work performed by Wentworth (1971) found the proportion of top-land crevice UHCs accounted for as much as 47-74% of the total engine-out UHCs depending upon speed and load conditions. This value is greater than that quoted by Min *et al* (see previous page) and is thought to be as a result of differing crevice sizes between both engines and different test conditions.

Amount of gas flowing into and out of crevice regions †

	% mass	ppm C
Total gas in all crevice regions	8.2	
Total gas back to combustion chamber	7.0	
Unburned back to combustion chamber	3.7–7.0‡	5000–9400
Unburned to blowby	0.5–1.2‡	
Total unburned escaping primary combustion	4.2–8.2‡	

† For V-6 engine operating at 2000 rev/min and wide-open throttle
‡ Depends on spark plug and ring gap location

Table 1.2: Proportion of UHC escaping the primary combustion process [Heywood (1988)]

Although the top-land crevice accounts for the major part of UHC emissions, Min *et al* (1994) found that the head gasket crevice volume was more sensitive to changes in its volume, than that of the top-land crevice. For the piston crevice, a 10 %, change in volume led to a 2% change in UHC emissions, but for the gasket crevice, a 2% change in volume led to a 12 % change in UHC emissions. The results appeared to be independent of speed and load. In addition, for a centrally-mounted spark plug, greater UHC levels were obtained if the gasket crevice was on the exhaust side rather than on the inlet side.

The reduction in UHCs through a decrease in the crevice volume does not occur uniformly over the whole of the engine cycle. This was shown by Boam *et al* (1992) who measured real-time exhaust UHC concentrations using a Cambustion fast flame ionisation detector (FFID). Figure 1.9 shows the UHC traces obtained from (i) using a standard piston and (ii) one which had its piston crevices virtually eliminated (here-on-in

referred to as a sealed piston). The most significant difference between the two traces occurred as the piston approached TDC exhaust, with the UHC concentration increasing significantly more with the standard piston than with the sealed piston. This may be explained if the flows into and out of the piston crevices are considered.

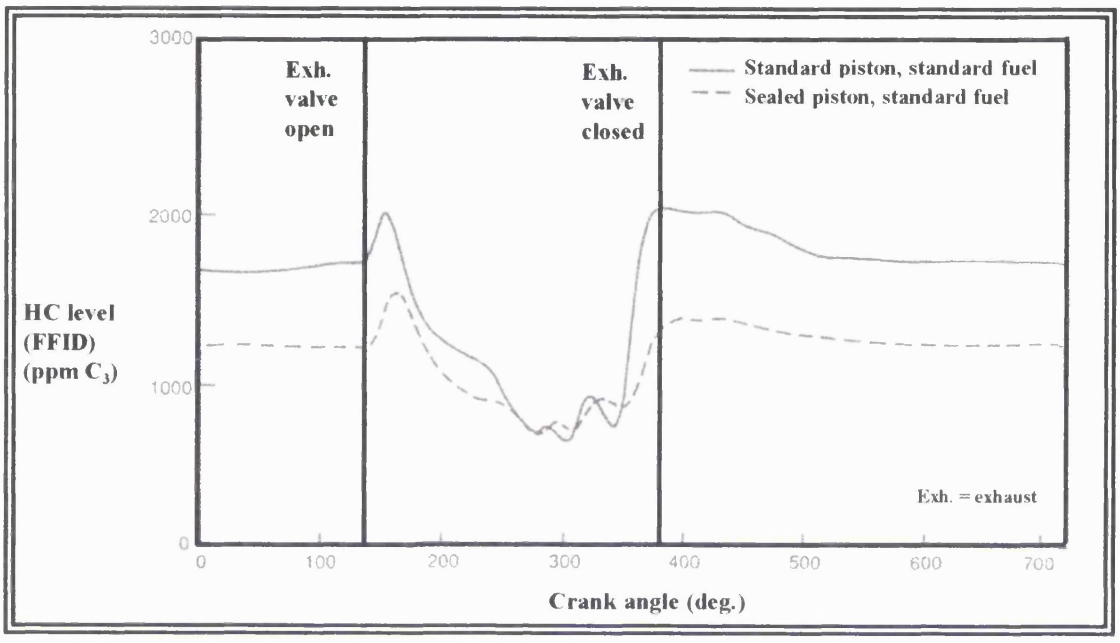

Figure 1.9: FFID exhaust HC trace for an engine with and without a piston ring crevice taken 100 seconds after a 20°C start [Boam *et al* (1992)]

During the compression stroke the piston moves from BDC to TDC, the cylinder pressure rises, and some of the inducted charge is forced into the crevices. The flow of unburnt charge into the crevices continues during combustion whilst the cylinder pressure continues to rise, until the arrival of the flame front whereupon burned mixture will flow into the crevices (as long as the cylinder pressure continues to rise). It is likely that the crevice entrance is so small that the flame front is unable to penetrate and is quenched at the entrance leaving the crevice charge unburnt. As the cylinder pressure decreases during the expansion stroke, a low velocity gas jet emanates from the top-land crevice and is laid along the cylinder wall. Flow reversal of the gas trapped in the crevice regions behind the top ring occurs as the jet flow starts from the top ring gap and the crevice pressure in this region exceeds the cylinder pressure. A proportion of this gas having escaped the primary combustion process, will expand into the bulk gases and at exhaust valve opening (EVO), may become entrained by the bulk gases and oxidise in the

rapid motion which occurs during blowdown, (Heywood (1988)). Some will however, be scrapped off the cylinder wall into a vortex by the upward motion of the piston during the exhaust stroke, leading to the relatively high UHC concentration in the exhaust port (figure 1.10). The elimination of the piston crevices prevents unburnt charge from becoming trapped in these volumes and thus reduces the quantity of charge released by the late storage mechanisms.

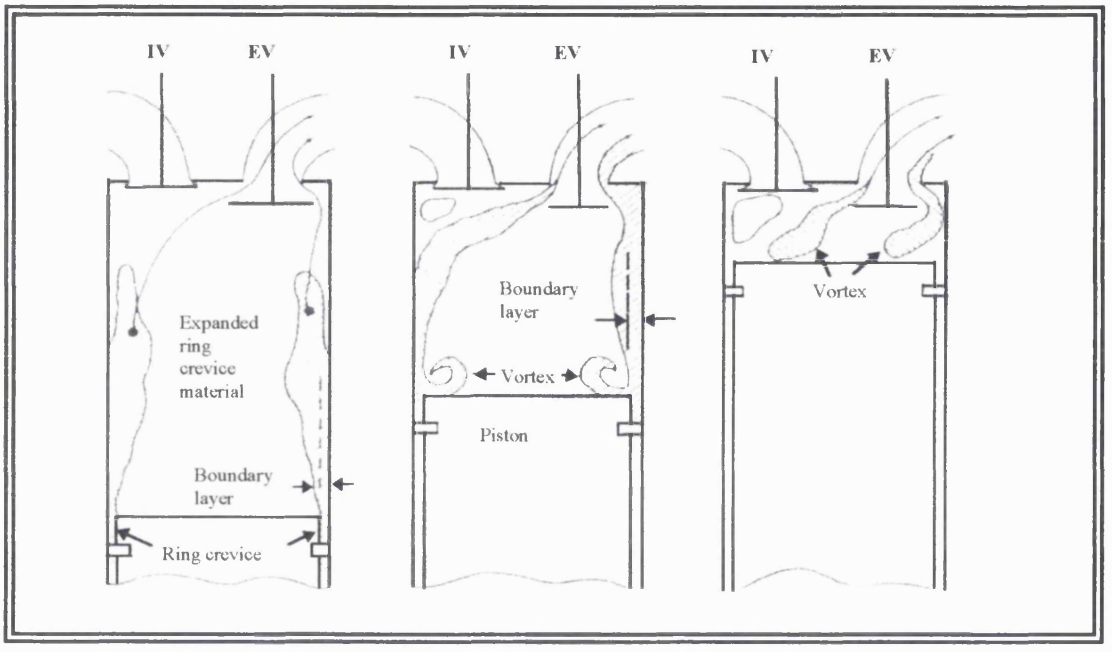

Figure 1.10: Flows into and out of the piston ring crevices during the exhaust stroke [Heywood (1988)]

Both the low and high velocity flows have been visualised and recorded using Schlieren photography techniques applied to a transparent engine (Namazian *et al* (1982)) and their concentrations measured with a FFID by Peckham *et al* (1993). Here, a FFID probe was mounted into the piston such that the in-cylinder UHC concentration was measured 0.5 mm and 20 mm away from the cylinder bore, the probe moving up and down with the piston through its stroke. Throughout the expansion and exhaust strokes high UHC levels were measured with the probe at 0.5 mm, but only at EVO with the probe situated in the 20 mm position, adding increased weight to the mechanisms described above.

Finally considering the spark plug crevice, Namazian and Heywood (1982) visualized charge emanating from this region using Schlieren photography techniques, however

Boam *et al* (1992) found experimentally that the spark plug crevice did not trap a significant amount of charge when compared with that trapped by the piston ring crevices and the cylinder head gasket crevice. The spark plug crevice did not therefore contribute significantly to the production of UHC emissions.

1.4.2 Absorption and Desorption of Fuel Vapour in Oil Films

It has been postulated (Kaiser *et al* (1981) that oil present on the walls of the combustion chamber can absorb fuel vapour during intake and compression and then desorb it during expansion and exhaust. Although some of the desorbed fuel vapour will mix with the high temperature gases and oxidise, that which remains in the cooler regions such as in the boundary layer, will remain unoxidised and eventually contribute to the UHC emissions. Similarly, the desorbed vapour which mixes with the cooler bulk gases later in the cycle may not be fully oxidised and again will contribute to UHC emissions. Kaiser *et al* (1981) showed that by increasing the oil layers up to 25 microns thick the UHC exhaust levels increased linearly, and Boam *et al* (1992) quotes from Ishizawa and Tagaki as having reported a 30% reduction when running an engine without oil lubrication.

1.4.3 Absorption and Desorption of Fuel in Deposits

The presence of deposits is known to increase UHC levels between 7-20 % (Heywood (1988)). The position and size of the deposit is important in determining the effect it will have on UHC levels, with locations close to the exhaust valves contributing to a greater degree.

1.4.4 Flame Quenching

During combustion, the gas temperatures can reach 2000 °C whereas the temperature of the cylinder wall remains at a relatively low temperature, approximately 200 °C. The cylinder wall acts as a heat sink, quenching the flame as it approaches and as a result there exists a thin boundary layer, or quench layer, of combustible mixture on the surface of the cylinder wall. Work investigating combustion in bombs (Adamczyk *et al* (1983)) has suggested that the gases in these quench layers diffuse into the burned gases and fully oxidise 1-2 ms after quenching. Under cold start conditions the scenario may be quite

different, with the quench layer being thicker and less readily consumed thus contributing to UHC emissions.

An alternative flame quenching process is bulk quenching. This can occur during the expansion stroke if the pressure and temperature in the cylinder fall too rapidly, causing the flame to be extinguished in the bulk gases. The probability of bulk quenching occurring may be reduced by increasing the combustion burn rate, thereby decreasing the time available for the flame to be extinguished.

1.4.5 The Effect of Liquid Fuel Present in the Cylinder

Boam *et al* (1992) carried out experiments both with a standard piston and a sealed piston. The engine was supplied with vaporised fuel and it was discovered that the effect of the vaporised fuel was not as great in terms of UHC emissions if the crevices were eliminated. The conclusion drawn was that some liquid fuel found its way into the crevices, thereby escaping combustion and contributing to the overall UHC emissions.

The rate of evaporation is increased significantly if the fuel is prepared as small droplets. Mineo *et al* (1990) quote an 8% reduction in UHC emission with the installation of fine atomisation injectors, and Matthes and McGill (1976) quantified the effect of the degree of atomisation of a carburettor, using a single-cylinder engine to eliminate the effect of cylinder to cylinder variability. In order to simplify the situation further, they also tried to eliminate the effects of air motion as much as possible by using different combustion chamber designs. They investigated three mean sizes of fuel droplets and showed greater amounts of UHCs being produced with larger droplets than with smaller droplets. The difference was as much as 20% for a particular engine speed and AFR.

1.4.6 Exhaust Valve Leakage

When the engine is new, exhaust valve leakage is not thought to be significant when compared with other UHC formation mechanisms (Boam *et al* (1992)). However, with wear of the valves and valve seats, this may become a significant.

1.5 Sources of CO

CO is formed in significant proportions whenever there is a deficiency of air to burn all the fuel. The cause may be that the overall mixture is rich of stoichiometric, or local regions are rich due to poor mixture preparation. Small quantities of CO are formed even with lean mixtures due to dissociation of CO_2 at the high combustion temperatures, followed by insufficient time for the reversion reactions to take place.

1.6 Sources of NOx

NOx is the name given to the oxides of nitrogen that are present in the exhaust gases, with nitric oxide (NO) accounting for over 90% of the total NO_x. The basic mechanism for the formation of NOx is the dissociation of oxygen and nitrogen molecules (O_2 and N_2) into oxygen and nitrogen atoms (O and N) which then combine to form NO. Three principal reactions (equations 1.3.1-1.3.3) are responsible for the formation (and destruction) of NO and are collectively referred to as the Zeldovich reactions (Heywood (1994)).

$$O + N_2 \Leftrightarrow NO + N \qquad (1.3.1)$$

$$N + O_2 \Leftrightarrow NO + O \qquad (1.3.2)$$

$$N + OH \Leftrightarrow NO + H \qquad (1.3.3)$$

[Heywood (1994)]

The bulk of these reactions occur in the post-flame gases with negligible amounts (except at very lean AFRs) being produced in the flame reaction zone. NO formation rates are strongly dependent upon temperature, the higher the peak combustion temperature, the greater the degree of dissociation, and so the greater the level of NOx emissions. A reduction in peak combustion temperature (for example through the addition of exhaust gas or the use of leaner mixtures) will lead to a decrease in the NOx levels as a result of an increase in the heat capacity of the cylinder per unit mass of fuel. Retarding the spark timing also reduces the peak temperatures due to a reduction in the peak cylinder pressure since a greater quantity of the fuel burns after TDC. However, this has an adverse effect on the power output and fuel economy of the engine. Thus, the concentration of NO being produced tends to decrease with increasing combustion time

because mixture which burns early is compressed to a higher temperature and pressure after combustion as the cylinder pressure continues to rise. Mixture which burns later is primarily compressed as unburned mixture and ends up after combustion at a lower burned gas temperature, the density of burned fuel being approximately 4 times less than that of unburned fuel. Another factor in determining NOx levels is the rate at which the gas cools during the expansion stroke. The slower the cooling, the greater the time available for the reverse reactions to occur, converting NO back to N_2 and O_2.

1.7 Abnormal Combustion

The mechanisms for the production of UHC, NO_x and CO have all been discussed so far in relation to 'normal' combustion. However, there are situations in which 'abnormal' combustion may take place. Two major abnormal combustion phenomena which are widely recognised are knock and surface ignition. Tests have shown that CO and UHC emissions are high when these abnormal combustion phenomena occur.

1.7.1 Knock

The compression ratio of a SI engine is usually between 8 and 12. If this compression ratio is set too high, then the resultant increase in the temperature and pressure of the end gas (i.e. the gas waiting to be burnt) caused by combustion can lead to some of the end gas undergoing a series of chemical reactions prior to the flame front reaching it. These reactions may cause autoignition, in which chemical energy is rapidly released at a rate of 5-25 times greater than for normal combustion (Heywood (1988)). A high frequency pressure oscillation occurs inside the cylinder which produces a sharp metallic knocking noise. Other factors which affect the tendency to knock are the chemical structure of the fuel and the speed of combustion.

1.7.2 Surface Ignition

Surface ignition refers to the ignition of fuel by any source other than the spark formed at the spark plug. Alternative sources could be an overheated valve or spark plug, or an incandescent hot spot somewhere else in the combustion chamber. Surface ignition may occur before the spark (preignition) or after the spark (postignition). Following surface ignition, a turbulent flame develops at each surface ignition point and propagates across

the chamber in a manner similar to that associated with normal combustion. Since there is less control over when surface ignition occurs, it may cause a loss in power output and driveability and contribute to increased emission levels.

1.7.3 Activated Radical Combustion

Engine researchers are looking at using abnormal combustion and the promotion of free radicals to help reduce emission levels. Ishibashi *et al* (1996) claim a reduction of approximately 60% from a 250 cm^3 two-stroke engine when using this abnormal combustion phenomenon known as activated radical combustion (AR combustion). The processes that occur are not yet fully understood and the literature does not discuss the reactions.

1.8 Emission Legislation

In the earlier days of IC engines, combustion was studied with a view to improving engine performance, but since the late 1960s the world's population has become increasingly aware of problems caused by pollution from exhaust gas products. Much of the current research into production is driven by the need to meet emission legislation, and so the following section discusses current and future legislation.

1.8.1 Transportation

The world's car population in the 1950s was less than 50 million, by 1986 this figure had increased by some 700% to a figure beyond 350 million and is likely to increase further right into the 21st century (Goldsmith (1990)). Considering Europe alone, there is a predicted increase in car ownership of some 52 million to a total of 167 million over the period 1987-2010 (Newman *et al* (1993)), and an increase in vehicle kilometres of 25% between 1990 and 2010 (Murley (1993)). The problem of vehicle pollution is therefore a serious one.

Legislation has evolved in an attempt to control the quantity of vehicle pollution entering the atmosphere. It varies from region to region, with the United Nations Economic Commission for Europe (ECE), and the European Economic Community (EEC) setting

standards for Europe, whilst the Environmental Protection Agency (EPA) and the California Air Resources Board (CARB) set the standards for the USA.

1.8.2 European Legislation

The ECE is responsible for most of the initial work in vehicle pollution control in Europe, with ECE Regulation Number 15 establishing the first emission standard criterion for all new cars (1968). These regulations have been superseded by the EEC Type Approval System for motor vehicles (defined by directives), set-up in 1970 to work alongside corresponding approval systems already in place in its member states.

1.8.3 Current Legislation

1.8.3.1 Test Cycles: Light Duty Vehicles

Several different test cycles exist in different parts of the world, however the cycle relevant to Europe is the ECE 15 (urban driving cycle) combined with EUDC 15 (suburban driving cycle) (Anon. Ford Motor Company (1994)). The combined driving cycle is shown in figure 1.11.

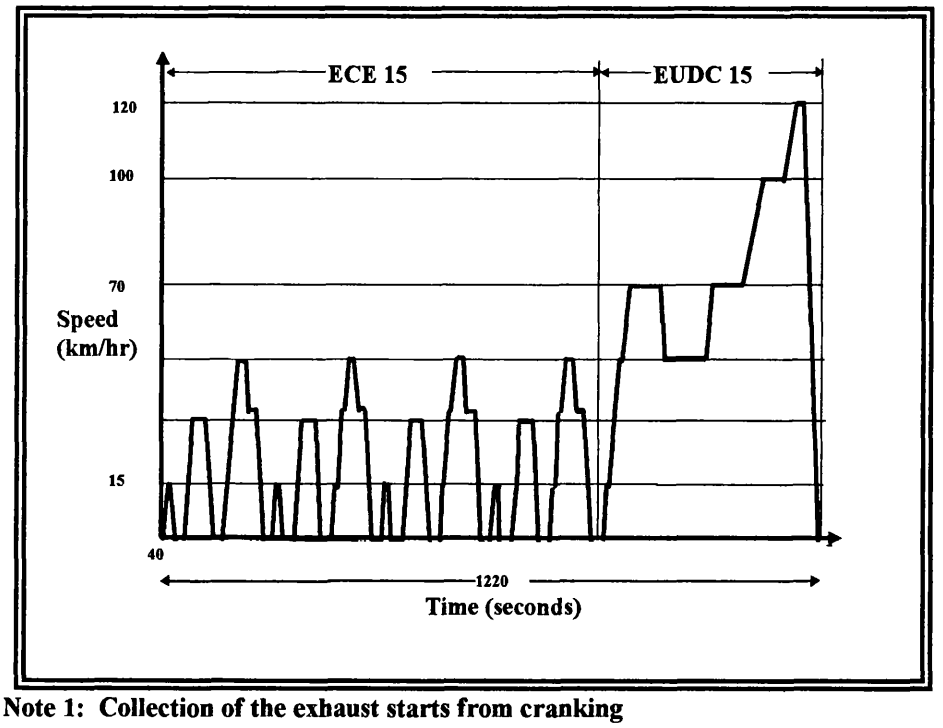

Note 1: Collection of the exhaust starts from cranking
Note 2: Test and soak temperatures are currently set at 20 °C and 30 °C
Note 3: Applicable to all new cars sold from the beginning of 1993 [Briesly *et al* (1993)]

Figure 1.11: EUDC 15 test cycle [Anon. Ford Motor Company (1994)]

1.8.3.2 Exhaust Pollutant Measurement

The method of measuring the exhaust gas pollutants has changed from the 'big bag' method to that of constant volume sampling (CVS), whereby a known quantity of exhaust gas is collected (Anon. DoT (1992)). Depending upon the test cycle used, the methods of measuring the pollutants may vary but, in general, to measure UHCs a flame ionisation detector is used, to measure CO_2 and CO, nondispersive infrared techniques are used and to measure NOx a chemiluminescent analyser is used (Heywood (1988)).

1.8.3.3 Pollutant Levels

Table 1.3 shows the European exhaust emission standards for all new cars effective from January 1997 and table 1.4 the standards proposed for the years 2000 and 2005.

Engine Type	CO (g/km)	($HC+NO_x$) (g/km)	Particulates (g/km)
Petrol	2.2	0.5	N/A
Diesel, indirect injection	1.0	0.7	0.08
Diesel , direct injection	1.0 +	0.9	0.1

+ di diesel standards are more relaxed than idi for three years

Table 1.3: European exhaust emission standards for all new cars effective from January 1997 [Anon. Automotive Engineer (1997)]

Engine Type	**CO** (g/km)	**HC** (g/km)	**NO_x** (g/km)	**Particulates** (g/km)
Petrol				
(2000/1)	2.3	0.2	0.15	N/A
(2005)	1.0	0.1	0.08	N/A
	CO	**$HC+NO_x$**	**NO_x**	**Particulates**
Diesel				
(2000/1)	0.64	0.56	0.50	0.05
(2005)	0.50	0.30	0.25	0.025

Table 1.4: European exhaust emission standards for the years 2000 and 2005 [Anon. Automotive Engineer (1997)]

1.8.3.4 US Legislation

The levels of allowable emissions for California and the other US states are shown in the tables 1.5 and 1.6 below. The levels are based on the FTP75 driving cycle which comprises of three stages. The first stage is the cold start transient stage (average speed 25.7 mph), the second stage is the cold start stabilised phase (average speed 16.2 mph) and the final stage is the warm start transient phase (average speed 25.8 mph). California is leading the way with a push towards 'zero emissions vehicles', which in practice are battery-powered vehicles.

Standard	**NMHC** g/mile	**CO** g/mile	**NOx** g/mile
Tier I (MY 1996)	0.25	3.4	0.4
Tier II (MY 2004)	0.125	1.7	0.2

Table 1.5: US passenger car pollution limits [Anon. Automotive Engineer (1997)]

Vehicle Class	**NMOG** g/mile	**CO** g/mile	**NOx** g/mile
MY 1993	0.250 (NMHC)	3.4	0.4
TLEV	0.125	3.4	0.4
LEV	0.075	3.4	0.2
ULEV	0.040	1.7	0.2
ZEV	0.000	0.0	0.0

Note 1: NMOG = non methane organic hydrocarbons, NMHC = non methane hydrocarbons, TLEV = transition low emissions vehicle, LEV = low emissions vehicle, ULEV = ultra low emissions vehicle, ZEV = zero emissions vehicle
Note 2: Standards are for 5 years/50,000 miles
ote 3: From 1998 2% of cars sold by each manufacturer in the state must be ZEV, this percentage increases to 10 % by 2003

Table 1.6: Californian passenger car pollution limits [Heimrich *et al* (1991)]

1.9 Exhaust Gas Treatments: The Catalyst

Existing legislation has led to the development and widespread use of catalysts. Here the main reduction in pollutant levels is achieved in the exhaust system where the catalyst is situated, rather than in improving the combustion process itself. The pollutants are made to undergo further reactions by the catalyst to produce N_2, H_20 and CO_2.

The two most common catalyst configurations are the monolith design and the pelletized design (figures 1.12 a and b). In both configurations the surface area of the catalyst is designed to be as large as possible in order to optimise the contact area between the catalyst and the exhaust gas. For a monolith structure, the ratio of catalyst volume to engine volume is 1.1:1 to 1.23:1 (Goldsmith (1990)).

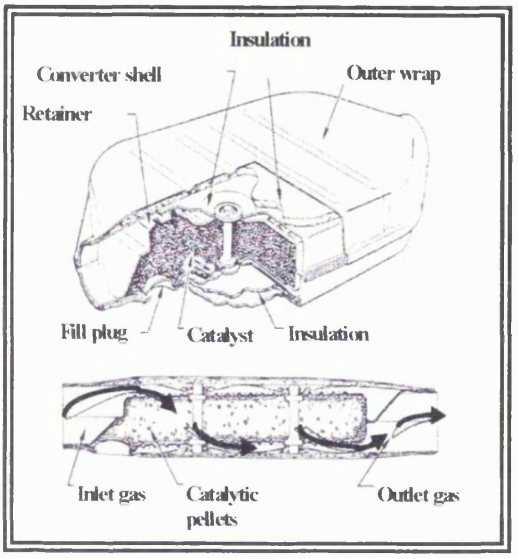

Figure 1.12a: Monolith catalytic converter for a SI engine [Heywood (1988)]

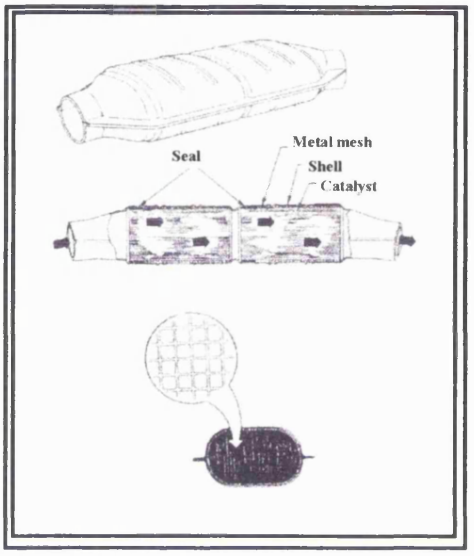

Figure 1.12 b: Pelletized catalytic converter for a SI engine [Heywood (1988)]

The three main types of catalyst are: the reduction catalyst, the oxidation catalyst (these may be used together and are called 'dual' catalysts) and the three-way catalyst. Each depends upon the use of a different AFR to achieve maximum efficiency (figure 1.13).

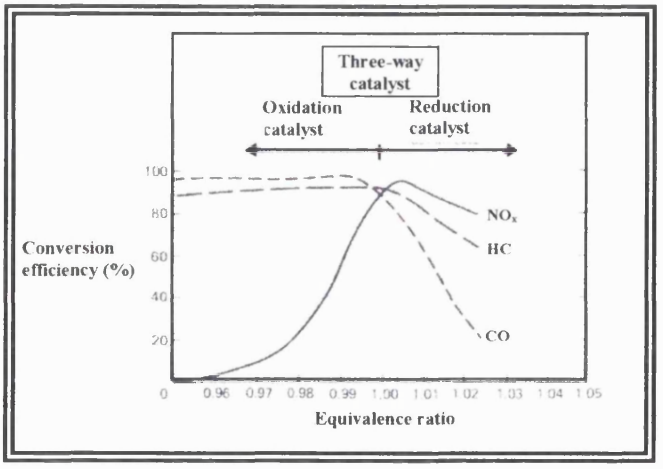

Figure 1.13: Variation of catalyst efficiency with air fuel ratio [Stone (1994)]

1.9.1 Oxidation Catalyst

Oxygen is required to oxidise the HCs and CO into CO_2 and H_2O through the following reactions.

$$4\ HC + 5\ O_2 \rightarrow 4\ CO_2 + 2\ H_2O \qquad (1.4)$$

$$2\ CO + O_2 \rightarrow 2\ CO_2 \qquad (1.5)$$

[Stone (1994)]

The excess oxygen may be provided by operating lean of stoichiometric or by using an air pump to introduce air into the exhausts ports upstream of the catalyst. NOx is controlled by retarding the ignition or using EGR (see section 1.10.2).

1.9.2 Reduction Catalyst

Removal of NO is afforded through promotion of reactions with CO, HC and H_2 which are also present in the exhaust gases, particularly so with rich mixtures (equations 1.6-1.6.6). To ensure all the CO and HC has been removed from the exhaust gas, a second oxidation catalyst is required downstream with air supplied between the two catalysts by a pump in order to provide the necessary oxygen for this oxidation process.

$$2\ NO + 5\ CO + 3\ H_2O \rightarrow 2\ NH_3 + 5\ CO_2 \qquad (1.6)$$

$$2\ CO + 2\ NO \rightarrow 2\ CO_2 + N_2 \qquad (1.6.1)$$

$$2\ NO + CO \rightarrow N_2O + CO_2 \qquad (1.6.2)$$

$$2\ NO + 2\ H_2 \rightarrow N_2 + 2\ H_2O \qquad (1.6.3)$$

$$2\ NO + 5\ H_2 \rightarrow 2\ NH_3 + 2\ H_2O \qquad (1.6.4)$$

$$2\ NO + H_2 \rightarrow N_2O + H_2O \qquad (1.6.5)$$

$$4\ HC + 10\ NO \rightarrow 4\ CO_2 + 2\ H_2O + 5\ N_2 \qquad (1.6.6)$$

[Stone (1988), Heywood (1994)]

1.9.3 Three-Way Catalyst

The three-way catalyst (TWC) requires only a single catalyst bed to simultaneously reduce NOx and oxidise CO and HC to form the products CO_2, N_2 and H_2O. It is the oxygen that is present in the NOx that is used to oxidise the HC and CO. However a

stoichiometric or close to stoichiometric AFR is required so that sufficient reducing and oxidising gases are present. Either side of this and the catalyst efficiency is drastically reduced. This is clearly demonstrated in figure 1.14 which shows there is a 80 % conversion efficiency window around stoichiometric. The feature of having all the reactions taking place in a single catalyst has led to manufacturers adopting three-way catalysts universally.

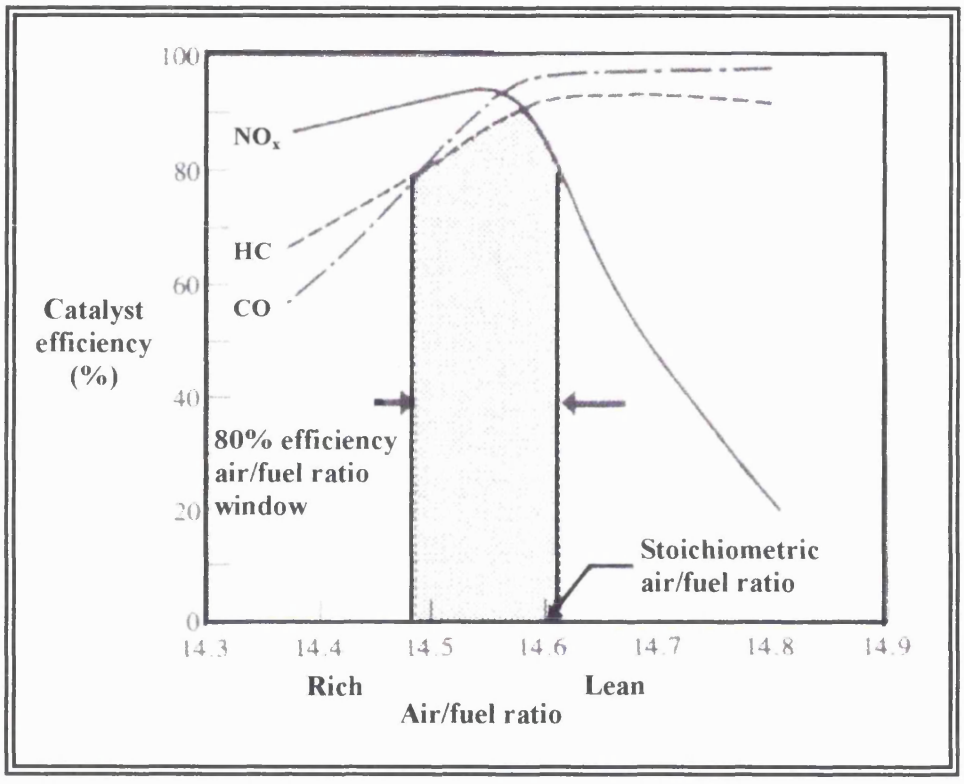

Figure 1.14: Conversion efficiency of a 3-way catalyst [Heywood (1988)]

The light-off temperature of the catalyst is that temperature at which the catalyst achieves a 50% conversion efficiency and is in the region of 300-400 °C. Catalysts can take up to 1-2 minutes to achieve this temperature, however 80 % of all UHC and CO emissions are produced in the first 45 seconds (Boyle *et al* (1993)). A possible means of decreasing the light-off time is to move the catalyst closer to the engine but this subjects the catalyst to even higher temperatures once the engine is warm, which could substantially decrease the catalyst durability unless careful development is undertaken. In order that catalysts continue to play a large role in the reduction of emissions, further improvements in the areas of light-off temperature and durability are required.

1.10 Reduction in the Formation of Exhaust Pollutants

Catalysts have shown their effectiveness in reducing pollutant levels, but it is still crucial to ensure that engine-out emission levels are as low as possible to start with, not least because the presence of UHCs mean a corresponding loss in engine efficiency. The following sections will discuss more fundamental methods for improving engine-out emissions, but first there will be a general discussion of the flow processes that occur within the cylinder.

1.10.1 In-Cylinder Air Motion

The characteristics of the intake flow and the resulting air motion that is established in the cylinder are dependent upon the intake port and cylinder head design. There are two types of predominant air motion, axial swirl and barrel swirl (figure 1.15). These organised air motions are important at part load conditions because they increase the in-cylinder charge motion, leading to high levels of small-scale turbulence just prior to and during combustion. Turbulent air motion aids the mixing and burning of the air and fuel, and then during combustion promotes rapid burning and flame growth. Without turbulence the flame propagation rate is substantially decreased to one which would be impractically low. An optimum degree of swirl exists beyond which burning becomes too fast and the flame front may be extinguished too early. In addition, noise may become a problem.

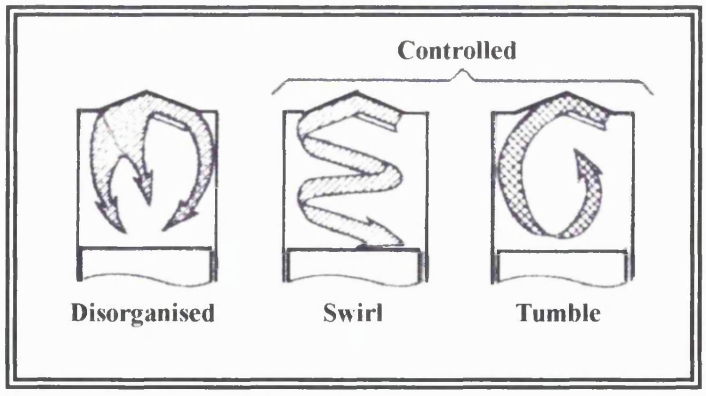

Figure 1.15: Ordered (barrel and axial swirl) and disorganised air motion [Boer *et al* (1990)]

1.10.1.1 Axial Swirl

Axial swirl is currently found mainly in direct injection (DI) diesel engines, or in some stratified charge SI engines. It may be induced in two ways. The first involves inducing

the swirling action *within the cylinder*, either by designing the intake port so that the flow enters the cylinder tangentially and is guided by the cylinder walls in a swirling downwards motion (figure 1.16 a), or by masking off or shrouding part of the valve area (figure 1.16 b). The third method of inducing axial swirl involves forcing the flow to rotate about the valve axis *before it enters the cylinder* using, for example, helical ports (figure 1.16 c). This method has a higher flow discharge coefficient at the valve seat (and hence higher volumetric efficiency), primarily as a result of the more uniform flow around the inlet valve seat.

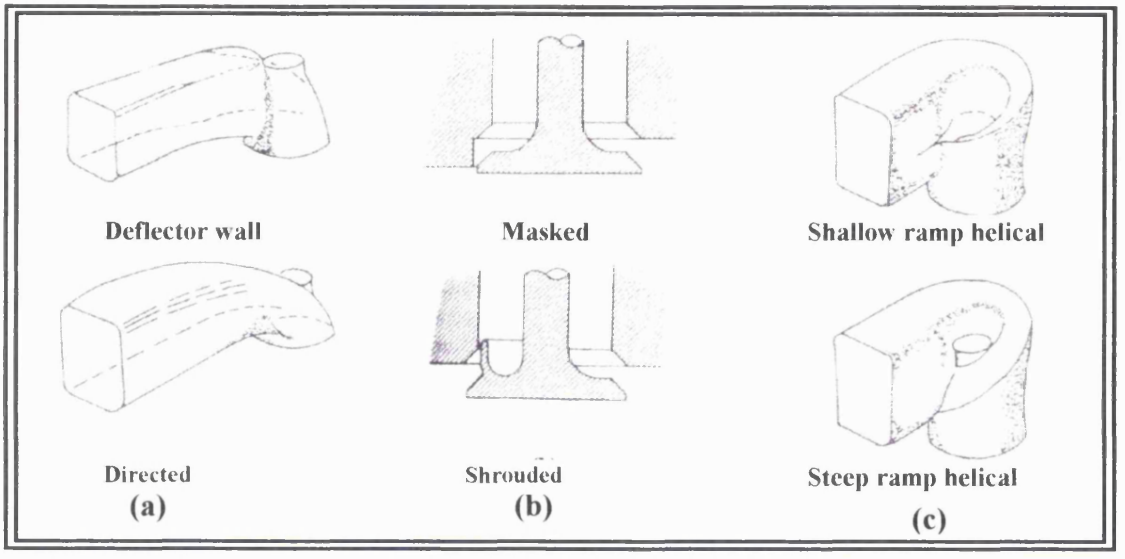

Figure 1.16 : Methods to induce axial swirl, a) tangential inlet ports, b) masked cylinder head and shrouded inlet valve, c) helical inlet ports [Heywood (1988)]

Axial swirl does not fully break down during compression and a large part of the bulk motion remains intact throughout the compression stroke and most of the expansion stroke, serving only to advect the flame around the combustion chamber (Benjamin (1993)). Small-scale turbulence levels are not as high as with tumbling regimes.

1.10.1.2 Barrel Swirl

Barrel swirl or tumble is usually found in 4-valve SI engines and can be produced by designing the inlet port and cylinder head such that the air motion is drawn over the top of the intake valves. During compression this tumbling motion is squashed until the bulk motion is broken down into a regime of turbulent vortices and eddies prior to combustion.

Unlike axial swirl, this tumbling air motion is also dependent upon the flow impinging on the piston. Various piston designs have been used to help promote the tumbling motion with one such design shown in figure 1.17.

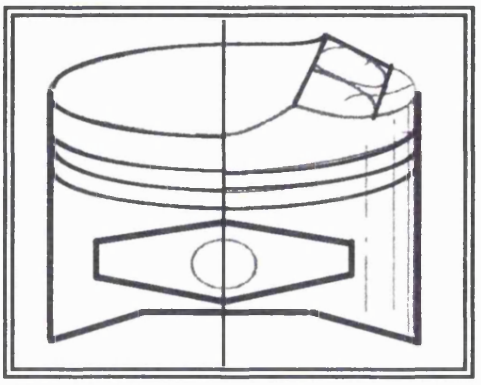

Figure 1.17: A design of piston to promote barrel swirl [Heywood (1988)]

In some engine designs, axial and barrel swirl are combined and the resulting motion maybe considered to be a single vortex rotating about an axis whose inclination is dependent upon the ratios between the two motions (Furuno *et al* (1990)).

1.10.1.3 Swirl Measurement Techniques

Hot wire anemometry techniques (HWA) and laser Doppler anemometry/velocimetry techniques (LDA/V) are used to provide quantitative information about both the bulk air motion and turbulence in an operating engine. A swirl ratio (R_s) is used to characterise bulk air motion in an operating engine (equation 1.7).

$$R_s = \frac{\omega_s}{2\pi N} \qquad (1.7)$$

where: ω_s = angular velocity of a solid body rotating flow (rad/s)

$2\pi N$ = crankshaft rotational speed (rad/s)

[Heywood (1988)]

Alternative techniques and swirl ratios are used to characterise air motion on a steady flow test rig. One such technique involves the use of an impulse swirl meter mounted in a dummy cylinder onto which a cylinder head is mounted. Air is then blown (or sucked) through the cylinder head into the dummy cylinder. The swirl meter comprises a honeycomb flow straightener which measures the total torque exerted by the flow with

the torque being equal to the flux of angular momentum through the plane coinciding with the flow straightener upstream face. Several swirl coefficients have been defined for use with the impulse swirl meter, one of the simplest being:

$$C_s = \frac{8\tau}{mv_o B} \qquad (1.8)$$

where C_s = Swirl coefficient

τ = torque

m = mass flow rate of air

v_o = characteristic velocity derived from the pressure drop across the valve

B = bore diameter

[Heywood (1988)].

1.10.1.4 Effect of Swirl on Part Load Engine Performance

Tumble rapidly breaks down close to TDC and produces high levels of small-scale turbulence which decreases the ignition delay and main combustion period albeit by differing amounts. Detailed flow modelling and 2-dimensional calculations of a tumbling regime suggested that combustion of the first 10 % of the charge occurred at a faster rate than the main combustion period (burning of 10 %-90 % of the charge) (Boer *et al* (1990)). This was due to the fact that the highest turbulence intensities close to TDC occurred approximately in the centre of the chamber which, coupled with the rotation of the bulk flow, combined to increase the flame area and promote rapid inward burning of the flame during the early stages of combustion.

Prior to the initiation of combustion the turbulence intensities remained relatively constant until approximately 80° BTDC whereupon they increased, peaking around 40° BTDC (figure 1.18). Rapid decay of the turbulence intensity occurred after this, allowing the main part of combustion to take place at a slower rate than that induced in the early stages. The relationship between burn rate and tumble measured on a steady-flow rig is shown in figure 1.19, while the corresponding changes in UHC and bsfc are illustrated in figure 1.20.

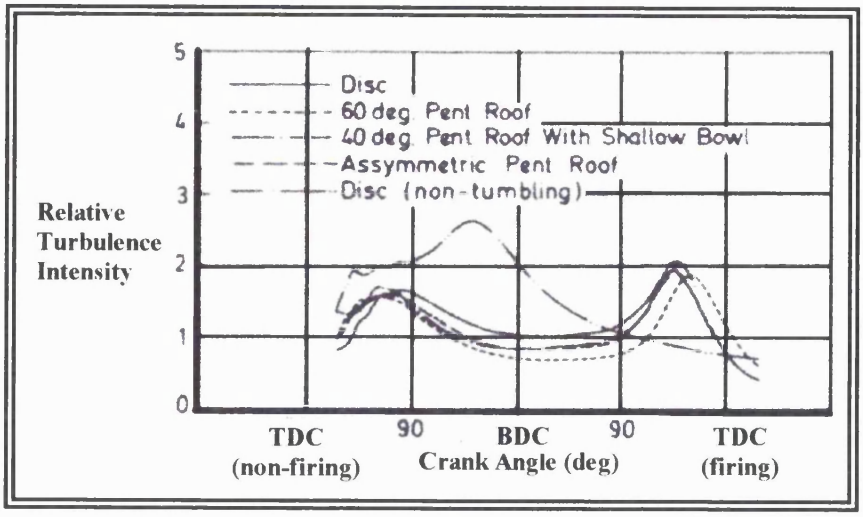

Figure 1.18: Variation of turbulence intensity with crank angle for different combustion chamber designs [Boer *et al* (1990)]

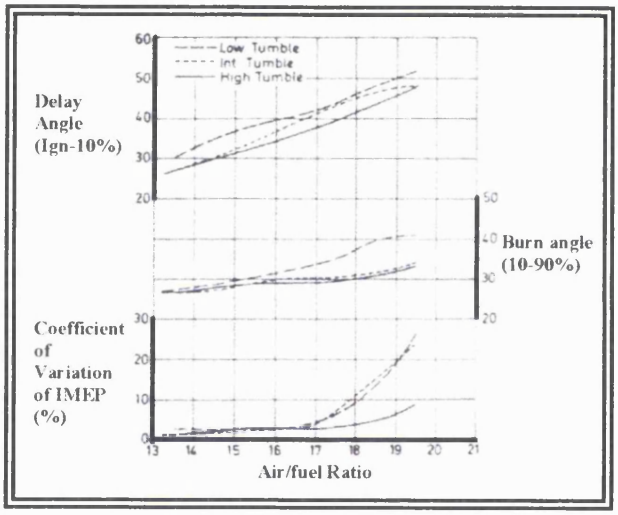

Figure 1.19: Effect of tumble on burning rates with crank angle for different combustion systems using a steady flow test rig [Boer *et al* (1990)]

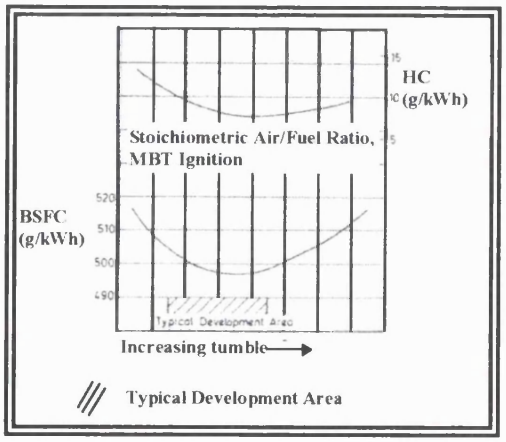

Figure 1.20: Effect of tumble at part load on bsfc and HC emissions [Boer *et al* (1990)]

Unfortunately tumble tends to increase NOx levels due to the increase in combustion temperature and pressure associated with rapid burning. At higher swirl ratios, UHC emissions also increase due mainly to the lower exhaust gas temperature caused by combustion occurring more quickly and thus leaving conditions less conducive to the oxidation of UHCs.

1.10.2 Exhaust Gas Recirculation (EGR)

Induced in-cylinder motion increases the tolerance of combustion systems to exhaust gas recirculation (EGR) which is beneficial in reducing emissions of NOx and part load fuel consumption (Stone (1993)). EGR may be internal or external with acceptable EGR levels being up to 30% depending on the engine configuration (Heywood (1988)). Internal EGR refers to that portion of burned gas which is not purged from the cylinder into the exhaust port, and also to the back flow of exhaust gases from the cylinder into the inlet port during valve overlap at low speed and load conditions. External EGR is additional EGR that may be added to the cylinder through a connection between the exhaust and inlet manifolds. In some cases it is preferable to limit internal EGR so that greater amounts of external EGR may be added over which there is better control but regardless of the means by which EGR is present in the cylinder, it acts as a heat sink, decreasing the combustion temperature and reducing NOx emissions.

The pumping work will also decrease with increasing EGR levels because EGR dilutes the charge. In order therefore to achieve the same power output, the throttle must be opened to restore the quantity of flammable mixture in the cylinder, thus increasing the manifold pressure during induction and reducing throttling losses. The presence of EGR results in more favourable values for the ratio of specific heats with a consequential increase in the Otto cycle efficiency (equation 1.2).

Unfortunately, the UHC emissions often tend to increase slightly with the addition of EGR because of the lower combustion temperature and hence lower rate of UHC oxidation in the exhaust. The effect can be counteracted to some extent if combustion

becomes significantly slower, thus restoring the temperature later in the expansion stroke, albeit with loss of efficiency.

The control of internal EGR at low speed and load conditions during the valve overlap period may be afforded by the use of port throttles situated in the inlet ports just upstream of the bifurcation on 4-valve engine designs (figure 1.21). (These port throttles can be used as well as, or instead of, a single throttle at the inlet to the manifold (Baker *et al* (1996)). The extra control of backflow allows the use of camshafts with a large valve overlap period, capable of giving high power output at high speeds. Without this additional restriction, excessive charge dilution would occur in the following cycle causing poor combustion and high exhaust emissions. The port throttles may take the form of butterfly valves (figure 1.22 a) or barrel throttles (figure 1.22 b).

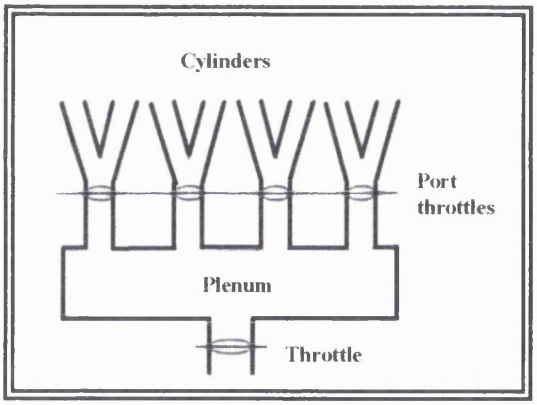

Figure 1.21 The position of port throttles [Baker *et al* (1996)]

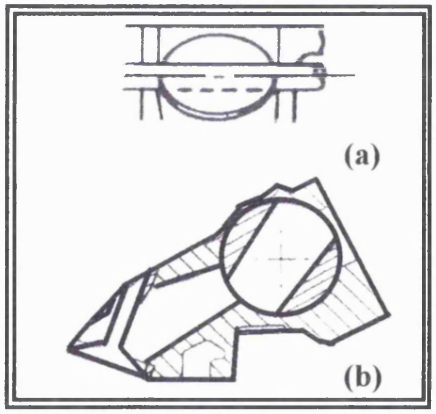

Figure 1.22 a: Butterfly valves [Baker *et al* (1995)], Figure 1.22 b: Barrel valves [Poole *et al* (1992)]

The use of port throttles affects a number of aspects of engine performance and these have been investigated by several researchers. Newman *et al* (1989) found experimentally that port throttling decreased the combustion burn rate as a direct consequence of reducing the backflow into the inlet port, and thus the mean forward velocity of the flow entering the cylinder was not so high leading to less in-cylinder motion. On the positive side, port throttling can lead to an overall reduction in the pumping work at idle and low loads (Newman *et al* (1989)). This is because the dominant effect on pumping work is the full or partial port pressure recovery in the intake port when the inlet valve is closed. (Complete port pressure recovery can only be

achieved at 800 rpm if the port volume is 22% or less than the swept volume (Newman *et al* 1989)). The cylinder pressure at the start of the intake stroke will be closer to the plenum manifold pressure before falling to its normal throttling pressure. On the pV diagram this manifests itself as a decrease in the pumping loop area, and hence a reduction in the pumping work.

1.10.3 Variable Valve Timing (VVT)

An alternative to port throttles for control of internal EGR is to apply variable valve timing (VVT). This more sophisticated method controls the phasing of either the intake, or exhaust camshafts, or both, thus allowing varying quantities of internal EGR to be induced into the cylinder at different speed and load conditions. Duckworth (1996) has made a comparison of the merits of VVT versus port throttling. Tests were carried out on a 2-litre, 16-valve, 4 cylinder engine, and the results showed that for optimisation of VVT, a camshaft swing from 86° to 128° ATDC was required. Significant improvement over a conventional engine design was achieved in terms of idle stability. which allowed the spark timing to be retarded with benefits in decreasing the catalyst light-off temperature. Other improvements resulting from VVT included a 4% reduction of fuel consumption at idle and 3% at part load conditions. Barrel throttles, however, showed no improvement in idle stability, but fuel consumption was improved by 4% at MBT and 8% at part load conditions.

Stein *et al* (1996) have made a thorough survey of the effects of different camshaft phasing strategies. They list 4 possible means of employing VVT through camshaft phase changes when twin overhead camshafts are used, and these are listed below. A summary of each method is also given together with a diagrammatic representation (figures 1.23 a-c).

1) Phasing only the intake camshaft (Intake Only)
2) Phasing only the exhaust camshaft (Exhaust Only).
3) Phasing both the intake and exhaust camshafts equally (Dual Equal).
4) Phasing both the intake and exhaust camshafts independently (Dual Independent).

1.10.3.1 Intake Only

At part load conditions, the camshaft is advanced so that the inlet valve opens earlier during the exhaust stroke and the valve overlap period is thus increased causing more of the burnt gases to flow into the inlet port to be recycled in the following cycle. The inlet valve also closes earlier in the compression stroke, thus decreasing the amount of fresh charge pushed into the inlet port by the upward movement of the piston.

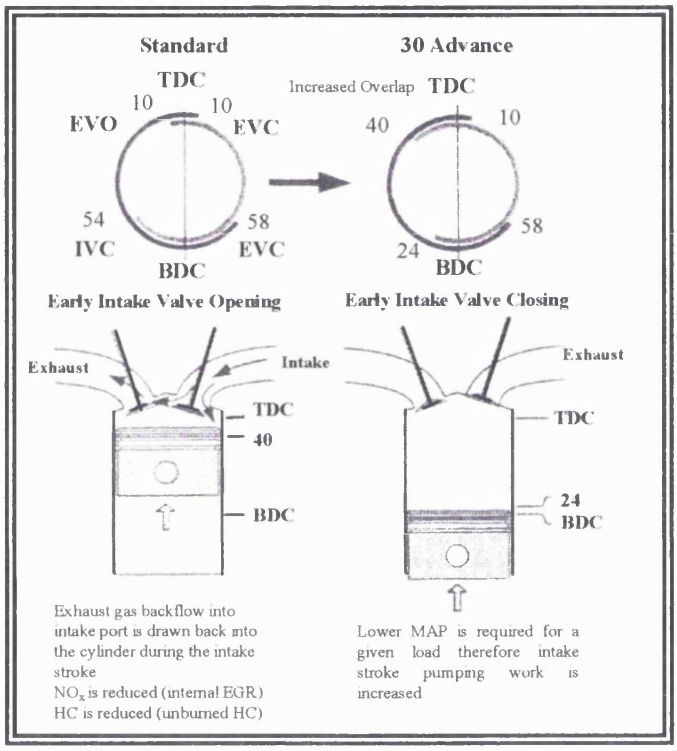

Figure 1.23 a: Inlet only camshaft phasing [Stein *et al* (1996)]

1.10.3.2 Exhaust Only

The exhaust camshaft is significantly retarded at part load conditions to increase the valve overlap and hence the amount of internal EGR. The late opening of the exhaust valve allows an increase in the expansion work (figure 1.23 b).

1.10.3.3 Dual Equal

The camshafts are significantly retarded at part load conditions. The objectives of this are: delayed valve overlap for increased residual dilution, late intake valve closing for pumping work reduction and late exhaust valve opening for increased expansion (Stein *et al* (1996)) (figure 1.23 c).

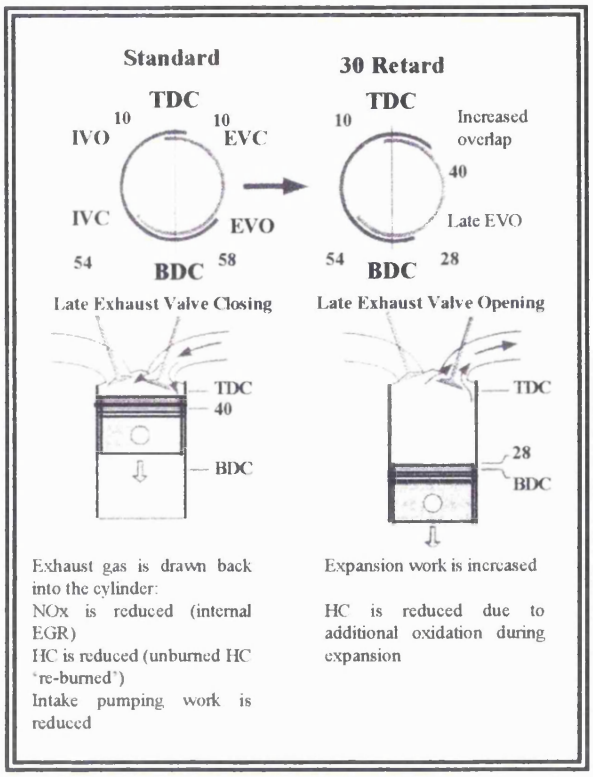

Figure 1.23 b: Exhaust only camshaft phasing [Stein *et al* (1996)]

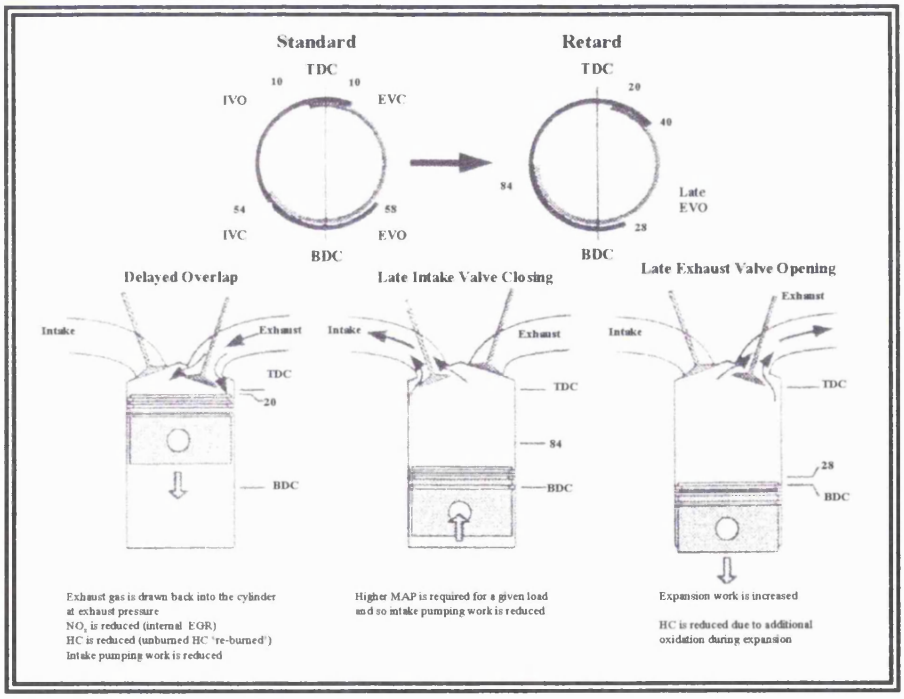

Figure 1.23 c: Dual inlet camshaft phasing [Stein *et al* (1996)]

1.10.3.4 Dual Independent

This method is essentially a refinement of dual equal retard. Both camshafts are significantly retarded but the overlap is variable rather than fixed.

The effects of valve timing on emissions and pumping work at low speed and low/part load are summarised in table 1.7.

Event	Effect	Explanation
Early EVO	Increased HC	Premature release of combustion products
	Increased NO_x	Higher peak cylinder temperature & pressure
	Increased fuel consumption	Wider throttle opening to maintain power
	CO unchanged	
Late EVO	Slight increase in NO_x No effect on HC and CO	
Early EVC	Decreased HC	Retention of HC-rich scroll-off gas
	Decreased NO_x	Increased residual gas fraction
	CO & fuel consumption unchanged	
Late EVC	Decreased HC	Re-introduction of HC-rich scroll-off gas
	Increased NO_x (for modest retard)	Lower residual gas fraction
	CO & fuel consumption unchanged	
Early IVO	Decreased HC	Retention of HC-rich scroll-off gas by re-introduction
	Decreased NO_x	Increased residual gas fraction
	CO & fuel consumption unchanged	
Late IVO	Increased NO_x	Lower residual gas fraction
	HC, CO & FC unchanged	
Early IVC[1]	HC, NO_x, CO & FC unchanged	
Late IVC[2]	HC, NO_x, CO & FC unchanged	

[1] Only small deviations from standard timings were investigated; NO_x might be expected to decrease slightly

[2] As 1; fuel consumption should also fall because of reduced pumping losses

Table 1.7: Effects of valve timing on emissions and pumping work at low speed and low/part load [Seabrook (1995)]

1.10.4 Lean Burn Engines

Lean burn engines normally use compact combustion chamber designs (figure 1.24) and require a sufficient amount of in-cylinder turbulence to allow the leaner mixtures to be burnt before combustion quality deteriorates to unacceptable levels and emission quantities increase. The compact combustion chamber design shortens the flame propagation distance and, coupled with high turbulence, the ignition delay and combustion duration are reduced.

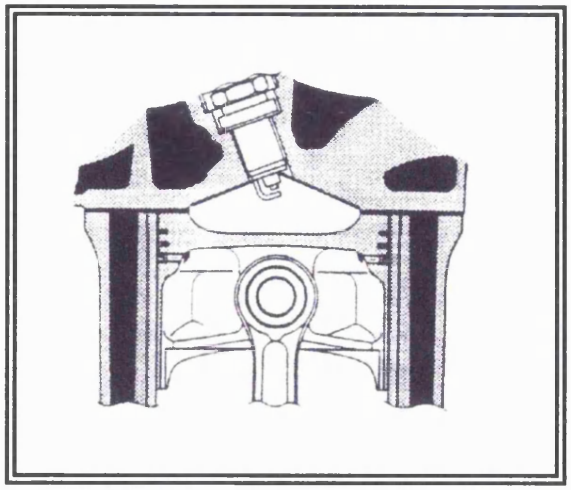

Figure 1.24: Compact combustion chamber design [Horie *et al* (1992)]

Lean burn engines have the capacity to decrease emission levels as well as being more efficient. This is partly because leaner mixtures require less throttling since the lean AFRs are realised not by reducing the amount of fuel, but rather by increasing the amount of air. The consequence is a reduction in pumping losses. In addition, more favourable values of γ (ratio of principal specific heats) are realised and, together with the higher compression ratios which may be utilised, lead to an increase in cycle efficiency as predicted by equation 1.2.

Lean burn engines require the charge to be as homogeneous as possible 'in order to gain the full benefit of lean combustion in terms of NOx reductions and good driveability' (Hardalupas *et al* (1995)). Unfortunately the widespread use of the lean burn engine has been inhibited due to difficulties in achieving legislative limits. The TWC cannot be used (section 1.9.3) and it is proving difficult to develop an alternative catalyst for operation with lean mixtures.

In the absence of a lean NOx catalyst, the obvious way of achieving NOx and fuel economy levels is to develop a combustion system with far greater EGR tolerance than at present, operating at stochiometric and hence allowing the use of a TWC to meet emission levels. One possible means is to stratify the EGR (Stokes *et al* (1994)). A general introduction to stratified charge engines is given before this is discussed.

1.10.5 Stratified Charge Engines

An alternative to the conventional spark ignition engine is the stratified charge (SC) engine. Here the fuel distribution within the cylinder is non-uniform, with a rich but ignitable mixture in the vicinity of the spark plug and a leaner non-ignitable mixture of air or exhaust gas in the remainder of the combustion chamber. Stone (1994) lists the following advantages of a stratified charge engine:

1) Lower exhaust emissions than conventional SI engines due to low NOx levels at lean mixtures (figure 1.7).
2) Improved efficiency since throttling losses are reduced.
3) Greater fuel tolerance.

SC engines have 2 basic configurations, divided chamber and open chamber (Ferguson (1986)). Several different designs of both exist. The jet/torch ignition SC engine is an example of the former configuration. This design uses a prechamber (hence the term divided chamber) which requires separate fuel and air intake systems. During the intake stroke the first fuel system provides the prechamber with a non-ignitable rich mixture, whilst the second fuel system provides the combustion chamber with a non-ignitable lean mixture. A portion of the lean mixture is then forced into the prechamber during the compression stroke, bringing the charge in the prechamber to one which is ignitable, albeit slightly rich. Combustion is initiated by a spark, and the rich burning mixture in the prechamber issues as a jet through the orifice into the main chamber igniting the leaner mixture (figure 1.25).

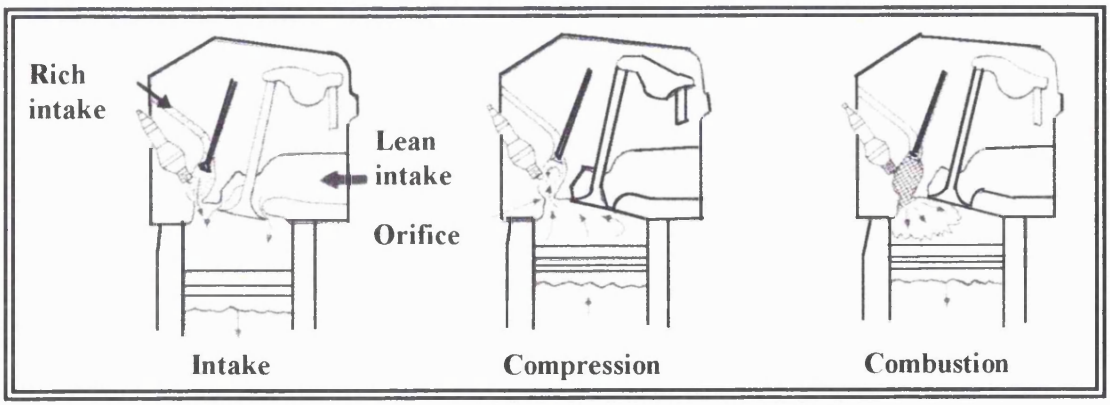

Figure 1.25: Three-valve torch-ignition SC SI engine [Heywood (1988)]

The use of a prechamber not only increases the complexity of the design, but the pumping losses are also higher as a consequence of the pressure drop between the two chambers during induction and expansion (Fry (1992)) and the transfer of charge into and out of the prechamber. The prechamber is also an additional source of heat loss and may act in a similar manner to crevices, trapping UHCs.

The Honda CVCC engine has a divided chamber configuration and was the first SC engine in regular production (Stone (1994)). Its prechamber volume was 5% of its clearance volume and it used a single 'large' nozzle (ratio of nozzle area to prechamber volume 0.04 cm^{-1}) rather than several smaller nozzles to connect the prechamber to the main combustion chamber (Heywood (1988)). The larger nozzle directs the burning prechamber mixture more slowly into the combustion chamber resulting in the lean mixture burning more slowly.

Open chamber SC configurations are more commonly used today. SC may be achieved through either direct injection (DI) or through port injection (PI). Both of these methods may employ either tumble, thus promoting barrel stratification, or swirl, thus promoting axial stratification. Both axial and barrel stratification are discussed below with reference to DI and PI SC engines.

1.10.5.1 Open Chamber SC Engines

1.10.5.1.1 Direct Injection Stratified Charge (DI SC)

Axial Stratification

Misumi *et al* (1990) investigated the potential of axial stratification by direct injection using a low pressure wide-angle fuel injector. To promote axial swirl the intake system comprised of a main port housing, a butterfly valve, and an auxiliary port situated tangentially to the cylinder bore. The butterfly valve was closed at part load conditions so that a vigorous axial swirl was induced in the cylinder. The use of a low pressure fuel injector, and the objective of achieving axial stratification, required the fuel to be injected around BDC of the intake stroke. A rich layer of fuel remained at the top of the cylinder and a leaner mixture beneath, adjacent to the piston.

Stable combustion was realised at AFRs as lean as 40:1. However, because of the design of the air blast fuel injector, it was necessary to limit the cylinder head water temperature to below 40°C to achieve these lean AFRs. These limitations prevented vaporisation and hence 'bubbling' of the fuel within the injector which impeded the flow of air conducive to producing a fine spray and good combustion quality. Even at these lean AFRs, the emission levels were not low enough to satisfy legislative requirements. The UHC levels were particularly high in comparison to port injection axial stratification (figure 1.26) as a direct result of excessive fuel impingement on the cylinder walls and the low cylinder head temperature (Misumi *et al* (1990)). There has been no further published work showing that low UHCs are possible with this concept.

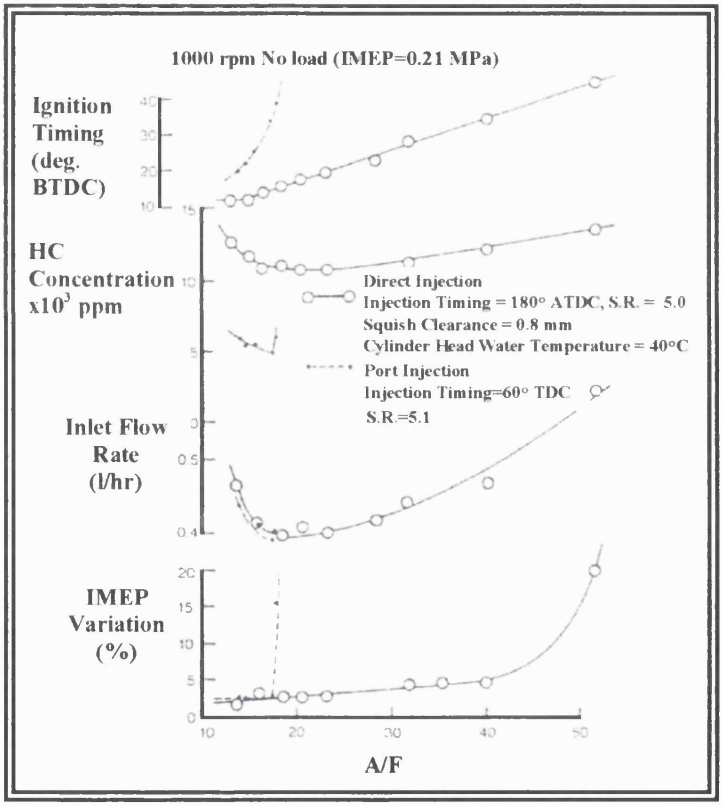

Figure 1.26: Comparison of PI and DI axial stratification [Misumi *et al* (1990)]

Barrel Stratification

Mitsubishi have developed a novel barrel stratification engine that was introduced into the Japanese market in 1996. The engine uses the following technologies (Kume *et al* (1996)):

1) Upright straight inlet ports to generate a tumbling motion that is in the opposite direction to conventional tumble.
2) A spherical compact piston cavity controlling the behaviour of the fuel spray and vaporised gaseous mixture.
3) A high pressure fuel feed pump with low driving loss.
4) An electromagnetic swirl injector to realise optimised spray dispersion and atomisation

Early injection produces a homogenous mixture which is required for high load conditions while late injection timing leads to a stratified charge mixture (figure 1.27). AFRs as lean as 100:1 can be achieved although in practice the engine is not operated with an AFR in excess of 40:1. A summary of the concepts and their objectives is given in table 1.8

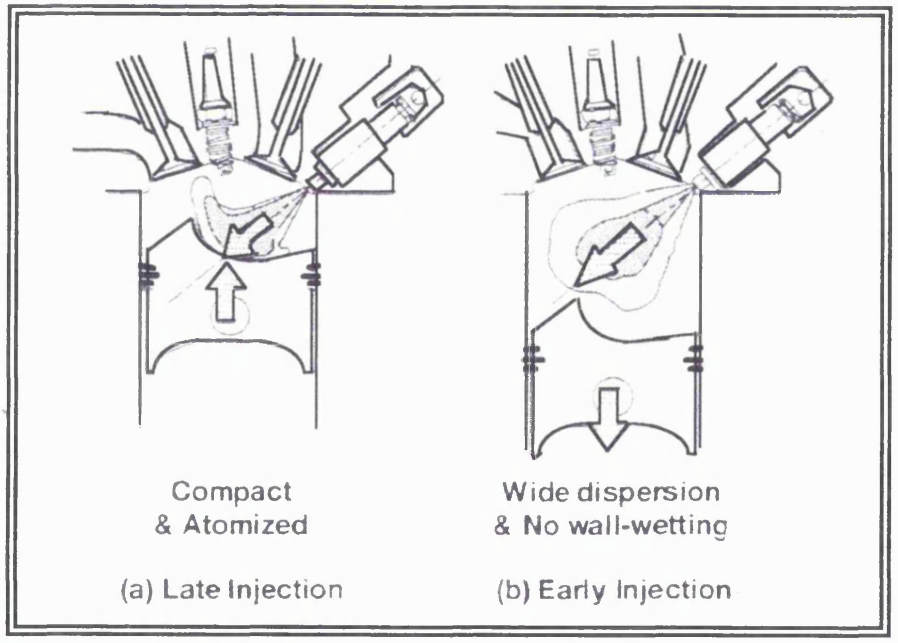

Figure 1.27: Early and late injection timings [Kume *et al* (1996)]

Condition	Injection Timing	Mixing	A/F Ratio
Partial Load	Later Stage of Compression Stroke	Stratified	25 - 40
Higher Load	Early Stage of Intake Stroke	Homo-geneous	Stoich./Rich or 20-25

Table 1.8a: The conditions of the Mitsubishi engine [Kume *et al* (1996)]

Concept			Goal	Measures
Flow		❑ Reverse tumble	❑ Fuel vapor transport to plug ❑ Higher port flow rate	❑ Vertical intake port ❑ Enhanced gas-dynamics effect by straight port
Injection		❑ Lower inj. pressure	❑ Lower fuel compres. loss	❑ Swirl injector
		❑ Engine-driven pump	❑ Lower driving loss	❑ Start by feed pump
Mixing	Higher Load	❑ Homogeneous (early injection) ❑ No wall-wetting ❑ Charge-air cooling	❑ Soot reduction in stoich. & rich conditions ❑ Knocking suppression ❑ Higher volumetric efficiency	❑ Suppressed spray tip penetration ❑ Widely dispersed fuel spray ❑ Enhanced reverse tumble
	Partial Load	❑ Stratified (late injection) ❑ Enhanced evaporation	❑ Stable leanburn ❑ Lower-soot-emission at high load	❑ Compact chamber ❑ Spray motion by reverse tumble ❑ Injection timing control
Ignition		❑ Conventional ignition system with confirmed reliability		
Emission		❑ High EGR	❑ NOx reduction in stratified charge	❑ Electronically actuated EGR valve
Intake		❑ High-speed & accurate air control	❑ Smooth operation ❑ Wider EGR zone	❑ Electronically actuated air control valve

Table 1.8b: Concepts and objectives of Mitsubishi engine [Kume *et al* (1996)]

Although DI SC engines offer great potential, by their very nature, the fuel injection system is likely to be very expensive due to the high injection pressures involved. Also more research is required into the durability of such systems as there is a tendency for fuel to carbonise in and on the injectors. A further concern is that the low-emission performance of these engines is very sensitive to ignition timing, and small changes in service could bring about a large increase in engine-out emissions.

1.10.5.1.2 Port Injection Stratified Charge (PI SC)

Axial Stratification

Axial stratification employs swirl as the mechanism for the enhancement of combustion. The fuel is introduced in the latter half of the intake stroke as the piston approaches BDC (Kiyota *et al* (1992)) in order that it moves with the swirling motion and minimal mixing occurs between the air in front of and behind the fuel band (Ohm *et al* (1993)). The combination of swirling motion and late injection allows a rich mixture of air at the top of the cylinder and a leaner mixture beneath to remain until the end of compression. The use of air, as opposed to EGR or a combination of EGR and air results in an overall lean mixture but one in which the fuel distribution is not homogeneous.

An example of a lean-burn axially SC engine that has achieved US legislative limits is the Honda VTEC-E engine (Horie *et al* (1992)). The VTEC-E engine uses a variable swirl

mechanism (figure 1.28) such that at low speed and load conditions the valve lift of one of the inlet valves is reduced to 0.67 mm and axial swirl is established in the cylinder. Both valves are fully activated at high speed and load conditions, thus preventing a decrease in volumetric efficiency. Straight ports with triangular cross sections achieve sufficient turbulence at low speed and load conditions without significantly compromising high speed and load running (Horie *et al* (1992)). In the Federal Test Procedure, an improvement in fuel economy of 8% was achieved at the low speed and load conditions and 12% in the highway mode. The US legislation limit on NOx was met.

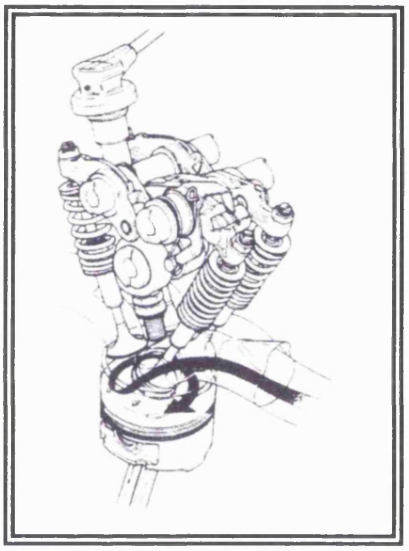

Figure 1.28: Honda VTEC-E mechanism [Horie *et al* (1992)]

There are three dominant factors to take account of when attempting to realise the full potential of axial stratification: swirl ratio injection timing and injector flow rate (Ohm *et al* (1993)). The swirl ratio is responsible for maintaining the rich mixture band up until the point of combustion, whilst the injection timing determines the position of the band. Bad injection timing will result in unfavourable stratification with the rich mixture band situated away from the spark-plug at the time of ignition.

With a swirl ratio greater than 3.7, Ohm *et al* (1993) found that there existed a single optimum injection timing (110°-130° CA ATDC depending upon the test condition and the exact swirl ratio) in which the lean misfire limit (LML) was a maximum. The LML taken here as being determined when the misfire frequency is greater than 1%. The

higher the LML, the greater the degree of fuel enrichment around the spark-plug. It was clear that true axial stratification was present with this arrangement. Systems that had a swirl ratio less than 3.7, exhibited different variations of LML with injection timing (figure 1.29).

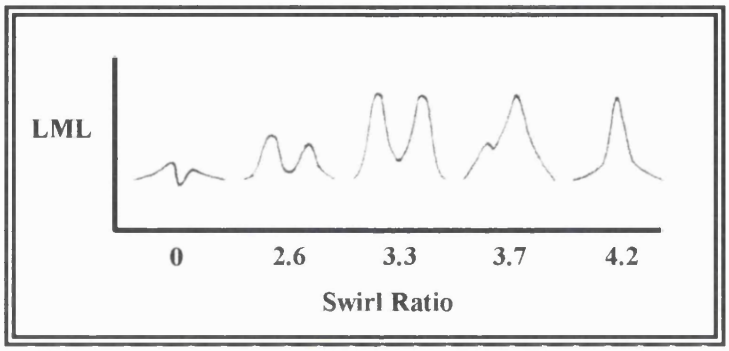

Figure 1.29: Variation of LML with injection timing and swirl ratio [Ohm *et al* (1993)]

In order to explain this, it was postulated that at the lower swirl ratio, there existed a small tumbling motion beneath the inlet valve during the early part of the intake stroke, and this motion is supported by the main swirling motion. The tumbling motion is not as intense as the swirling motion and tends to be destroyed relatively early (figure 1.30). The greater the swirl ratio, the lower the tendency for this tumble motion to be created.

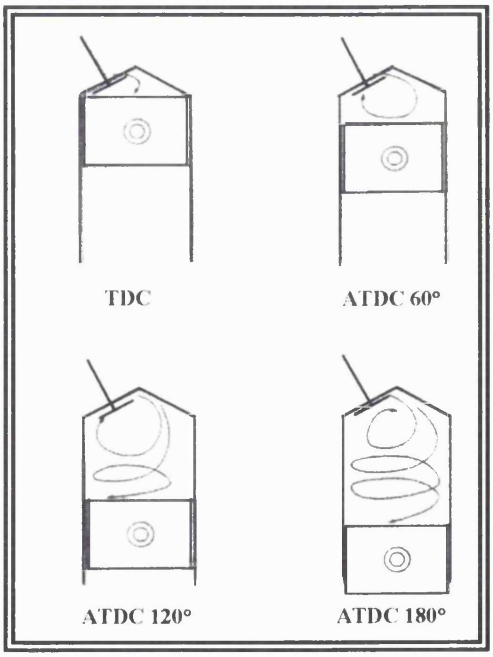

Figure 1.30: Schematic of air flow mechanisms with axial stratification and swirl ratios less than 3.7 [Ohm *et al* (1993)]

The degree of stratification for a given swirl ratio and injection timing will increase with fuel flow rate. However, an optimum flow rate exists beyond which although stratification may increase, combustion stability decreases. Ohm *et al* (1993) found this rate to be 200 cc/min, and they postulated that although stratification is increased with higher rates, bad atomisation becomes the dominant factor with a resulting decrease in LML.

Under the Federal Test Procedure, the improvement in fuel economy using axial stratification is approximately 10%. Engine-out NOx emissions is reduced by 80% with 5% EGR. Unfortunately engine-out UHC emissions are higher but after treatment with a catalyst, the UHC levels are lower than a conventional SI engine.

Barrel Stratification

A fuel/air mixture is injected down the primary inlet port, with only air (or EGR) passing down the secondary port. A single exhaust valve is used in some designs with the spark plug usually across from the port housing the fuel injector in the position of what would have been the second exhaust valve (figure 1.31).

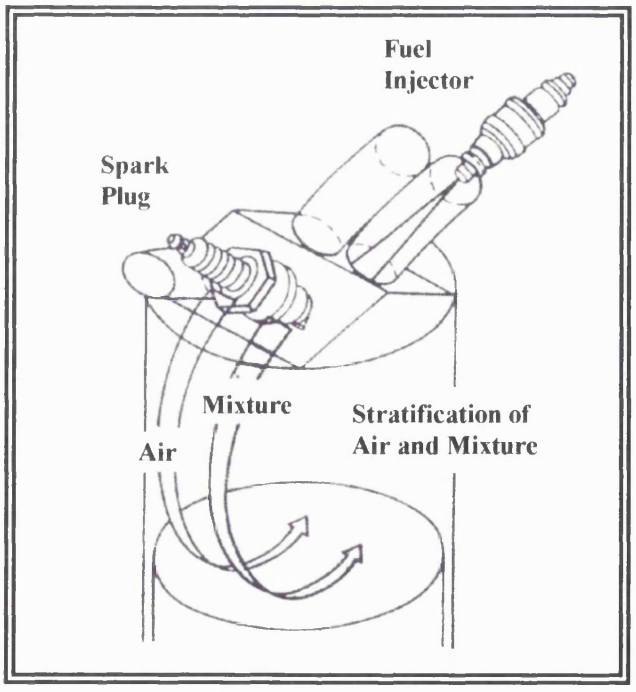

Figure 1.31: Barrel stratification [Stokes *et al* (1994)]

The Mitsubishi Vertical Vortex (MVV) engine employing barrel stratification enabled stable combustion to occur at air fuel ratios of 30:1 (Kiyota *et al* (1992)). Although no actual emission figures have been given (based on a test cycle), a comparison was made between a 4-valve uniform mixing with and without the tumble regime and a 3-valve barrel SC engine which employed triangular inlet ports. The favourable results are given in the figure 1.32.

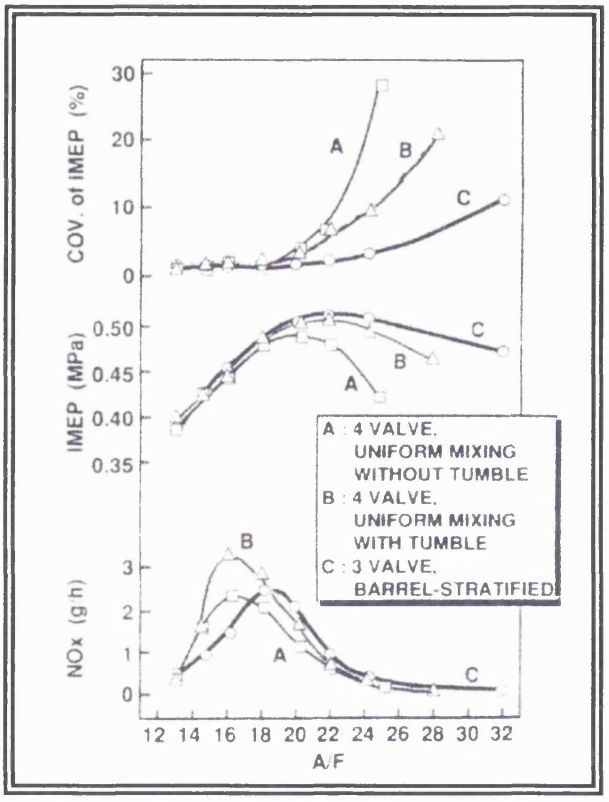

Figure 1.32: Effects of barrel stratification [Kiyota *et al* (1992)]

The use of 3-valve engines (as opposed to 4-valve engines) results in a loss of performance. Mitsubishi realising this, have developed a 4-valve SC engine, again employing tumble as the air motion (figures 1.33).

The Mitsubishi 4-valve SC engine achieves stratification with a central spark plug by having a sandwich of rich mixture. That is the rich mixture circulates in the centre of the barrel swirl with leaner mixture circulating on each side. Key features in achieving this are a discussion in each of the inlet ports to keep the rich mixture in its central position and a profiled piston to promote the tumbling air motion within the cylinder.

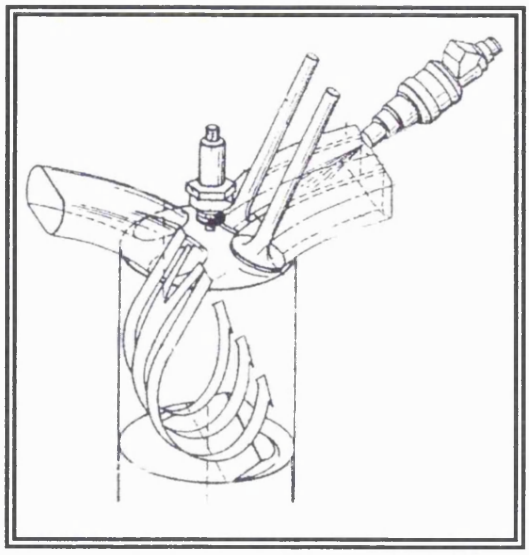

Figure 1.33: The Mitsubishi 4-valve SC engine employing tumble as the air motion [European Patent Publication Number 0 558 081 A]

1.10.5.2 Stratification With EGR

Stratification using EGR rather than air as the second gas has been investigated by several researchers (Endres *et al* (1990), Jackson (1996)). The advantage of using EGR rather than air is that the overall AFR is stoichiometric rather than lean, and hence a TWC may be used. Endres *et al* (1990) looked at axial stratification by introducing the EGR either into the manifold or into the second inlet port (fuel injected into the primary inlet port), downstream of a throttle disc of a 3-valve engine (figure 1.34). The results of the investigation are shown in figure 1.35.

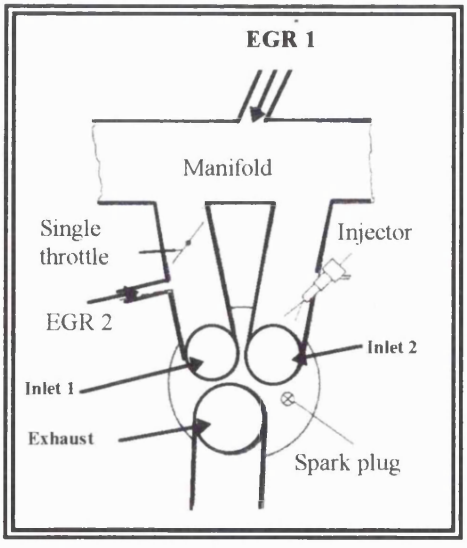

Figure 1.34: Axial stratification with different EGR concepts [Endres *et al* (1990)]

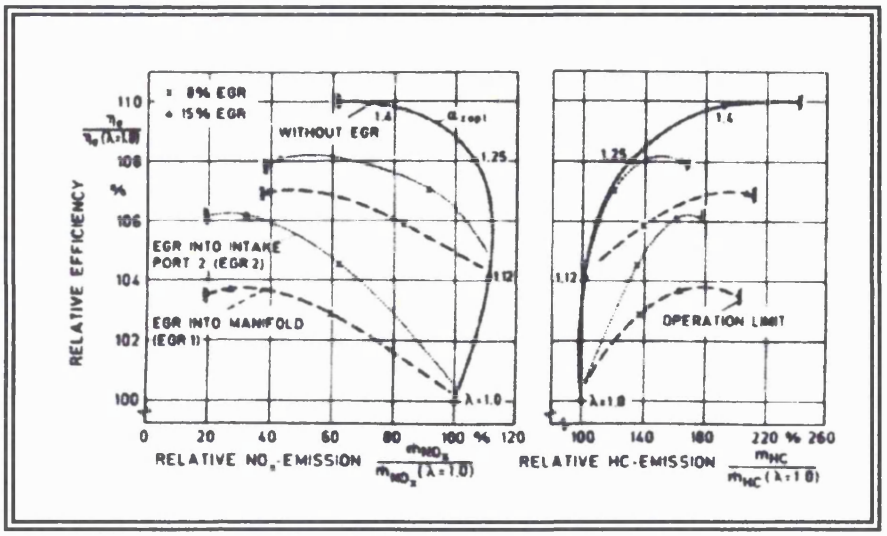

Figure 1.35: Comparison of lean burn operation and different EGR concepts (2000 rpm, 2 bar bmep) [Endres *et al* (1990)]

In addition to running at an overall AFR of 14.7:1, stratified EGR has a positive effect on the UHC emissions and also produces low NOx and good efficiency. There is a 6% decrease in bsfc and raw NOx emissions are reduced by 70% when measured over the Federal test cycle.

Ricardo with their barrel swirl SC engine have employed EGR rather than air (Stokes *et al* (1994)). They refer to this as the CCVS system (combustion control by vortex stratification). The ports are designed to establish tumbling motion. A summary of the operational modes is given in figure 1.36 a-e (Jackson *et al* (1996)). At the boundaries of the two flows, there is a certain amount of mixing due to the presence of turbulent eddies between the inlet valves, although the bulk of the charge remains stratified.

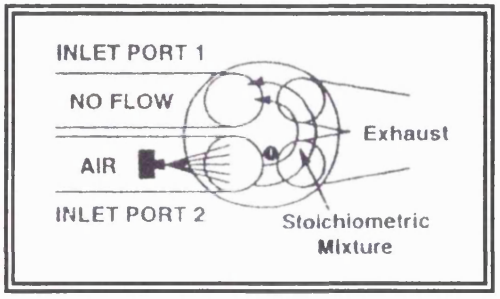

Figure 1.36 a: CCVS system, idle condition [Jackson *et al* (1996)]

Port 1 is deactivated setting up a high degree of axial swirl. No EGR is introduced at this condition.

Operates at a stochiometric AFR in the cylinder.

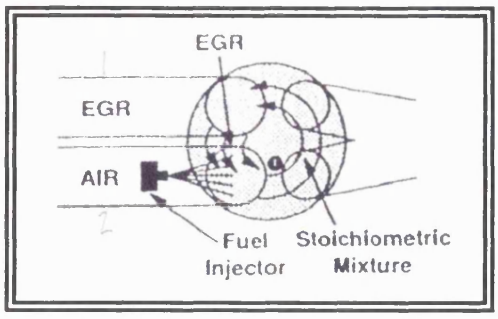

Figure 1.36 b: CCVS system, low load, low EGR rate [Jackson *et al* (1996)]

100% EGR is introduced down port 1. The low EGR rate down port 1 results in a mixture of tumble and swirl.

Operates at a stochiometric AFR in the cylinder with a homogeneous charge distribution.

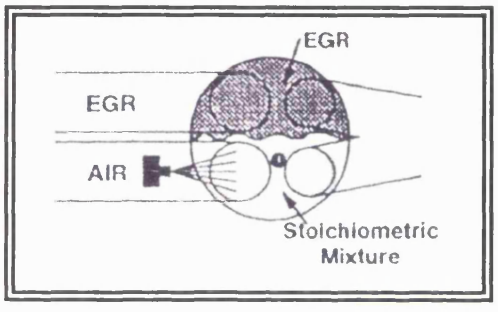

Figure 1.36 c: CCVS system, low load, high EGR rate [Jackson *et al* (1996)]

100% EGR is introduced down port 1. High EGR rate, thus charge stratifies into an EGR region and an air and fuel region.

The overall mixture is stoichiometric.

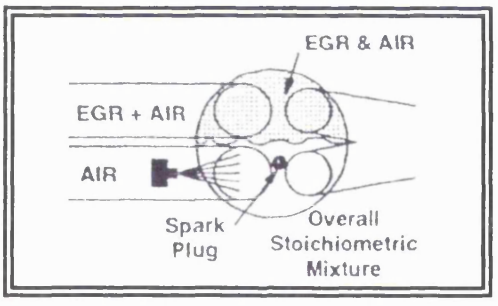

Figure 1.36 d: CCVS system, high load [Jackson *et al* (1996)]

At medium and high loads, a mixture of EGR and air go down port 1 and air and fuel down port 2.

In both cases the overall mixture is stoichiometric in the cylinder.

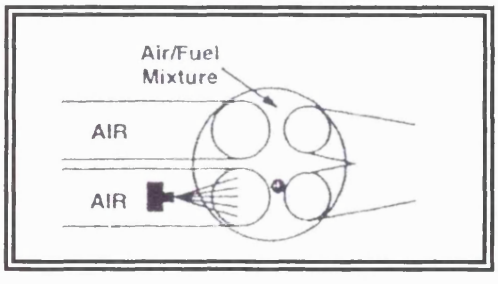

Figure 1.36 e: CCVS system, full load [Jackson *et al* (1996)]

At full load, no EGR is introduced.

The CCVS system reduced fuel consumption by 6.3% and NOx by 90% (when used with a TWC) at part load conditions as compared with a central plug homogeneous charge engine, but UHC emissions increased by 20%. This is lower than with stratification using air as the second gas. They postulated a theory which was validated in some later work (Jackson *et al* (1996)) based on FFID exhaust traces. FFID probes was situated in the exhaust and inlet ports (figure 1.37).

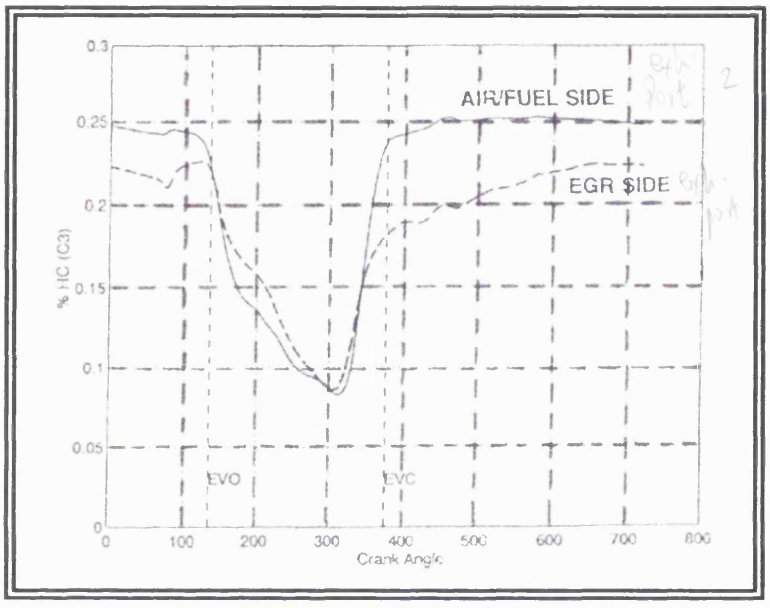

Figure 1.37: Barrel stratification with EGR FFID exhaust traces [Jackson *et al* (1996)]

Jackson *et al* (1996) postulated that the lower UHC emissions were due to the oil film on the EGR side not desorbing fuel due to the presence of a protecting layer of EGR. Also less UHC would get trapped in the top land region as indicated by the lower release of UHCs from the crevice regions. Min *et al* (1994) found that when the gasket crevice was on the exhaust side, the exhaust UHCs were greater than if it were on the inlet side. The addition of EGR has a similar effect to decreasing the crevice regions. The proportion of EGR with which the engine would run in a stable manner was calculated to be as high as 40%, although no direct measurements were made. This compares with an EGR tolerance of between 10-20% on conventional engines.

1.11 Summary of PI SC Engines

This approach offers considerable promise for several reasons:

1) The pumping work is reduced due to its ability to run with considerable charge dilution (either utilising air or exhaust gas).

2) The potential of lower exhaust emissions through its ability to run with considerable charge dilution (again with either air or exhaust gas), hence low NOx levels. However there is the challenge of keeping the UHCs low, but results have shown this to be more promising with PI than with DI.

3) The fuel system requirements are considerably less demanding than for DI, and the durability of PI systems is proven.

4) There is less likely to be degradation of performance in service with PI than with DI systems.

1.12 A Way Forward

From this literature survey, it has been shown that work is proceeding on two approaches by which exhaust pollutant levels may be reduced to meet emission legislation requirements. The first area of work makes use of a post-treatment device (catalyst) in which the pollutants are made to undergo a series of reactions. This has proved to be a very effective method but one major problem is the high level of emissions released into the atmosphere during the warm-up period whilst the catalyst is below its operating temperature.

The second approach is to improve the basic combustion process so that the levels of pollutants leaving the cylinder are considerably reduced. This can be a particularly attractive approach as improvements are possible in cycle efficiency as well as cleanliness of exhaust gas. Possible methods range from improving the mixture preparation through the use of, for instance, air-assisted injectors, to more fundamental approaches such as the development of stratified charge combustion. Although it is unlikely that any of these methods will reduce emission levels such that after treatment devices are no longer required, the situation may be significantly improved. An engine running at stoichiometric would require a TWC, whilst lean burn engines require a lean NO_x catalyst to reduce the NO_x emissions to acceptable levels.

The industrial sponsors of the project, the Ford Motor Company, specified that the initial aim of the project should be to concentrate on the second approach by determining whether improvements in the combustion process, and hence lower emission levels, would follow from making improvements to the mixture preparation on their standard medium-capacity engine, the 4-cyclinder, 4-valve, Ford Zetec engine. The investigation would be more fundamental than simply comparing emission results from different fuel preparation systems, it would employ high-speed cine photography to study the motion of liquid fuel within the cylinder. It was intended that this study would indicate which fuel system would give the best test results (to be confirmed elsewhere by engine emissions testing), and possibly would also allow deductions to be drawn as to how further improvements could be made. It follows that an optically-accessed engine would be required for this study and such an engine is described in the following chapter.

Chapter 2

Optically-Accessed Single-Cylinder SI Research Engine

Engines are currently evolving expeditiously because of the greater demands being placed on fuel efficiency, low emission levels and possible future changes in their fuels. They therefore now require a much better understanding of the fundamental sciences on which their design and development is based so that further progression may be made without compromising engine performance and driveability (Milton (1995)). This understanding may be obtained through the development of scientific techniques that investigate the processes occurring over one or many engine cycles. The optical approach is one such set of techniques and includes the use of high speed film, high resolution photography, laser absorption or flame pyrometry, to observe the behaviour of liquid fuel in the inlet port or combustion chamber (Plimon *et al* (1987)). The optical approach requires optical access to the engine to illuminate the area of interest, and to record the events. However, it is important that the modifications made to provide the optical access, (or to provide access for another technique), does not alter the engine design significantly, or seriously disrupt the processes occurring.

This chapter describes an optically accessed single-cylinder spark-ignition research engine, used initially to conduct an investigation into the behaviour of liquid fuel in the combustion chamber for a standard design of cylinder head and inlet port arrangement. The means of recording the fuel events and the method of illumination are also described and the results of the investigation are presented and discussed in chapter 3.

2.1 Description of the Engine

The optically-accessed, single-cylinder, SI research engine used for the experimental investigations was designed and manufactured at UCL. The research engine comprised of a 4-cylinder, 1.8-litre, Ford Zetec cylinder head, which utilised standard camshafts to actuate the inlet and exhaust valves at their normal timings. Only one cylinder was used for testing purposes. The cylinder head was mounted onto a specially-designed, single-cylinder block, which in turn was mounted onto the crankcase of a Lister TS1, single-

cylinder, diesel engine (Plate 1). The research engine was installed on a test bed and attached to an ac dynamometer unit (manufacturers Laurence Scott and Electromotors Ltd, model NS 1962, serial # 261601) which allowed the engine speed to be varied up to a maximum speed of 3000 rpm. Standard grade pump gasoline was supplied to the fuel injector from a sealed vessel to which regulated mains air pressure was applied.

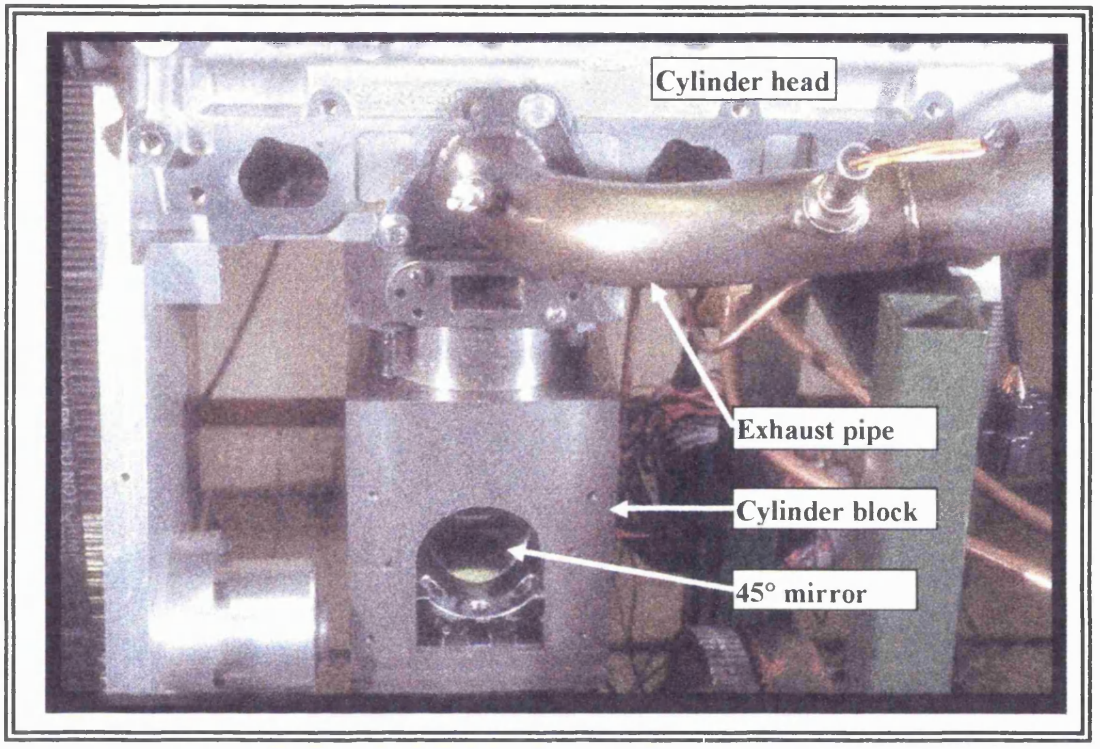

Plate 2.1: Optically-accessed, single-cylinder, SI research engine

The Lister crankcase was employed rather than the Zetec crankcase primarily because of time constraints. A coupling to the dynamometer unit already existed for the Lister crankcase, in addition to attachments for the cylinder block and head, thus only relatively minor modifications needed to be carried out. These modifications included regrinding the Lister crankshaft eccentrically to achieve the Zetec stroke of 88.0 mm, and reducing the Lister connecting rod length. The connecting rod length was reduced by 5 mm to a length of 160 mm, by inserting an eccentric bush into the little end. Compared with the Zetec length of 136 mm, the modified connecting rod length was still some 24 mm longer than desired but for the current application the difference in lengths was deemed to be acceptable. The specifications of the engine are given in table 2.1 on the following page.

Bore			80.6 mm
Stroke			88.0 mm
Number of valves per cylinder			4
Capacity per cylinder			450 cc
Compression ratio			9.1:1
Location of spark plug			Central
Injection system			Port
Timing			
Inlet valves open	**Inlet valves close**	**Exhaust valves open**	**Exhaust valves close**
10° BTDC	222° ATDC	44° BBDC	8° ATDC
Peak Lift			8.1 mm
Timing of peak lift: inlet stroke			108° ATDC
Timing of peak lift: exhaust stroke			108° BTDC
Period			232°

Table 2.1: Specifications of the Zetec engine

2.1.1 Intake System

The intake system is shown in figure 2.1. It comprised a throttle body connected to a plenum, (which allowed the manifold depression and air flow through the system to be altered), which in turn was attached to a standard Zetec manifold. The whole assembly was mounted onto the cylinder head.

The air flow into the engine was measured with a Zetec hot-wire air flow meter situated downstream of the throttle body. This air flow meter is normally used to measure the flow rate of air into four cylinders. Consequently in order to measure the lower flow rates associated with the single-cylinder engine more accurately, the main passage way through the air flow meter was partially blocked, thus forcing a greater proportion of the air to flow through the smaller parallel flow path that contained the hot wire (figure 2.2). The modified unit was calibrated against a Fischer and Porter rotameter and a calibration curve of flow rate (g/s) against meter output (Volts) was plotted (appendix A, figure A1).

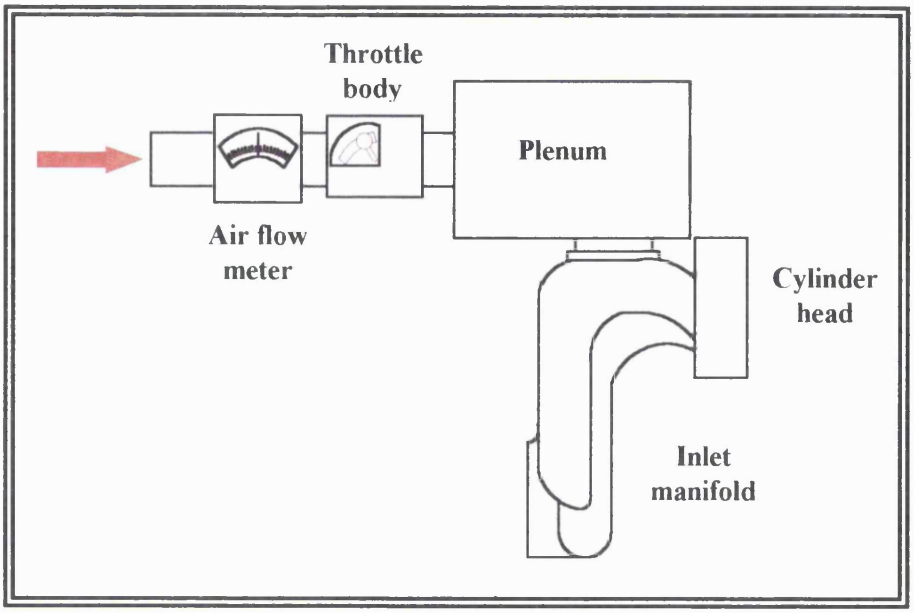

Figure 2.1: Air intake system

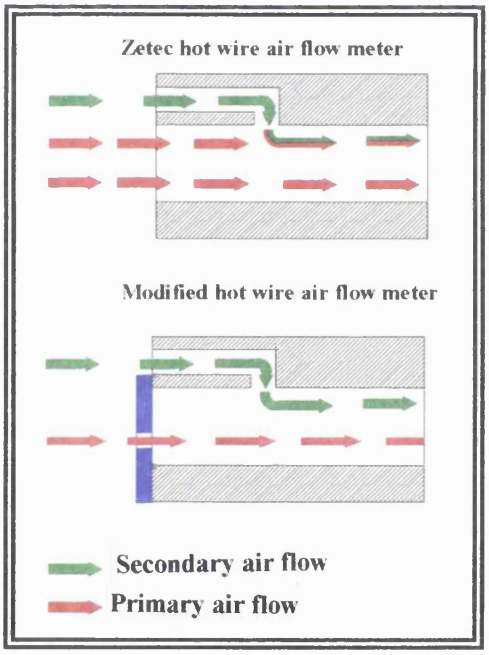

Figure 2.2: Modified air flow meter

2.1.2 Optical Access

2.1.2.1 The Optical Piston

An optical path was provided into the combustion chamber via a specially designed piston and cylinder block arrangement. The optical piston was manufactured in two parts that screwed together. The top section (here-on-in referred to as the 'piston cap') was a

housing to keep in place a quartz cylinder block which formed the piston crown, and the bottom section which was partially hollowed out and had a front section removed, formed the main part of the piston body (plate 2.2). The quartz section gave a viewing area of 85 % of the combustion chamber. The piston cap was manufactured from a high carbon steel and the main piston body from an aluminium alloy (L168) with an ultimate tensile strength (UTS) of 531 MPa (Fry (1994)).

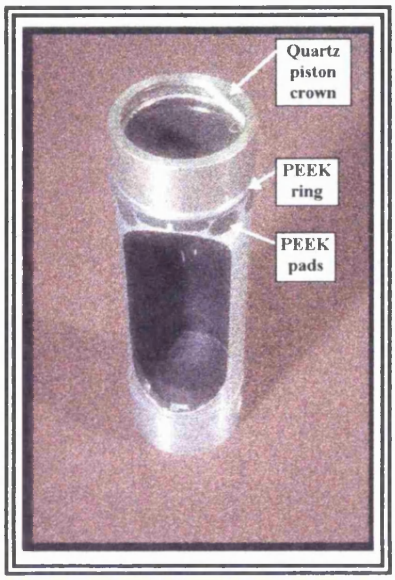

Plate 2.2: Optical piston

Two rings were fitted to the lower end of the piston for the purpose of oil control. The top ring was a standard Zetec second compression ring and the bottom ring was a standard Zetec three-piece scraper ring. Both of these rings, combined with good oil drainage facilities, minimised the amount of oil that passed up the cylinder bore and contaminated the quartz piston crown. A compression ring and dry sliding bearings were fitted just beneath the piston cap, some 36 mm and 46 mm to their respective mid points beneath the piston crown. These distances were the minimum that they could be fitted beneath the piston crown without the top ring traversing the joint made by the access port plugs machined in the top of the cylinder block (section 2.1.3). This meant that the top land crevice was abnormally large, with a volume of 1.74×10^{-6} m^3, but since comparative tests were to be carried out which did not include engine-out emission tests, the large top land crevice did not compromise the results. The compression ring and dry sliding bearings were manufactured from ICI Victrex PEEK (polyetheretherketone),

grade 450FC30, which was filled with carbon fibre, graphite and ptfe to enhance the mechanical and tribological properties of the polymer. The engine was run without any lubrication of the compression ring.

2.1.3 Cylinder Block

The front portion of the cylinder block was removed and a mirror mounted inside (and hence inside the piston) at 45° (figure 2.3). Whilst the piston moved up and down through its stroke, the mirror remained stationary, thus providing a view through the quartz piston crown of the combustion chamber over the entire engine cycle.

In addition, the cylinder block incorporated two access ports, one on the inlet side, and the other on the exhaust side in order to provide access to the quartz piston crown to allow it to be cleaned in between tests. Initially they were fitted with solid removable plugs that had inside faces that were flush with the cylinder bore but some limited testing was performed with the solid plugs replaced by plugs containing small quartz windows (chapter 4).

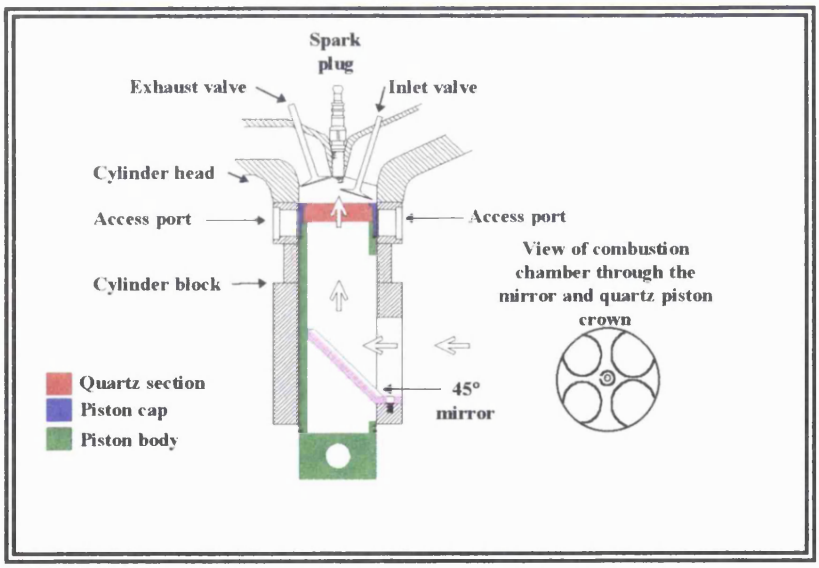

Figure 2.3: Optical path into the combustion chamber and the optical view of the combustion chamber

2.2 Engine Control System

The initiation of fuel injection, the injection timing, pulsewidth and the number of injector

pulses, were all controlled by a program written by the author that used the graphical software package LabVIEW (Laboratory Virtual Instrument Engineering Workbench). LabVIEW was installed on a Macintosh II computer, and employed the National Instruments board NB-MIO-16 to interface between the computer and external physical devices. The virtual control panel created by the software allowed the user to alter the fuel injection parameters listed above and is shown in figure 2.4.

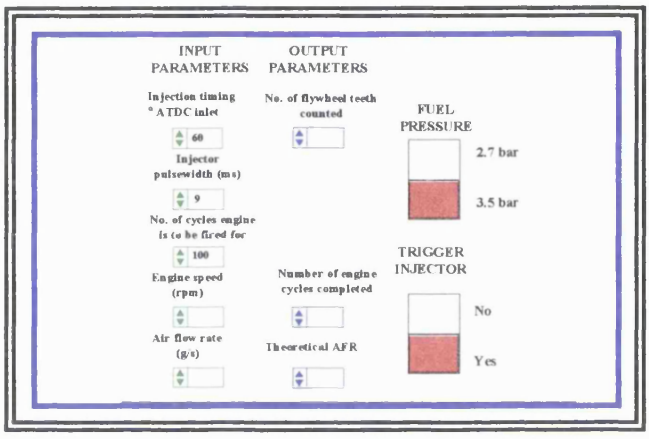

Figure 2.4: LabVIEW control panel for the user

At the start of the program (figure 2.5) the injection timing and the fuel injection pulsewidth were converted to the equivalent number of flywheel teeth, (blue box). Consequently both of these parameters remained constant from cycle to cycle although throughout an engine test the engine speed was known to increase by about 40 rpm. The program then waited until the fuel injection sequence was initiated by the user (green box). This feature allowed the required engine conditions to be established prior to the start of fuel injection. Once the fuel injection sequence was initiated, there was a second delay whilst the program waited for a signal from the engine that was set to occur at BDC (red box). The signal was provided from an opto-switch, that comprised of a light emitting diode (LED) and an integrated photodetector positioned around a cutter disk mounted onto the camshaft (Plate 2.3). A slot was cut into the circumference of the cutter disc such that the infra-red beam produced from the LED was uninterrupted for a finite time. This caused the output from the opto-switch to increase from 0 V to 5 V, and then back to 0 V when the cutter disc again interrupted the beam. The increase from 0-5 V was set to occur at BDC of the inlet stroke and was used as the reference point from which the computer program set all of its timings.

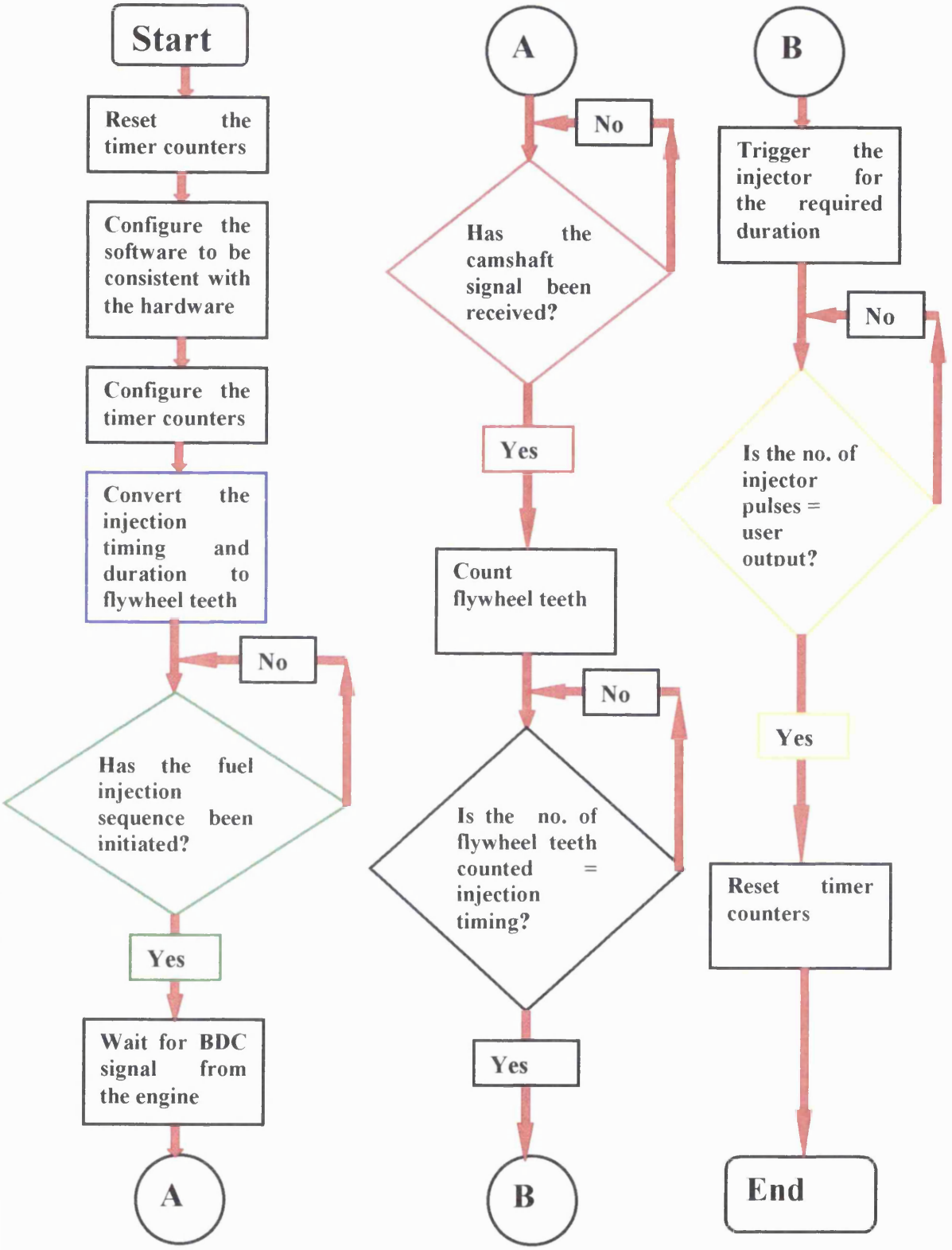

Figure 2.5: Flow chart for engine control system

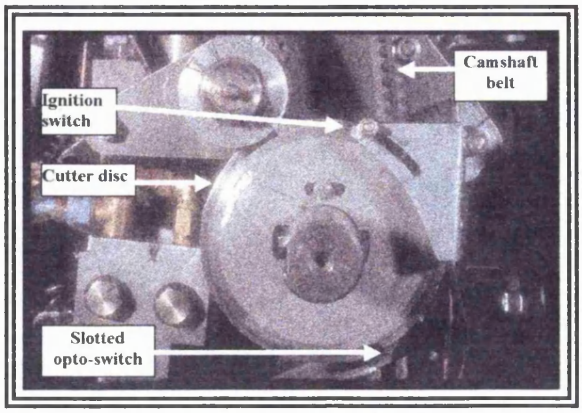

Plate 2.3: View of cutter disk and slotted opto-switch (positioned at 5 o'clock) which provided the BDC signal

An inductive transducer was positioned near the engine flywheel so that it responded to the movement of flywheel teeth past its pole piece and produced a 0-5 V TTL square wave output for each passing tooth. When the BDC signal was received from the slotted opto-switch, the program began to count the number of low to high edges of the transducer output and when this was equivalent to the injection timing (yellow box), the fuel injector was triggered for the required duration. These events were all completed prior to next BDC inlet signal being received from the opto-switch and the process was repeated until the number of required injection pulses was achieved. The angle between each flywheel tooth was 3°. Hence the error in the fuel injection timing from using the flywheel teeth for reference was no greater than 3°.

The ignition system was a Luminition opto-electronic system which used an optical switch to trigger an electronic coil switching unit. The optical switch was mounted so as to be interrupted by the same cutter disk used by the injection timing system (Plate 2.3). Variation of the ignition timing was effected by mechanically moving the position of the optical sensor.

2.3 Copper Vapour Laser and High Speed Camera System

Illumination of the combustion chamber was provided by a Class 3 copper-vapour laser (Cu15-AL), the specifications of which can be found in appendix A, table A1. The main advantages of the copper-vapour laser for this application were its short pulse duration

(10-40 ns), which enabled the motion of the fuel spray to be frozen in mid flight and its high pulse repetition rates. For the current application, the pulse repetition rate was determined by the framing rate of the camera, set at 10, 000 pictures per second (pps) as in previous work carried out by Fry (1994).

The laser light was directed onto the 45° mirror via a fibre optic cable where it was deflected 90° through the quartz piston crown into the combustion chamber. The fibre optic cable had an effective diameter of 1 mm and a transmission efficiency of 80 %. Its position was important in order to obtain the most intense back illumination, whilst not obscuring any areas of interest with the bright spot formed by the direct reflection of the laser light. A blanking strip was placed in front of this reflected portion of the beam. The combustion chamber surface and the valves were polished to achieve a highly reflective surface in order to provide back illumination of the fuel spray, which appeared as dark droplets against a bright background.

The majority of the photographic work was performed with a Hadland Hyspeed S-2 16 mm rotating prism camera. The camera supplied a signal each time the film frame was aligned correctly and in so doing triggered the laser to give a pulse of light. It was found that the optimum exposure of the film (400 ASA) was obtained with an aperture setting of F3.6. An 80 mm lens was used to provide a view of the whole combustion chamber and a K2 stand-off microscope lens was employed for observing small areas of interest. The film used was Ilford HP5 Plus 400 ASA negative black and white motion picture film, type 782, 16 mm by 100 ft and the number of consecutive engine cycles that could be recorded for each engine speed is listed in table 3.1, chapter 3. An automatic processing machine was used to develop the films which were ready in approximately 1 hour.

2.4 Discussion of Engine Testing

It was decided to concentrate testing on the behaviour of liquid fuel in the combustion chamber during the period of cold start and warm-up. This was because significant

overfueling is applied during these periods in a port-injected SI engine to minimise the number of cycles between fuel injection and first fire and to avoid subsequent mis-fire (Fox *et al* (1992)). The excess fuel causes a significant increase in UHC and CO in the exhaust at a time when the catalyst has still to reach its light-off temperature. Although recent advances in catalyst technology have reduced this delay period and therefore has reduced the overall engine-out UHC emissions, Horie *et al* (1995) state that the emissions during the first 30 cycles of a ULEV engine, (when the catalyst is not yet operating efficiently) with a standard fuelling system, account for 17% of the overall FTP-75 mode HC emissions. Additionally, Jackson *et al* (1996) showed that within the first three seconds of fuel injection, the UHCs emitted, peaked at a level 95 % greater than that experienced when the engine was fully warm. The area of cold start and warm up is one which still provides tremendous scope for the engineer in reducing the emission levels, and thus was the most fruitful region on which to concentrate an investigation into mixture preparation.

Chapter 3 describes an investigation into the in-cylinder liquid fuel behaviour obtained for three current designs of fuel injection systems during the area of cold start. The research engine and high speed cine arrangement described in this chapter were used for the tests.

Chapter 3

In-cylinder Behaviour of Liquid Fuel for Conventional Fuel Injection Systems

3.1 Mixture Preparation

3.1.1 Fuel Injector Characteristics

Two factors that affect the amount of liquid fuel that escapes combustion, and consequently the degree of enrichment required during warm-up are the fuel injector characteristics and also the targeting of the injector. The fuel injector characteristics can affect the in-cylinder drop size as well as the quantity of fuel impacting on the port and combustion chamber surfaces (Kelly-Zion *et al* (1995)). Decreasing the droplet size, through for example the use of an air-assisted injector, can assist rapid first fire due to an increase in the surface area of the fuel available for evaporation. Additionally, droplets that have diameters of the order of 20 μm or less are more likely to follow the air stream than their larger counterparts, and hence are less likely to impact on a surface before entering the combustion chamber (Fry *et al* (1994)).

Before attempting to make improvements to existing hardware, it is necessary to know what is presently occurring in the engine and to be able to suggest reasons for the observed behaviour. As such three different designs of fuel injector were investigated using the optical engine described in chapter 2, under cold engine operating conditions. The three fuel injectors were the Bosch twin-spray injector, the Bosch four-hole injector and the Nippon Denso twin-spray air-assisted injector. In each case the injector was mounted in the standard position in the intake manifold and the fuel spray distribution within the combustion chamber was recorded over several consecutive engine cycles using the high-speed cine camera and copper-vapour laser arrangement described previously (chapter 2 section 2.3).

3.2 Engine Test Conditions

The test conditions are listed in table 3.1. For each engine test, the engine was motored

and the required conditions were established. This took approximately 10-20 seconds. The fuel injection system was then initiated and when the engine was seen to fire, the high-speed cine camera and the copper-vapour laser were triggered to start recording the in-cylinder events. The engine was allowed to cool to room temperature between each test.

Engine conditions			
Engine speed (rpm)	200	880	1500
Air flow rate (g/s/cylinder)	Throttle in idle position	0.7	2.0
Manifold depression (kPa)	Throttle in idle position	73	56
Ignition timing (degrees)	10° BTDC	15° BTDC	23° BTDC
Fuel injection parameters			
Injection timing (degrees)**	Open-valve 60° ATDC*	Open-valve 60° ATDC	Open-valve 60° ATDC
	Closed-valve 90° BTDC**	Closed-valve 90° BTDC	Closed-valve 90° BTDC
Fuel pressure (bar)	2.7***	2.7	2.7
Fuel pulsewidth (ms)	8	6.5	7
Average no. of cycles recorded	4-5	6-7	10-11

*** end of injection**
**** end of injection with reference to non-firing TDC**
***** with respect to manifold depression**

Table 3.1: Engine test conditions investigated

3.3 Results

General

For all three injectors investigated, the majority of the fuel appeared to enter the combustion chamber from that area between the inlet valves closest to the cylinder bore, and travel downwards to impact on the piston. This was true for most of the speeds and

injection timings (open-valve injection ends 60° ATDC and closed-valve injection) considered. The piston impaction areas were at their greatest for cranking and at their least for idle. It was quite difficult to distinguish the droplets as they entered the combustion chamber, but their subsequent impaction on the piston crown was very obvious on the cine film. Much, but not all, of the fuel would then evaporate before or during combustion and fresh fuel would be deposited during the next cycle. Comparison of the piston impaction areas for each injector at the different engine speeds and injection timings was made, and some of the results are shown in figures 3.1 a-3.1 c. The figures show the approximate areas of the piston crown covered by the liquid fuel, from the second recorded cycle. A discussion of the results then follows.

3.3.1 Comparison of Fuel Impaction Areas at Different Engine Speeds

Cranking Results

For the cranking condition closed-valve injection (figure 3.1 a), the twin spray injector and the air-assisted injector produced similar piston impaction areas which were beneath the inlet valves. The Bosch 4-hole injector had an impaction area beneath the spark plug. For open-valve injection, however, the impaction area for the air-assisted injector was biased to one side whilst that obtained for the twin spray was relatively central between the two inlet valves, and indeed was very similar to that produced for closed-valve injection. It is not known whether the biasing of the impaction area for the air-assisted injector was a true biasing phenomenon or rather as a consequence of small variations in the injector location. The impaction area for the Bosch 4-hole injector had increased to beneath the inlet valves as well as encompassing the area beneath the spark plug as noted for closed-valve injection.

Idle and 1500 rpm Road load Condition Results

For the idle and 1500 rpm road load conditions, the Bosch 4-hole injector and the air-assisted injector produced remarkably similar impaction areas. The fuel spray characteristics for the twin spray injector at idle was one in which a fine droplet cloud travelled across the combustion chamber in the direction indicated on the figure. Again with the Bosch 4-hole injector for 1500 rpm (but not for idle), some of the fuel impacted on the piston beneath the spark plug but this was not as great as at cranking. At the 1500

rpm road load condition, no fuel was observed for the twin spray injector although the engine was seen to fire.

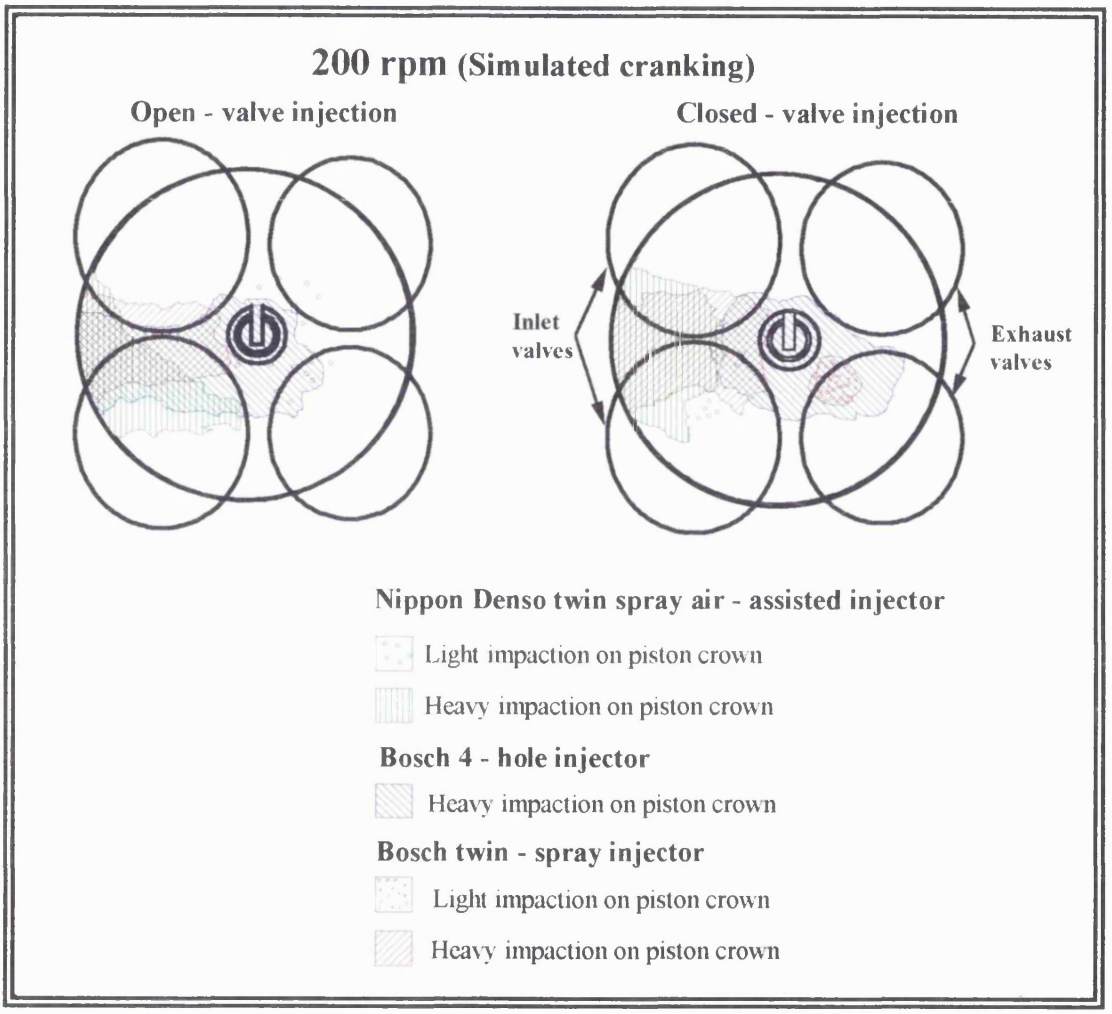

Figure 3.1 a: Comparison of the areas of impaction on the piston crown for open and closed-valve injection at an engine speed of 200 rpm

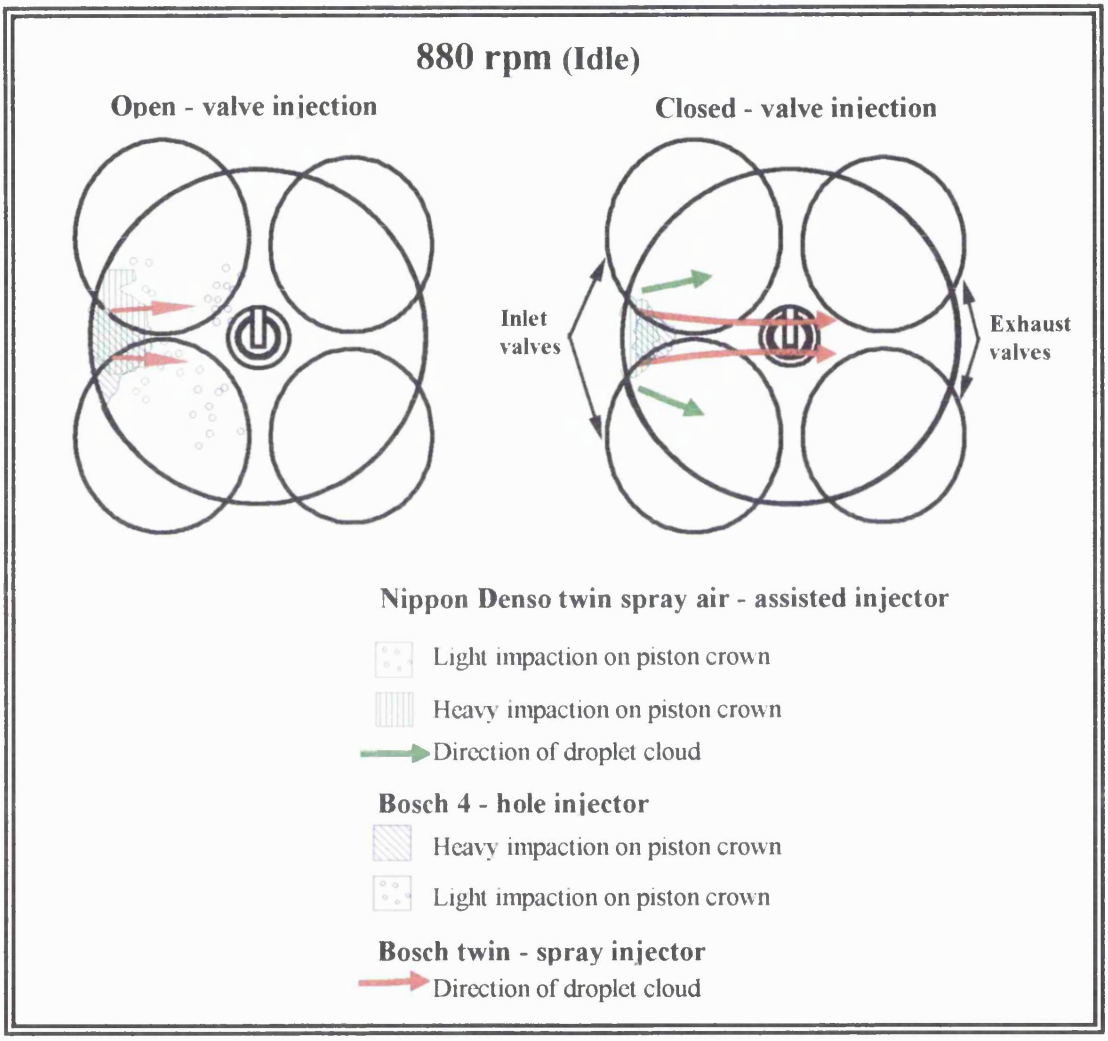

Figure 3.1 b: Comparison of the areas of impaction on the piston crown for open and closed-valve injection at an engine speed of 880 rpm

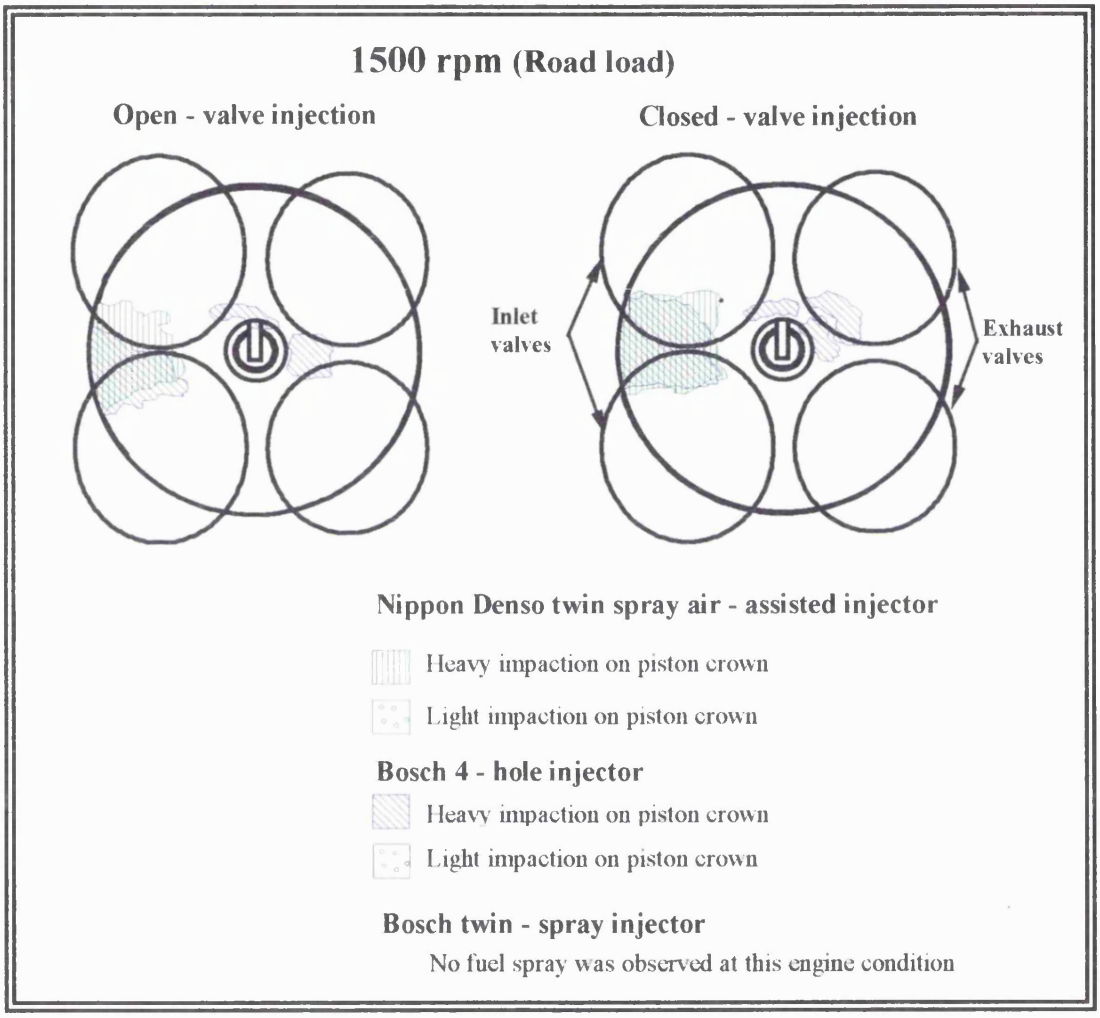

Figure 3.1 c: Comparison of the areas of impaction on the piston crown for open and closed-valve injection at an engine speed of 1500 rpm

3.3.2 Possible Mechanisms Responsible for Impaction Areas

The impaction area for the Bosch-4-hole injector at cranking encompassed that region directly beneath the spark plug (and also for 1500 rpm road load but not to such a large extent), which was a different region to the other two injectors. The reason for this difference was explained by focusing of the camera on the area around the inlet valve (figure 3.2), and observing how the fuel entered the combustion chamber for each injector. These results will be explained for the open-valve injection timings, however the mechanisms were the same for closed-valve injection.

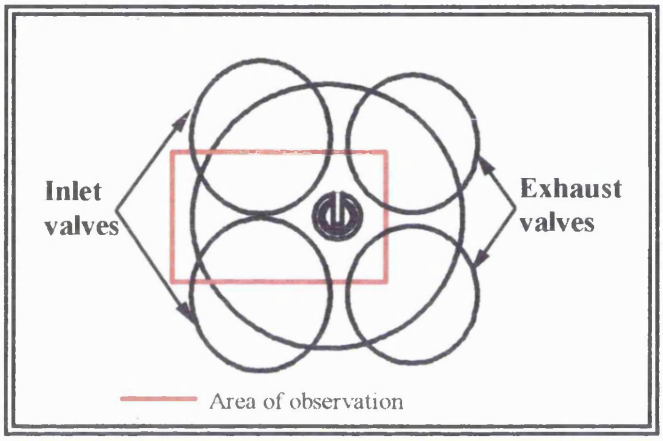

Figure 3.2: Area of observation for the fuel entry characteristics

For the Bosch-4 hole injector a proportion of the fuel entered the combustion chamber as droplets, some of which skimmed around the periphery of a segment of the inlet valve circumference before becoming detached (figure 3.3 a-c). The droplets then traversed downwards and across the combustion chamber volume to impact on the piston crown. The droplet velocities were estimated to be in the region of 13.5 m/s for open-valve injection and 12 m/s for closed-valve injection. Other droplets entered the combustion chamber directly and impacted on the piston.

In contrast, for the twin spray injector, initially it was possible to discern a number of droplets around a segment of the inlet valve (figure 3.4 a). These droplets moved downwards and outwards as more droplets entered in the same region, such that it was no longer possible to discern individual droplets, but rather a cloud of fine droplets (figure 3.4 b). A similar mechanism existed for the air-assisted injector except no

individual droplets could be identified, only a fine droplet cloud as it impacted on the piston.

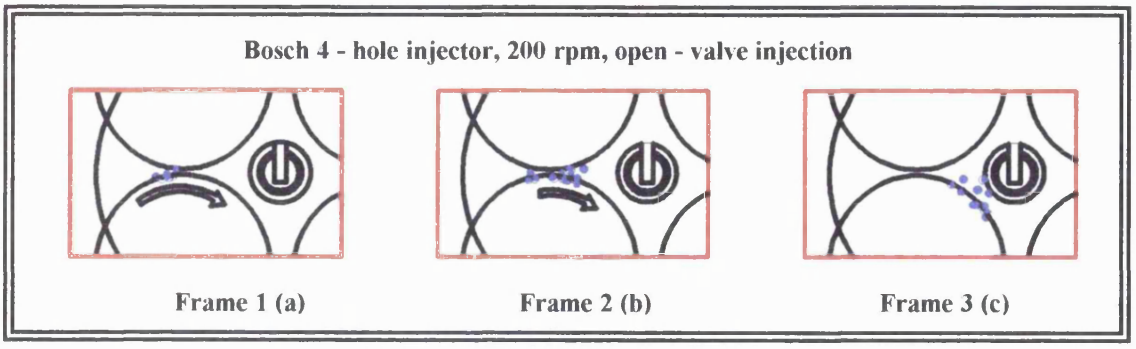

Figure 3.3 a-c: Fuel entry characteristics for the Bosch 4-hole injector at an engine speed of 200 rpm

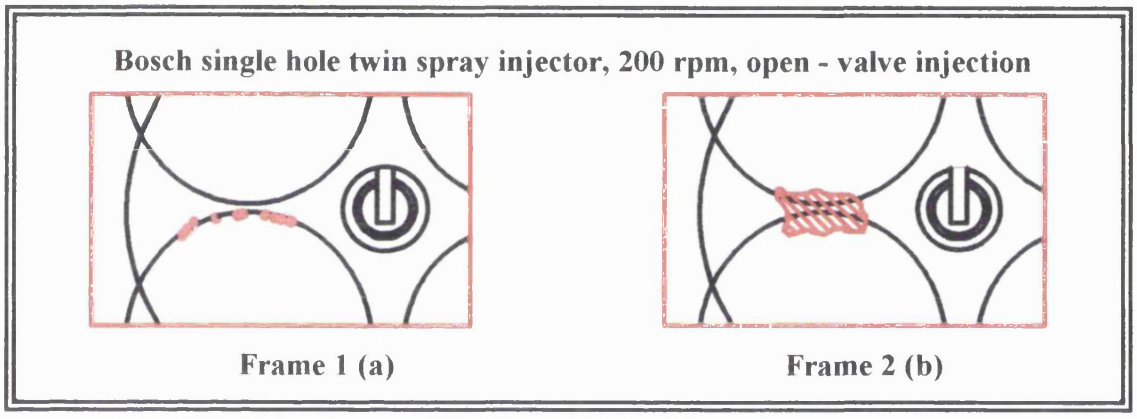

Figure 3.4 a and b: Fuel entry characteristics for the Bosch twin spray injector at an engine speed of 200 rpm

For the remaining engine conditions of idle and 1500 rpm road load with the Bosch-4 hole injector, the fuel entered as a droplet cloud (similar to that produced in figure 3.4 b) that moved vertically downwards to impact on the piston crown. Only a few individual droplets could be seen to move over the top of the inlet valve at idle but a larger proportion appeared to be present at 1500 rpm.

The similarity of the fuel spray distributions for the air-assisted injector for all the engine tests is shown in figure 3.5. A quantitative overall assessment of the behaviour of the three fuel systems can be obtained from table 3.2 which shows the percentage of the visible piston area on which the fuel impacted.

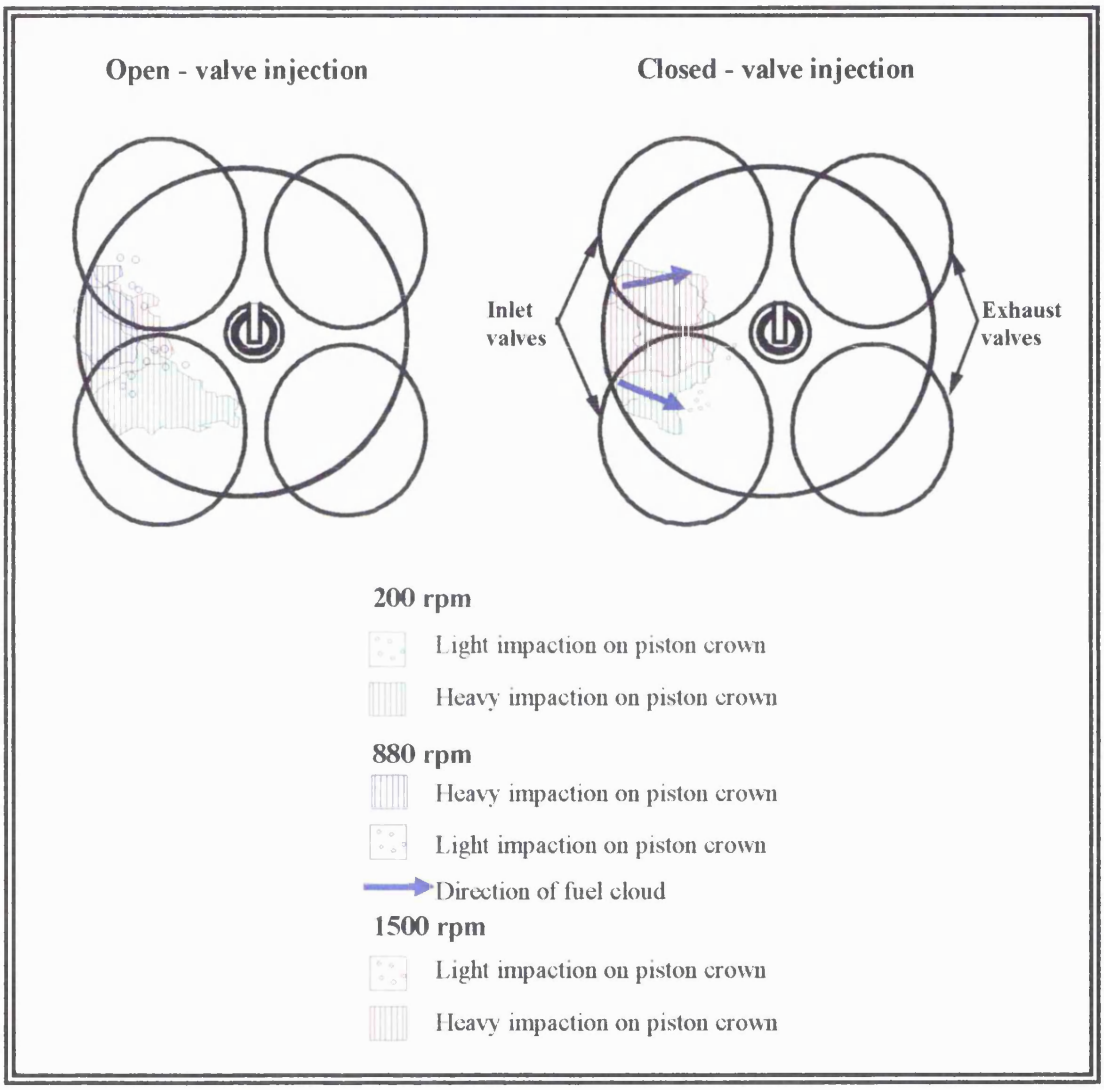

Figure 3.5: Fuel spray characteristics for open and closed-valve injection timings for the air-assisted fuel injector over the range of engine speeds

Engine speed and injection timing	Injector		
	Nippon Denso twin spray air-assisted injector	Bosch twin-spray injector	Bosch 4-hole injector
200 rpm (simulated cranking), open-valve injection	8.8 % -	8.1 % ≤1	15.5 % -
200 rpm (simulated cranking), closed-valve injection	10.0 % ≤1 %	11.0 % 2.6 %	12.3 % -
880 rpm, open-valve injection	5.7 % ≤1 %	- -	4.7 % ≤1%
880 rpm, closed-valve injection	3.1 % -	- -	1.6 % -
1500 rpm road load, open-valve injection	8.5 % -	- -	9.4 % -
1500 rpm road load, closed-valve injection	10.9 % -	- -	12.7 % -

The numbers in red relate to heavy impaction (figures 3.1 a-c)
The numbers in blue relate to light impaction (figures 3.1 a-c)

Table3.2: Impaction areas as a percentage of the total viewing area

3.4 Summary of Results

The results from the cine films have been summarised and tabulated below (table 3.3).

Observation of the cine films showed that the manner in which the fuel entered the combustion chamber for each injector and engine test carried out was remarkably similar. This is more surprising when considering work carried out by Fry (1994) where changing from a pintle-type injector to an air-assisted injector produced a dramatic change in the behaviour of the liquid fuel within the cylinder. The pintle-type injector wet the combustion chamber roof, and some liquid fuel was even observed to pass straight out of the exhaust valves having escaped combustion by being hidden in the crevices around the exhaust valve. This contrasted with the air-assisted injector which gave a fine cloud of droplets which mostly impacted on the piston.

Injector Type	Engine Speed (rpm)	End of Injection w.r.t. Valve Timing	In Focus	None	Slight	Moderate	Severe	Inlet Side	Exhaust Side
Twin Spray	200	Open (60° ATDC)	Valves				X	X	X
Four Hole	200	Open (60° ATDC)	Valves				X	X	X
Four Hole	200	Open (60° ATDC)	Valves				X	X	
Air-assisted	200	Open (60° ATDC)	Valves				X	X	
Twin Spray	200	Closed	Valves				X	X	
Four Hole	200	Closed	Valves				X	X	X
Air-assisted	200	Closed	Valves				X	X	
Twin Spray	880	Open (60° ATDC)	Valves	X					
Twin Spray	880	Open (60° ATDC)	*		X			X	
Four Hole	880	Open (60° ATDC)	Valves	X					
Air-assisted	880	Open (60° ATDC)	Valves				X	X	
Air-assisted	880	Open (60° ATDC)	Valves				X	X	X
Twin Spray	880	Open (60° ATDC)	Crown	X					
Four Hole	880	Open (60° ATDC)	Crown	X					
Twin Spray	880	Closed	Valves	X					
Twin Spray	880	Closed	*		X			X	
Four Hole	880	Closed	Valves	X					
Air-assisted	880	Closed	Valves	X					
Closed	880	Closed	Crown			X		X	
Air-assisted	880	Open (60° ATDC)	Close-up	X					
Air-assisted	880	Closed	Close-up	X					
Four Hole	1500	Open (60° ATDC)	Valves				X	X	X
Air-assisted	1500	Open (60° ATDC)	Valves				X	X	
Four Hole	1500	Open (10° ATDC)	Valves				X	X	X
Four Hole	1500	Closed	Valves				X	X	X
Air-assisted	1500	Closed	Valves				X	X	
Twin Spray	1500	Open (60° ATDC)	Valves				X	X	X

- *** The plane of focus was approximately 6 mm below the edge of the spark plug.**

Table 3.3: Summary of the high speed cine results for a range of fuelling systems

3.5 Cylinder Bore Wetting

As a consequence of the design constraints for the housing of the quartz piston crown (chapter 2 section 2.1.2.1), only 85 % of the combustion chamber could be viewed. It was not possible to see right to the edge of the combustion chamber and observe whether some of the fuel spray impacted on the cylinder bore just beneath the inlet valves or not. It was thought that this was an important detail which needed elucidation, as impaction on the cylinder would mean fuel entering the crevice above the top piston ring and adding significantly to the UHC emissions. It was decided to employ a technique developed from an approach reported by Miller *et al* (1991) to qualify and quantify (where applicable) the amount of fuel that impacted on the cylinder bore and is reported in the following.

3.5.1 Fuel Systems Test Facility

The comparison was performed in the Fuel Systems Test Facility which is an environmental chamber that incorporates a pulsating flow test rig (section 3.5.1.2) to allow different engine fuelling systems to be investigated in controlled and safe conditions. The main components (section 3.5.1.2) are shown in figure 3.6.

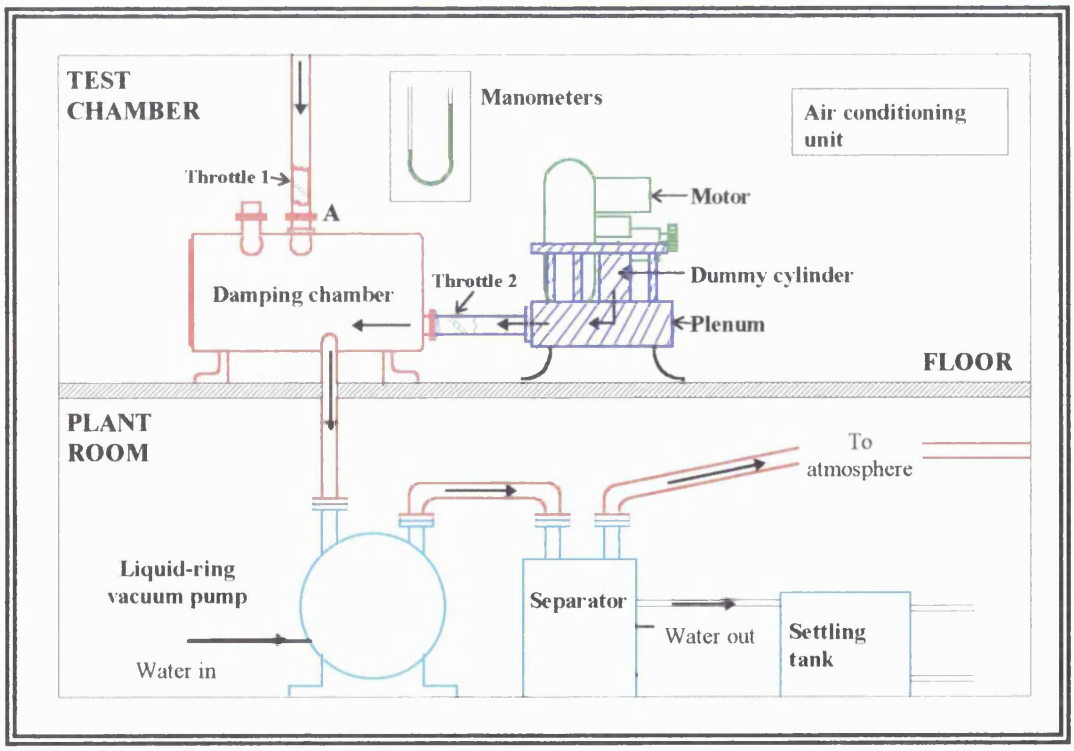

Figure 3.6: Fuel Systems Test Facility

Suction was applied to the pulsating flow ring from a Hick Hargreaves CHR 1200 liquid-ring vacuum pump via a large damping chamber. The damping chamber served two purposes. The primary purpose was to dilute the air/fuel mixture produced from the pulsating flow rig to a level well below the explosive limit, and the second was to damp out any fluctuations of the air flow caused by the pumping of the vacuum pump. Beneath the Fuel Systems Test Facility test chamber is a ventilated plant room which houses the liquid-ring vacuum pump and also two separator chambers. The first separator chamber separates the liquid phases from the gas phases, and the second separates the liquid hydrocarbons from the water.

3.5.1.2 Pulsating Flow Rig

The pulsating flow rig comprised a Ford Zetec standard cylinder head and intake system (chapter 2 section 2.1) mounted on a dummy cylinder which, in turn, was mounted onto a plenum attached to the damping chamber (figure 3.6). The camshafts were motored using a 220/240 V, 3 kW, variable-speed motor (Lenze Simplabelt Type 11.331.20.16.2). Standard grade pump gasoline was supplied to the injector from a sealed vessel to which mains air pressure could be applied and the fuel injector was triggered using a Malvern instrumentation delay unit that used a signal from a Malvern infra-red sensor mounted onto the camshaft. The air flow to the pulsating flow rig was controlled by an air-spill valve in the damping chamber (throttle 1, figure 3.6), in conjunction with a second throttle (throttle 2, figure 3.6), in the supply pipe. Using the system of throttles it was possible to set the required depressions and air flows through the test rig, and the motor was adjusted to give the required engine speed. A mercury manometer was used to measure the manifold depression and a Zetec hot wire air flow meter (chapter 2 section 2.1.1) to measure the air flow rate.

3.5.2 Measurement Technique for the Cylinder Bore Wetting

Miller's (1991) method was used to quantify the amount of fuel impacting on the bore. This involved concentrating on one combustion chamber and fitting a porous bronze ring (plate 3.1) around the top of the dummy cylinder. Suction was applied to the other three cylinders, but no measurement were made of cylinder bore wall film. The porous ring was divided into eight equal segments.

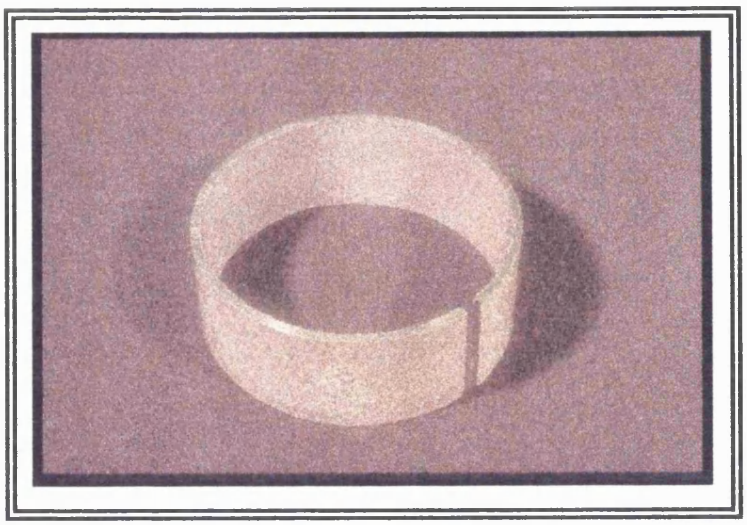

Plate 3.1: Porous bronze insert

Any fuel which impacted on each segment was sucked through the insert by applying a depression across the insert just in excess of the cylinder depression. The fuel was collected in test tubes which were contained in a large glass vessel. The method of applying the depression across the insert and the method of fuel collection is shown in figure 3.7, for clarity only one of the pressure tappings has been shown connected to the test tube.

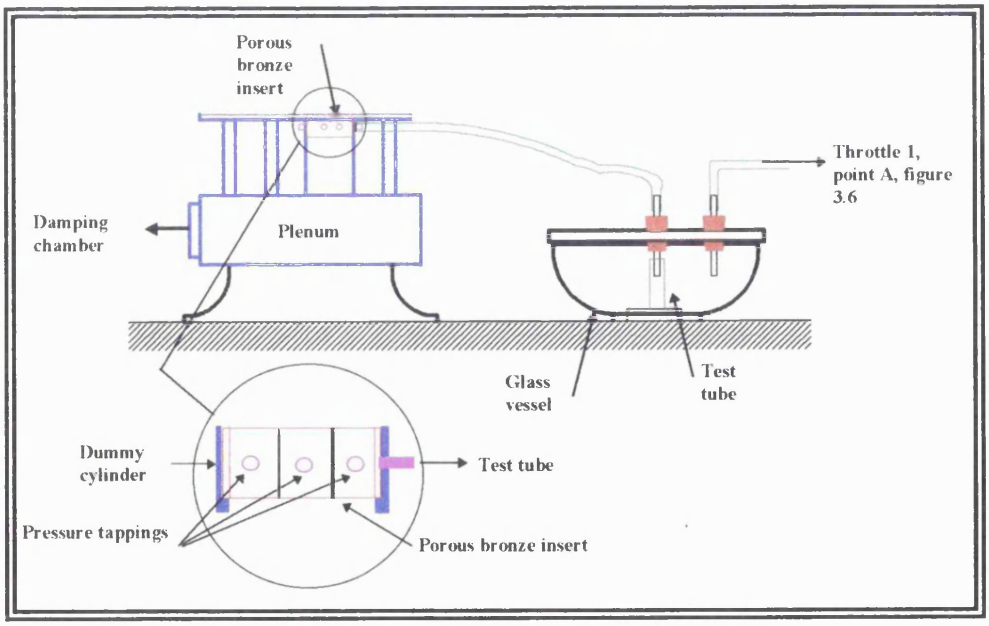

Figure 3.7: Method of applying the depression across the porous bronze insert

The depression across the porous bronze insert had to be large enough to suck any

deposited fuel into the test tubes, but could not be so great as to cause airborne fuel droplets to be sucked out of the air stream. Miller (1991) showed that the amount of fuel collected increased as the depression across the insert was raised, until a point was reached at which the amount of fuel collected achieved a plateau (figure 3.8). Based on this graph a depression was chosen that was a short distance from the start of the plateau.

Each fuel injector was investigated at the engine speeds and injection timings listed in table 3.1, and each test lasted for 40 minutes. For all the test conditions and injectors a negligible amount of fuel was collected. It was decided to check whether evaporation effects were playing a role in preventing any fuel from being measured and so the tests were repeated with the test fluid SBP3 which had a similar relative density and surface tension to gasoline, but was significantly less volatile (boiling point (bp) around 110 °C). In these tests, negligible amounts of SBP3 were collected as well.

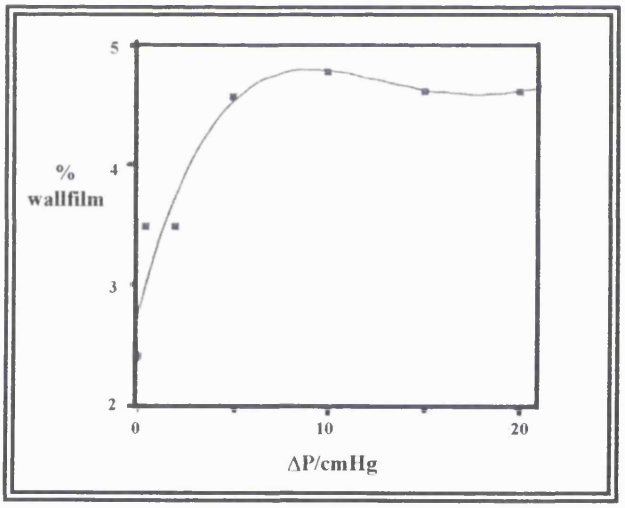

Figure 3.8: Fuel collected versus depression across porous insert [Miller (1991)]

3.5.3 Observation of the Fuel Spray

A spark plug adapter was manufactured to allow an endoscope to slide into the dummy cylinder through the spark plug hole (plate 3.2). Illumination was provided by a high powered light source secured into the bottom of the plenum, directly beneath the endoscope and with this arrangement it was possible to observe the fuel spray as it came through the inlet valves.

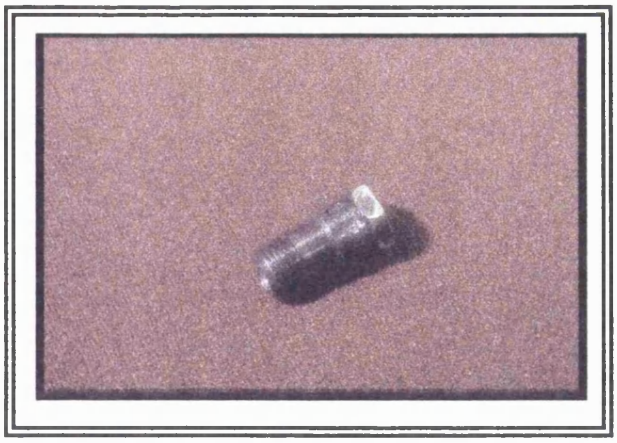

Plate 3.2: Spark plug adapter

3.6 Concluding Comment

These visualisation tests showed that the fuel was entering the cylinder from the back of the inlet valves in a sheet form that appeared to be away from the cylinder bore. This would account for why no fuel was collected with the cylinder bore wetting rig. Due to insufficient illumination it was not possible to record this sheet and so an alternative means was sought.

Chapter 4

A Novel Image Capture Technique to Record the Fuel Distribution Across the Cylinder Bore

The previous chapter investigated the fuel spray distribution within the cylinder for three different injector types. It was observed that the majority of the fuel impacted on the piston crown, with small differences in the impaction area for different injector and engine conditions. Due to the need to fit a cap to retain the quartz piston window, it was not possible to see right to the edges of the combustion chamber and consequently observe whether the fuel impacted on the cylinder bore. A wall skimming technique was employed to attempt to measure any fuel that may have impacted on the cylinder bore, but although the tests ran for 40 minutes, no measurable amounts of fuel were collected. Observation of the fuel with an endoscope placed down the spark plug hole showed the fuel to be entering the combustion chamber in the form of a sheet that travelled vertically downwards. Due to insufficient illumination, it was not possible to record the journey of the fuel and so an alternative method was sought to investigate and record the presence of the vertical sheet of fuel.

The work described in this chapter had two combined purposes. These were firstly to record the downward motion of the fuel observed in chapter 3 section 3.5.3, and secondly to develop a system of recording images of droplet motion within the cylinder that did not rely on the use of a powerful, but expensive, copper-vapour laser.

4.1 Modifications to the Optical Research Engine

The optical engine (chapter 2) was modified to incorporate a second optical path across the cylinder bore. The removable plugs positioned close to the top of the cylinder block, which were used initially to provide access to the combustion chamber in order to clean the quartz piston crown (section 2.1.2.1), were replaced with optical plugs designed by the author (plate 4.1).

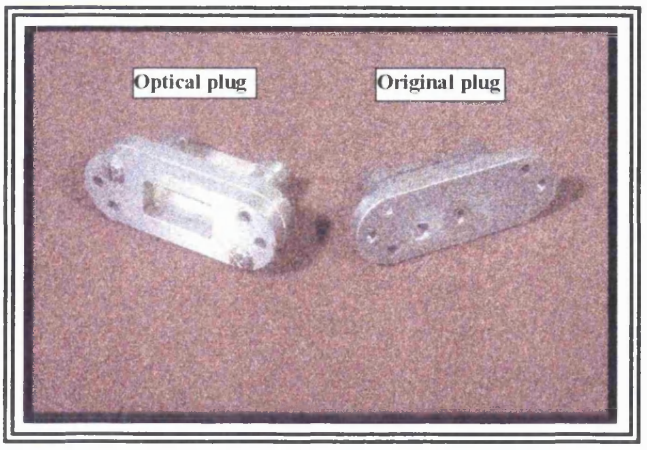

Plate 4.1: Optical and original plugs

The design parameters for the optical plugs are listed below:

1) to allow images to be recorded using back illumination as this allows the use of a relatively low intensity light source,
2) to maximise the viewing area,
3) to use flat windows but to minimise the inevitable crevice volume between the piston bore and quartz windows,
4) to prevent the top piston compression ring from traversing across the joint between the quartz housing and the cylinder bore,
5) to provide windows which would withstand the worst loading case of 50 bar (Stone *et al*, (1994)) (although in reality the worst loading case was not likely to exceed 25 bar (Fry (1994)))

4.1.1 Calculation of the Quartz Window Thickness

The height and width of the quartz block were determined by considering points 2-4 listed above while the thickness of the quartz was calculated to withstand the worst loading case. The following formula was used (Young (1989)):

$$W_u = \beta \sigma_y t^2 \qquad (4.1)$$

where W_u = total load require to collapse window (= pA)

p = pressure (kPa)

A = area of window face (mm^2)

β = constant = 5.64 (Young (1989))

σ_y = yield point of the material

t = thickness (mm)

and assuming σ_y = 54 MPa = UTS of quartz.

Including a safety factor of 5, the minimum thickness required for the quartz block to withstand the worst loading case was 9.0 mm. In order to simplify the quartz housing design the thickness of the window was increased such that it sat flush with the outside of the cylinder block, allowing a flat metal plate to be mounted on the outer surface to retain the quartz (plate 4.1).

4.2 Camera and Illumination Arrangement

The arrangement of the camera and illumination system used to record the liquid fuel in the combustion chamber is shown in figure 4.1. A 45° mirror had to be inserted between the cylinder block and the flash unit so that the unit could be mounted to one side in order to avoid the blocking effect of the inlet manifold. The camera was positioned to view through the quartz window on the exhaust side.

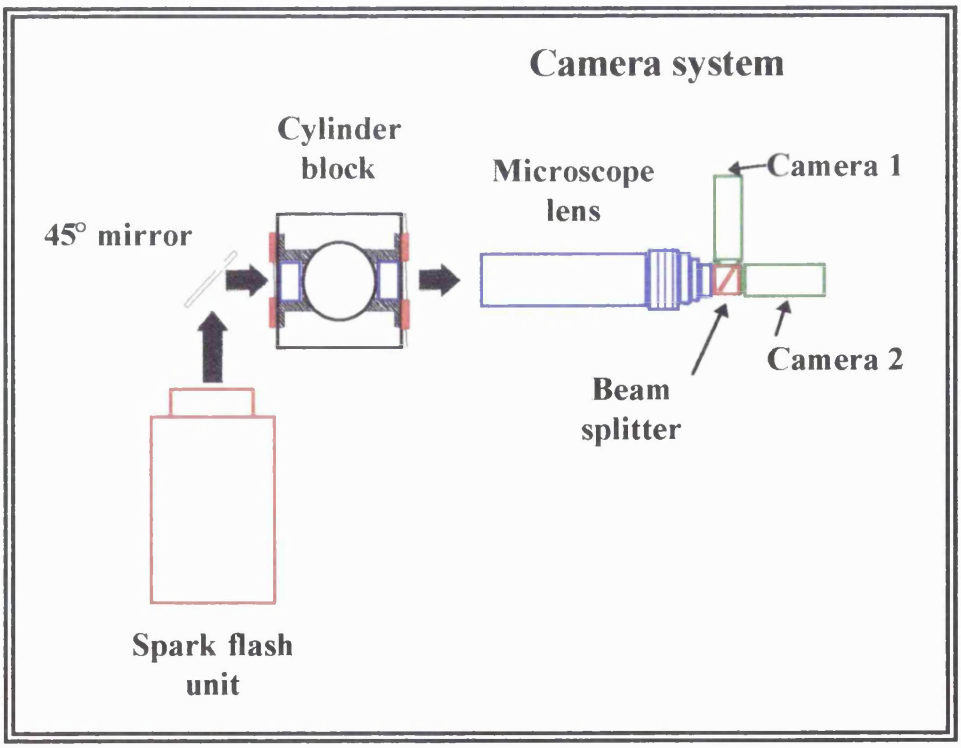

Figure 4.1: Camera and illumination arrangement

4.2.1 The Camera System

The capture of an image on film has historically had a greater degree of resolution than those images recorded by a personal computer employing image capture technology. However the use of film involves lengthy developing processes and laborious analysis of the data. Increasing technological advancements made in the area of video image capture have meant that the resolution of the computer-based images can begin to approach that of film, with the added advantage that the image to be analysed is already in computer format. Software packages may therefore be readily employed to analyse or display the data.

Typical CCD cameras employ interlace scanning techniques to produce a high resolution picture. In this manner the data is captured in two fields: the first field containing all the odd lines, and the second field all the even lines. A high resolution picture is obtained by projecting both of these fields together to obtain a single image. Horizontal and vertical synchronisation pulses are required to ensure that the odd and even lines occur at the correct times relative to one another. In Europe, horizontal synchronisation occurs at a period of 63.5 μs, and vertical synchronisation at a period of 20 ms (Salter *et al* (1996)). The transfer of the data from each semi-conductor storage element to a similar storage element where the image may be retrieved is accomplished by either by a frame transfer process or by an interline transfer process. The difference between the two is the manner in which the data is arranged for transfer. The frame transfer technique has a greater resolution than the interline technique, but has the disadvantage that the image may be partially or wholly damaged by extraneous light during the transfer of the data.

CCD cameras employing these techniques are perfectly adequate if the cameras are allowed to view the object for a reasonable length of time (20 ms for a 50 Hz field rate). However serious losses in resolution can occur with a short duration light source which may illuminate the area of interest for a duration of less than 20 ms. This loss in resolution may be understood by considering figure 4.2 below. The pixel elements on the CCD chip are scanned as two fields that contain the odd and even lines as previously described. The scanning is overlapped with respect to time and hence it is critical when

pixels are exposed. If the pulse of light was to occur at the position of flash 1 then only half the pixels would be illuminated, and consequently half the resolution would be lost. Alternatively, if the pulse of light occurred at the position of flash 2, then all the pixels would be illuminated and the greatest resolution for the given configuration would result. The camera shutter therefore needs to be accurately synchronised to the light pulse.

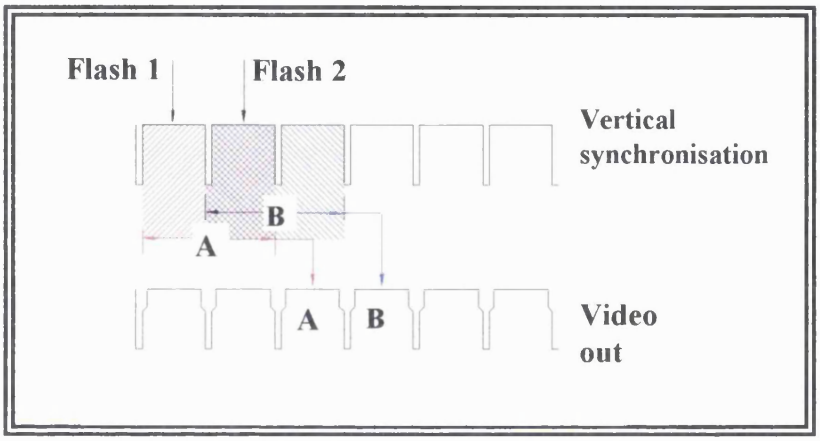

Figure 4.2: Integration timing of a standard CCD camera

In addition, it is useful to allow the camera to only accumulate an image for a portion of time that may be significantly less than the 20 ms previously required. This is possible by utilising a CCD camera that allows the CCD chip to be asynchronously triggered. A substrate drain built underneath the CCD chip expels the charge from all the pixels simultaneously until the start of the shutter period, when the charge is stored and the image is accumulated.

The cameras employed for the current application were two factory-modified progressive-scanning Pulnix TM-9700, full frame shutter, asynchronous reset, high resolution monochrome CCD cameras. The progressive-scanning feature allowed all the pixels to be scanned during the shutter process as opposed to the odd and even lines being read in turn. There is consequently no loss in resolution during the shuttering process. The cameras used an interline transfer 2/3 inch monochrome CCD with a resolution of 768 x 484 (horizontal by vertical) pixels. A substrate drain type shutter process was employed with a maximum shutter speed of 63μs. The cameras were also modified so that they could be started and stopped exactly when required. Only a few

CCD cameras can be reset and these only after reaching the end of a digital line of data. Resetting the cameras can therefore take anywhere between 0 and 63.5 μs depending on where along the digital data line the camera lies, at the time of reset. Both cameras were positioned to view the same area of the combustion chamber using a beam splitter. A long distance stand-off microscope lens was employed and the depth of focus of the cameras was 4 mm. The image from each camera was captured by a high-speed Alacron digital data acquisition system and displayed on a personal computer screen. This image capture system was designed and set up for an earlier project (Salters *et al* (1996)) which used a copper-vapour laser for illumination of sprays in a DI gasoline engine. It was employed by the author for the different work described here.

The cameras were triggered using a control box connected to the control system described in chapter 2 section 2.2. In this instance, the injector trigger was divided so as to produce two TTL square waves, one to trigger the injector and the second to trigger camera 1 to take a picture at a controlled time after receiving this signal, the delay being a user input on the control box. During the shutter period of camera 1 (the shutter period could be up to a maximum of 63 μs), the light source (section 4.2.2) was pulsed. Camera 2 was then automatically triggered at a controlled time after camera 1, this delay again being a user input on the control box, and similarly the light source was pulsed for a second time during this shutter period. The cameras were activated within 100 ns of receiving a trigger as opposed to the 63.5 μs required for standard CCD cameras to be reset. The camera trigger control system is shown schematically in figure 4.3.

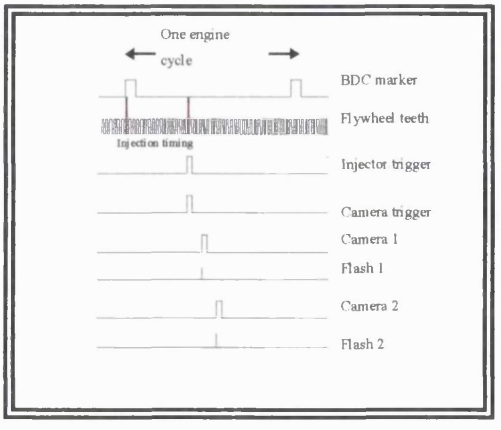

Figure 4.3: Camera and spark flash triggering sequence

4.2.2 Illumination System

Back illumination was provided by a spark flash unit (Palflash 500, Photonics Analysis Ltd) that provided two very high intensity spark flashes close together. The duration of the flash was 500 ns which was sufficient to freeze the fuel in mid-flight and was controlled by the control box. The delay between the two flashes was set to 80μs.

4.2.3 Focusing Planes for the Cameras

The cameras were focused by removing the window on the exhaust side of the engine and placing a transparent scale inside the combustion chamber. Focusing at different planes was achieved by moving the scale into the appropriate place. Print 4.1 shows the transparent scale placed inside the combustion chamber along the spark plug centreline. Each interval on the scale represents 1 mm, and hence the dimensions of the image were approximately 14 mm (length) by 9 mm (height).

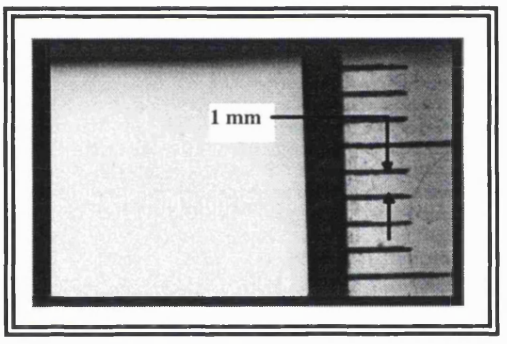

Print 4.1: Scale inside the combustion chamber midway across the cylinder bore

Initial engine testing was spent focusing at different planes within the combustion chamber and on different areas of the quartz window trying to locate fuel droplets to ascertain the best field of view and camera trigger timings. This preliminary work indicated the difficulty of capturing the droplets as they had both time and space to move in. For brevity and to aid understanding of the processes occurring, this preliminary work has not been included in this chapter. However, it enabled location of the most relevant viewing area (figure 4.4) and of the most productive focal planes (figure 4.5). These focal planes were the cylinder bore centreline, halfway between the centreline and quartz window on the inlet side, 5 mm from the quartz window on the inlet side and on the quartz window. For each focal plane, images were recorded every 15°, starting from 5°

after the end of injection, to a timing after the inlet valves had closed, namely 205° ATDC.

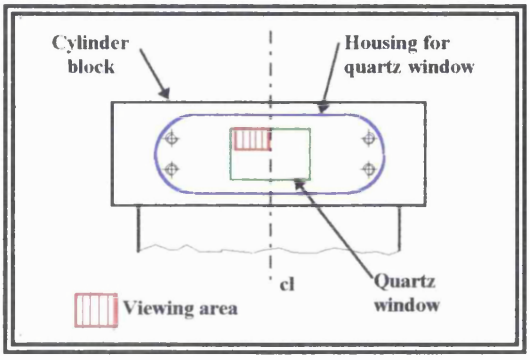

Figure 4.4: Viewing area of the quartz window

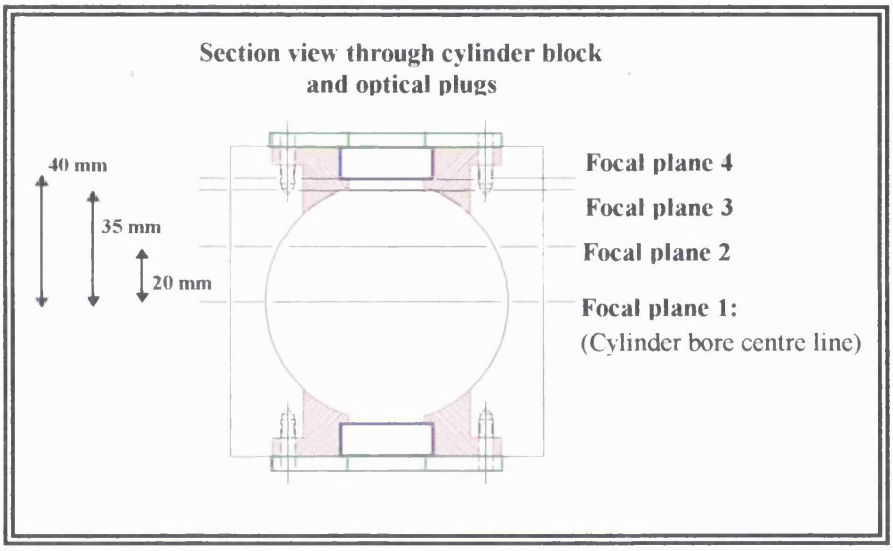

Figure 4.5: Focal planes on which images were recorded

4.3 Test Procedure

When the camera was focused on the required focal plane, the windows were replaced and background pictures were taken with both cameras. The engine was motored and the required engine conditions were set. The injector was then triggered, and when the engine was seen to fire, the cameras were initiated.

Testing was only carried out at an engine speed of 880 rpm (with a corresponding air flow of 0.7 g/second and manifold depression of 73 kPa) because the results from the first phase of testing (chapter 3) showed fairly similar behaviour between typical engine

operating conditions. The fuel pressure was set at 2.7 bar relative to manifold depression and ignition timing was set to 15° BTDC. A Bosch 4-hole injector was used throughout. Open-valve injection was used with injection set to finish at 60° ATDC.

4.4 Processing of the Results

Prints 4.2 a and b show raw background images recorded at focal plane 1 (along the spark-plug centreline) with cameras 1 and 2 just prior to the first engine test being carried out and prints 4.3 a and b, raw images recorded 95 °ATDC with cameras 1 and 2 when the engine was firing.

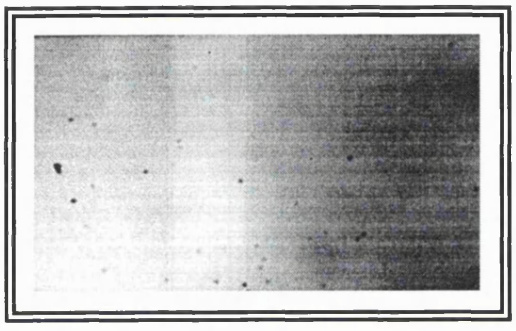

Print 4.2 a: Background image recorded along the spark plug centre line with camera 1, open-valve injection, Bosch 4-hole injector, raw data, idle condition

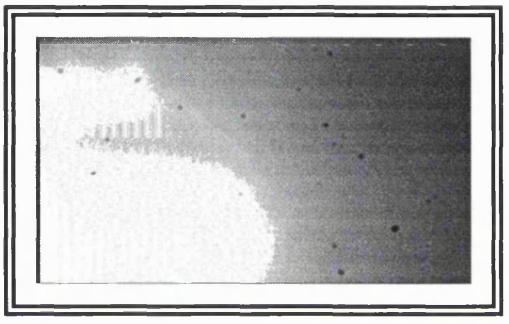

Print 4.2 b: Background image recorded along the spark plug centre line with camera 2, open-valve injection, Bosch 4-hole injector, raw data, idle condition

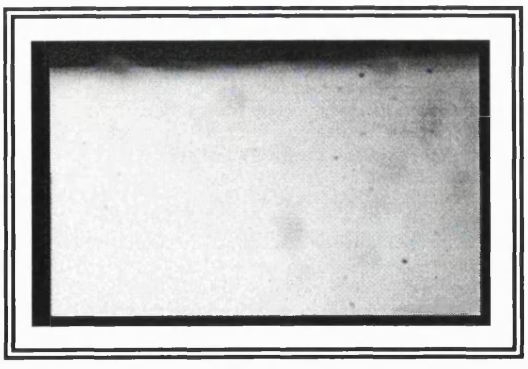

Print 4.3 a: Image recorded along the spark plug centre line with camera 1, 95° ATDC, open-valve injection, Bosch 4-hole injector, raw data, idle condition

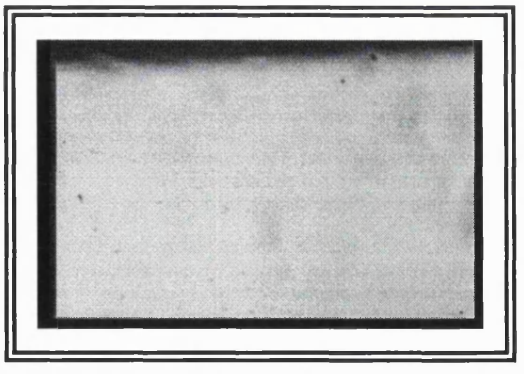

Print 4.3 b: Image recorded along the spark plug centre line with camera 2, 95° ATDC, open-valve injection, Bosch 4-hole injector, raw data, idle condition

Processing of the results was carried out with the software package *Visilog 4* in the following steps:

1) The images were imported into *Visilog 4.*

2) Both the background readings and the corresponding test runs were filtered to remove any extreme pixel values caused by noise. The particular filter chosen was a basic median filter which assigned to each particular pixel the average value of its eight surrounding neighbours. The advantage of this filter is that small objects such as fuel droplets are not lost.

3) There are 255 grey levels present in an image. When the images are recorded, not all of these grey levels are necessarily used. The second stage of processing adjusted the histogram of grey levels so that most, if not all of the grey levels were used. This improved the definition between the background and any particles present. A histogram equalisation technique was employed.

4) The particles were then tracked manually and their direction recorded on a subsequent image.

Prints 4.4 a and b show images 4.3 a and b after the above filtering and histogram equalisation techniques had been applied. It is also possible to carry on the process of image enhancement to include threshholding followed by subsequent labelling and analysis of the particles. This was not performed for this particular investigation as it was thought that the limited benefits would not be worth the extra effort involved.

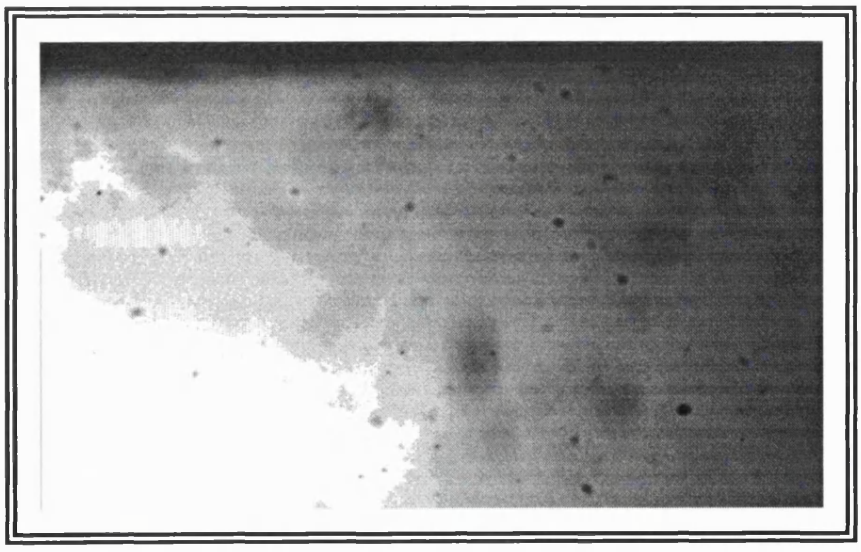

Print 4.4 a: Image recorded along the spark plug centre line with camera 1, at 95 °ATDC, open-valve injection, Bosch 4-hole injector, processed data, idle condition

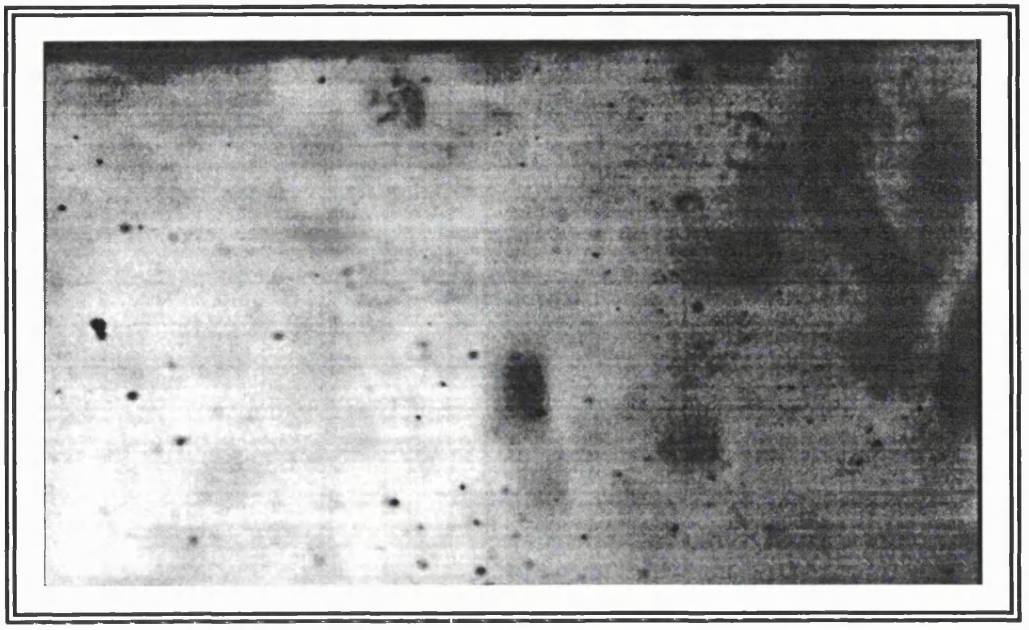

Print 4.4 b: Image recorded along the spark plug centre line with camera 2 at 95 °ATDC, open-valve injection, Bosch 4-hole injector, processed data, idle condition

Figure 4.6 shows the manual tracking of the droplets

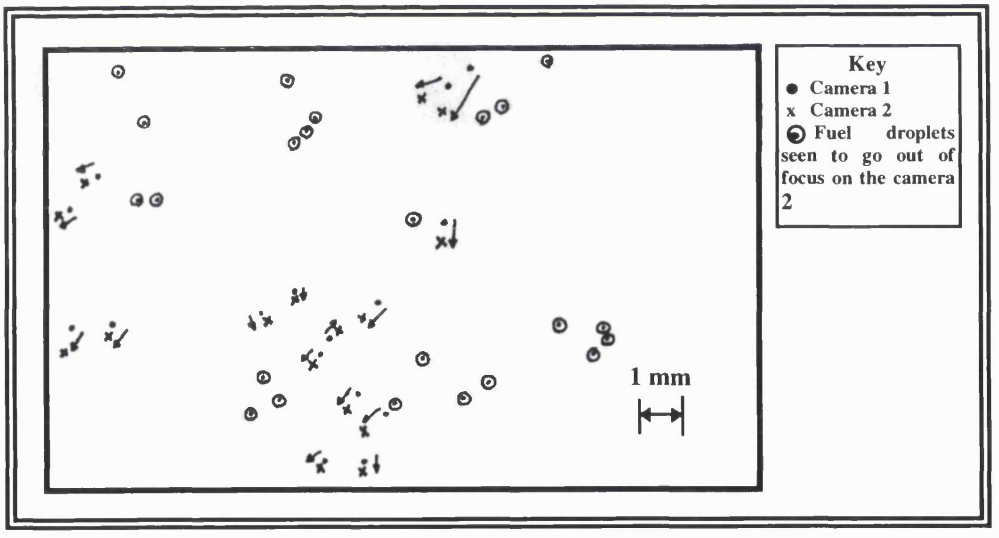

Figure 4.6: Manual tracking of the droplets for prints 4.4 a and b

4.5 Results

At each focal plane, images were recorded at least every 15° crank angle, starting from 5° after the end of injection (namely 65° ATDC on the intake stroke) to a time after the inlet valves had closed (namely 205° ATDC). The engine was stopped between each test to allow it to cool back to room temperature and to allow the quartz windows to be

cleaned.

4.5.1 Focal Plane 1: Along the Cylinder Bore Centre Line

The first sets of results were taken along focal plane 1, on the spark plug centreline. The results recorded the presence of fuel droplets in the images from both cameras from 95° ATDC to 125° ATDC and at 165° ATDC with no individual droplets being recorded after this. In fact, the fuel droplets were first recorded at 80° ATDC although only in the image obtained from camera 1. This may be because the droplets were moving too fast to be captured by both cameras, either by moving out of focus or moving completely out of the frame. At 95° ATDC the fuel droplets had a direction of movement either downwards or towards the window (prints 4.4 a and b, and figure 4.6). Velocities in the region of 3-14 m/s were estimated from the two images, (having assumed the fuel droplet to be travelling in the plane of focus). Results from a further 15° later (110° ATDC) showed clusters of fuel droplets with only two individual droplets travelling alone (prints 4.5 a and b). At 125° ATDC a relatively large number of fuel droplets were again observed (Prints 4.6 a and b). The droplets at this timing appeared slightly larger than those observed at 95° ATDC and somewhat less in number. Images recorded 150° ATDC showed no fuel droplets but one final observation was made at 165° ATDC in which the presence of possible clusters of fuel droplets was suspected in the lower right hand corner. After this no droplets or clusters were recorded.

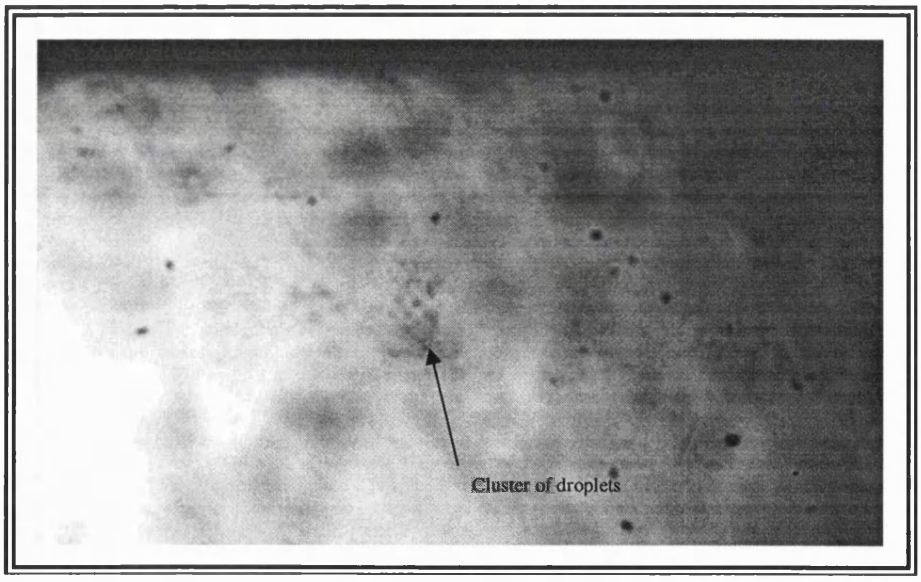

Print 4.5 a: Image recorded along the spark plug centre line, camera 1, 110 °ATDC, open-valve injection, Bosch 4-hole injector, processed data, idle condition

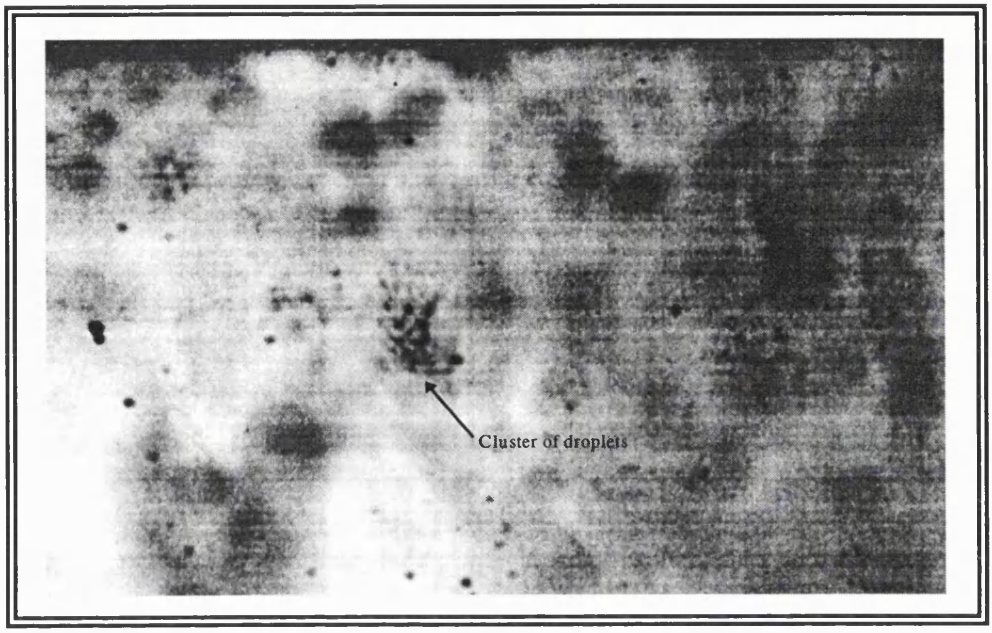

Print 4.5 b: Image recorded along the spark plug centre line, camera 2, 110 °ATDC, open-valve injection, Bosch 4-hole injector, processed data, idle condition

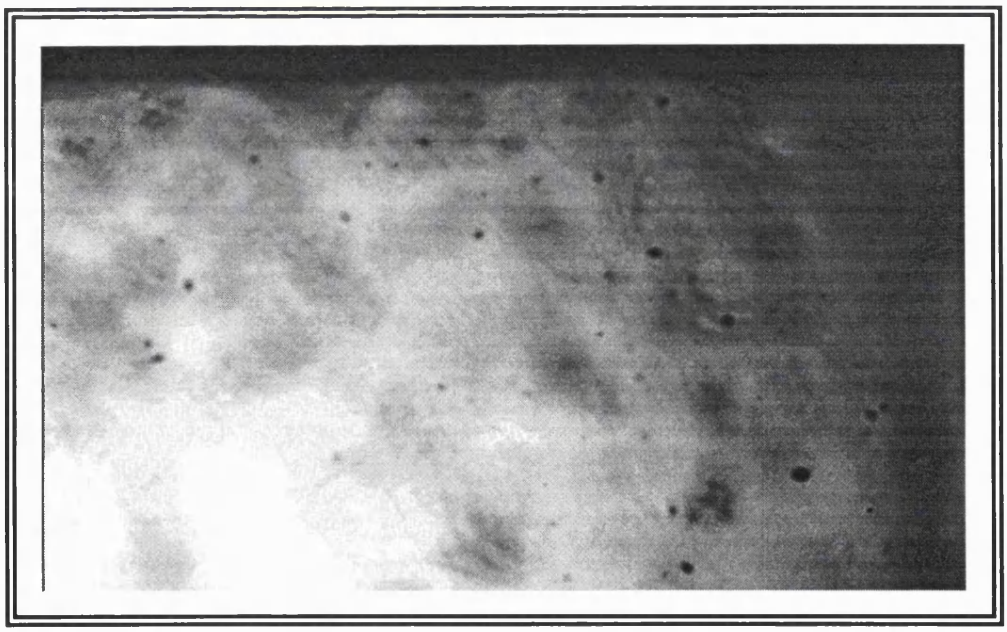

Print 4.6 a: Image recorded along the spark plug centre line, camera 1, 125 °ATDC, open-valve injection, Bosch 4-hole injector, processed data, idle condition

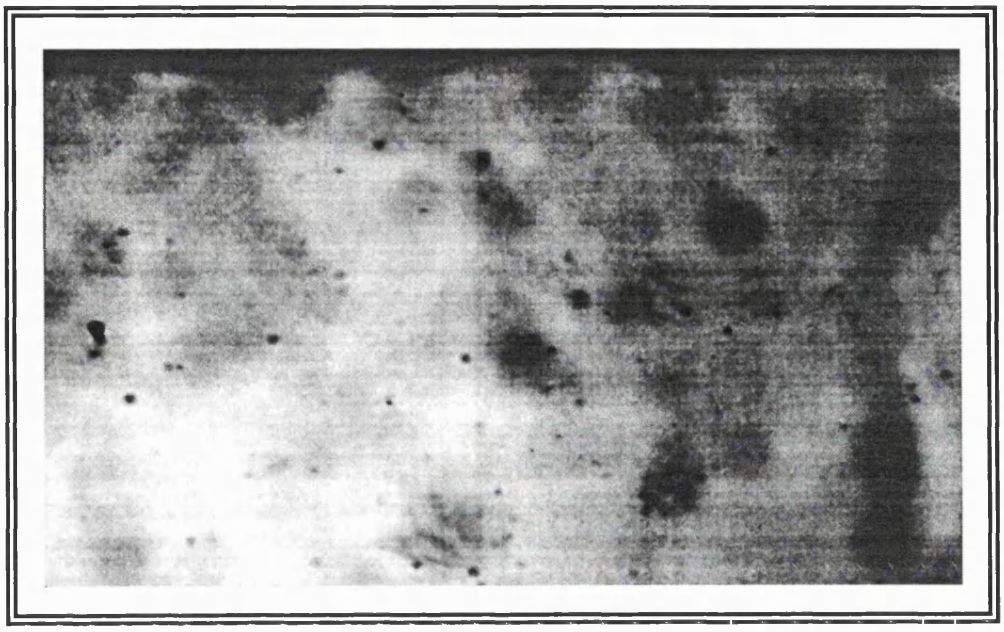

Print 4.6 b: Image recorded along the spark plug centre line, camera 2, 125 °ATDC, open-valve injection, Bosch 4-hole injector, processed data, idle condition

4.5.2 Plane 2: Halfway Between Spark Plug and Quartz Window

In contrast to the previous set of results, a shimmering wave effect could be seen before any fuel droplets appeared. Prints 4.7 a and b show this effect at 95° ATDC although it was first observed at 80° ATDC and continued to be present for most of the tests up until 165° ATDC. At this timing fuel droplets were also present. The wave effect was thought to be due to one of the two following explanations. The first was that fuel was wetting the quartz window on the inlet side and the second was that a sheet of fuel was travelling downwards at a distance away from the bore.

Fuel droplets of varying size were also recorded at 110° ATDC, although for brevity only the image captured with camera 1 is presented (print 4.8). In general, these droplets tended to be of larger size than those captured near the spark plug, although the velocities were similar (3-14 m/s). Images recorded after 110° ATDC indicated no more fuel droplets but again the shimmering effect was observed. The wave effect was most pronounced (with both cameras) at 125° ATDC (print 4.9). This is shown when comparing prints 4.7 a and 4.9. After this it diminished until there was no difference between the background readings and the test runs.

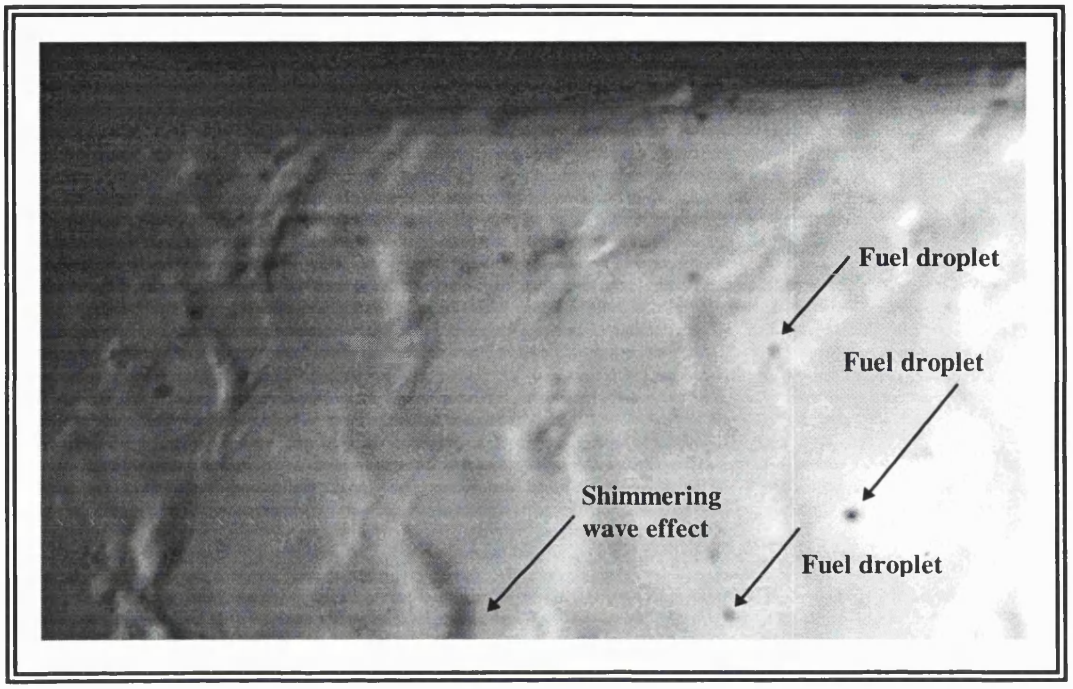

Print 4.7 a: Image recorded half way between the spark plug and quartz window with camera 1, 95 °ATDC, open-valve injection, Bosch 4-hole injector, processed data, idle condition

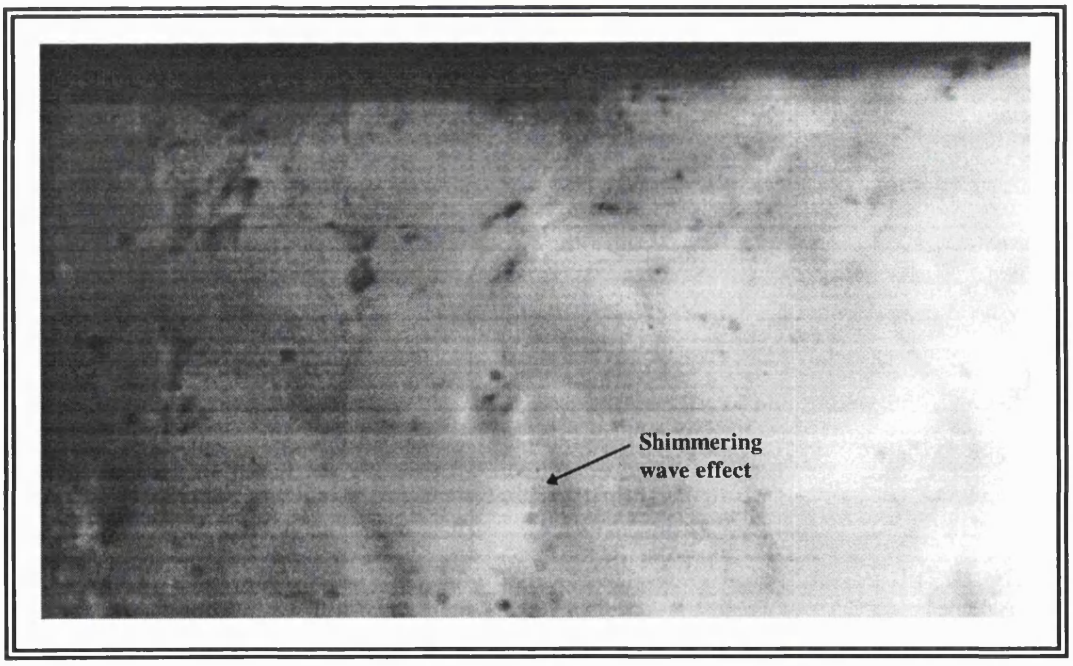

Print 4.7 b: Image recorded half way between the spark plug and quartz window with camera 2, 95 °ATDC, open-valve injection, Bosch 4-hole injector, processed data, idle condition

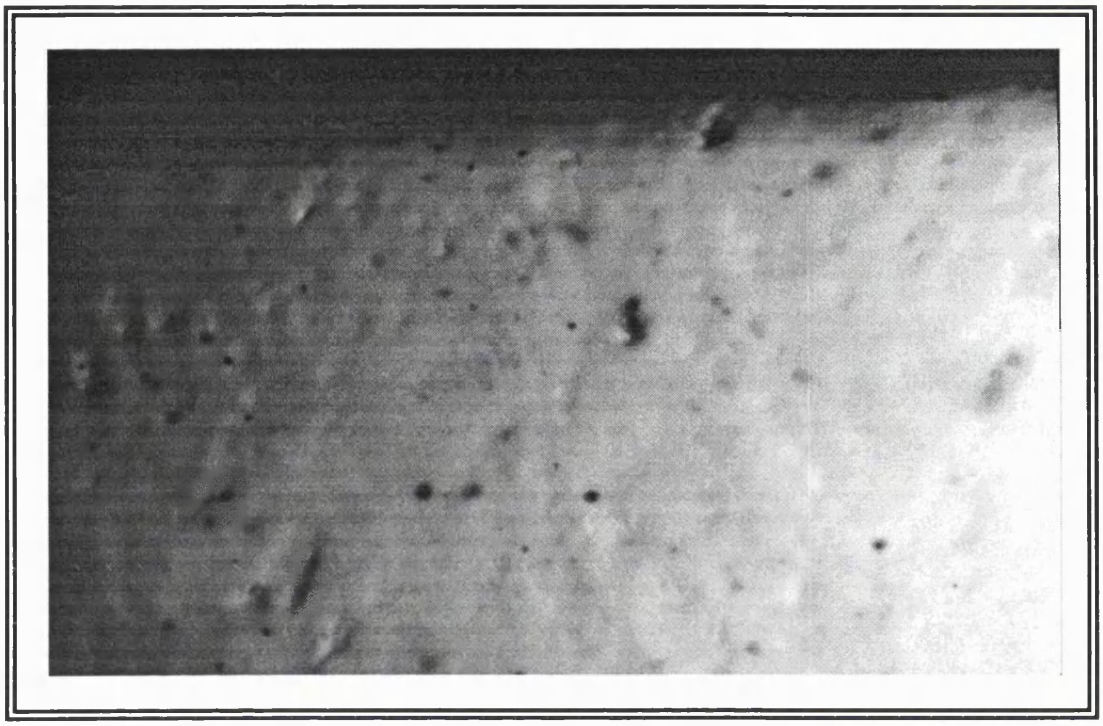

Print 4.8: Image recorded half way between spark plug and quartz window with camera 2, 110 °ATDC, open-valve injection, Bosch 4-hole injector, processed data, idle condition

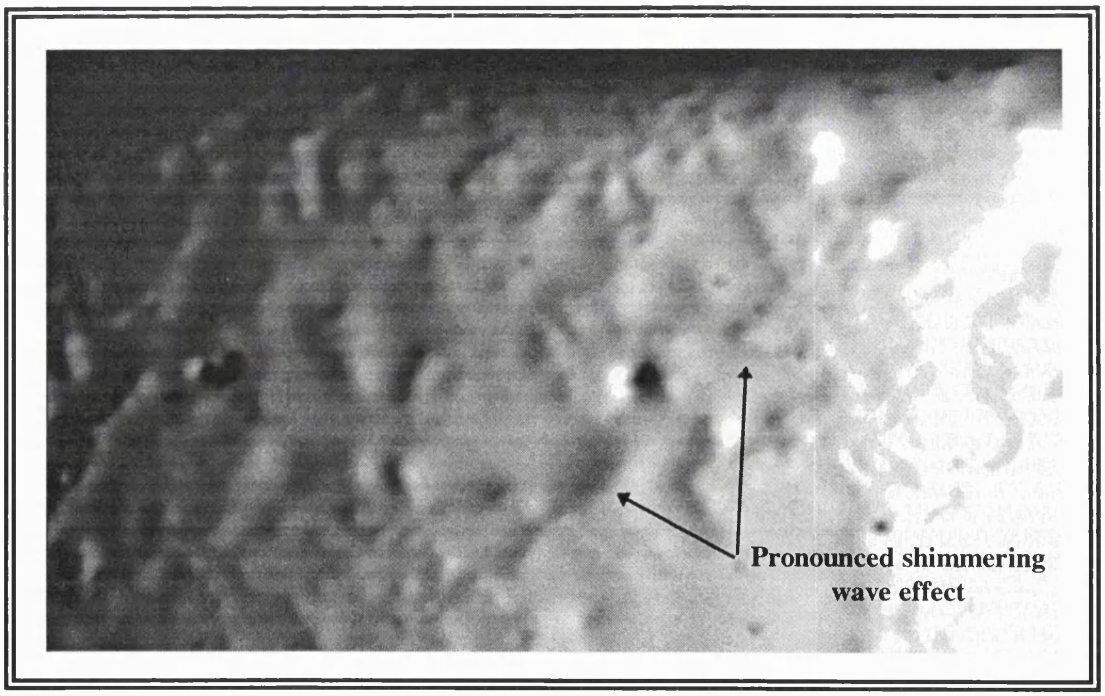

Print 4.9: Image recorded half way between spark plug and quartz window with camera 1, 125 °ATDC, open-valve injection, Bosch 4-hole injector, processed data, idle condition

4.5.3 Plane 3: 5 mm from Back Window

The results recorded in this focal plane showed the most extreme manifestation of the shimmering wave effect recorded between 65°ATDC and 135°ATDC. In fact, the waves were so extreme that they appeared to be more like craters (prints 4.10 a and b). Had the copper-vapour laser been available, it is believed that its higher intensity would have revealed more of the structure of the waves and given a better indication of their nature.

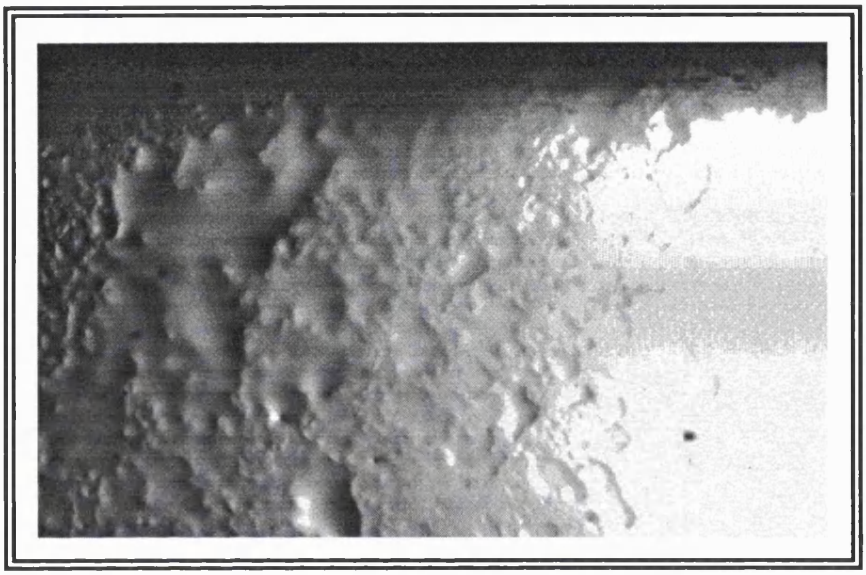

Print 4.10 a: Image recorded 5 mm from quartz window with camera 1, 65 °ATDC, open-valve injection, Bosch 4-hole injector, processed data, idle condition

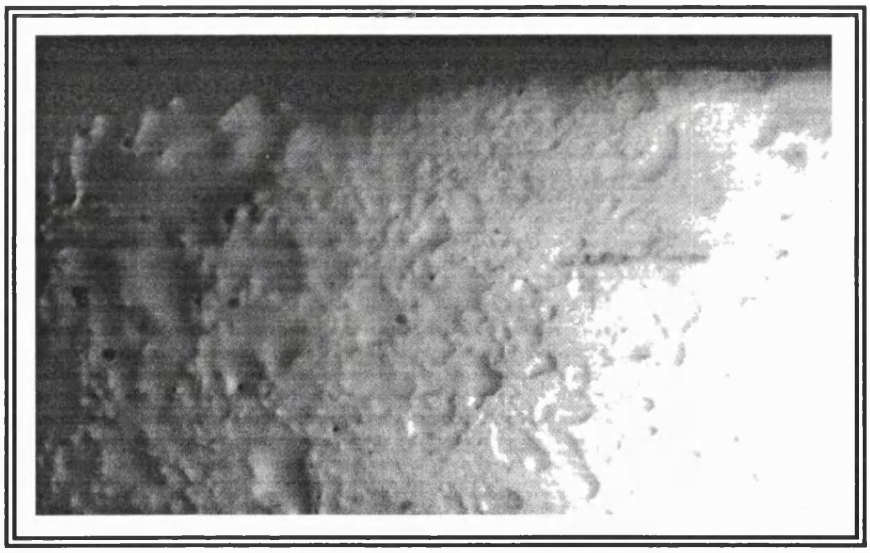

Print 4.10 b: Image recorded 5 mm from quartz window with camera 2, 65 °ATDC, open-valve injection, Bosch 4-hole injector, processed data, idle condition

4.5.4 Plane 4: Back Window

Although a number of tests were carried out at this focal plane, no difference could be seen between the background readings and the test runs themselves. This was taken as fairly positive confirmation that the shimmering wave effect was a sheet of fuel travelling downwards, a few millimetres away from the window, rather than fuel impacted on the window.

4.6 Repeatability of Test Results

The repeatability of the test results was investigated by performing several tests at the same condition. The tests were repeated allowing for a minimal amount of time for the engine to cool back to room temperature and also allowing several hours to pass between the tests. All test results showed good repeatability. The images captured from one of the repeated tests are shown in prints 4.11 a and b for camera 1 and 4.12 a and b for camera 2. The results are from tests repeated at 100° ATDC, along focal plane 2, the engine was allowed to cool for several hours between the tests.

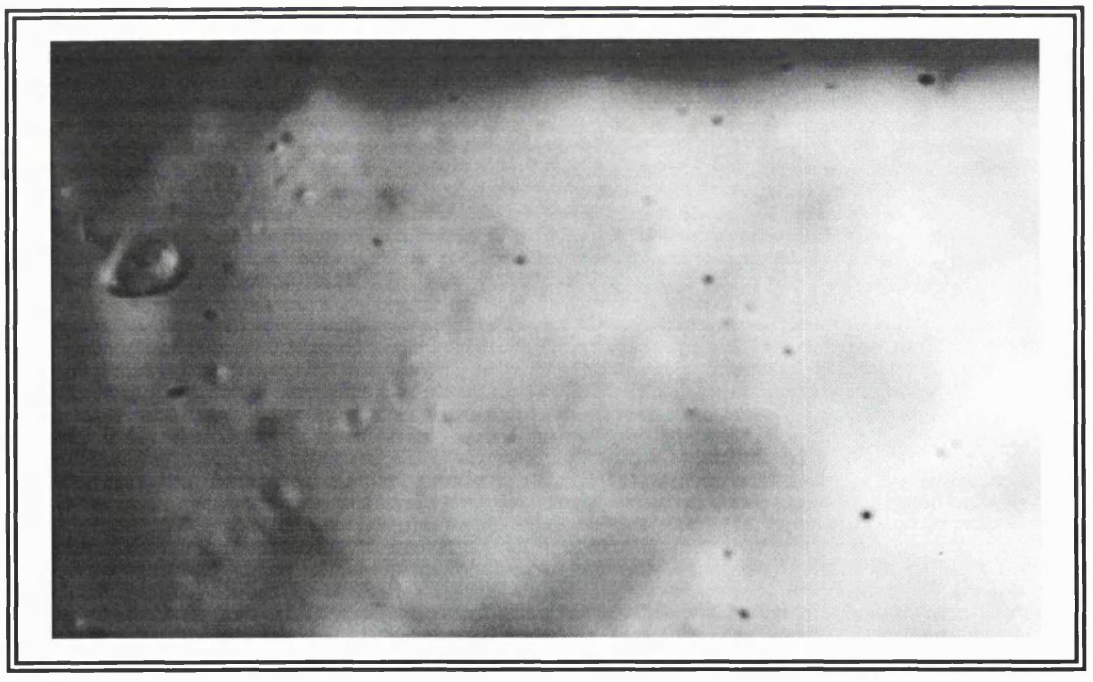

Print 4.11 a: Repeatability of test results, image recorded midway between spark plug and cylinder bore, with camera 1, 100 °ATDC, open-valve injection, Bosch 4-hole injector, processed data, idle condition

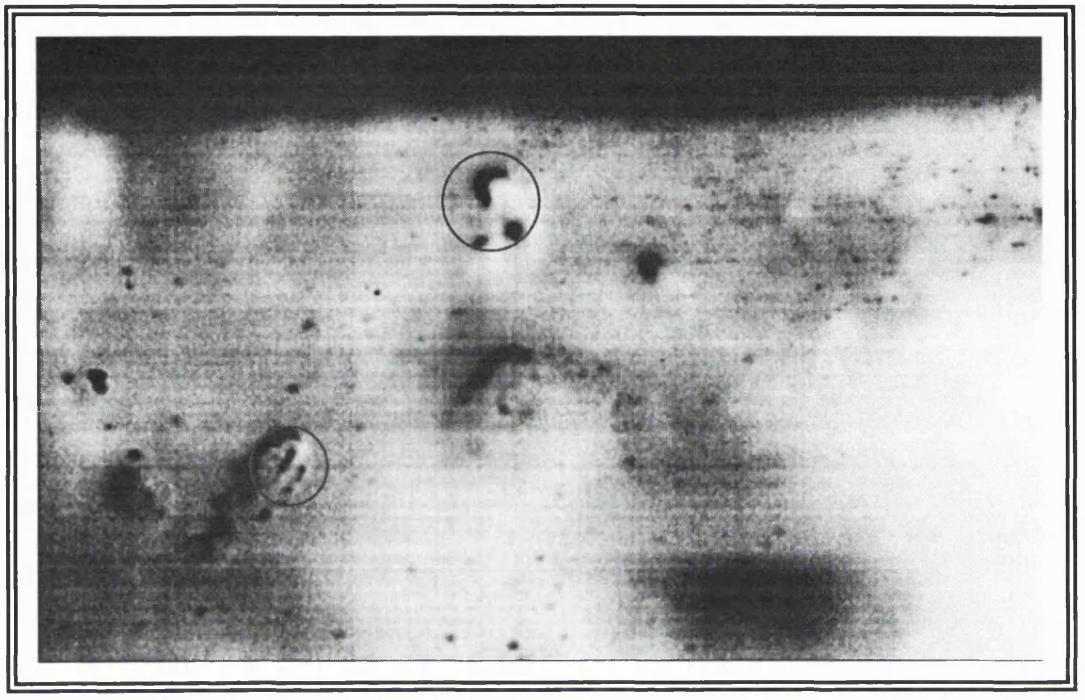

Print 4.11 b: Repeatability of test results, image recorded along focal plane 2 with camera 1, 95 °ATDC, open-valve injection, Bosch 4-hole injector, processed data, idle condition

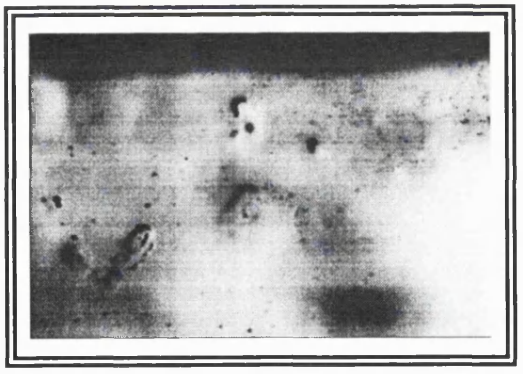

Print 4.12 a: Repeatability of test results, image recorded along focal plane 2, with camera 2, 95 °ATDC, open-valve injection, Bosch 4-hole injector, processed data, idle condition

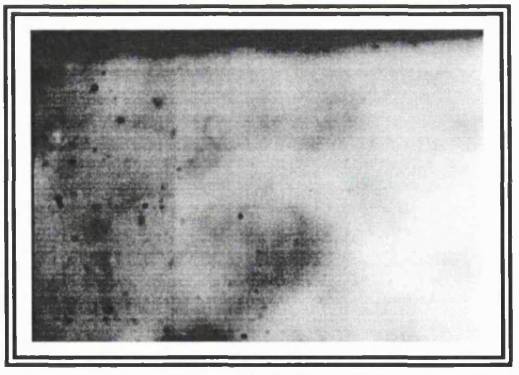

Print 4.12 b: Repeatability of test results, image recorded along focal plane 2, with camera 2, 95 °ATDC, open-valve injection, Bosch 4-hole injector, processed data, idle condition

4.7 Concluding Comments

The results of this chapter have provided further evidence of how the liquid fuel enters the cylinder in the design of engine tested. The high-speed cine results described in the first part of chapter 2 indicated that a significant amount of fuel was impacting on the

piston crown, but it was not clear whether or not fuel was landing on the cylinder bore. The wall skimming tests described in the later part of chapter 3 showed that virtually no fuel was present on the bore walls which was partially validated by the endoscope visualisation technique. With this method it was not possible to record the fuel entry characteristics. The spark flash images described in this chapter provide evidence of a significant quantity of liquid fuel travelling vertically downwards a few millimetres away from the cylinder bore on the inlet side of the inlet valves.

Furthermore, the work has demonstrated that it is possible to record images of liquid fuel droplets and films within the cylinder of a firing IC engine using a relatively low intensity light source. The spark flash light source is a relatively low cost unit (circa £6000) and consequently is readily available. In contrast, the copper-vapour laser used for the tests described in chapter 3 is a high cost item (circa £80 000) and was only available on loan from the EPSRC loan pool for a 3-month period, or on hire for a shorter period. The testing showed that useful results could be obtained with the spark flash unit although the extra intensity of the copper-vapour laser would have benefited the quality of the images in most cases. A brief comparison of the light sources is given in table 4.1.

	Duration	**Pulse energy**	**Wavelength**
Spark Flash	100ns-1μs	1-10 J	White light
Copper-vapour laser	10-40ns	2 mJ (max)	510-6-578.2 nm

Table 4.1: Comparison of copper-vapour laser and spark flash unit

The test results from each condition have also been summarised and are presented in table 4.2 on the following page.

Focal Plane	Timing	Individual Droplets Observed Camera 1	Camera 2	Grade	Clusters of Droplets	Shimmering Effect
1	80° ATDC	Yes	No	1	Possibly	No
	95° ATDC	Yes	Yes	4-5	No	No
	110° ATDC	Yes	Yes	1	Possibly	No
	125° ATDC	Yes	Yes	3	Possibly	No
	135° ATDC	Yes	Yes	2-3	Possibly	No
	150° ATDC	Yes	Yes	1-2	Possibly	No
	165° ATDC	Possibly		1	Possibly	No
	180° ATDC	Possibly		1	Possibly	No
	195° ATDC	No	No	-	No	No
	210° ATDC	No	No	-	No	No
2	80° ATDC	No	No	-	Possibly	Yes
	95° ATDC	Possibly		1	No	Yes
	110° ATDC	Yes	Yes	5	No	Yes (Slight)
	125° ATDC	No	No	1	No	Yes
	135° ATDC	No	No	-	Possibly	Yes (Slight)
	150° ATDC	No	No	-	No	Yes (Slight)
	165° ATDC	No	No	-	No	Yes (Slight)
	180° ATDC	No	No	-	No	Possibly
	195° ATDC	No	No	-	No	No
	210° ATDC	No	No	-	No	No
3	80° ATDC	No	No	-	No	Fuel Film
	95° ATDC	No	No	-	No	Fuel Film
	110° ATDC	No	No	-	No	Fuel Film
	125° ATDC	No	No	-	No	Fuel Film
	135° ATDC	No	No	-	No	Fuel Film
	150° ATDC	No	No	-	No	Fuel Film
	165° ATDC	No	No	-	No	No
	180° ATDC	No	No	-	No	No
	195° ATDC	No	No	-	No	No
	210° ATDC	No	No	-	No	No
4	No difference noted between background and test results					

Grading system: Grade 1 = one or two droplets present
Grade 5 = large number of fuel droplets

Table 4.2: Summary of test results

Chapter 5

Fuel Injection Mounting Block for Achieving Stratified Charge

5.1 Introduction

The overall conclusion from the first part of the project was that there was considerable similarity between the three injection systems tested in terms of behaviour of the fuel once it reached the cylinder. The high-speed cine photography showed that the fuel impacted on the piston crown for all three types of injector, open or closed-valve injection. The skimming tests showed that negligible amounts of fuel were impacting on the cylinder wall in each case, and this was further confirmed by the more limited photographic investigations using the spark flash for illumination. These results were considered to be very satisfactory as impaction on the cylinder bore would have led to higher levels of UHC emissions resulting from some of the impacted fuel finding its way into the crevice volume above the to piston ring, particularly when the engine was cold. It is inevitable that the majority of fuel entering the cylinder in the form of droplets will impact on some surface, as only exceedingly small droplets (less than 20 μm in diameter) stand any chance of following the air flow. It is preferable that the droplets should impact on the piston rather than the cylinder bore.

In view of the similarity between the performance of the three injection systems, it was interesting to make comparisons with results obtained from emissions tests performed by Shayler *et al* (1996) with the same injection systems. They reported very similar results between the same injection systems when the engine was fully warm. There were some differences in emission results between the systems during the warm-up period, but these could be attributed to the different ways in which fuel was deposited on the walls of the intake ports

The results of the first part of the project were discussed with the sponsor, and it was agreed that the project should continue by concentrating on developing a more advanced

fuelling concept as no obvious detail improvements could be made to the standard arrangement. It was decided to attempt the development of a port-injected, stratified-charge, approach in view of the advantages of such an arrangements (1.10.5.1.2). The concept is discussed in the next chapter, and the early stages of its development in the remainder of the chapter.

5.2 Concept

A fuel injection mounting system was proposed to promote stratification within the 4–valve SI optical engine. The system incorporated a pencil-jet fuel injector positioned in one of the inlet ports, downstream of the bifurcation, such that the solid column of fuel produced from the injector was targeted at an open inlet valve (figure 1 a). In this manner it was hoped that the fuel spray would be deflected by the open inlet valve in the direction of the spark plug, and remain there up to the point of ignition. Axial swirl was induced in the cylinder at part load conditions through deactivation of the second inlet port, achieved for the purposes of initial testing by sealing a brass insert into the port (figure 5.1 b). It was thought that the relatively ordered air flow structure that existed with axial swirl would serve to maintain a rich central core around the spark plug and a leaner mixture elsewhere in the combustion chamber.

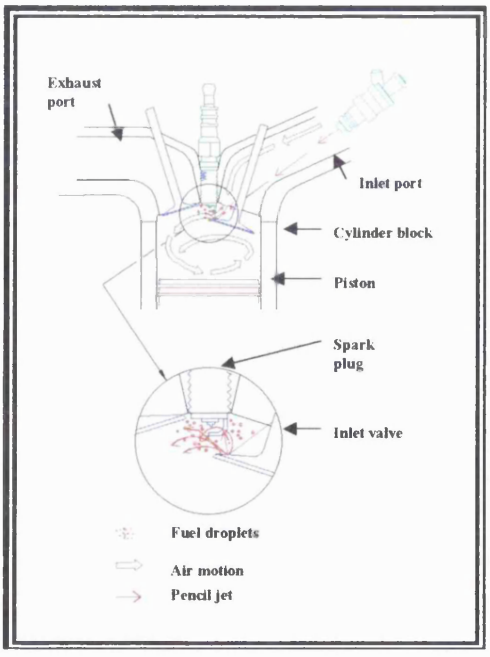

Figure 5.1 a: Concept of stratification (side view)

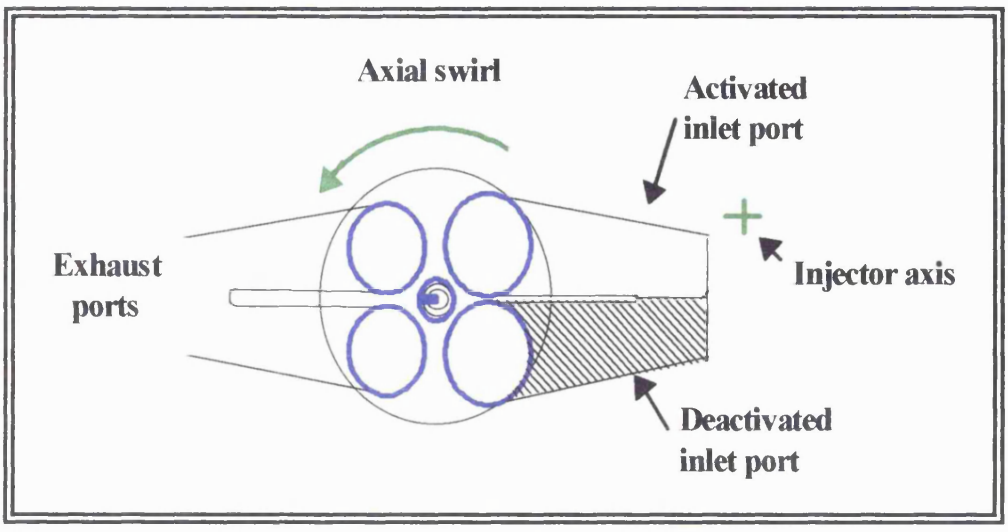

Figure 5.1 b: Concept of stratification (plan view)

5.3 Development of Concept: Injector Type and Positioning

The initial development of the concept concentrated on the targeting of the fuel injector, such that the impaction point of the fuel column on the inlet valve resulted in the greatest quantity of fuel terminating around the spark plug.

5.3.1 Pencil-Jet Injectors

Two injectors were used for this investigation; a low flowrate Weber pencil-jet injector (part number 95BF-BA) with a nominal cone angle of 5°, and a high flowrate pintle-type Bosch injector (part number 88WF–A1A). The Weber pencil-jet injector was the only pencil-jet injector available at the start of the development period and was considered to be adequate for the development of the fuel injection mounting system and the testing to be carried out at the lowest engine speed of 880 rpm. However, it was obvious that for the concept to work at higher engine speeds, a high flowrate injector would be required to keep the injection period as short as possible relative to the inlet valve opening period. Since no high flowrate pencil-jet injectors were available at the time of testing, it was necessary to modify a pintle injector and so its tip was ground as shown in figure 5.2 to produce a pencil-jet spray. The flowrate of the modified injector was typically 8.2 mg/pulse with a fuel pulsewidth of 7 ms as compared with the flowrate of the Weber injector of 14.6 mg/pulse for the same pulsewidth.

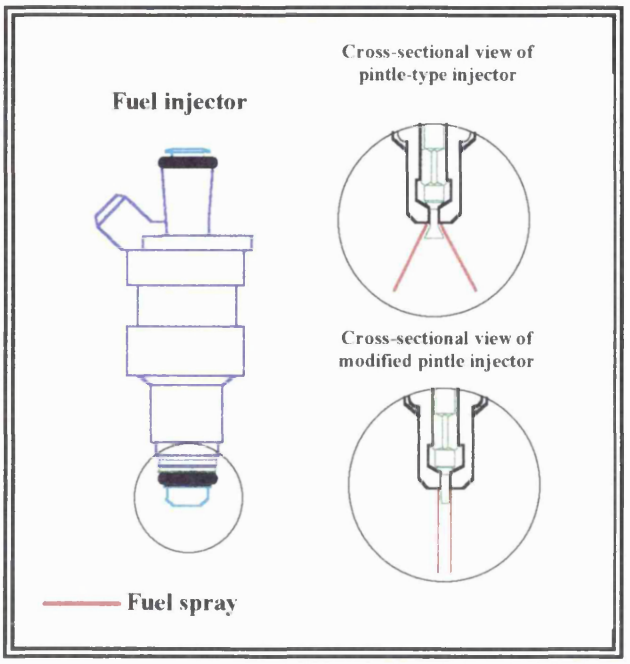

Figure 5.2: Modified pencil-jet injector

Images were recorded for both injectors spraying into quiescent air to determine the distance the fuel spray remained intact. Plates 5.1 a–b show the images recorded for the low flow rate injector, first with the fuel injector in view and then 80 mm downstream when the pencil jet begins to break up. For the low and high flowrate injectors, the fuel remained as a solid column for approximately 80 mm before it began to break up. It was thought that this was the *minimum* distances the fuel spray would remain intact, as under running engine conditions the depression established in the inlet manifold would aid the fuel column remaining intact over a longer distance (Williams *et al* (1994)).

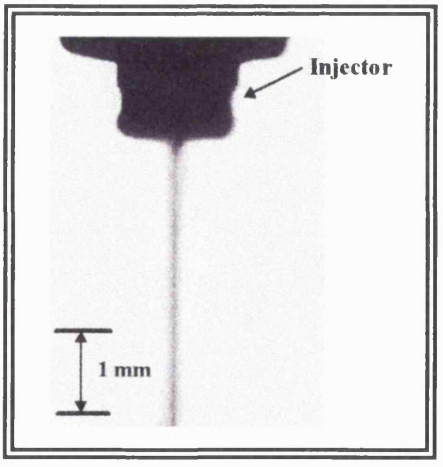

Plate 5.1 a: First section of fuel spray for low flowrate injector (95BF-BA)

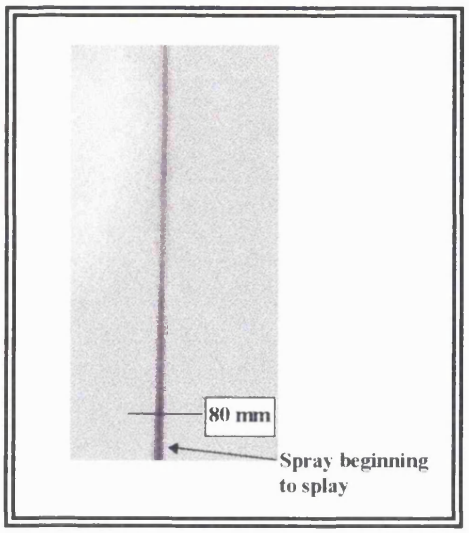

Plates 5.1 b: Lowest section of fuel spray for low flowrate injector (95BF-BA)

5.3.2 Development Test Rig

A test rig was designed and manufactured to allow the position of the pencil-jet fuel injector to be altered with respect to a section of the cylinder head. It was assumed that under low load conditions, the airflow would not deviate the pencil-jet fuel spray significantly and so the initial development work was carried out without airflow. The front section of one of the inlet ports was removed in order to facilitate the observation of the fuel spray (plate 5.2). For a particular injector location and valve lift, observation was made as to where the column of fuel impacted and the subsequent behaviour of the liquid fuel after impaction.

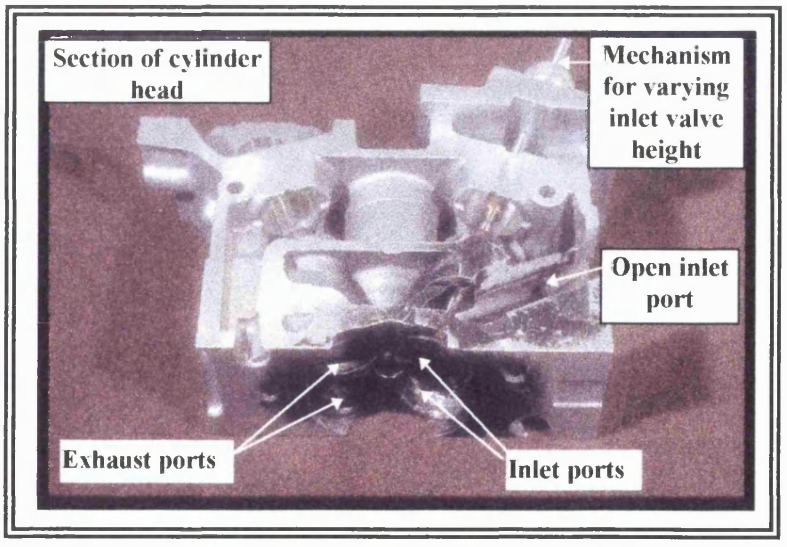

Plate 5.2: Injection mounting development test rig

5.3.3 Recording the Direction of Deflected Fuel Spray

Although visual observation of the fuel spray before and after it impacted on the inlet valve was relatively easy, some means of recording the direction of the deflected fuel spray for a particular injector location was required. An investigation into the different droplet sizing techniques available was carried out (appendix B), as it was thought that it would be possible to readily adopt one of them to obtain information on fuel spray distribution around the inlet valve for the current application.

Having reviewed the droplet sizing techniques, it was decided to simplify matters and concentrate on recording the overall behaviour of the spray as opposed to measuring the droplet size distribution and velocities. A very simple, but effective, method was chosen to record the fuel spray distribution, and it was a variation on a mechanical droplet sizing technique that involved the spray impacting on a coated glass slide (Williams (1976)). The method chosen used circular absorptive impaction plates mounted onto the base of the inlet valve. The plates were kept in position with a metal disc that could be removed, and which allowed the circular absorptive impaction plates to be replaced at the start of each test (figure 5.3).

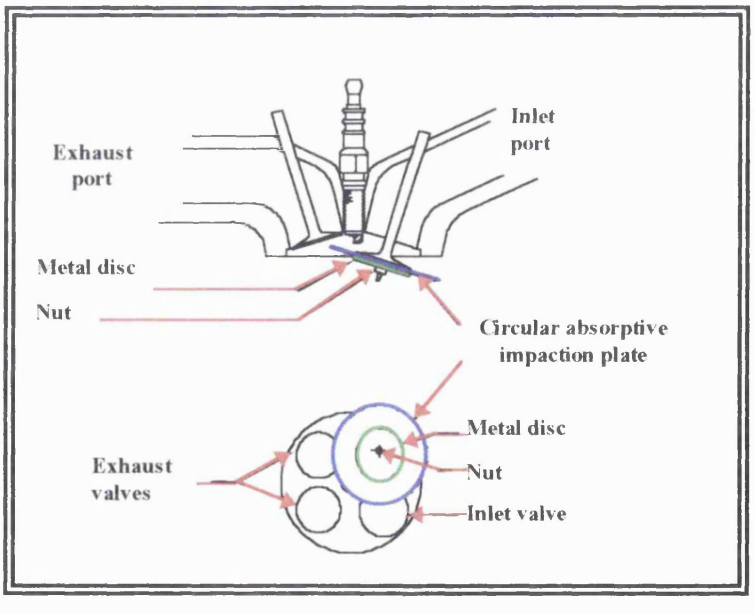

Figure 5.3: Mounting of the circular absorptive impaction plates

The fuel was dyed red with a biological reagent (Michrome Oil Red 'O'), in order to

facilitate observation of the fuel spray on the impaction plates. The result was a red area on the plate where fuel had impacted, and this was immediately traced around. Knowing the position of the impaction plate and, in particular the position of the dye mark relative to the face of the inlet valve, meant that the overall direction of the deflected fuel spray could be deduced. Some initial work was carried out to see if the dye had an effect on the pencil-jet qualities of the injector. Two results are shown in plates 5.3 a and b in which the injector is sprayed into quiescent air with and without dye added. The injector calibration was also checked with and without the addition of dye and it was found that the differences were very small indeed.

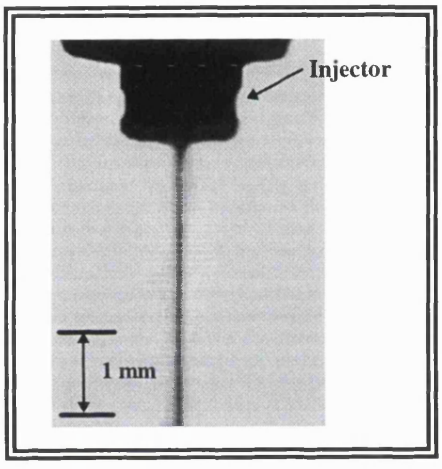

Plate 5.3 a: Injection with dye

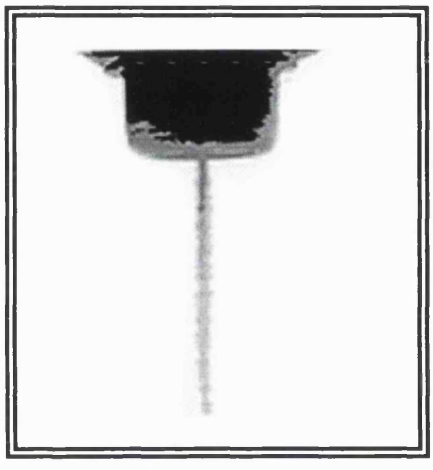

Plate 5.3 b: Injection without dye

For a range of injector locations, the valve lift was decreased from a maximum valve lift of 8.0 mm to a valve lift of 3.0 mm in increments of 1.25 mm, and the fuel spray distribution was recorded on the impaction plates for each case. Approximately twenty different injector positions were investigated. Comparison of the impaction plates for different injector locations enabled an optimum injector position to be chosen (figure 5.4) which appeared to fulfil the objectives.

It was recognised that, since the initial development was carried out under ambient and quiescent conditions, no account could be taken of the effect the airflow would have on the liquid fuel once it had impacted and been formed into droplets. Indeed the method chosen for recording the direction of the deflected fuel spray would not be suitable for use with airflow as the impaction plates would cause significant disruption to the

around the inlet valves. Although the method of recording the fuel distribution did provide a good indication of the general direction of the fuel spray, it could not distinguish between the direction of the individual droplets. It was decided that some means of incorporating a variable injector location into the fuel injection mounting block was needed to take account of any effect that the airflow might have on the deflected fuel spray under actual engine running conditions.

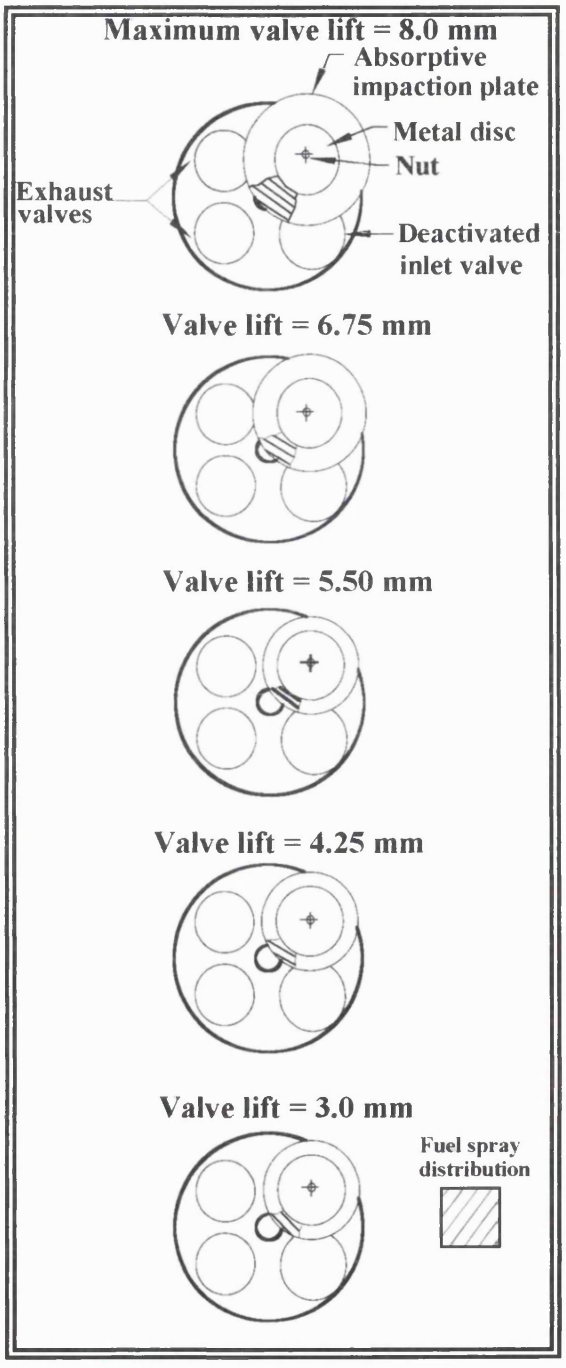

Figure 5.4: Impaction plates for most promising fuel distribution

5.3.4 Photographic Investigation

A CCD camera and illumination system were set up in order to investigate the effect that the injector location, fuel pulsewidth and fuel supply pressure had on the direction of the deflected fuel spray. The photographic arrangement also provided an opportunity to validate the trends recorded with the circular absorptive impaction plates for the different injector locations previously described. The work carried out was performed with a new low flowrate injector of the same type but which had had no dye passed through it.

Two camera locations were chosen. The first camera position recorded the fuel spray as it impacted on the inlet valve, and the second the fuel spray as it emerged into the combustion chamber after it was deflected off the inlet valve. Illumination was provided by conventional photographic flash guns which were positioned so as to illuminate the area of interest uniformly. They were chosen over the spark flash unit due to their compact size which allowed them to be mounted in positions to give even illumination. Significant preparatory testing was required to identify the optimum position for the flash guns.

The flash guns were triggered simultaneously and the duration of illumination was approximately 1/8,000 of a second which was not sufficiently fast enough to freeze the fuel spray in motion. Consequently, a streaking effect of the fuel occurred on the recorded images. Rather than detracting from the images, the streaking of the fuel spray indicated the path of the fuel spray. Plates 5.4 a-b show results for both views taken with the injector at the 'optimum' location and at maximum valve lift 10 ms after the start of injection.

The position and orientation of the fuel injector were found to be critical if the fuel was to be deflected in the intended way. This is borne out in plate 5.5 which shows how the fuel distribution may be significantly altered by moving the injector away from its optimum orientation. A proportion of the fuel no longer impacted on the inlet valve and the deflected spray no longer travelled towards the spark plug (plate 5.5). The

corresponding distribution on the plates is shown in figure 5.5. In contrast plate 5.4 a taken at the optimum injector location, shows, all the fuel to travel across the spark plug region. On the running engine it was hoped that the swirling air motion would take up the deflected fuel spray preventing the larger droplets from travelling across the streamlines, thus maintaining a rich central core and a leaner mixture elsewhere.

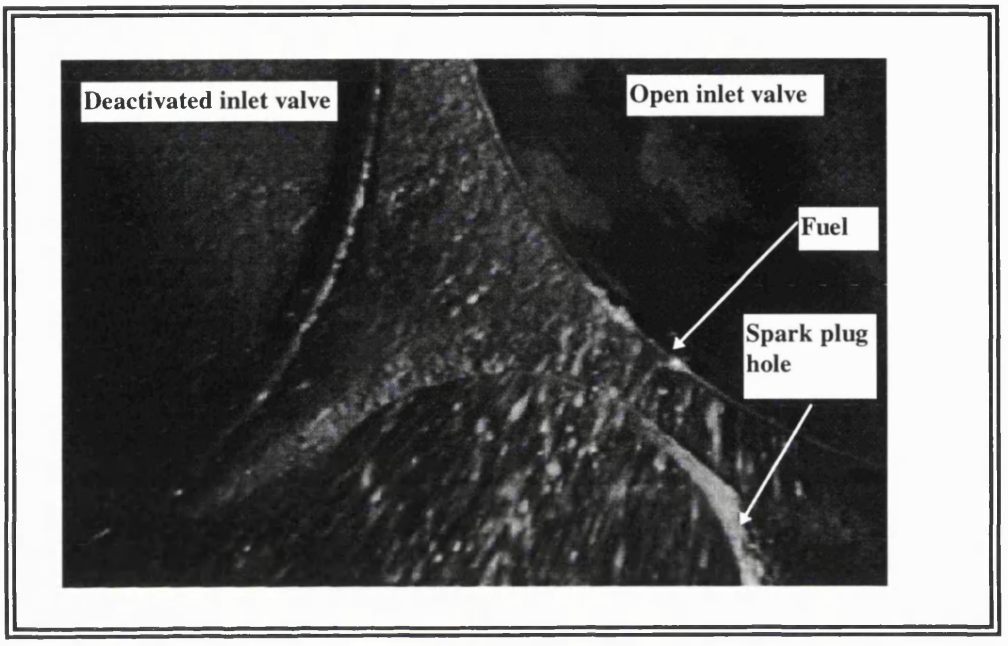

Plate 5.4 a: Optimum injector location, global view, fuel pressure 3.5 bar, injection period 7 ms, maximum valve lift

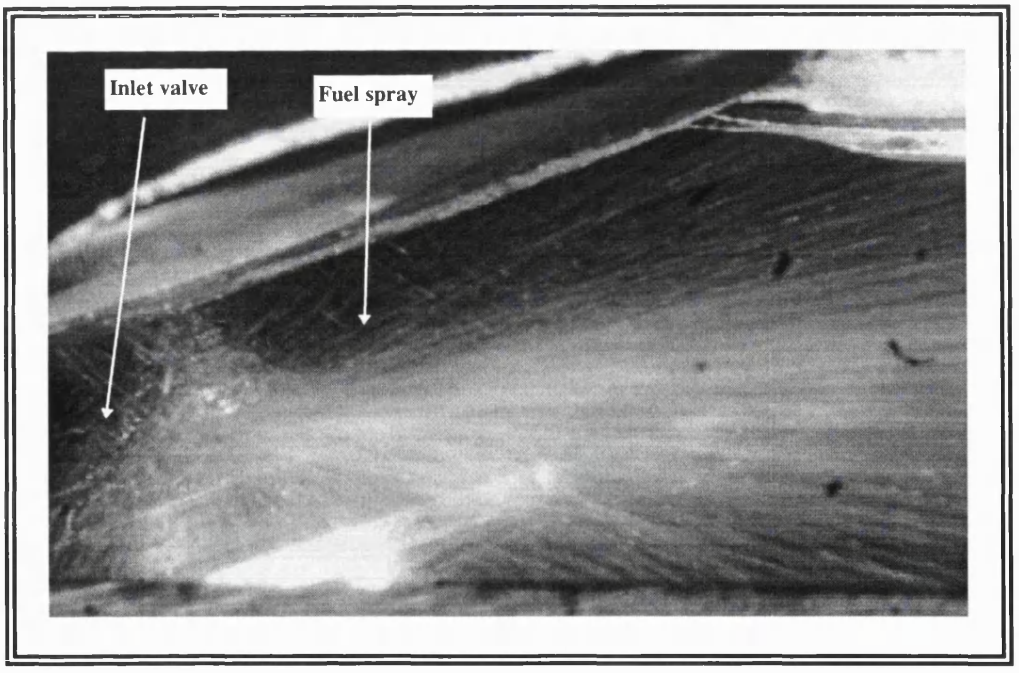

Plate 5.4 b: Optimum injector location, side view, fuel pressure 3.5 bar, injection period 7

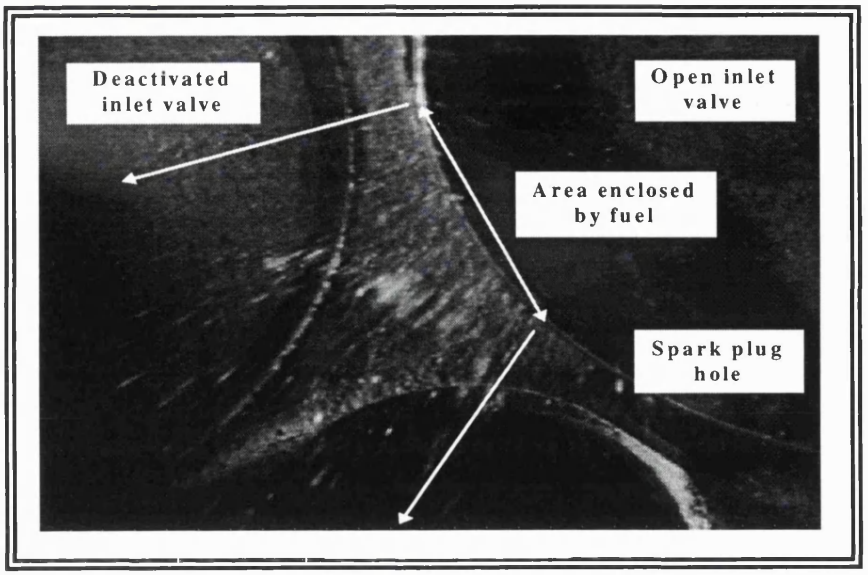

Plate 5.5: Injector moved away from optimum orientation, global view, fuel pressure 3.5 bar, injection period 7 ms, maximum valve lift

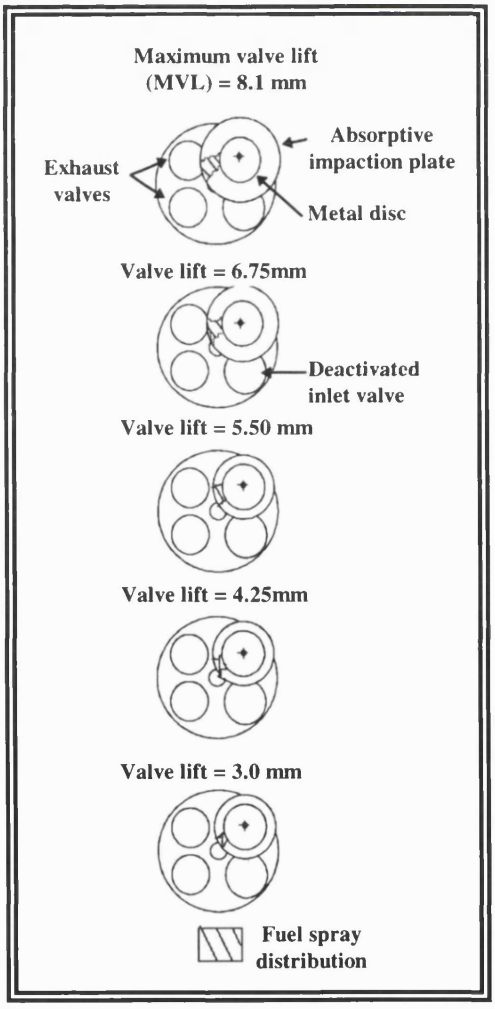

Figure 5.5: Fuel spray distribution on circular absorptive impaction plate for injector location away from the optimum

The images taken after fuel injection had ended (image recorded 19 ms after the start of injection) showed fuel to be present in the atmosphere around the valve and also to be dripping from the inlet valve. Indeed fuel can be seen starting to drip from the valve even during the injection period very slightly (9 ms after the start of injection (plate 5.6)) and becoming more pronounced with increasing delay. It was thought that with airflow the dripping effect would be affected by a tendency for the fuel to become entrained in the air stream.

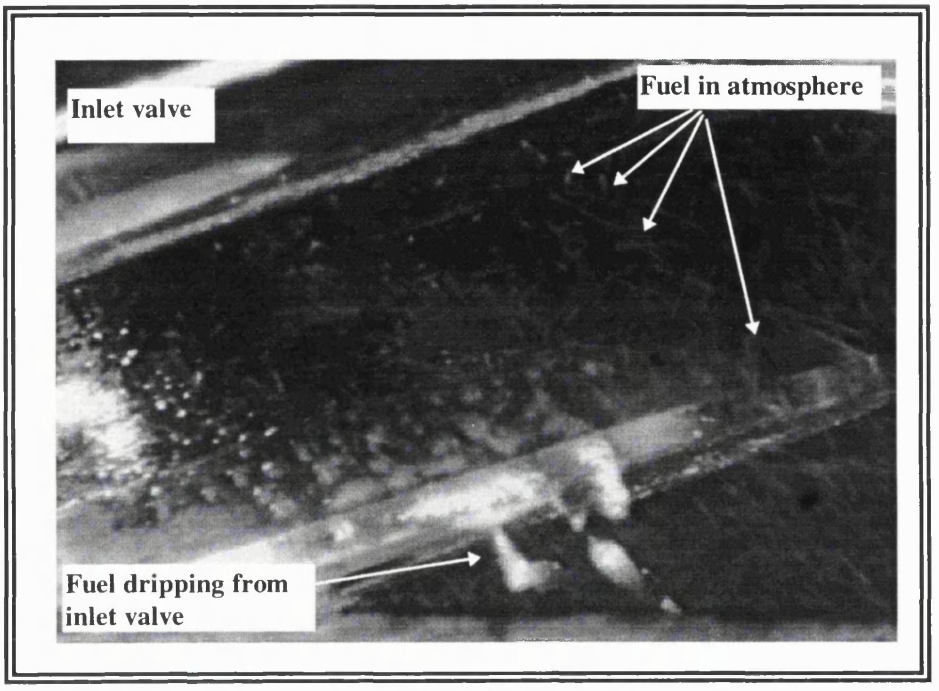

Plate 5.6: Injector at the optimum location, global view, fuel pressure 2.7 bar, injection period 9 ms, maximum valve lift

5.4 Design of Injector Mount

Based on the optimum position and orientation of the injector identified from these tests, an injector block was designed and manufactured (plate 5.7) which positioned the injector at this optimum location when mounted onto the single-cylinder research engine (chapter 2). Some movement of the injector within the mounting block was afforded in two planes to investigate the effect of small movements away from its optimum location (figure 5.6). It also allowed adjustments to be made to compensate for the effects of airflow on the deflected fuel spray in the light of engine running experience.

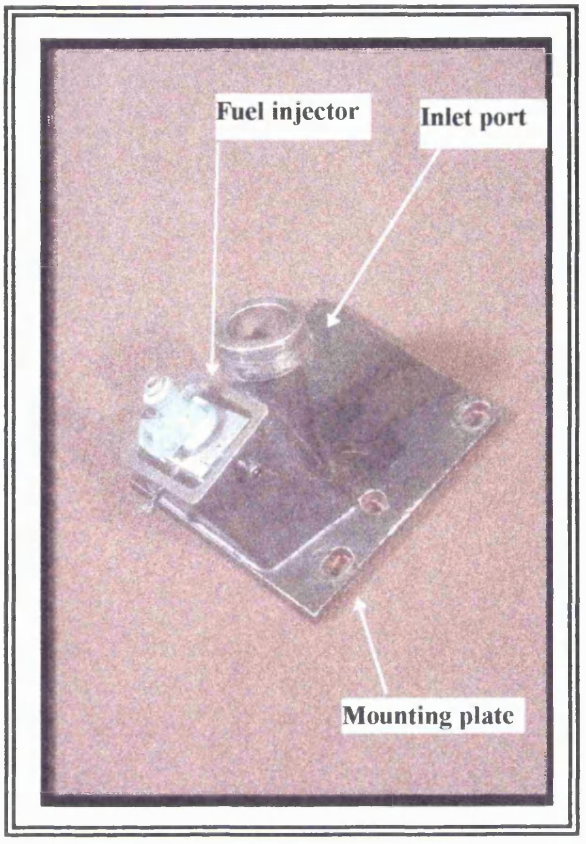

Plate 5.7: Injector mounting block

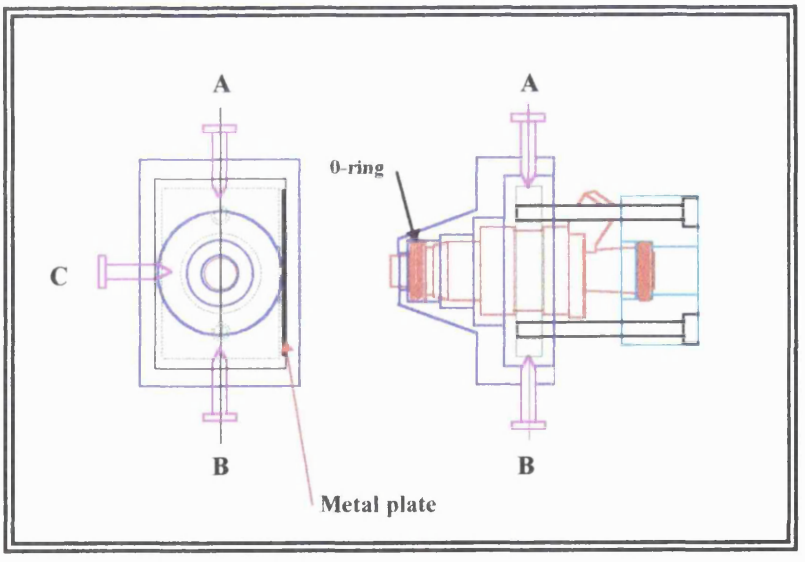

Figure 5.6: Description of injector movement

Considering figure 5.6, the fuel injector was gripped and sealed by the O-ring at the end from which the fuel was injected. The 0-ring, in turn was located through its fit in the bore of the mounting block. At its centre, the injector was held by 3 screws (A, B and C) and a metal plate allowing adjustment in two planes

5.5 Impaction of Liquids on Surfaces

Since the manner in which the fuel spray impacted on the inlet valve was a key element to the fuel being directed in the appropriate direction, an investigation into the impaction of liquids on surfaces was carried out.

The hydrodynamic details of droplet-droplet and droplet-liquid film interactions on solid surfaces are believed to have a significant role in spray impingement phenomena (Al-Roub *et al* (1996)). The characteristics of the spray prior to impaction (the kinetic energy, the Weber number and the distribution of the droplets) and the characteristics of the impaction surface (surface finish and temperature) will also affect the impaction process and whether the spray impacts and bounces off the surface, or whether a liquid film is formed on the surface, or both. After the initial impaction, further interactions occur between the droplets which affect the secondary atomization and coalescence processes, and the stability of any film formed. Several researchers have looked at the thermal effects on droplet impaction and lifetime, and have attempted to model various processes such as the evaporation and ignition of fuel droplets on a surface, droplet dynamics and heat, mass and momentum transfer (Dwyer *et al* (1984), Dwyer *et al* (1994), Gulder *et al* (1984)). These models tend to be relatively simple and do not cover the range of droplet impaction processes that can occur.

Useful experimental data on impaction processes is hard to obtain, since over-simplification (e.g. single droplet collision) does not take into account the effect other droplets would have on the impaction process, whilst more complex systems may obscure what is happening and the understanding of the processes involved. Al-Roub *et al* (1996) carried out extensive experimental work to observe the characteristics of 1, 2 or 3 droplets impacting onto a film of fuel situated on a surface normal to the axis of the droplets, with the liquid in different stages of boiling (figure 5.7). This was thought to be applicable to the work carried out here since some of the spray that impacted on the inlet valve is likely to spread out and form a film (figure 5.7).

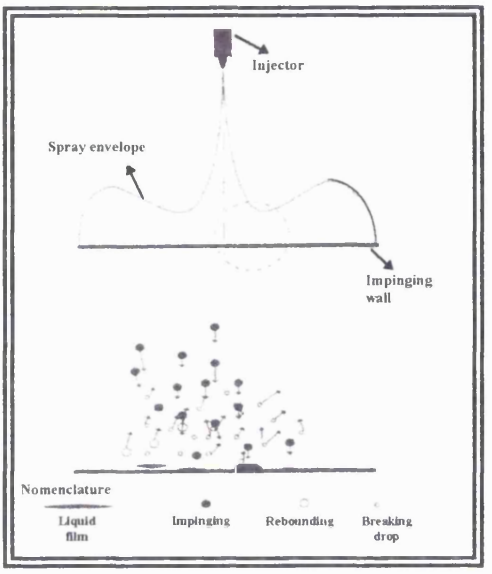

Figure 5.7: Formation of a fuel film on the inlet valve [Al-Roub *et al* (1996)]

Al-Roub *et al* observed that multiple droplet impactions onto the liquid film gave the potential for breaking up the film. The most significant factors as to whether the film broke up or not was the kinetic energy (KE) of the droplets and the thickness of the film. However, the timing and distribution of the impacting droplets also had an effect, since these factors would determine whether constructive or destructive wave interference occurred throughout the liquid film. If constructive wave interference occurred, the film would destabilise and eject some of its mass as droplets with considerable momentum. These would then undergo a secondary atomization process with a proportion of the droplets breaking up into smaller droplets while others coalesced with adjacent droplets. The potential for breaking the film up diminished with increased Weber number when the droplet diameters were held constant.

The impaction processes involved with the new injector arrangement are even more complex due to the angle of impaction, the curved impaction surface and the impaction of a solid column of fuel as opposed to individual droplet impaction. Nevertheless some insight can be gained as to how the droplets may be formed by the impaction of the fuel jet onto the back of the valve. Hardalupas *et al* (1992) used PDA to investigate the spray impinging on a disc at surface angles of 0°, 20° and 45° to the horizontal (the 20° angle being the most appropriate to this work). The injector tip was 40 mm away from the disc. They found that the Sauter mean diameter for the injector spray impacting on the

20° plate was 80-120μm which covered a greater range (and greater average diameter) than for the other two plate angles. They concluded that this was because of the reatomisation of the liquid film on the plate. Indeed the size and range of droplets produced by reatomisation processes was very dependent on the resultant angle between the fuel spray and impaction plate. Almost all the droplets that left the plate inclined at 20° were generated by reatomisation.

5.5.1 Surface Temperature Effects

In order to consider the effect surface temperature (in this instance the temperature of the valve), it is necessary first to look at the variation of the temperature of an inlet valve with time. Shin *et al* (1994) measured the temperature in the inlet port 43.0 mm from the cylinder entrance and also at two points on the inlet valve (figure 5.8 a and b). The valve was pinned to prevent the valve from rotating on its seat and the results for closed-valve injection are shown in figure 5.9 a. The surface temperature of the inlet valve at point B was higher than that at A because the distribution of the back flow of exhaust gases into the inlet port was biased around point B (point B being closer to the exhaust valve than point A, and also the back flow of the gas was restricted around point A because of the close proximity of the cylinder wall).

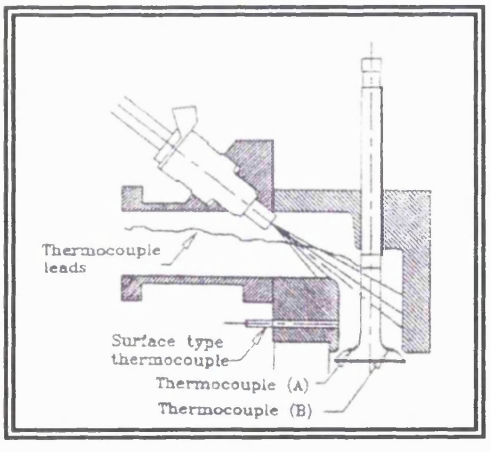

Figure 5.8 a: Location of thermocouples, side view [Shin *et al* (1994)]

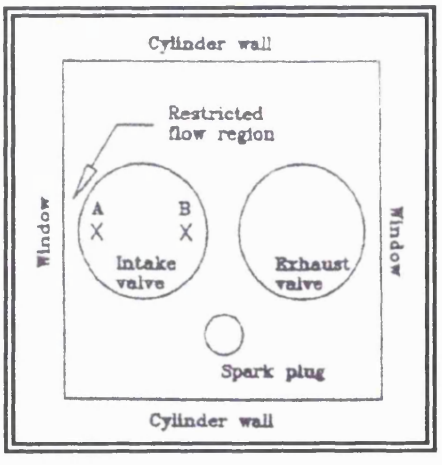

Figure 5.8 b: Location of thermocouples, plan view [Shin *et al* (1994)]

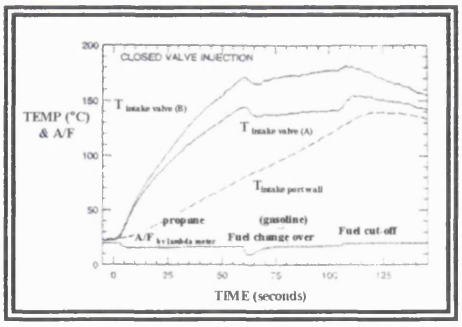

Figure 5.9 a: Temperature distribution across an inlet valve [Shin *et al* (1994)]

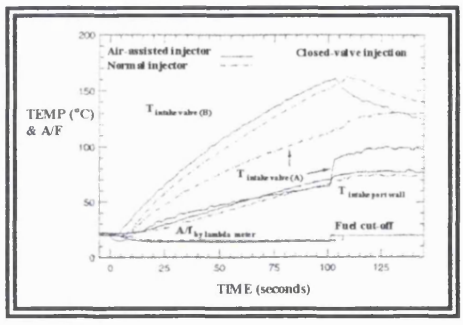

Figure 5.9 b: Temperature distribution across an inlet valve for different impaction regimes [Shin *et al* (1994)]

Considering figure 5.9 a, in the first 60 seconds propane was used as the fuel to eliminate the cooling effects the fuel would have on the valve, and from 60-120 seconds a standard grade of gasoline was used. Changing the fuel from propane to standard petrol decreased the surface temperature of the valve by approximately 10 °C indicating that the gasoline had a cooling effect on the valve. The greater the fuel impaction, the greater this cooling effect was found be (figure 5.9 b).

Developing this further it is necessary to take into account the possibility of a vapour cushion forming on the inlet valve when the fuel impacts onto a hot valve. The formation of the film vapour is complicated in the case of gasoline because of the multitude of hydrocarbon components. The range of boiling temperatures of the different components of standard grade petrol vary widely from near room temperature to over 200 °C (Swindal *et al* (1995)).

Keeping figures 5.9 a and b, in mind, at surface temperatures higher than the Leidenfrost point of the liquid (defined as that temperature at which the drop has the longest total evaporation time in film boiling (Nelson *et al* (1986)), the droplet rests (or floats) on a layer of its own vapour. This vapour cushion is created by the heat transfer from the hot surface to that portion of the liquid in contact with the surface (Gulder *et al* (1984)). The liquid above this vapour cushion tends to be insulated from the high temperature of the surface and consequently takes longer to evaporate. The Leidenfrost temperature indicates the presence of this effect. Al-Roub *et al* (1996) found that the vapour cushion

in the film boiling regime altered the direction of the spreading droplets so that impaction normal to the surface resulted in droplets with velocities mostly tangential to the surface. In addition the droplet normal rebound velocity for transition boiling was an order of magnitude greater than that in the film boiling regime.

Impaction of the solid column of fuel on the inlet valve will have a cooling on the valve in this region of the order of 50 °C (figure 5.9 b) and hence should minimise the Leidenfrost effect. The question remains as to whether the Leidenfrost temperature is exceeded if the engine is run for a longer period of time. The engine was fired for periods of over one minute during the hydrocarbon sampling tests reported in chapter 8.0, and there was no significant change in the stratification achieved within the cylinder. Again, it seemed that no vapour cushion was being formed. However, it is certainly possible that the Leidenfrost temperature would be exceeded if the engine is run for a longer period at higher loads, and this is an area for future work (chapter 10).

5.6 Concluding Comments

An injector block was designed and manufactured which could be mounted on the optical engine (chapter 2) such that it would position a pencil-jet fuel injector in one of the inlet ports so that the fuel column could be deflected off the open inlet valve in the direction of the spark plug. The second port was to be deactivated at part load conditions in order to promote axial swirl within the cylinder.

The initial development of the optimum injector location was carried out on a test rig under ambient and quiescent condition. It was not known what effect the airflow would have on the impacted spray and whether the Leidenfrost effect would become significant under running conditions. Some movement of the injector was afforded in two planes, (as described earlier on in the chapter, section 5.4), to take account of these two factors. The following chapter describes tests performed on the optical engine which had the aim of applying high-speed cine photography to study whether the droplets would rebound off the inlet valve in the intended manner on a running engine. It would also give some

indication as to whether the Leidenfrost effect was occurring by comparing engine cycles recorded at the start and end of the cine film.

Chapter 6

In-Cylinder Photographic Testing with the Targeted Fuel Injector

6.1 Introduction

The high-speed cine camera and copper vapour laser system described in chapter 2 were used to record the motion of liquid fuel within the combustion chamber for the angled injector arrangement. The injector housing (described in chapter 5) was mounted onto the single-cylinder, optically-accessed, engine (described in chapter 2 and chapter 5), and the high-speed camera was set to view the combustion chamber via the 45° mirror. Initially the camera field of view was the entire area of the quartz piston crown but subsequently areas of particular interest were viewed at higher magnification. The engine was motored, as before, at the required test condition and allowed to stabilize before the start of fuel injection. When the engine was seen to fire, the high-speed camera was initiated and between 7 and 12 consecutive engine cycles were recorded for each test, the exact number of cycles depending on engine speed. The engine was allowed to cool back to room temperature and the quartz piston crown was cleaned between tests. The test conditions and the injection timings investigated are to be found in table 6.1.

Engine Speed (rpm)	Injection Timing † (° ATDC inlet)	Engine Speed (rpm)	Injection Timing † (° ATDC inlet)
880 *	Closed-valve injection ‡	1500 **	Closed-valve injection ‡
	Injection ends 60° ATDC		Injection ends 60° ATDC
	Injection starts 95° ATDC		Injection starts 95° ATDC
	Injection starts 135° ATDC		Injection starts 130° ATDC
	Injection starts 145° ATDC		Injection starts 135° ATDC
	Injection starts 155° ATDC		Injection starts 140° ATDC

* Airflow = 0.7 g/s/cylinder, manifold depression = 73 kPa, ignition = 15° BTDC, ** Airflow = 2.0 g/s/cylinder, manifold depression = 56 kPa, ignition = 20° BTDC, † Timings refer to open valve timings unless otherwise stated, ‡ Injection ends 90° ATDC

Table 6.1: Engine conditions and injection timings

6.2 Analysis

An LS-1000 Nikon 35 mm film scanner was used to digitize the first engine cycle from each cine film. Some of these digitized images were then imported into *Visilog 4*, an

image processing package which can be used to calculate droplet velocities, sizes and concentrations. It was necessary to remove all the background features (inlet and exhaust valves and the spark plug) from each cine frame before *Visilog 4* could be used to analyse the fuel spray. This proved not to be feasible because, although the software allowed images to be subtracted from one another, small movements of the background features, through vibration and the opening and closing of the valves, meant that the background features were not necessarily in the same place for consecutive cycles. Subtraction of one image from another left a shadow where features had moved. Also the loss in resolution of the digitized image reduced the contrast between the background features and the fuel spray, making it difficult to prevent unintentional degradation and removal of parts of the spray when subtracting the images. Similar analysis problems for in-cylinder high-speed cine films were reported by Fry 1994. Thus a more manual approach was adopted.

A 16 mm Visual Instruments Selecta Frame 5, type 16N2BX2, analysis projector was used to project individual frames of interest from the second recorded cycle of each cine film onto paper. These images were then traced around and digitized with a KP-M1 black and white CCD camera (figure 6.1 a) before being imported into *Microsoft Word* where the 'draw' facility was used to improve the presentation (figure 6.1 b). Several such figures were obtained for each injection timing. Those produced for an injection timing of 95° ATDC, 1500 rpm road load, are shown in figures 6.2 a-j. In these images and in subsequent images only the camera field of view is shown. In figure 6.1 b the periphery of the quartz crown, that is the camera field of view (red line) and also the cylinder bore (blue line), are indicated on the figure.

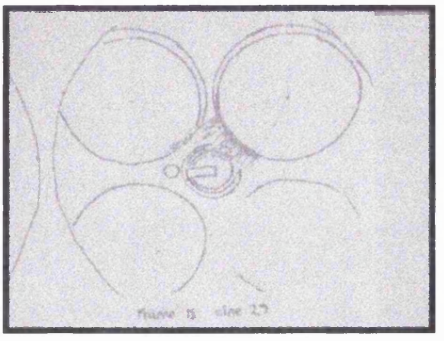

Figure 6.1 a: CCD image of projected frame

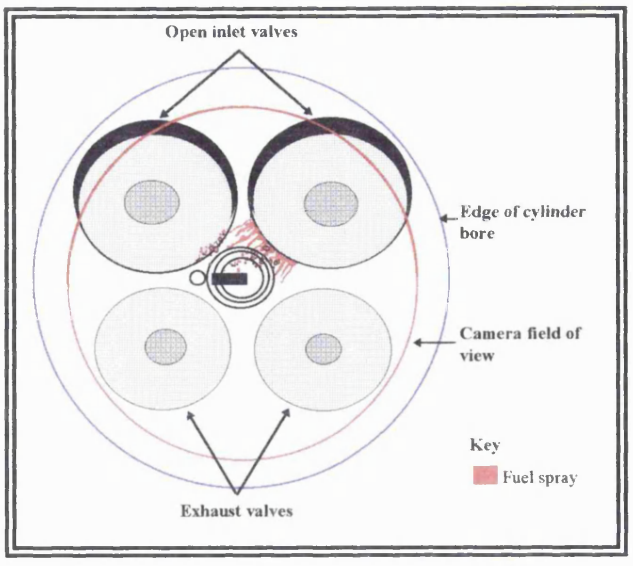

Figure 6.1 b: Image after importing into the *Microsoft Word* 'draw' facility

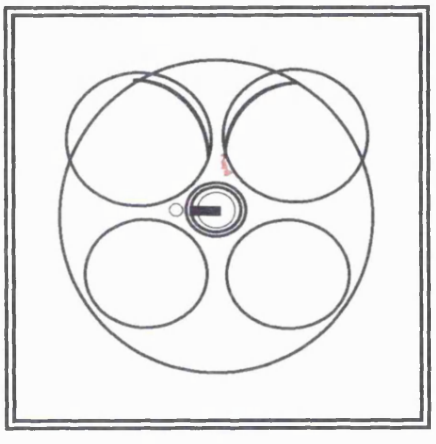

Figure 6.2 a: 1500 rpm, injection starts 95° ATDC, frame 1

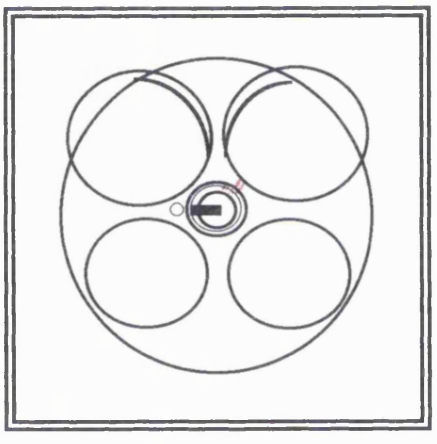

Figure 6.2 b: 1500 rpm, injection starts 95° ATDC, frame 14

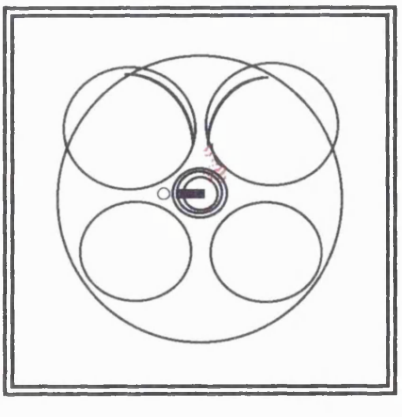

Figure 6.2 c: 1500 rpm, injection starts 95° ATDC, frame 15

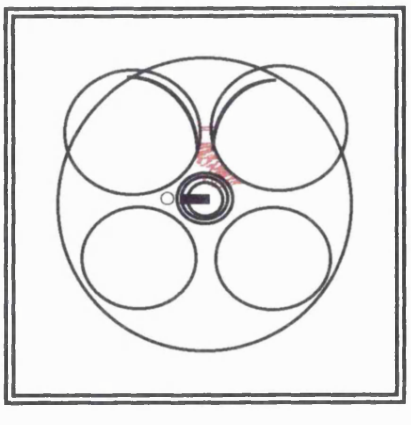

Figure 6.2 d: 1500 rpm, injection starts 95° ATDC, frame 16

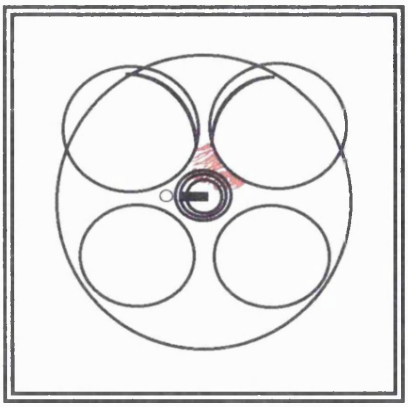

Figure 6.2 e: 1500 rpm, injection starts 95° ATDC, frame 17

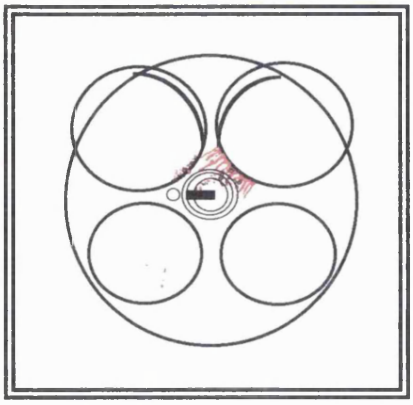

Figure 6.2 f: 1500 rpm, injection starts 95° ATDC, frame 18

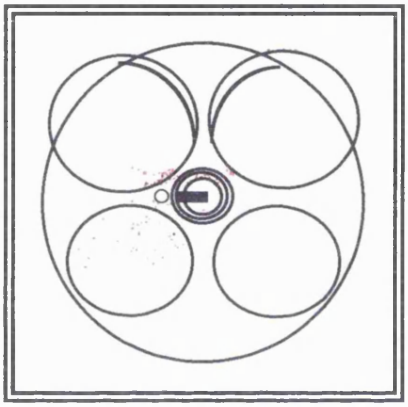

Figure 6.2 g: 1500 rpm, injection starts 95° ATDC, frame 19

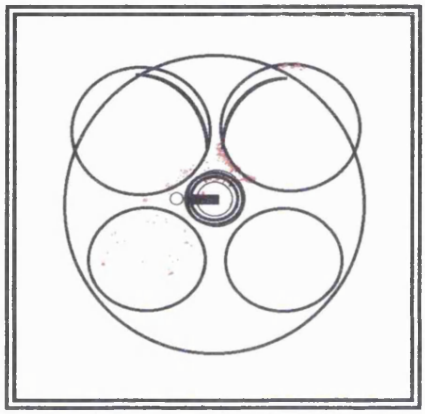

Figure 6.2 h: 1500 rpm, injection starts 95° ATDC, frame 20

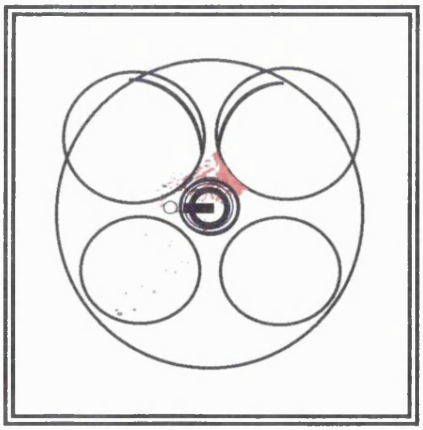

Figure 6.2 i: 1500 rpm, injection starts 95° ATDC, frame 21

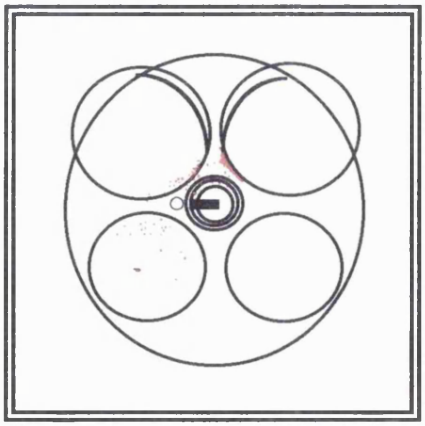

Figure 6.2 j: 1500 rpm, injection starts 95° ATDC, frame 22

The following information was extracted from the digitized images and the above diagrams:

1) The fuel spray characteristics on entry into the combustion chamber: whether as a liquid fuel film or as droplets.
2) Areas of impaction.
3) The angle of entry and arrival time of the fuel spray.

The results will now be discussed in some detail for the engine tests listed in table 6.1.

6.3 Results

6.3.1 Fuel Spray Characteristics for the Standard Injection Timings of 60° ATDC and Closed-Valve Injection

6.3.1.1 End of Injection 60° ATDC

For both the idle and 1500 rpm road load condition, a cloud of fine droplets emerged from the fuel entry valve and travelled across the combustion chamber. In both instances the lack of contrast between the cloud and the background made it impossible to record the journey of the cloud accurately, and one was only left with an impression of where the cloud had moved by running the cine film. For idle it appeared that the cloud travelled diagonally across the spark plug region from the fuel spray entry point towards the exhaust valve, whereas for 1500 rpm road load, the cloud emerged from the left hand portion of the inlet valve and impacted on the second inlet valve where it dispersed still further (figure 6.3 a).

In addition to the fine droplet cloud, at 1500 rpm road load, a portion of the fuel emerged as a series of larger droplets from the lower right hand portion of the inlet valve (figure 6.3 a). Some of these larger droplets were dragged over the inlet valve lip and along its surface (drawn in red, figure 6.3 b). The distance travelled by these droplets varied from cycle to cycle but all stayed within the boundary of the inlet valve circumference. The remainder of the larger droplets (drawn in green, figure 6.3 b) took a slightly wider route around the valve and travelled upwards to impact and bounce off the

neighbouring inlet valve. Some of these droplets then travelled as far as the cylinder bore.

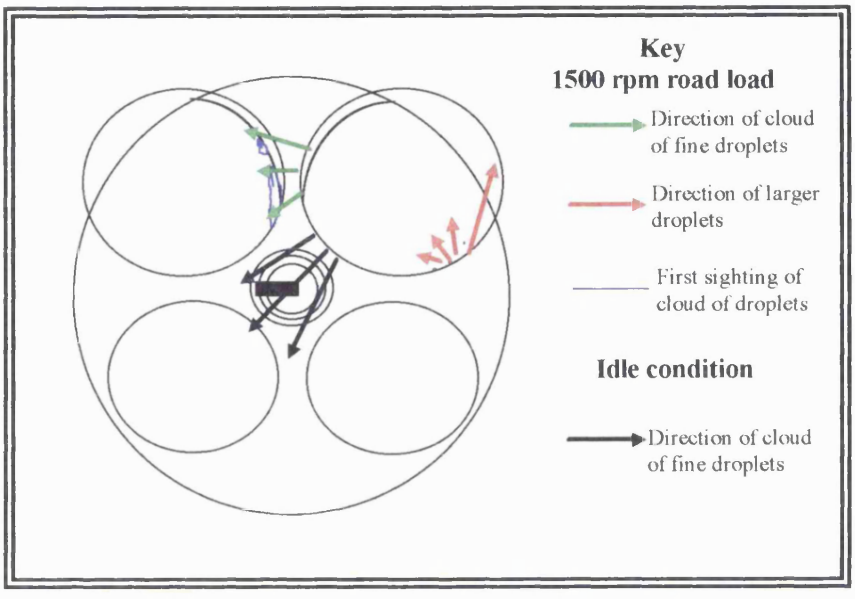

Figure 6.3 a: Entry of fuel into combustion chamber end of injection 60° ATDC, idle and 1500 rpm conditions

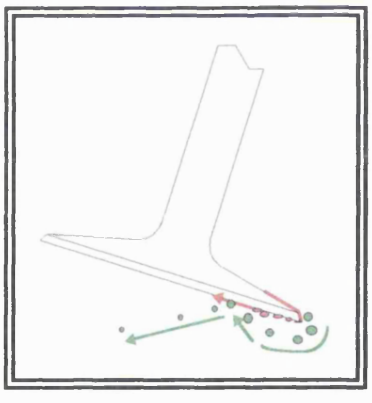

Figure 6.3 b: Movement of fuel over the inlet valve for injection timing ending at 60° ATDC, 1500 rpm road load condition

The average times (over 12 cycles) when the cloud and the larger droplets were first observed for the 1500 rpm road load condition were 87.5° and 81° after the start of fuel injection, respectively. It should be noted that the time recorded for the entry of the fuel cloud was when it was observed on the second inlet valve and not as it emerged into the combustion chamber. Therefore, in reality, the cloud would have entered earlier than the

recorded 87.5°. It was not possible to record the time the fuel cloud entered into the chamber for the idle condition due to the lack of contrast with the background.

6.3.1.2 Closed-Valve Injection

For the 1500 rpm road load condition, the fuel entered the combustion chamber as droplets from over the top left hand portion of the inlet valve and travelled downwards to impact on the piston (figures 6.4 a and b). The fuel on the piston evaporated quickly leaving no trace. On closer examination of the cine film, a fuel film was also seen to enter from the lower portion of the inlet valve. This fuel film was dragged along the valve seat area onto the cylinder head to the right of the spark plug where it remained until combustion occurred (figure 6.5).

No fuel could be observed entering the combustion chamber at the idle condition although the engine was seen to fire. It is likely therefore that the fuel entered as a very fine droplet cloud or as a thin and rapidly evaporating film.

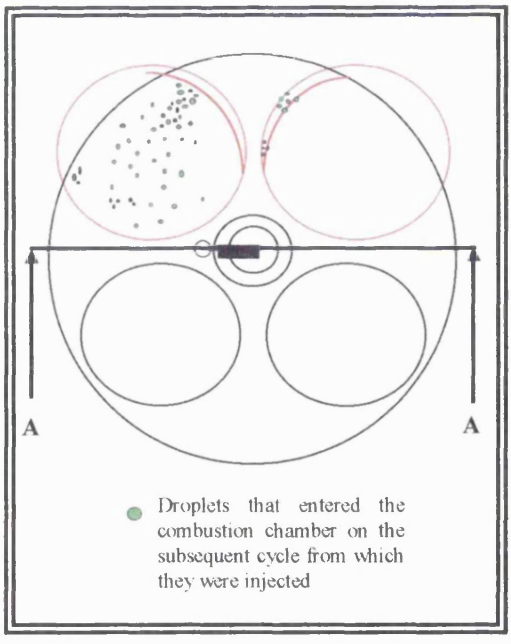

Figure 6.4 a: General trends for closed-valve injection, plan view, 1500 rpm road load

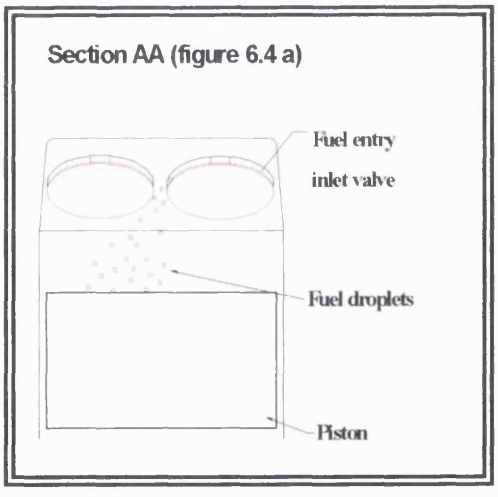

Figure 6.4 b: General trends for closed-valve injection, side view, 1500 rpm road load

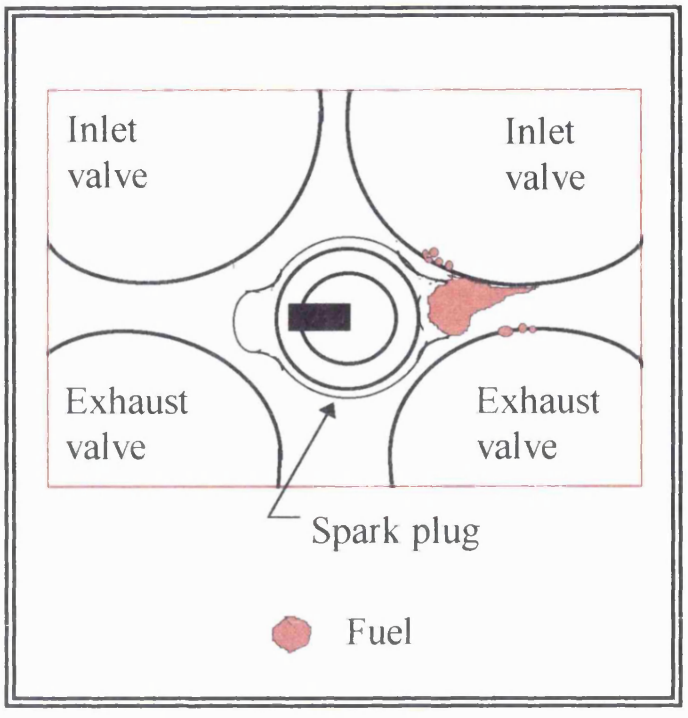

Figure 6.5: Fuel at valve seat, 1500 rpm road load for closed-valve injection

6.3.2 Fuel Spray Characteristics at a Range of Alternative Open-Valve Timings

6.3.2.1 Injection Starts 95° ATDC

For both idle and 1500 rpm road load conditions there were two modes of fuel entry, one of which was common to both test conditions. With the common mode of fuel entry, the fuel appeared as ligaments that were drawn off the inlet valve surface into the combustion chamber (figure 6.6 a). Some of the first ligaments to enter the combustion chamber impacted on the cylinder head around the spark plug region or on the exhaust valve diagonally across from the point of fuel entry, whilst the rest sheared into smaller ligaments and eventually into droplets as they traversed across the combustion chamber. This shearing effect occurred mainly as a consequence of the motion of the air relative to the fuel ligaments, but at idle the formation of the smaller ligaments and droplets was aided by the larger ligaments impacting on the spark plug electrodes and at 1500 rpm road load by impaction on the second inlet valve (figure 6.6 b). General trends for droplet motion and ligaments entry are shown in figure 6.7 for the 1500 rpm road load condition.

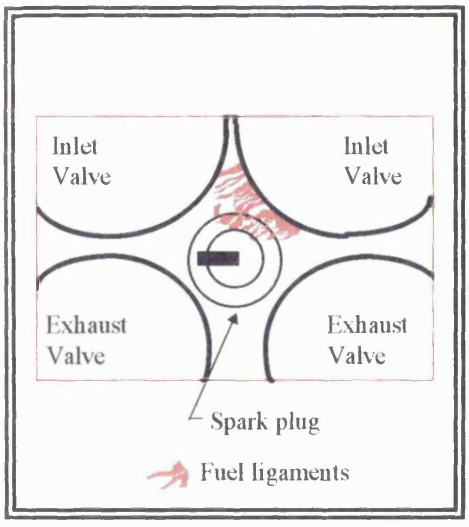

Figure 6.6 a: Ligaments about to impact on the second inlet valve for 95° ATDC injection, 1500 rpm road load

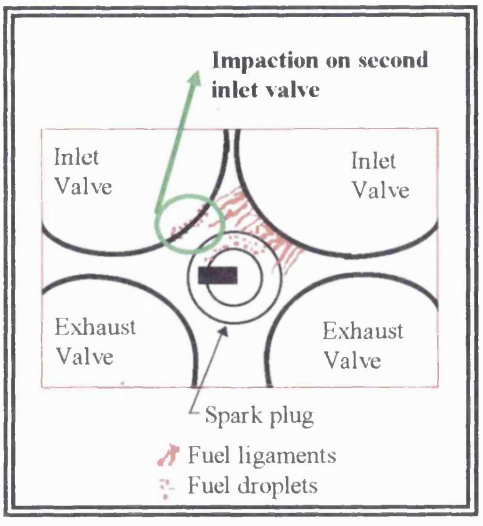

Figure 6.6 b: Ligaments impacting on the second inlet valve for 95° ATDC injection, 1500 rpm road load

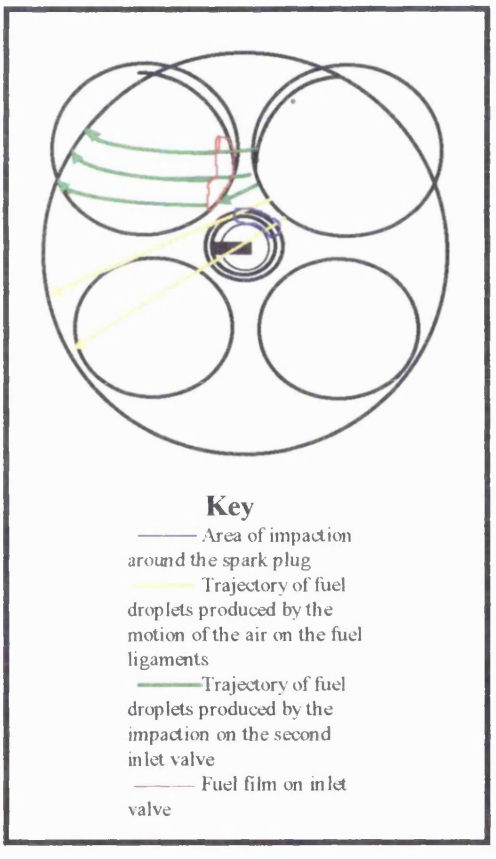

Figure 6.7: General trends of droplet direction and ligament entry point for 95° ATDC injection, 1500 rpm road load

In the second mode of fuel entry, for idle, a small proportion of the ligaments remained attached to the inlet valve and became elongated as the valve closed until they detached

themselves from the valve. The detached fuel did not appear to impact on the piston but a fuel film was left on the fuel entry inlet valve (figure 6.8). For the 1500 rpm condition, a cloud of fine droplets was also observed. The contrast between this cloud and the background was not very marked and no other characteristics were recorded other than its presence.

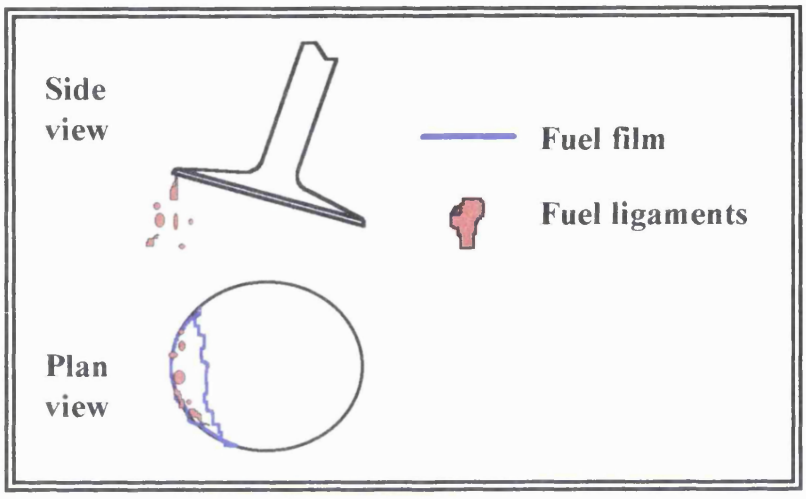

Figure 6.8: Trajectory of droplets that remain on the inlet valve until inlet valve closure for 95° ATDC injection, 880 rpm idle

The average time at which the ligaments were first observed entering the combustion chamber was 83° after the start of fuel injection for the1500 rpm condition.

6.3.2.2 Late Open-Valve Injection Timings

The fuel entered the combustion chamber as ligaments at idle for injection timings of 135°, 145° ATDC, whereas the fuel was in the form of droplets at the 1500 rpm road load condition at 130°, 135° and 140° ATDC timings. For both test conditions (but particularly so for 1500 rpm road load) the majority of the fuel impacted on the cylinder head around the spark plug region and remained there until combustion occurred (figure 6.9). That fuel which did not stay in this region had a number of paths that were common to both test conditions (points 1-3 below).

1) Some droplets bounced off the cylinder head from around the spark plug region and continued to travel across the combustion chamber. Further impaction occurred on

the exhaust valve diagonally across from where the fuel entered and also on the cylinder bore.

2) Other droplets impacted on the exhaust valve diagonally across from the fuel entry point without having first impacted on another surface. These droplets either remained on the exhaust valve until combustion, or bounced off and impacted on the cylinder bore.

3) A few droplets impacted on the cylinder bore without having first impacted another surface.

For 1500 rpm, the number of cycles which exhibited the trend of droplets continuing past the spark plug decreased as the injection timing was retarded , and at the timing of 140° ATDC no fuel was observed to travel past the spark plug. However, less fuel also impacted around the spark plug at this timing. This was because at the two timings of 135° ATDC of 140° ATDC was that not all the fuel entered the combustion chamber during the cycle in which it was injected. This was true for some of the cycles at 135° injection timing, and all of the cycles for 140° timing. Consequently, when the inlet valve opened on the subsequent cycle, this fuel entered immediately from the top left hand portion of the inlet valve and travelled downwards to impact on the piston (figures 6.10 a and b). This fuel evaporated quickly and left no trace.

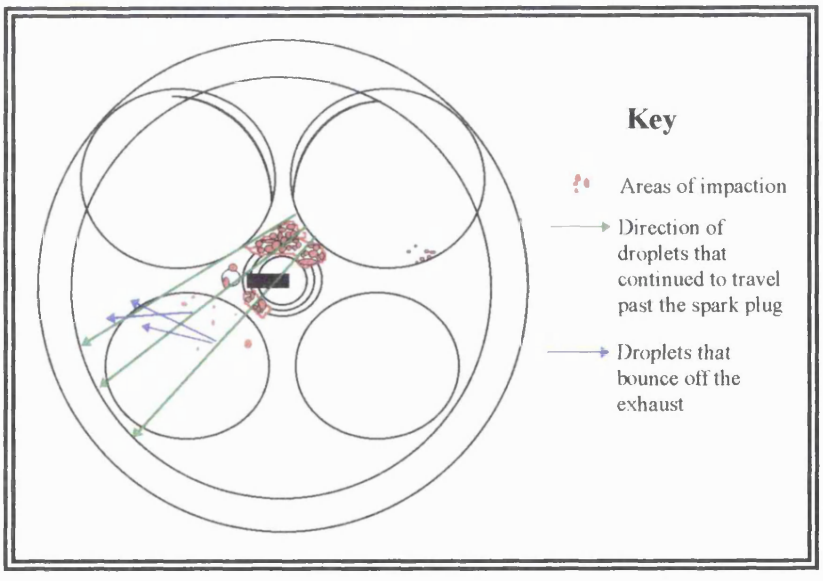

Figure 6.9 a: General trends for an injection timing of 130° ATDC, 1500 rpm road load

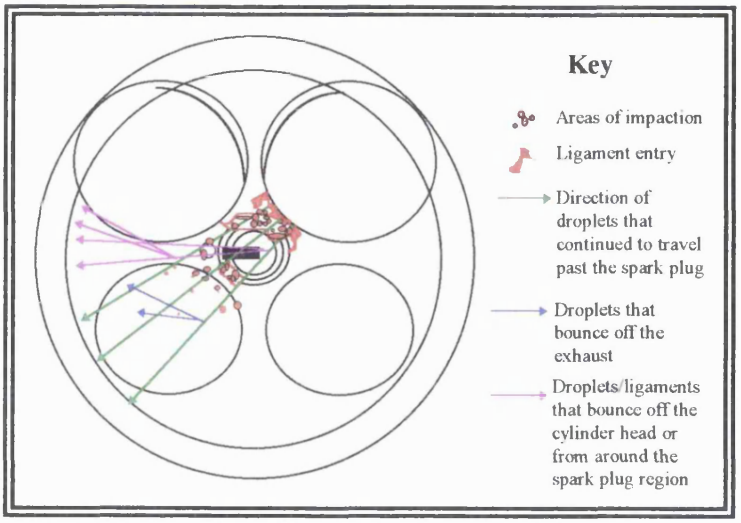

Figure 6.9 b: General trends for an injection timing of 130° ATDC, 880 rpm low load

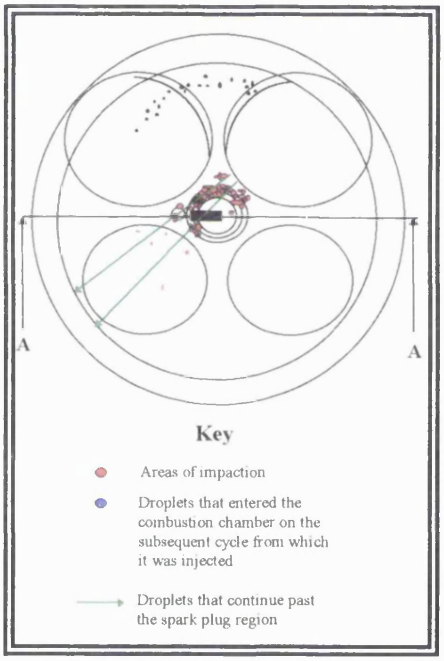

Figure 6.10 a: General trends for an injection timing of 135° ATDC, 1500 rpm road load

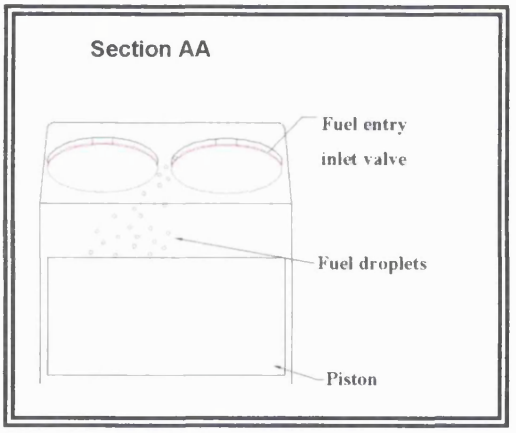

Figure 6.10 b:Trajectory of fuel impacting on the piston, 1500 rpm road load

For idle, a few of the ligaments impacted on the spark plug electrodes and on the second inlet valve, causing the fuel to break up into droplets. These smaller ligaments/droplets continued across the combustion chamber. Similar to the timing of 95° ATDC, a number of recorded cycles showed that some of the ligaments remained attached to the inlet valve until the valve began to close at which point they became detached and travelled

over the valve and then vertically downwards. A fuel film was once again left on the inlet valve. Some of these droplets were taken up with the swirling motion of the air and appeared to rotate around the spark plug (figure 6.11) at an injection timing of 140° ATDC.

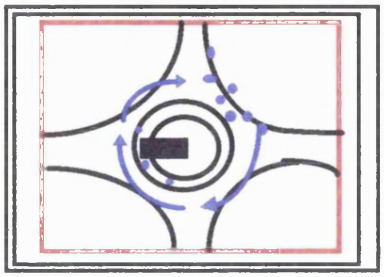

Figure 6.11: Trajectory of droplets that remain on the inlet valve until inlet valve closure, and swirl around the spark plug, injection timing 140° ATDC, idle condition

The average time at which the fuel was first observed was 62° after the start of fuel injection at an injection timing of 130° ATDC. The average times for 135° ATDC for observing the fuel emerging from the lower and upper regions of the inlet valve were 61° and 636° respectively, and for an injection timing of 140° ATDC the values were 68° and 618° respectively. The results are summarized in table 6.2

Injection timing °ATDC	Speed (rpm)	Characteristics	Fuel first seen, ° after the start of fuel injection
End of injection 60°	880 1500	Fine cloud Fine cloud and Large drops	87.5° 81°
Start of injection 95°	880 1500	Ligaments Fine cloud and Ligaments	- 83°
Start of injection 130°	1500	Droplets	62°
Start of injection 135°	880 1500	Ligaments Droplets	- 61°, 636°
Start of injection 140°	1500	Droplets Fuel film	68°, 618°
Start of injection 145°	880	Ligaments	-
Closed-valve	880 1500	None Droplets and Fuel film	- -

Table 6.2: Summary of results

6.4 Discussion

From the analysis of the results it was apparent that the manner in which the fuel entered the combustion chamber was strongly dependent on the injection timing. Depending on this timing, the fuel entered in a manner consistent with one or a combination of the following ways:

1) a rapidly moving cloud of very fine fuel droplets,
2) a number of large visible fuel droplets,
3) ligaments of fuel drawn off the inlet valve to shear into droplets.

Variation in injection timing altered the portion of the inlet valve on which the solid column of fuel impacted, and indeed whether it impacted on a downward or an upward moving valve. Injection timing and its effect on spray formation was therefore a function of valve lift.

6.4.1 Injection Timing in Relation to Valve Events

A better appreciation can be obtained of the processes that occur when the solid column of fuel impacts on the back of the inlet valve if one considers the likely values of valve lift during the period of impaction. The injection timings are shown in relation to valve lift in figure 6.12

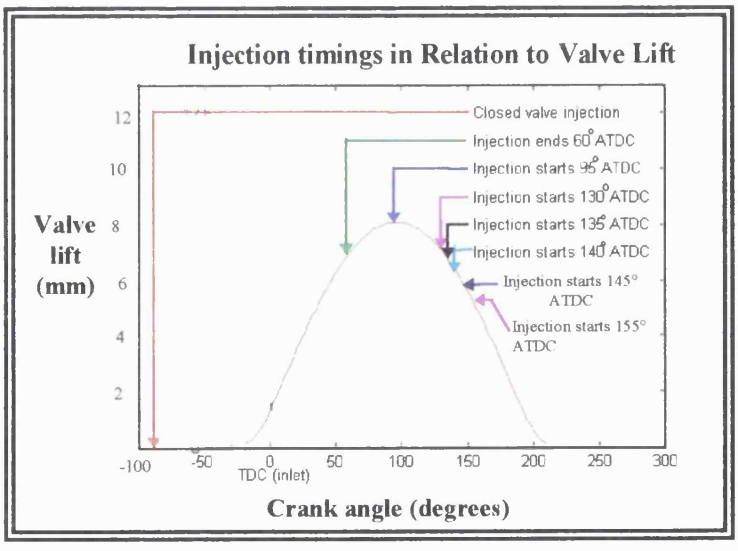

Figure 6.12: Injection timing and valve lift

With a knowledge of the fuel pulsewidth and engine speed, the start and end of the injection period at the injector nozzle exit and the start and end of impaction on the inlet valve can be related to the valve lift. The valve lift at the start of fuel injection differed from that at which impaction first occurred on the inlet valve because of the finite transport time. The distance between the injector tip and the inlet valve was 90 mm when the valve was fully closed. The velocity of the pencil jet was found to be 12 m/s for the low flow rate injector and 18 m/s for the high flow rate injector from the photographic records of the fuel column (chapter 5) when spraying into quiescent air. This resulted in a delay of 7.5 ms and 5 ms respectively before the fuel reached the inlet valve (calculated on the basis of the fully-closed position).

Figures 6.13 a-f show the injection duration at the injector nozzle exit (represented by the distance between the red lines), and at the start and end of fuel impaction on the inlet valve (represented by the distance between the blue lines), in relation to valve lift for the idle condition. All of the injection timings investigated for this condition are shown on these figures. Figures 6.13 g and h, however only show these parameters for the earliest and latest injection timings investigated at 1500 rpm road load. From these figures (figures 6.13 a-f) it can be seen whether the fuel impacted on a downward or an upward moving valve.

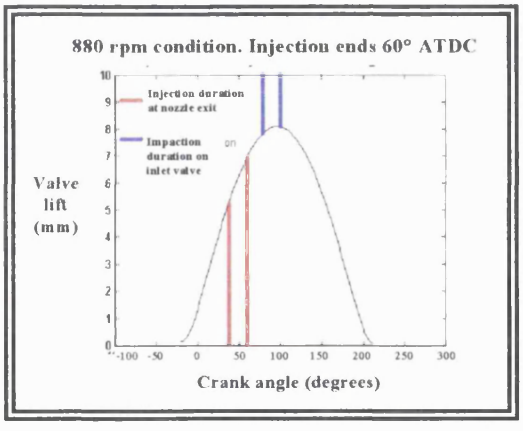

Figure 6.13 a: Injection duration at nozzle exit and impaction duration on inlet valve in relation to valve lift, low flow rate injector

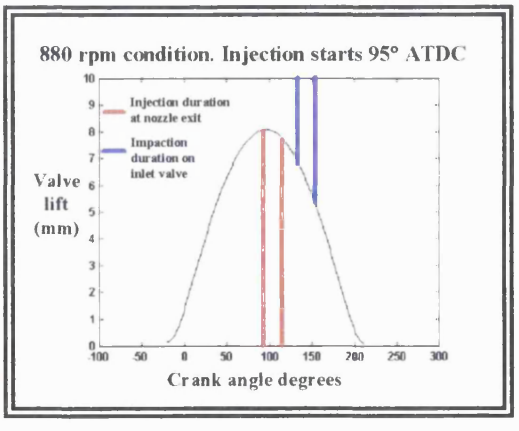

Figure 6.13 b: Injection duration at nozzle exit and impaction duration on inlet valve in relation to valve lift, low flow rate injector

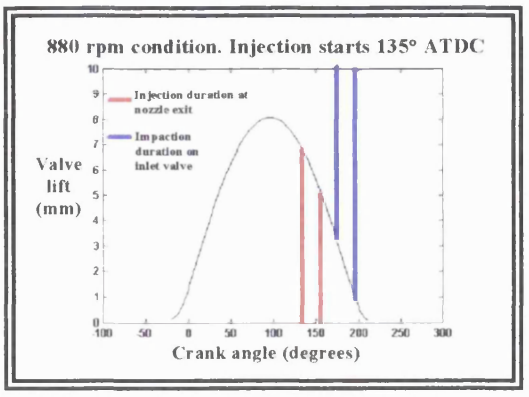

Figure 6.13 c: Injection duration at nozzle exit and impaction duration on inlet valve in relation to valve lift, low flow rate injector

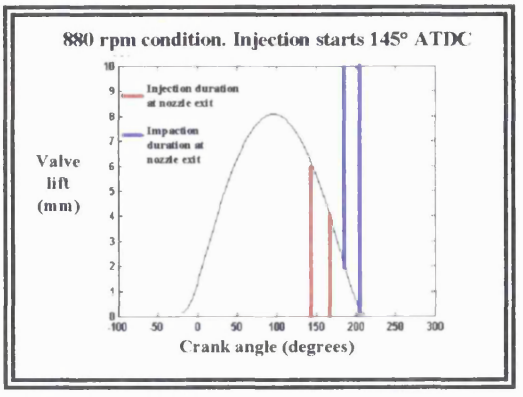

Figure 6.13 d: Injection duration at nozzle exit and impaction duration on inlet valve in relation to valve lift, low flow rate injector

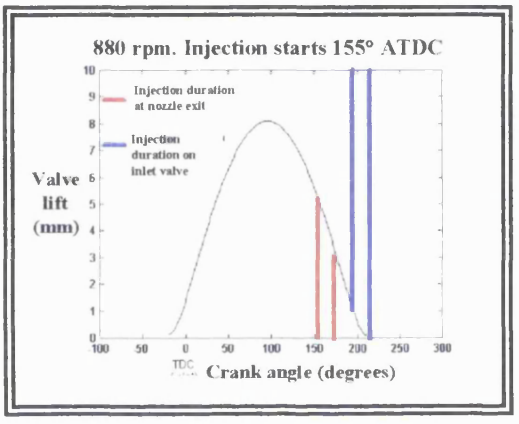

Figure 6.13 e: Injection duration at nozzle exit and impaction duration on inlet valve in relation to valve lift, low flow rate injector

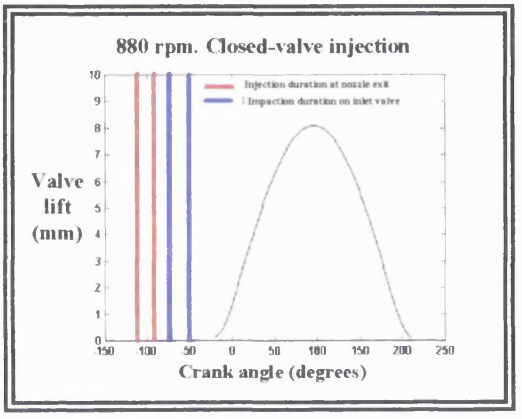

Figure 6.13 f: Injection duration at nozzle exit and impaction duration on inlet valve in relation to valve lift, low flow rate injector

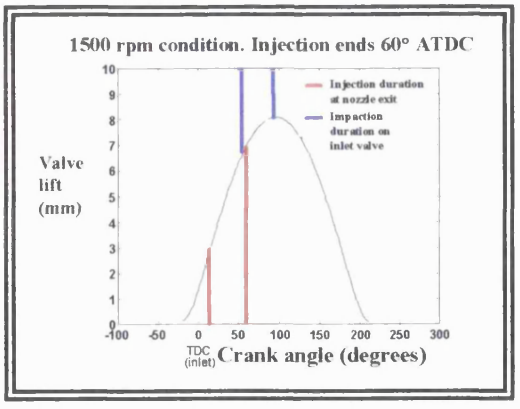

Figure 6.13 g: Injection duration at nozzle exit and impaction duration on inlet valve in relation to valve lift, high flow rate injector

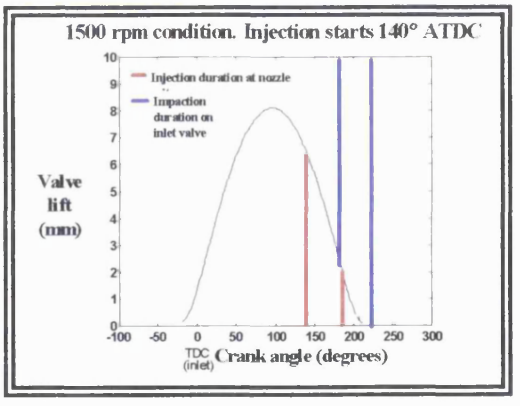

Figure 6.13 h: Injection duration at nozzle exit and impaction duration on inlet valve in relation to valve lift, high flow rate injector

In addition, the valve velocity at the time of impaction can be calculated from the gradient of the valve opening characteristic (figures 6.13 a-h). For idle at an injection ending 60° ATDC, the average valve downward velocity during impaction was 0.12 m/s (and hence relative velocity between the fuel and the valve, 11.88m/s) and for the remaining injection timings the upward velocity was approximately 0.33 m/s (relative velocity between fuel and air 12.33 m/s). The motion of the valve does not add significantly to the relative impact velocity, because the velocity of the fuel is considerably greater than the velocity of the inlet valve at any one instant. Thus, the fuel may be considered to be impacting on a stationary inclined plate at any instant in time (chapter 5, section 5.5). The relative velocity would obviously be greater for higher engine speeds (at the later timings) but the effect of the valve motion would still not be particularly significant.

6.4.2 Air Velocity Distribution at Valve Curtain Area

As well as having an appreciation of valve lift and velocity during injection, a knowledge of air flow direction and magnitude is also important in understanding the processes involved in distributing fuel after its impaction on the inlet valve. For the idle condition, depending on the open-valve injection timing, impaction of the fuel on the inlet valve occurred either around the time of maximum valve lift or as the inlet valve was closing (figures 6.13 a-f). Baker (1995) investigated the air flow distribution around the inlet valve, with a stagnation pitot tube attached to a standard inlet valve that had a hollow stem (figure 6.14), for a range of valve lifts and air flows.

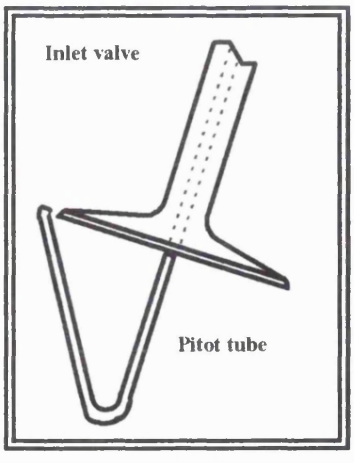

Figure 6.14: Pitot tube arrangement

The work was carried out using hardware from a Ford Zetec engine, similar in specification to the one used in the investigation reported here (also with one valve deactivated), and so his results may be taken as being directly relevant to this work. He concluded that the major influence of valve deactivation was on the velocity of the incoming air (almost doubling it, since the flow area was halved). The velocity distribution around the valve was reasonably uniform (figure 6.15), with only a slight biasing towards the exhaust valve. Although Baker does not provide individual plots of the velocity profiles across a range of engine conditions he reported the velocity profile for 1500 rpm road load as being typical.

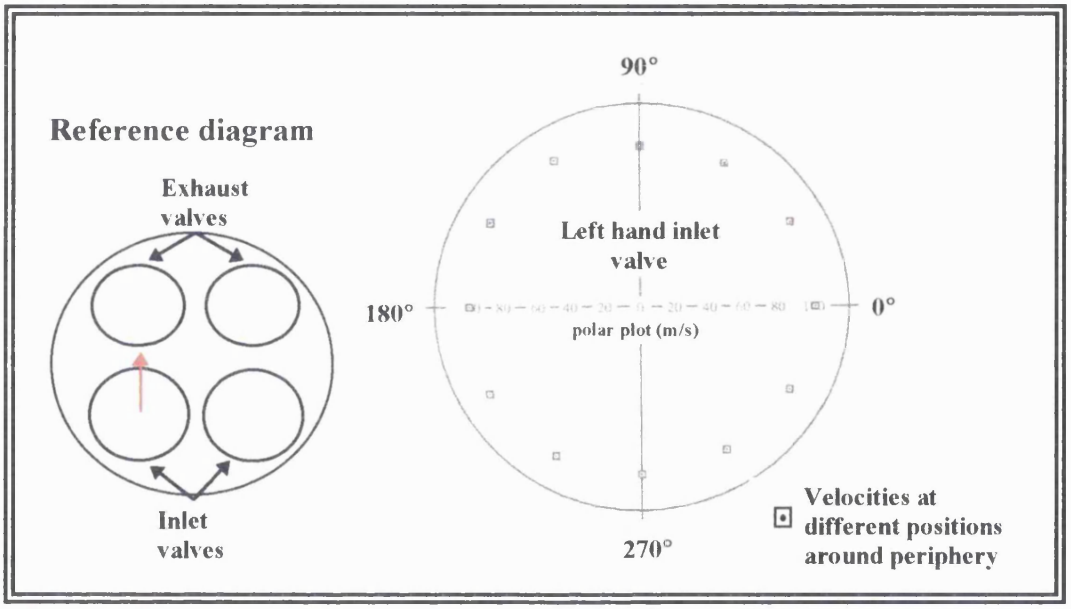

Figure 6.15: Velocity profile generated at a simulated 1500 rpm road load condition, valve deactivation, air flow = 5 g/s, valve lift 5 mm [Baker (1995)]

It may be concluded that the position of the point of impaction of the fuel spray was not critical in terms of finding rapidly moving air streams on one side of the inlet valve compared with the other.

6.4.3 Relative Velocities Between the Fuel and Air

Having established that the air flow velocity is relatively uniform around the periphery of the inlet valve, an attempt will be made to assess how the magnitude of velocity varies with crank angle, and hence valve lift

Virtually identical mass flow characteristics across the inlet valves were predicted by Baker (1995) at idle with both valves in operation, and those predicted by Newman *et al* (1989) with valve deactivation. (It should be noted that although the bore and stroke of the engines were very similar, different engines were used by Newman and Baker). Valve deactivation appeared not to have a significant effect on the mass flow characteristics across the valves. It was therefore possible to calculate the velocities across the inlet valve and in the inlet port using values for the mass flow rate predicted by Baker *et al* (1995) for a Zetec engine with no valve deactivation coupled with a knowledge of the cross-sectional area of the inlet port and appropriate valve lift. The results are given in tables 6.3 and 6.4 for the idle condition.

Injection (° ATDC)		**Valve lift (mm)**		**Velocity in inlet port (m/s)**		**Impaction (° ATDC)**		**Valve lift (mm)**		**Velocity in inlet port (m/s)**	
starts	ends	start	end	start	end	starts	ends	start	end	starts	end
39	60	5.3	6.9	16.9	20.8	79	100	7.8	8.1	20.8	18.1
95	116	8.0	7.7	12.8	12.9	135	156	6.8	5.1	20.0	18.4
135	156	6.7	5.1	8.6	5.1	175	196	3.2	0.9	1.2	-3.1
145	166	6.0	4.1	7.4	2.7	185	206	2.1	0.2	-1.2	-5.1
69*	90	0.0	0.0	0.0	0.0	-20	1	0.15	1.5	2.35	-25.5

*** Closed valve injection**

Table 6.3: Inlet port velocities for different valve lifts at different times in the cycle, idle condition

Injection (° ATDC)		**Valve lift (mm)**		**Velocity across valve curtain (m/s)**		**Impaction (° ATDC)**		**Valve lift (mm)**		**Velocity across valve curtain (m/s)**	
starts	ends	start	end	start	end	starts	ends	start	end	start	end
39	60	5.3	6.9	24.6	23.3	79	100	7.8	8.1	20.6	17.2
95	116	8.0	7.7	20.1	13.0	135	156	6.8	5.1	22.8	28.0
135	156	6.7	5.1	10.0	7.7	175	196	3.2	0.9	2.8	-27
145	166	6.0	4.1	9.6	5.2	185	206	2.1	0.2	-4.3	197.5
69*	90	0.0	0.0	-	-	-20	1	0.15	1.5	-227	-131.6

*** Closed valve injection**

Table 6.4: Velocity flow rates across the inlet valve and valve lifts at different times in the cycle, idle condition

The velocities in the inlet port at the start and end of injection (left-hand-side of table 6.3), and the velocities in the region of the valve curtain area at the time of impaction (right-hand-side of table 6.4) may be compared to the velocity of the pencil jet (12 m/s) at different injection timings.

Before the fuel impacts on the inlet valve, it is subjected to shear forces resulting from its motion relative to the air in the inlet port. The velocity of the air in the inlet port is therefore another factor in determining the fuel entry characteristics. The velocity of the air is greater than the fuel velocity for the earliest open-valve injection timing. Consequently the shear stresses between the surface of the fuel column and the adjacent air are greater than for the later timings where the air is more quiescent. An indication as to the likelyhod of the fuel column breaking up before it reaches the inlet valve is given by the aerodynamic Weber number. The aerodynamic Weber number is a dimensionless number that is the ratio of the aerodynamic forces to surface tension forces (equation 6.1):

$$We = \frac{\rho_g u_r d}{\sigma_l} \qquad (6.1)$$

where We= aerodynamic Weber number

u_r = relative velocity (m/s)

d = column diameter (m)

ρ_g = air density

σ_l = surface tension (kg/s^2)

The Weber number determines the rate of growth of capillary waves or ripples on the liquid surface (through the ratio of aerodynamic forces to consolidating surface tension forces) with high values of Weber number indicating large capillary waves and therefore an increased chance of the formation of small droplets. This coupled with the high shear stresses implies that the surface of the fuel column is likely to shear into fine droplets.

The complexities of the processes occurring are further increased when it is considered that the fuel spray is injected at an angle to the air flow (figure 6.17). Williams *et al*

(1994) calculated the relative velocity of the air flow and fuel flow using the cosine rule and reports that although a gross simplification, it is adequate to provide comparative data. Thus using this approach, the relative velocity between the fuel and air at an injection timing of 60° ATDC was calculated as 10.9 m/s at the nozzle exit for the start of injection and 13.9 m/s at the end of injection. The remainder of the relative velocities are tabulated in table 6.5 together with the Weber numbers of the flows. These are the Weber numbers calculated in relation to the flow in the inlet port as the fuel leaves the injector nozzle.

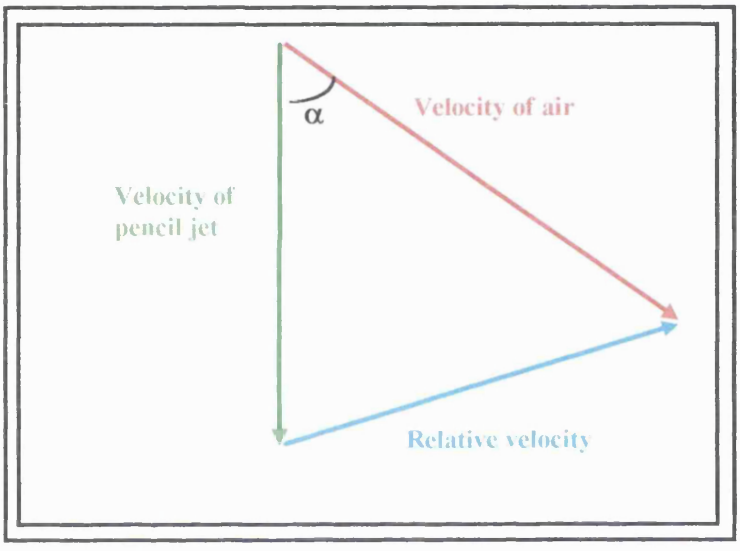

Figure 6.16: Relative velocity of fuel and air

Injection (° ATDC)		**Relative velocity between fuel and air (m/s)**		**Weber number**	
starts	ends	start	end	start	end
39	60	10.9	13.9	0.64	0.81
95	116	8.9	8.5	0.55	0.50
135	156	7.7	8.7	0.45	0.51
145	166	7.9	8.1	0.46	0.47

Table 6.5: Weber numbers of the flows at the time of injection (across injector nozzle)

It can be seen that the higher Weber numbers occurred at the earlier injection timings, and this could explain the cloud of droplets that was apparent at the 60° ATDC end of injection timing (section 6.3.1.1).

Apart from some break-up at the higher Weber numbers it is concluded that the column of fuel mainly arrives at the inlet valve fully intact. Considering the period of impaction, at the two early open-valve injection timings of 60° and 95° ATDC, the velocity at the valve curtain area was significantly greater than that of the pencil-jet. The droplets produced by impaction are likely to be taken up by the air motion and brought into the cylinder quite readily.

For an injection timing of 135° ATDC the velocity around the valve curtain area is relatively quiescent at the start of impaction but by the time impaction ends there is a significant amount of backflow into the port. The backflow velocities increased significantly for the end of injection at the later injection timings. At the start of impaction the fuel for these late injection timings is more likely to be dragged off the inlet valve into the combustion chamber or drip off the inlet valve rather than entering readily. By the end, some of the fuel will be pushed back up the inlet port due to the backflow. For idle some of the fuel was seen to drip of the inlet valve for the later injection timings, however this was also observed at 95° ATDC. Interestingly the fuel dripping of the inlet valve was also observed in the photographic work carried out in chapter 5 (development of injector mounting block). Here the tests were carried out without airflow and so were similar to the quiescent conditions noted in these tests for the later injection timings at the start of impaction. Some similarity between the test results can be expected.

The flow separation characteristics of the air around the inlet valve also has an effect on the manner in which the fuel enters the combustion chamber. This is further considered in the following chapter.

6.4.4 Flow Separation from the Inlet Valve

The air flow separates from the valve seat (Annand and Roe (1974)) at high valve lifts and promotes the passage of the fuel droplets off the inlet valve into the cylinder. Therefore fuel that entered the combustion chamber early on in the cycle, such as with closed-valve injection and the open-valve injection timing of 60° ATDC, is likely to have mixed better with the air at the later open-valve injection timings, particularly so because of the high air velocities at the valve curtain area.

For the remainder of the open-valve injection timings at idle, the start of fuel injection occurred around the time of maximum valve lift (figure 6.13 b) or as the valve was closing (figures 6.13 c-e). Fuel impaction always occurred on a closing inlet valve. Because of the low port velocities and Weber numbers during this portion of the cycle, any droplets or ligaments produced will tend to be large in size (section 6.3.2). It would appear for idle a significant proportion of fuel does not bounce off the inlet valve but enters the combustion chamber by a process of strip atomization. This fuel impacts on the valve and is drawn towards the cylinder by the shear stresses of the intake flow. This film flow stops at the valve periphery due to the diverging flow field as the intake air enters the cylinder (Annand and Roe (1974)). The fuel is trapped in this region, its thickness being dependent on the surface tension, gravity and the shear forces produced by the air flow. At the very low valve lifts the fuel is squeezed into the cylinder between the valve and valve seat. The upwards action of the valve causes the fuel to eventually break away from the valve. At the low valve lifts the air motion is predominantly axial swirl and with an injection timing of 145° ATDC, the late droplets to enter the combustion chamber can be seen to swirl around the spark plug

6.5 Concluding Comments

The high-speed cine films have shown the behaviour of liquid fuel within the cylinder with the angled injector arrangement. It was apparent that the behaviour was very dependent on injector timing with a significant proportion of the fuel from the earlier open-valve injection timings tending to be carried past the spark plug region. Injection timings of around 130°/135° ATDC were relatively successful in retaining the fuel

around the spark plug. Calculations for the timing of 135° ATDC suggested that the air velocities in the port and at the valve curtain area were relatively low, and it is thought that this would favour the establishment of a stratified charge within the cylinder.

Chapter 7

Instrumentation for the Measurement of In-Cylinder Hydrocarbon Concentrations

The high-speed cine photography results discussed in the previous chapter suggested that the injector approach was, at least, partially successful in its goal of introducing the fuel into the cylinder in the vicinity of the spark plug. It was decided that the next logical step was to attempt to measure the in-cylinder HC concentration at key points and to do this with a Cambustion HFR400 fast flame ionisation detector.

7.1 Cambustion HFR400 Fast Flame Ionisation Detector

A Cambustion HFR400 Fast Flame Ionisation Detector (FFID) was used to measure 'real time' in-cylinder HC concentrations at specific points in the combustion chamber. The high frequency response of the FFID (2 ms) is obtained by the sample gas being delivered directly to a nozzle exit via short sample lines, whereupon it is mixed with the fuel gas and burnt (figure 7.1 a). With conventional FID designs the sample is supplied via a pump (figure 7.1 b), and the frequency response is typically 1 second (Cambustion HFR400 FFID User Manual (Version 1.3)).

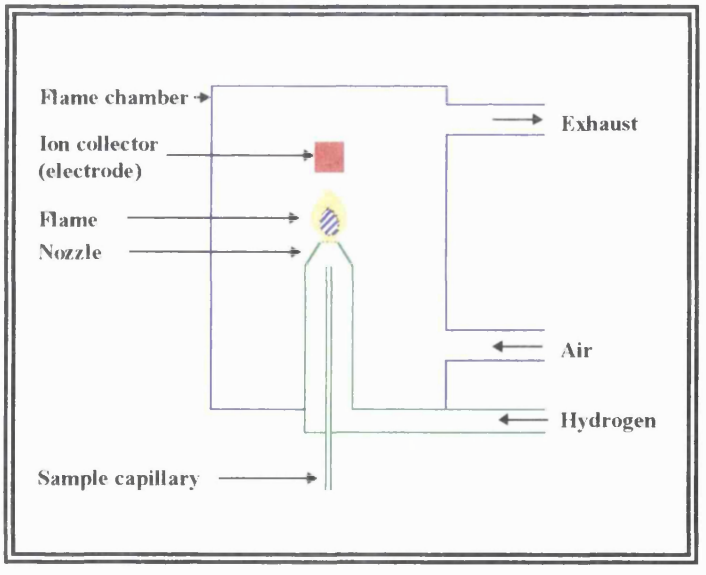

Figure 7.1 a : Cambustion FFID arrangement

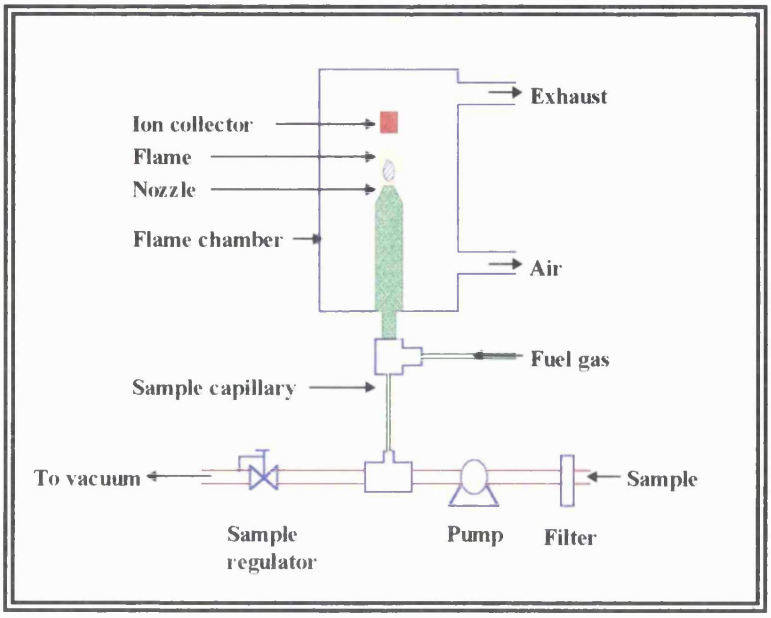

Figure 7.1 b: Conventional FID arrangement

Under normal flame temperatures, if the sample gas contains hydrocarbons, negative ions are produced when it is burnt. It is these ions that are collected at the electrode and used to generate an electrical output which is proportional to the number of carbon atoms burnt in hydrocarbon form. Since the volume of the sample gas being burnt at any time in the system is dependent on the pressure differential between the sample entry point and the constant pressure (CP) chamber, and between the CP chamber and the flame chamber (figure 7.2), the output is therefore also proportional to the mass flow of the sample gas through the system.

It is important to maintain a constant flow of sample gas into the nozzle, regardless of the pressure fluctuations that may occur at the sample entry point (Cambustion HFR400 FFID User Manual (version 3.1) and Ladommatos *et al* (1995)). The exit from the FID tube must not become choked (Crawford *et al* (1996)). Since the FID tube forms a static pressure tapping on the tee-top, the flow through it is independent of dynamic pressure effects, and will only vary if the pressure in the CP chamber varies (or more precisely if the pressure at point A varies (figure 7.2). A constant pressure in the CP chamber can be maintained by making the CP chamber volume large in comparison to the sample flow fluctuations and using bleed flow regulators, together with careful selection of the FFID tube diameters and the FID flame chamber pressure (Cambustion HFR400 FFID User

Manual (version 3.1)). Ladommatos *et al* (1995) demonstrated the insensitivity of the FFID output signal to sample pressure, by supplying the end of the FFID probe with calibration gas of known concentration at a pressure of 1.7 bar, and then rapidly increasing the sample pressure to 44 bar. The FFID output was seen to remain constant although the sample pressure altered.

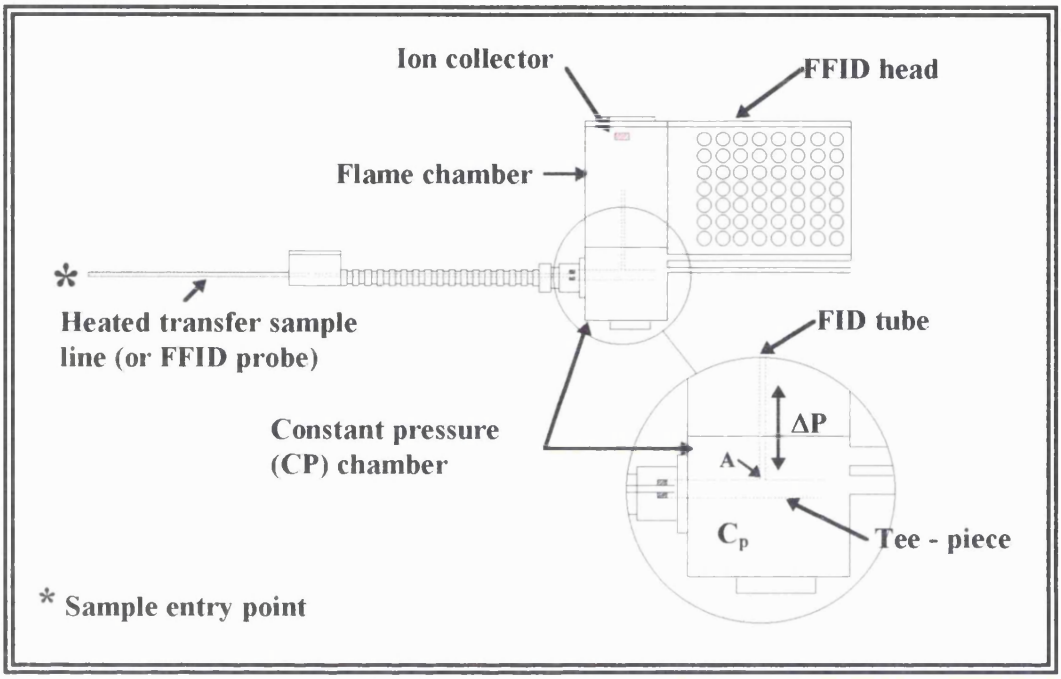

Figure 7.2: FFID head and probe

The pressure independence of the FFID system used in the current work was also investigated. The engine was motored whilst the FFID was used to sample from the combustion chamber. No fuel was injected into the combustion chamber because of the complexities involved in ensuring that a homogeneous air fuel mixture existed every cycle in the cylinder. Both the motored cylinder pressure and the FFID output were recorded on an oscilloscope. A constant output from the FFID was obtained although the cylinder pressure varied.

This method for determining pressure independence is not completely satisfactory in that the motored cylinder pressure is lower than the cylinder pressure achieved when the engine is fired. Additionally, the rate of increase in pressure in the motored cylinder pressure trace will not be as great as that encountered under firing conditions (chapter 1,

figure 1.5) Pressure independence over the entire range of cylinder pressures encountered under normal firing conditions has therefore not been fully proven for the particular application investigated here. However it will be seen that the readings are used more in a comparative way than as absolute readings. Also cylinder pressure was monitored throughout the testing and was found to be relatively consistent for a particular test condition.

The depressions set in the flame chamber and in the CP chamber were values recommended by the manufacturer of the FFID (table 7.1).

ΔP (mmHg)	160
C_p (mmHg)	300
T * (°C)	150
Span Gas	5% C_3 in N_2

* Temperature of heated sample line

Table 7.1: Specifications of the FFID (see figure 7.2)

7.2 Typical In-Cylinder FFID Trace

Figure 7.3 shows two superimposed in-cylinder HC traces taken at two different points in the combustion chamber over one complete engine cycle. It may be assumed that the fuel and air mixture in the cylinder was homogeneous. The output is recorded in terms of voltage versus time but, with a knowledge of the system calibration, the voltage output can be converted to HC concentration (second x-axis marked in red).

The x-axis does not have a uniform scale but rather it contracts and expands over an engine cycle. This is because the time taken (transit time) for a sample to enter the probe and be measured is a function of cylinder pressure. The transit time is also dependent on the diameters of the internal FID tubes, and the depressions set in the flame and the CP chamber. As the cylinder pressure is increased the transit time will decrease, and vice versa. *SATFLAP,* a software program provided by the manufacturers, can be used to

estimate the transit time for different system dimensions, and it enables features such as BDC or TDC to be marked on the diagrams.

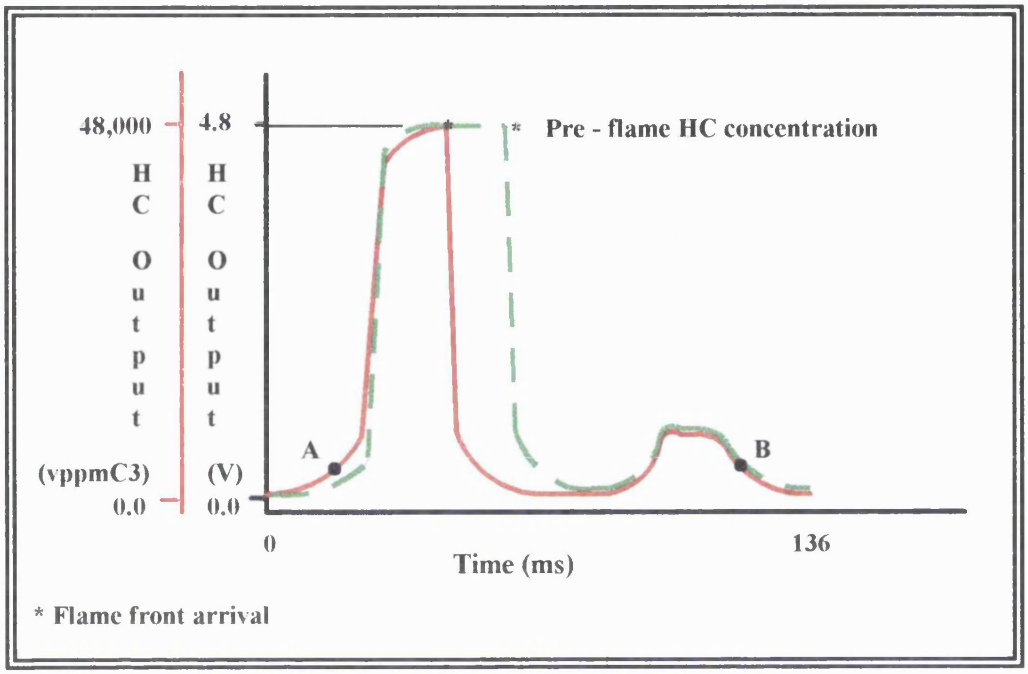

Figure 7.3: Two typical in-cylinder FFID traces superimposed

With reference to figure 7.3, (red line), towards the end of the intake stroke (point A), the cylinder pressure has increased to a level such that there is sufficient flow through the probe and the signal becomes 'valid'. The output begins to increase as it detects the evaporated fuel in the intake charge. During compression the output increases further until it approaches a maximum value at which it begins to level off. This maximum value represents the pre-flame HC concentration in the cylinder at the sample point prior to flame arrival, and it is this maximum value that holds the most interest for the current application. At ignition the fuel begins to burn, and when the flame front reaches the probe (*), the UHCs in the vicinity are rapidly burnt and the output abruptly falls to a low level. Somewhat later in the cycle the exhaust valve begins to open, causing the unburnt hydrocarbons (UHCs) to be sucked out of the crevices. The output measured by the FFID will increase if these UHCs pass in the vicinity of the probe. Again when the cylinder pressure decreases beyond a critical value, there is no longer sufficient flow along the probe and the signal becomes invalid once more (point B). This occurs when the inlet valves open if the engine is running under throttled conditions.

The output voltage from the FFID can only be considered representative of the HC concentration if it reaches a stable plateau (Crawford *et al* (1996)). The further the distance between the probe and the spark plug, the greater the available time for the HC concentration to achieve its 'true' maximum. This will manifest itself on the HC trace as indicated by the green line.

7.3 Calibration of the FFID

Prior to each engine test, the FFID probe, tee-piece and FID tube (figure 7.2) were cleaned and the system checked for any leaks. Leak testing involved applying a concentrated source of hydrocarbon gas (lighter fuel) around the FFID probe and FFID head, whilst the output was monitored on an oscilloscope. A constant output indicated that no gas was leaking into the system. The system was then calibrated by flooding the FFID probe with a calibration gas (5% propane in nitrogen) and optimising the fuel and air flows to give a maximum voltage output. On completion, the span control was adjusted so that an output of 1.0 V was equivalent to 10,000 vppm propane (C_3) and the probe was inserted into the engine. After each engine test, the system was again leak tested and the calibration was checked to ensure the probe had not become blocked during the test, and that the calibration had not drifted significantly. If the calibration was $\pm$ 3 % away from the original calibration, or the system was found to be leaking, the test was repeated.

It is important to note that the calibration carried out was a static calibration and not a dynamic calibration. The advantage of dynamic calibration is that it allows the FFID system to be calibrated when the engine is running, and therefore the temperatures and pressures are similar to those exhibited during an engine test. A static calibration is carried out at room temperature and pressure. For identical sample gas concentrations, the dynamic calibration will yield a lower output than a static calibration. This is because the FFID output is proportional to the number of carbon atoms burnt in HC form. The number of carbon atoms burnt will decrease as the density of the sample gas through the FFID probe decreases, which can be caused by an increase in the temperature of the

FFID probe, and thus the sample gas itself (Cambustion HFR400 FFID User Manual (version 3.1)). A dynamic calibration was not chosen due to the constraints of space close to the spark plug. The dynamic calibration system required the FFID probe to be inserted into an adapter which was 5 mm in diameter as compared to the FFID probe which was 3 mm in diameter. The available space at the chosen sample location was only 4 mm. For the purpose of this investigation, a static calibration was thought to be satisfactory because comparative data was required as opposed to absolute data.

7.4 Test Conditions and Procedures

The FFID testing was divided into two stages:

1) measurement of the HC concentration at two specified locations (section 7.4.2,),
2) HC measurements at a number of other locations throughout the combustion chamber volume (chapter 9).

and where applicable, measurement of the in-cylinder HC concentration for the following tests were carried out for each stage:

(i) closed-valve injection,
(ii) various open-valve injection timings,
(iii) skip-firing tests,
(iv) different injector locations,
(v) variation of the fuel pressure.

For both stages the following test procedure was used.

7.4.1 Test Procedure

The optical research engine and its control system, as described in chapter 2, were used for the testing described here. The FFID system was leak tested and calibrated as above and the probe(s) were positioned at their relative points in the combustion chamber. The engine was then motored and the speed and manifold depression were set to the required values, and the air flow was checked for consistency with the test condition. The fuel

injection system was initiated and the engine was fired for 1 minute. The output from either or both sample probes were simultaneously displayed on a *Nicolet* digital oscilloscope and recorded on a *Nicolet XF-44/2* dual disk recorder, together with the fuel injection pulse and cylinder pressure (the cylinder pressure was measured with a Kistler pressure transducer type 7121a). Each sweep displayed by the oscilloscope had to be recorded before a second sweep could be taken. At idle, a sweep comprised of 6-7 consecutive engine cycles which took approximately 4 seconds to record and write to disk. A total of 15 sweeps could be recorded within the period of 1 minute.

7.4.2 Stage 1: HC Concentration at Two Locations Close to the Combustion Chamber Surface

For the first stage of testing, the FFID was used to measure the HC concentration simultaneously at two points in the combustion chamber. The first probe measured the HC concentration in the region of the sparking plug, and the second at a point on the exhaust side of the cylinder bore, 23 mm beneath the cylinder head surface (figure 7.4). The cylinder bore location was chosen to check whether the fuel, having been deflected from the inlet valve, continued to travel past the spark plug and impact on the cylinder bore on the opposite side. In addition, if this proved not to be true, the reading would also provide an indication of the degree of stratification that existed within the cylinder between these two locations.

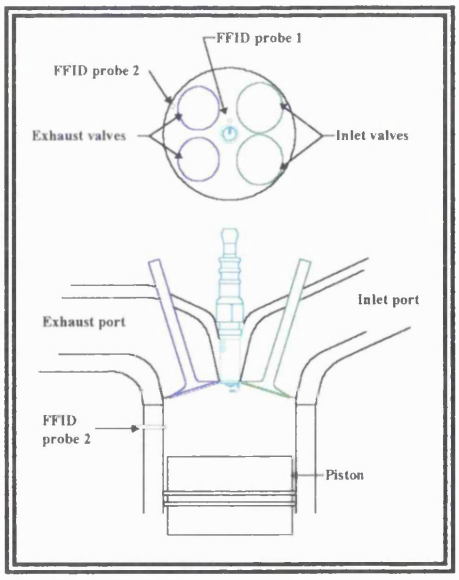

Figure 7.4: Cylinder head showing position of both probes

The last 20 mm of each probe was threaded to allow them to be screwed into position. Also because the probes had to be frequently removed for calibration, they were fitted with sleeves so that they could be relocated into the cylinder with an accurately set protrusion of 2 mm (plate 7.1). The location of the second probe meant that it was covered by the piston for 22.5° either side of TDC, and because it protruded into the cylinder, it was necessary to cut a small slot in the piston cap to prevent the probe tip from coming into contact with the piston (figure 7.5).

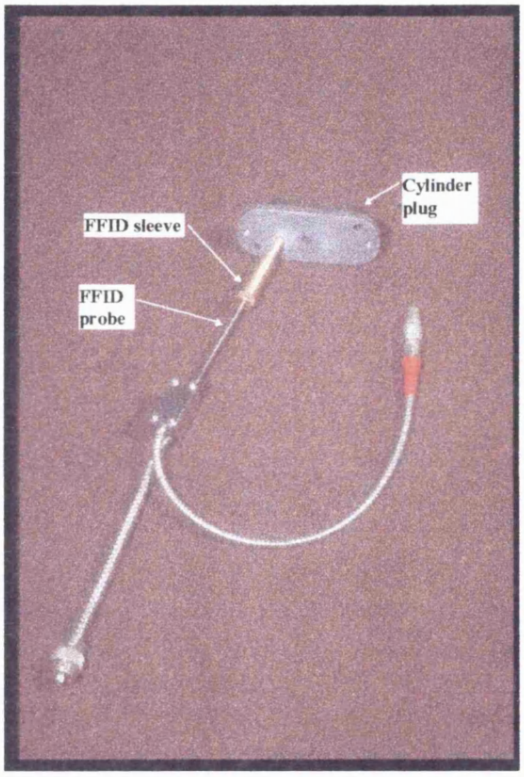

Plate 7.1: FFID probe and sleeve

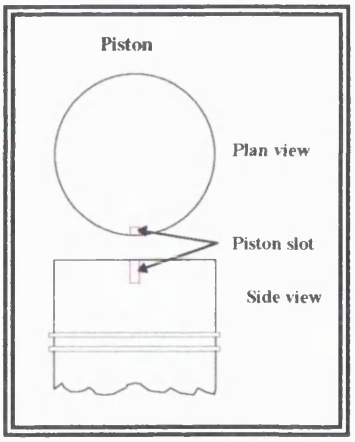

Figure 7.5: The slotted piston

7.5 Concluding Comments

A method for measuring the in-cylinder HC concentrations at specific points in the combustion chamber was decided upon. The two following chapters describe and discuss the test results obtained.

Chapter 8

In-cylinder Hydrocarbon Concentration Measurements

This chapter describes how the degree of stratification achieved with the targeted injector arrangement was estimated by comparing the output from the FFID (chapter 7) at the spark plug for open and closed-valve injection timings. This comparison was made on the basis that closed-valve injection timings would tend to produce mixtures in the cylinder that approached homogeneity, whereas open-valve injection timings would result in stratification.

With closed-valve injection the injected fuel is ready to enter the cylinder as soon as the inlet valve opens. The initial backflow period aids the mixing as the fuel is pulled back up the inlet port, and only on flow reversal does it begin to travel in the direction of the cylinder. The fuel is located at the front of the swirling motion and In-Young *et al* (1993) postulate that it cannot be moved with the strong swirling motion so good mixing occurs (figure 8.1). Similar conclusions were drawn by Winklhofer *et al* (1992) for closed-valve injection but through a different mechanism. They observed the fuel vapour (through the infra-red laser light radiation being absorbed by the hydrocarbon molecules) to hang around the inlet valve where it was purged and diluted with the air that entered the cylinder later on. This combined with the initial low levels of bulk turbulence but high air velocities caused good mixing between the fuel and air, with the resulting distribution within the cylinder approaching homogeneity. With open-valve injection, the interaction between the initial back flow of gas and the fuel can be avoided by initiating injection after the back flow has finished. As such it was thought that the fuel would move with the bulk air motion as a pocket of fuel with swirling air in front and behind it. No significant degree of mixing between the air and the fuel would occur and the overall charge would be stratified (In-Young *et al* (1993)).

The HC concentration was also measured at a single point on the cylinder bore (chapter 7 section 7.4.2 figure 7.4) and comparison of the cylinder bore and spark plug data gave a further insight into the stratification effect as will be shown later in this chapter.

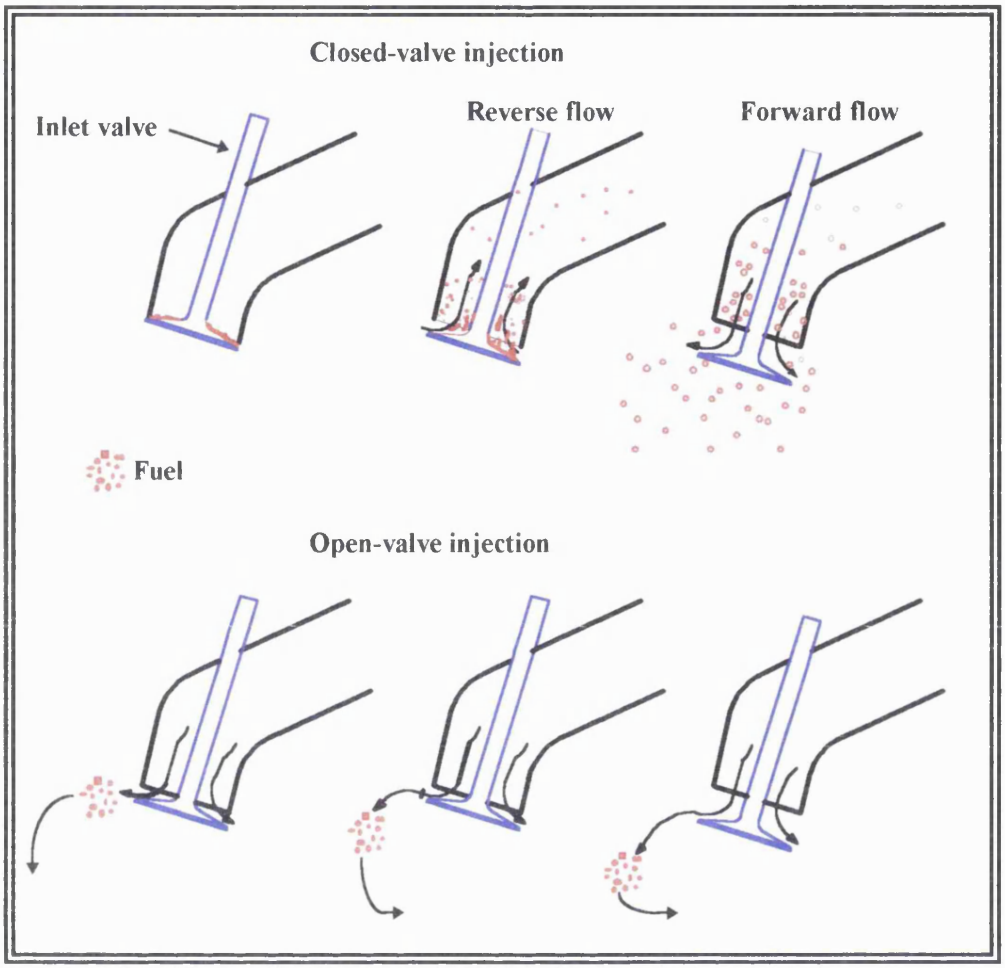

Figure 8.1: Mixing of fuel with open and closed-valve injection

8.1 FFID Analysis

The variation in voltage output from both FFID probes, the output from the cylinder pressure transducer and an injection pulse (y-axis), were recorded simultaneously with respect to time (x-axis). A typical set of results recorded for sweep 2 (taken approximately 4 seconds after initiation of the fuel injection) is shown in figure 8.2. The red trace represents the HC concentration at the spark plug, and the blue trace the HC concentration at the cylinder bore. The green square wave shows the start (as the signal goes from low to high) and end (as the signal goes from high to low) of fuel injection for each cycle. For clarity cylinder pressure has not been included in the figure.

Several programs were written using *Matlab* software to convert the data into more appropriate units (time into crank degrees, and to convert the voltage output from the

FFID into HC concentration measured in vppm propane) and to analyse and present the data. Although the engine speed did not vary greatly during a test, there was a gradual increase of around 40 rpm during the test period. The *Matlab* programs accounted for the variation in engine speed by applying a cubic spline interpolation to the raw data in order to calculate the FFID output every 0.5° crank angle. This allowed the HC trace obtained for individual cycles within a sweep to be superimposed onto one another. A complete cycle was defined as being from the start of fuel injection in one cycle (0° crank) to the start of fuel injection in the subsequent cycle (720° crank). Good agreement was achieved between the curve-fitted data and the raw data (appendix C figure C1). The key below is for all subsequent FFID traces unless otherwise stated.

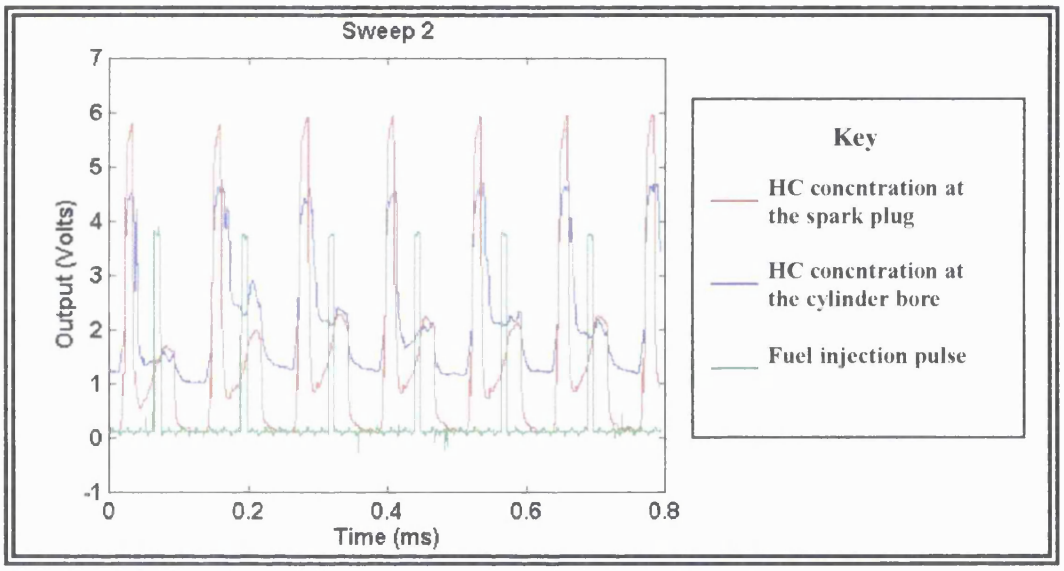

Figure 8.2: Closed-valve injection traces recorded 4 seconds after the start of fuel injection, idle condition

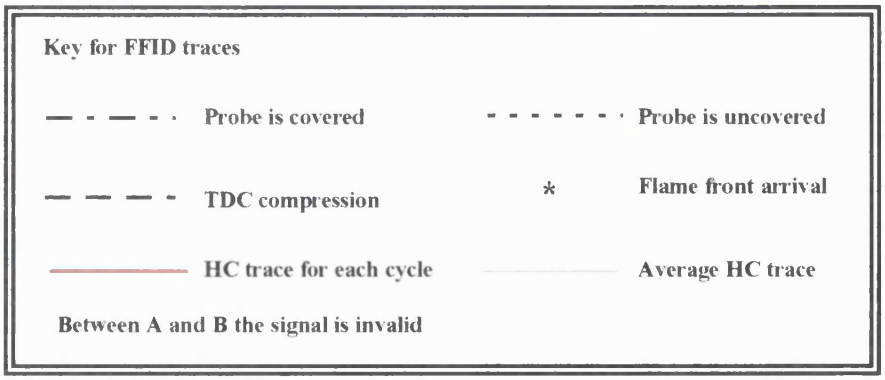

In the analysis of the FFID results, the first recorded sweep was not considered. This is because the engine often did not fire continuously throughout the first sweep, leading to high HC levels which would be unrepresentative of the levels obtained throughout the rest of the sweeps. The results for the idle condition (chapter 3, section 3.2, table 3.1) are discussed first.

8.2 Results, Idle Condition

8.2.1 Condition 1: Closed-Valve Injection

The in-cylinder HC traces obtained at the spark plug and at the cylinder bore for each cycle within sweep 2 (taken approximately 4 seconds after the start of fuel injection) and sweep 15 (taken approximately 60 seconds after the start of fuel injection) have been superimposed on separate graphs and are shown in figures 8.3 a and b, and 8.4 a and b respectively for the idle condition.

Both sets of figures show that *within* a sweep the HC traces were very similar, and in particular the maximum HC concentration achieved did not vary significantly. The maximum HC concentration is known as the pre-flame HC concentration. It is important to be aware when applying this term to the maximum HC level obtained at the cylinder bore that the probe is covered by the piston for approximately 22.5° either side of TDC. Therefore the maximum value obtained in each cycle is not necessarily the pre-flame HC concentration for this location since the probe is covered prior to flame arrival (ignition occurs 15° BTDC), and can only sample the gases in the top land crevice rather than in the bulk gases. It will also be considered later on that the maximum value achieved at the spark plug is not necessarily the absolute value of the pre-flame HC concentration.

For the results shown in figure 8.3 a and b and 8.4 a and b, the maximum pre-flame HC concentration varied less than 2 % away from the average, except for one instance at the cylinder bore where the variation was 2.6 %. Since the accuracy of the FFID is nominally 2 % (Cambustion HFR400 FFID User Manual (Version 3.1)), it is unlikely that the variation in the pre-flame HC concentration within a sweep is due to cycle to cycle variations in the HC concentration, but rather, is the random variation in the FFID's

measurement of any true variation (Lipson *et al* (1973)). The minimal amount of cycle to cycle variation exhibited for closed-valve injection is clearly shown in figure 8.5 where the average pre-flame HC concentration measured for each sweep at the spark plug and at the cylinder bore have been plotted together with their standard deviations.

The average traces obtained at the spark plug for sweep 2 (figure 8.3 a) and sweep 15 (figure 8.3 b) and the average traces obtained at the cylinder bore for sweep 2 (figure 8.4 a) and sweep 15 (figure 8.4 b) have been superimposed and are shown in figures 8.6 a and b.

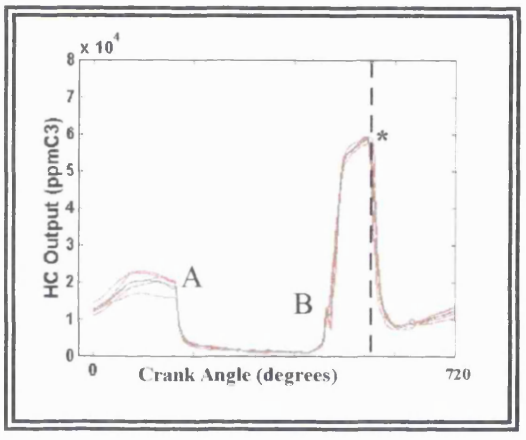

Figure 8.3 a: Sweep 2, probe at spark plug, closed-valve injection, idle condition

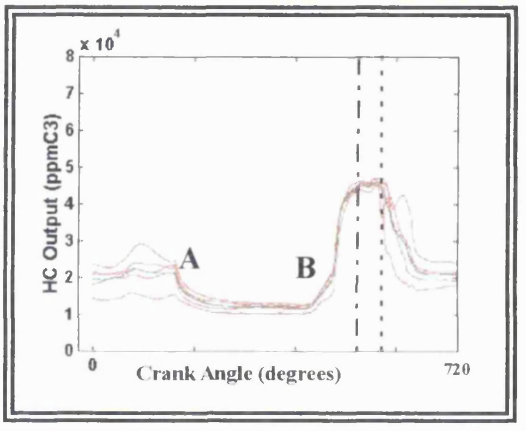

Figure 8.4 a: Sweep 2, probe at cylinder bore, closed-valve injection, idle condition

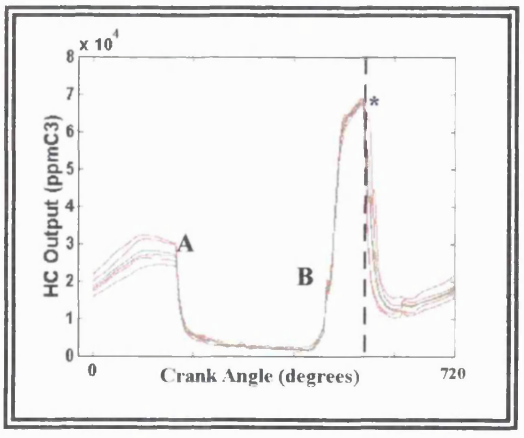

Figure 8.3 b: Sweep 15, probe at spark plug, closed-valve injection, idle condition

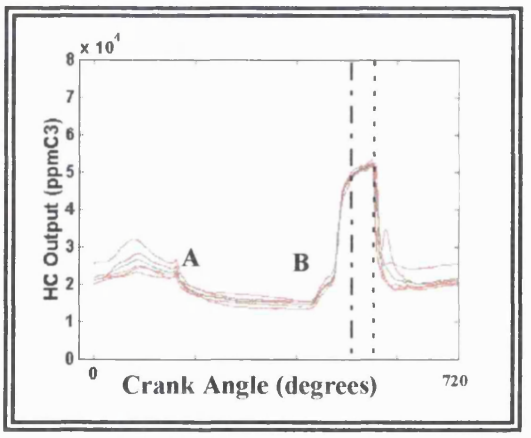

Figure 8.4 b: Sweep 15, probe at cylinder bore, closed-valve injection, idle condition

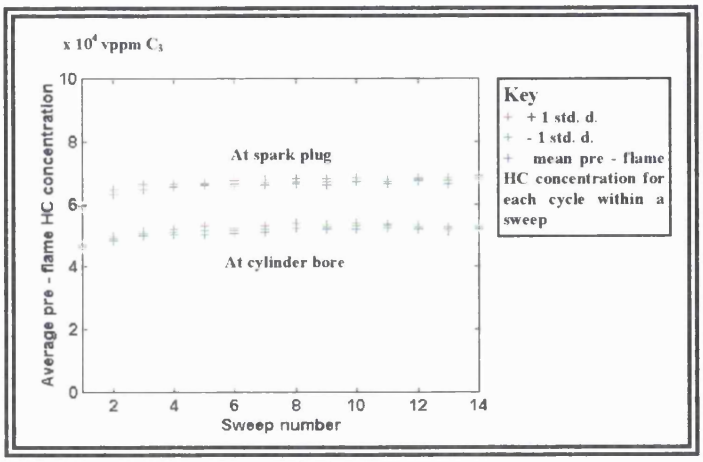

where std.d. = standard deviation

Figure 8.5: Average pre-flame HC concentration at the spark plug and cylinder bore for each sweep together with ± 1 std. d., closed-valve injection, idle condition

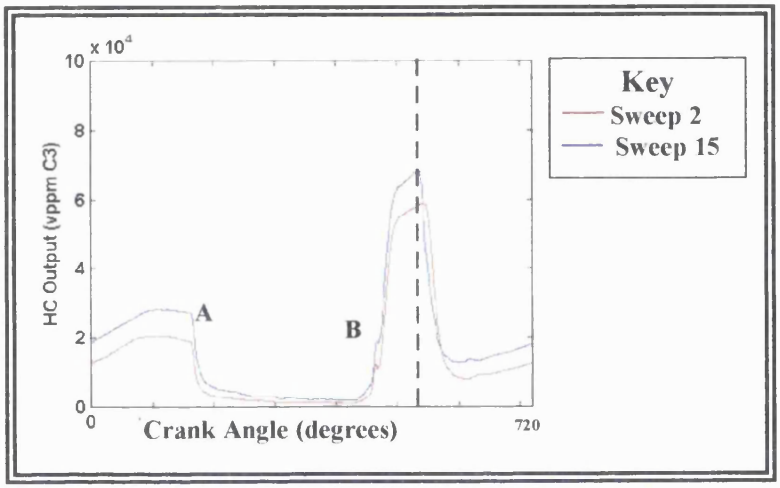

Figure 8.6 a: Average HC trace at the spark plug for closed-valve injection, sweeps 2 and 15, idle condition

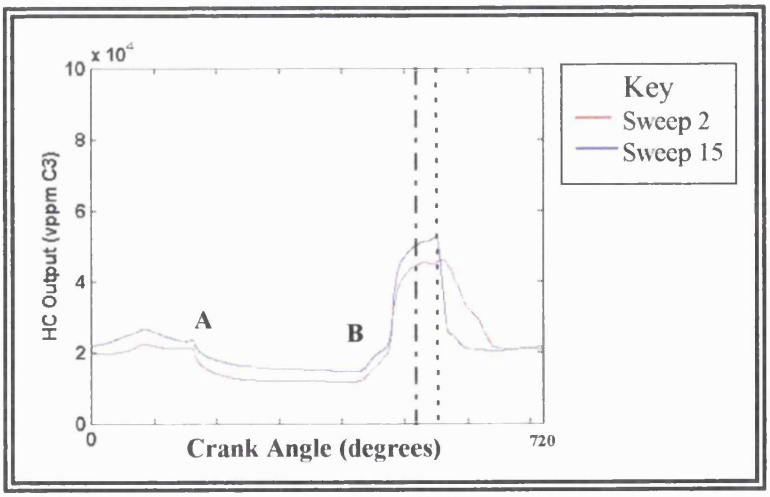

Figure 8.6 b: Average HC trace at the cylinder bore for closed-valve injection, sweeps 2 and 15, idle condition

Considering the HC concentration at the spark plug, the average value for the pre-flame HC concentration achieved during each sweep, gradually increased from an initial peak of 5.90 x 10^4 vppm propane to 6.85 x 10^4 vppm propane from start to end of a test, an increase of 16 %. There was a gradual increase of 13 % at the cylinder bore. This increase can be explained because fuel evaporation and the establishment of a stable inlet port wall film are time-dependent processes (Winklhofer *et al* (1994)). Considerable wetting of the port surfaces can occur and fuel films begin to form as a consequence of the backflow period even though the fuel injector is targeted at a specific point on an inlet valve. As the port and combustion chamber surfaces warm up, the rate of evaporation of the fuel increases and its viscosity decreases, thereby facilitating the passage of the fuel from the inlet port film into the engine. Shin *et al* (1995) measured an increase in the port wall temperature 43 mm from the cylinder entrance of approximately 50° C (to a temperature of 75° C) over the first minute of engine firing. An increase in the temperature of this order almost halves the viscosity of petrol (Brown *et al* (1991)).

Several researchers (Ladommatos *et al* (1995), Schurov *et al* (1995), Brown *et al* (1991)) have looked at the wetting of the port surfaces, and have measured or modelled the percentage of the injected fuel that has remained on the port walls as opposed to entering the combustion chamber. Under steady engine conditions, the fuel that is deposited on the port floor will reach a stable value. At this point, the quantity of fuel impinging on the fuel film and adding to it is equivalent to that which is removed by vaporisation, flow into the cylinder or by re-entrainment (Ladommatos *et al* (1995)). It is thought that the increase in the pre-flame HC level from start to end of a test is due to changes in balance between these processes. Further evidence for this is provided by investigating the rate at which the average pre-flame HC concentration increased with time from sweep to sweep (figure 8.7). The increase in HC concentration measured in the cylinder will begin to level off as the equilibrium film level is achieved. Chen *et al* (1996) estimated that it would take approximately 30 seconds for the liquid fuel flow to approach a steady state at an engine speed of 1000 rpm road load. This corresponds to a point around sweep 8 in figure 8.7.

It was found that a difference in the maximum levels achieved did exist between that measured at the spark plug and that measured at the cylinder bore (figure 8.8). In sweep 2 this difference was of the order of 21 % and by sweep 15 it was 23 %. Although at first glance it would appear that some stratification effect did exist for closed-valve injection, it is more likely that the masking effect of the piston on the probe prevented true measurement of the HC concentration, and the pre-flame HC level was underestimated for the cylinder bore probe. However, this may not account for all of the difference as the traces diverge even before the probe at the cylinder bore is covered.

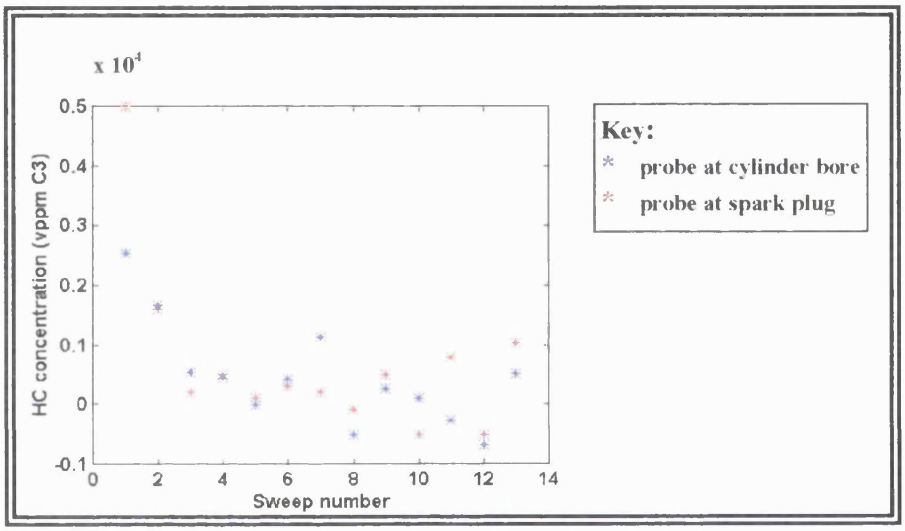

Figure 8.7: Rate of increase of the pre-flame HC concentrations at the spark plug and cylinder bore for closed-valve injection, idle condition

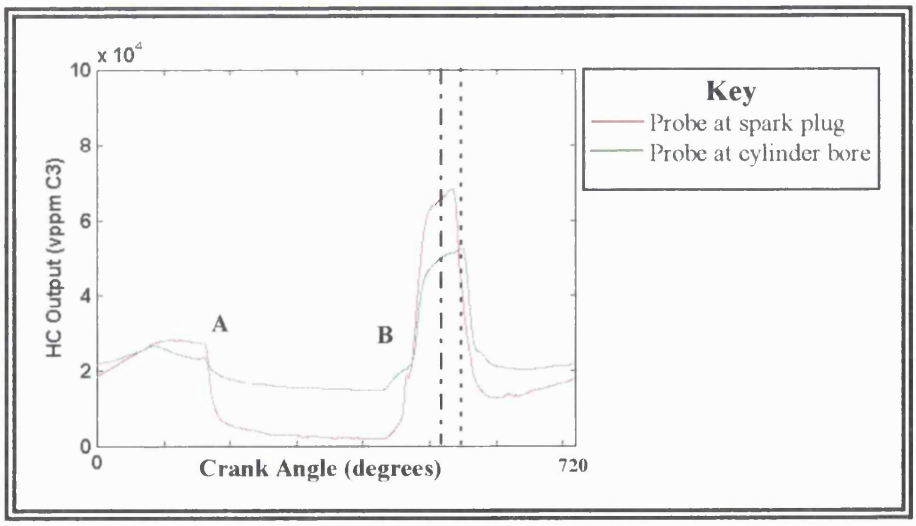

Figure 8.8: Traces from probe at spark plug and cylinder bore superimposed for sweeps 2 and 15, closed-valve injection, idle condition

8.2.2 Condition 2: Open-valve Injection, Idle Condition

The degree of stratification that may be obtained with open-valve injection can vary with injection timing. Consequently, the open-valve injection timings were varied between start of injection 65° ATDC to 135° ATDC in 10° intervals for the idle condition. An additional test was performed with the end of injection timed at 60° ATDC. The FFID traces obtained at the spark plug and cylinder bore from sweep 2 for all the open-valve injection timings have been plotted in figures 8.9 a and b to 8.17 a and b.

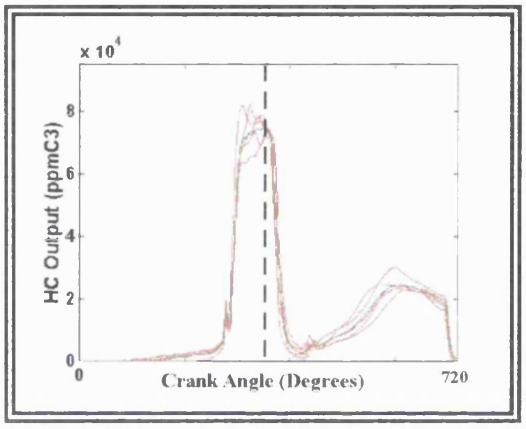

Figure 8.9 a: Sweep 2, probe at spark plug, end of injection timing 60° ATDC, idle condition

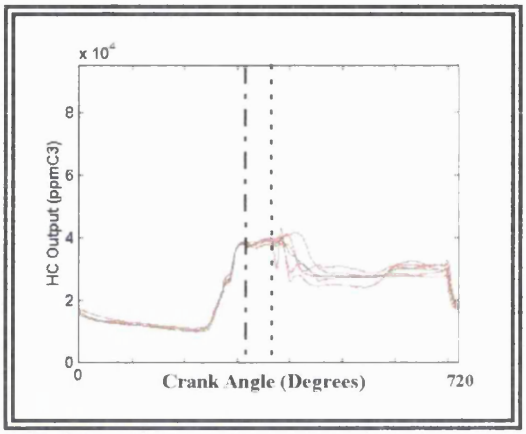

Figure 8.9 b: Sweep 2, probe at cylinder bore, end of injection timing 60° ATDC, idle condition

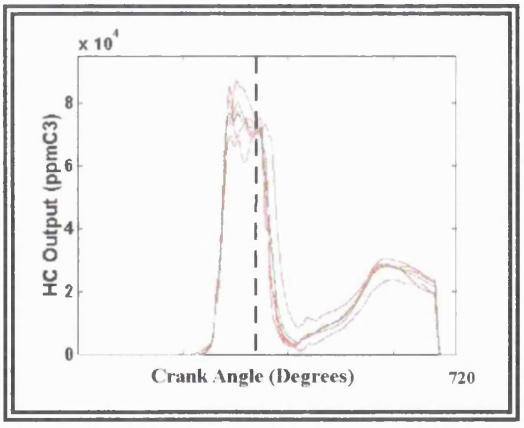

Figure 8.10 a: Sweep 2. probe at spark plug, injection timing 65° ATDC, idle condition

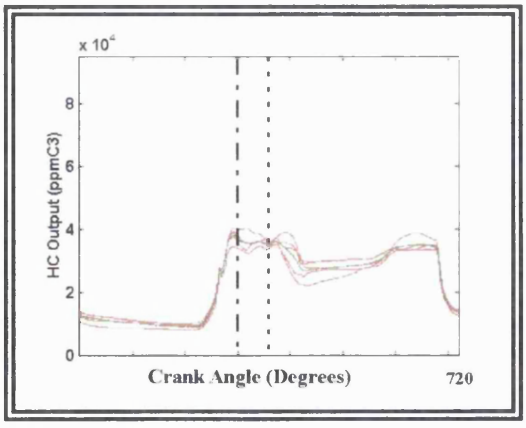

Figure 8.10 b: Sweep 2, probe at cylinder bore, injection timing 65° ATDC, idle condition

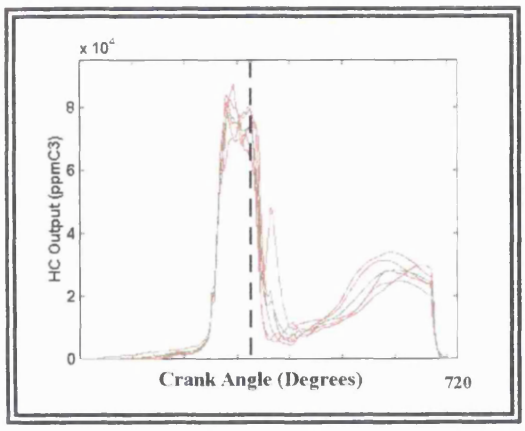

Figure 8.11 a: Sweep 2, probe at spark plug, injection timing 75° ATDC, idle condition

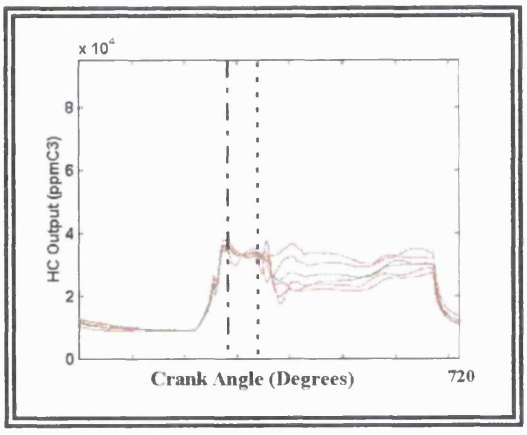

Figure 8.11 b: Sweep 2, probe at cylinder bore, injection timing 75° ATDC, idle condition

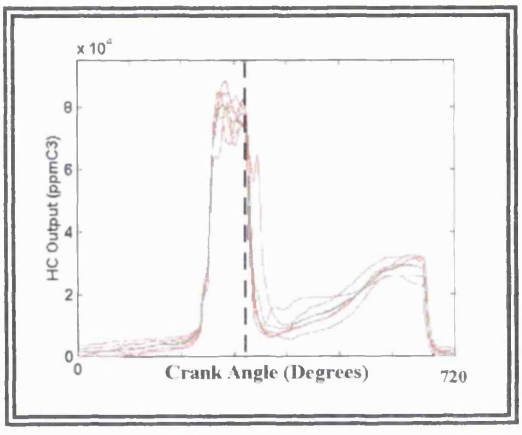

Figure 8.12 a: Sweep 2, probe at spark plug, injection timing 85° ATDC, idle condition

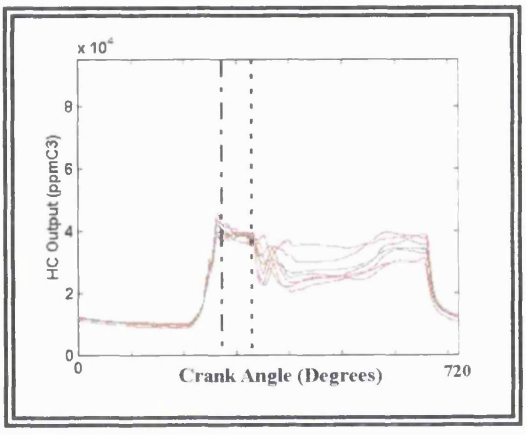

Figure 8.12 b: Sweep 2, probe at cylinder bore, injection timing 85° ATDC, idle condition

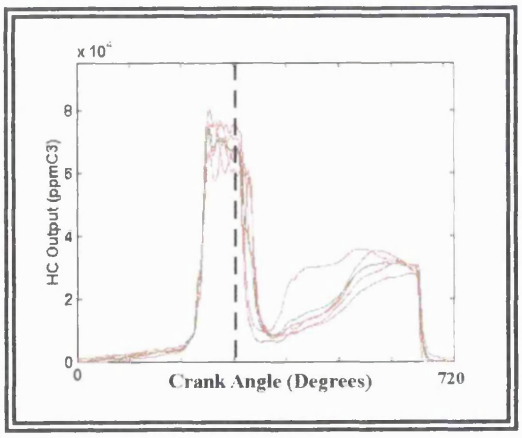

Figure 8.13 a: Sweep 2, probe at spark plug, injection timing 95° ATDC, idle condition

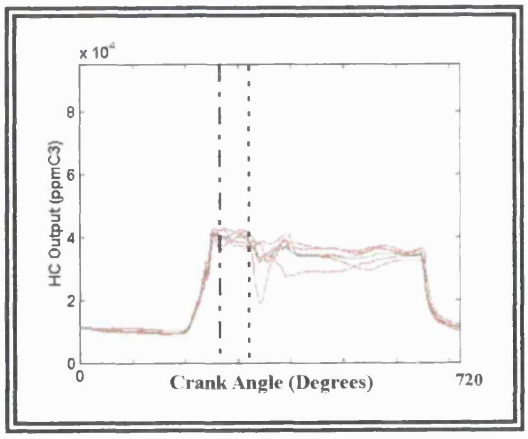

Figure 8.13 b: Sweep 2, probe at cylinder bore, injection timing 95° ATDC, idle condition

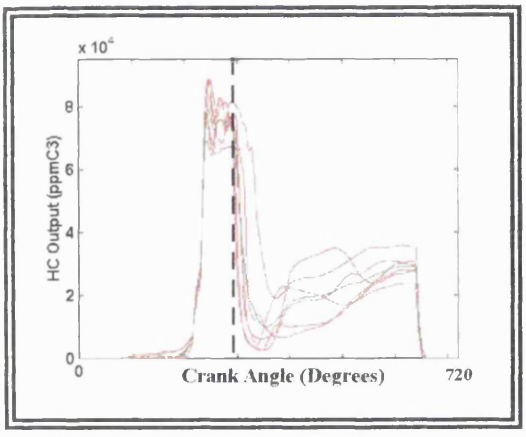

Figure 8.14 a: Sweep 2, probe at spark plug, injection timing 105° ATDC, idle condition

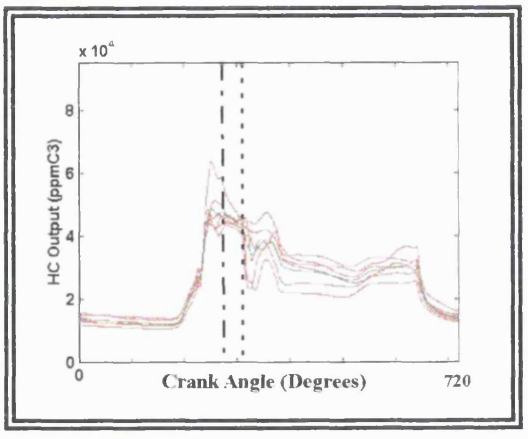

Figure 8.14 b: Sweep 2, probe at cylinder bore, injection timing 105° ATDC, idle condition

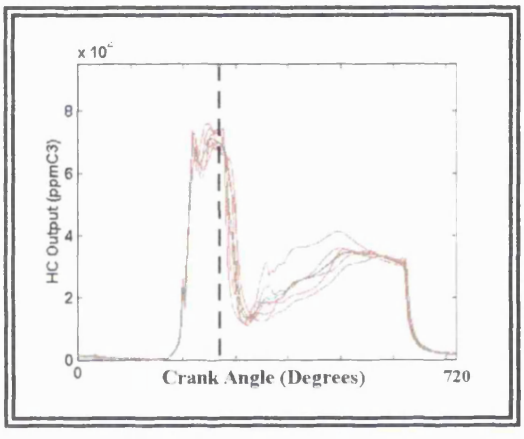

Figure 8.15 a: Sweep 2, probe at spark plug, injection timing 115° ATDC, idle condition

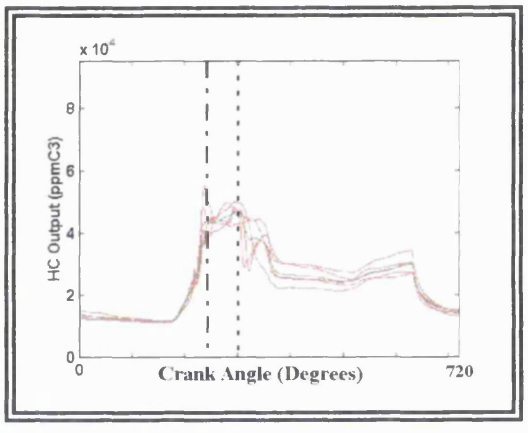

Figure 8.15 b: Sweep 2, probe at cylinder bore, injection timing 115° ATDC, idle condition

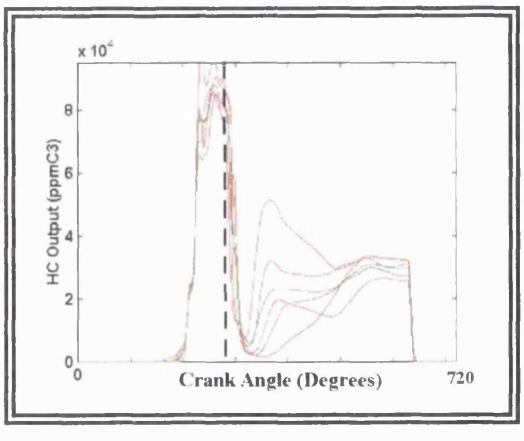

Figure 8.16 a: Sweep 2, probe at spark plug, injection timing 125° ATDC, idle condition

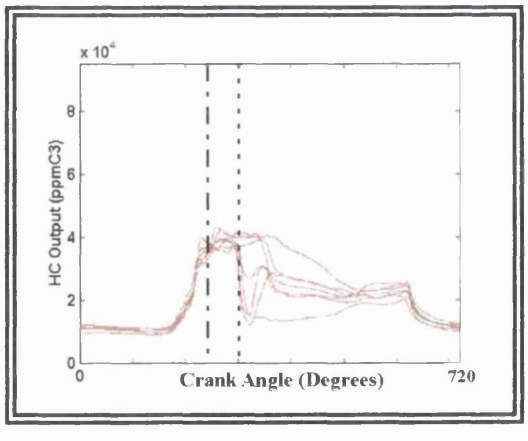

Figure 8.16 b: Sweep 2, probe at cylinder bore, injection timing 125° ATDC, idle condition

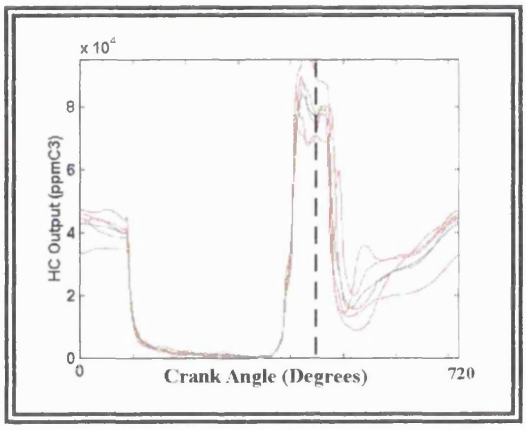

Figure 8.17 a: Sweep 2, probe at spark plug, injection timing 135° ATDC, idle condition

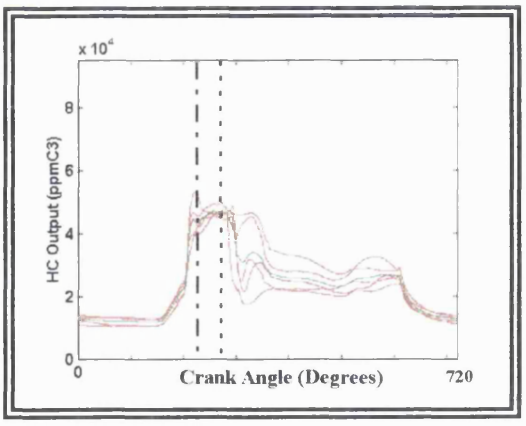

Figure 8.17 b: Sweep 2, probe at cylinder bore, injection timing 135° ATDC, idle condition

Considering the traces obtained at the spark plug (figures 8.9 a-8.17 a), the pre-flame characteristics varied significantly from cycle to cycle. With closed-valve injection there was a gradual flattening of the curve prior to flame arrival and the cycle to cycle variability was minimal (figures 8.3 a and 8.5). In contrast, the pre-flame HC level for open-valve injection exhibited a jagged appearance and comprised of a number of peaks and troughs. It was thought that these peaks and troughs represented real-time HC concentration fluctuations due to rich clouds of vapour or fuel droplets passing the probe.

Summaries of the results shown in figures 8.9 to 8.17 a and b are given in figures 8.18 and 8.19. Figure 8.18 shows the peaks of HC readings for each sweep plotted against cycle number for the probe situated at the spark plug, the different colours refer to the different injection timing. Although the amount of fuel injected was the same in each case, it can be seen that the higher HC concentrations were recorded for all open-valve injection timings compared with the closed-valve injection timing (circles). The timing that gave the highest readings, and hence most stratification, was when injection started 135° ATDC. The pattern is not so clear for the probe situated in the cylinder bore (figure 8.19), and this is to be expected considering that it was covered by the piston. Here only the results for closed-valve injection and the open-valve injection timings that gave the lowest and highest peaks for each cycle have been plotted, together with the peaks per

cycle for an open-valve injection timing of 135° ATDC.

Key For Figures

Injection starts 50° ATDC	Injection starts 105° ATDC
Injection starts 65° ATDC	Injection starts 115° ATDC
Injection starts 75° ATDC	Injection starts 125° ATDC
Injection starts 85° ATDC	Injection starts 135° ATDC
Injection starts 95° ATDC	Closed-valve Injection

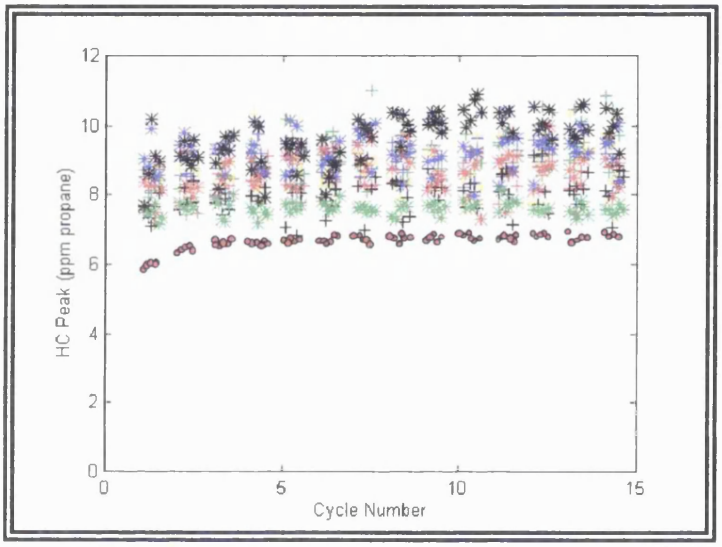

Figure 8.18: Peak obtained in each sweep at the spark plug for each injection timing against sweep number, idle condition

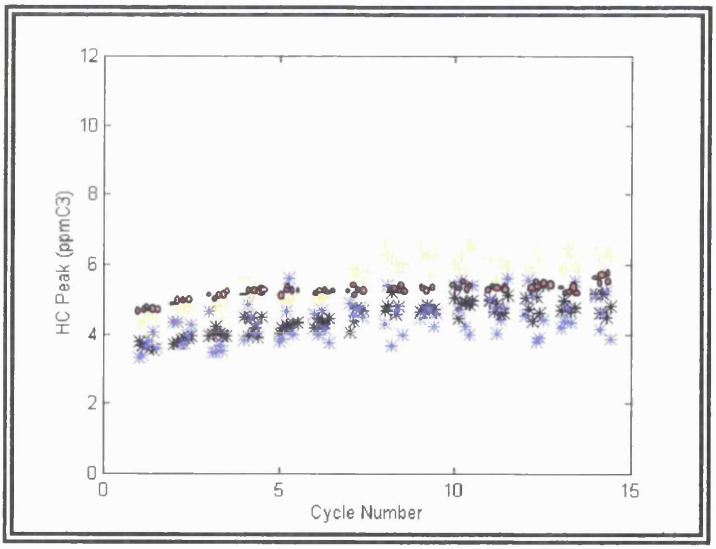

Figure 8.19: Peak obtained in each sweep at the cylinder bore for each injection timing against sweep number, idle condition

8.3 Results, 1500 rpm, Road Load Condition

Similar trends were obtained at 1500 rpm road load condition. Again with closed-valve injection there was a gradual flattening of the curve prior to flame arrival, and with open-valve injection the shape of the curve prior to flame arrival consisted of a number of peaks and troughs. The pre-flame HC concentrations obtained with all the open-valve timings at the spark plug were greater than those obtained for closed-valve injection, and those at the cylinder bore were always less. The closed-valve injection traces obtained for each cycle in sweep 2 at the spark plug have been superimposed onto one another and is shown in figure 8.20. Similarly the open-valve traces obtained at the spark plug for that injection timing that gave the greatest stratification effect has also been plotted and is shown in figure 8.21.

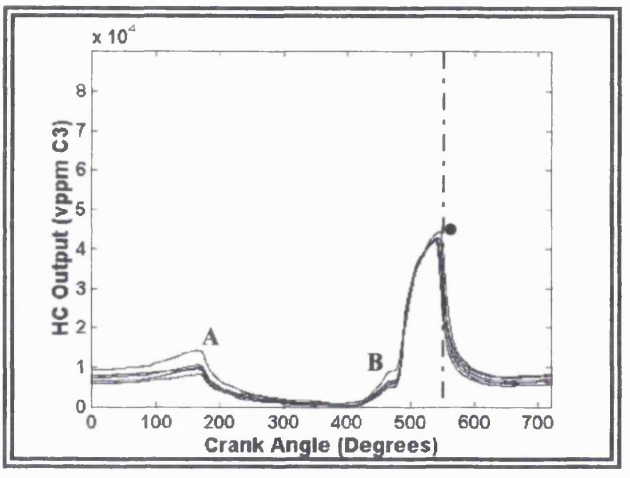

Figure 8.20: Sweep 2, probe at spark plug, closed-valve injection, 1500 rpm road load condition

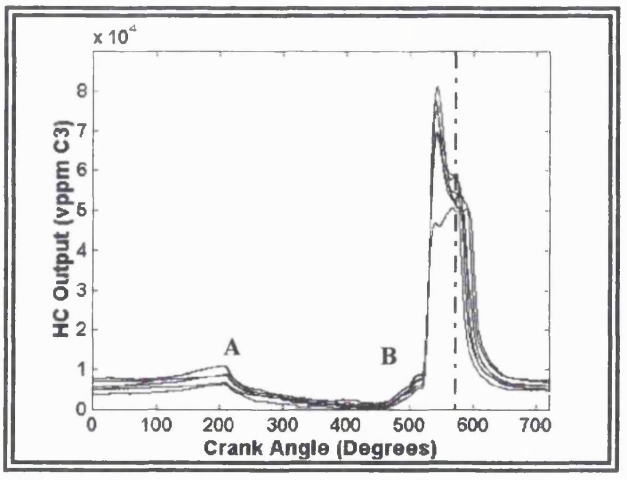

Figure 8.21 a: Sweep 2, probe at spark plug, injection starts x° ATDC, 1500 rpm road load condition

8.4 Comparison of Open and Closed-Valve Injection

The pulsewidths of injection were equivalent to 22° crank angle at idle and 45° crank at the 1500 rpm road load condition. These pulsewidths corresponded to the relatively rich overall AFR of 9.7:1 for idle and 13:1 for the 1500 rpm road load condition, and were common to all injection timings for each engine speed. The nominal overall AFR was calculated from a knowledge of air and fuel flow rates, and were chosen to give a rapid first fire from initiation of injection so as not to accumulate liquid fuel in the combustion chamber.

The HC concentration of a stoichiometric mixture is around 47,000 vppm propane for a typical gasoline but an allowance has to be made for residual exhaust gas from the previous cycle when applying this to the in-cylinder FFID measurements. This modifies the HC concentration to 42,000 vppm propane for a stoichiometric mixture if allowance is made for a 12 % dilution by exhaust gas [Baker (1995)]. This gives the calculated pre-flame AFRs at the spark plug as being 9.2:1 for closed-valve injection and 6.4:1 for an open-valve injection timing of 135° ATDC at the idle condition. For the 1500 rpm road load condition, these figures are 14.2:1 and 9.2:1 respectively. One of the assumptions made is that all the fuel is vaporised by the time the flame reaches the probe.

There is moderately good agreement at idle between the AFR calculated from measured air and fuel flow rates (9.7:1) and that measured by the FFID in the cylinder for closed-valve injection (9.2:1) when the mixture is nominally homogeneous. The comparison at the 1500 rpm condition does not show such good agreement (13.1:1 from air and fuel flow measurements compared with 14.2:1 from the FFID measurements). One possible explanation is that not all of the fuel in the cylinder had evaporated because the readings were taken from sweep 2, around 10 seconds after the engine started firing consistently. The effect is likely to be more significant at 1500 rpm due to the shorter time available for evaporation.

8.5 Number of Cycles to First Fire

For all open-valve injection timings the engine began to fire after approximately 5-7 cycles, except for an injection timing of 125° ATDC which took at least 10 cycles. Closed-valve injection took at least 14 cycles before the engine began to fire. This provides some further evidence of the stratifying effect present with open-valve injection, while also suggesting that plug-wetting may not be a problem when the fuel is deflected off the valve.

8.6 Skip Firing Tests

Some skip firing tests were also carried out where the spark plug was disabled for one cycle and the in-cylinder HC concentrations were recorded with the FFID. This was to investigate whether the FFID had enough time to measure the 'true' in-cylinder HC concentration rather than measuring a percentage of it. It was found that the HC concentration recorded for the disabled cycle was greater than that recorded for the previous cycles. However the increase was comparable for both open and closed-valve injection timings. Thus it was concluded that although the absolute values may not be representative of the true in-cylinder HC concentrations comparisons between the open and closed-valve injection HC traces were valid.

8.7 Variation of Injector Location and Fuel Pressure

The injector block had been designed in such a way that it was possible to make small adjustments away from its datum position and this allowed investigation of the effects of production tolerances on engine performance. The effect of a relatively small movement (1-2°) changed the peak pre- flame HC concentration significantly (table 8.1), thus indicating a loss in the stratifying effect. In addition the characteristic of the peaks and troughs obtained for the open-valve injection timings with the injector accurately targeted was no longer present to such a significant degree. Further testing showed that the stratifying effect was fairly insensitive to changes in the fuel supply pressure between 2.7 and 3.5 bar (table 8.1)

	Average of peaks for sweep 2
Correct alignment: 3.5 bar fuel pressure*	92 x 10^4 vppm C_3
Mis-aligned: 3.5 bar fuel pressure*	45 x 10^4 vppm C_3
Correct alignment: 2.7 bar fuel pressure*	88 x 10^4 vppm C_3

*** relative to manifold depression**

Table 8.1: Comparison of average peak of HC concentration for spark plug probe, idle condition

8.8 Concluding Comments

It was evident that the targeted injector arrangement was achieving some degree of stratification, more so at the 1500 rpm road load condition than at idle. It might be thought that the variable nature of the peaks of the FFID traces for open-valve injection is undesirable, but it is probably an inevitable consequence of being able to concentrate the fuel close to the sampling point. The variability was probably caused by pockets of vapour and/or droplets passing the end of the probe.

The optimum timing was start of injection 135° ATDC for both idle and the 1500 rpm road load condition. It was apparent that the degree of stratification was sensitive to injection timing, although not overly so. More significant was the sensitivity to the alignment of the injector, which means that production tolerances would have to be carefully controlled with this concept. There was much less sensitivity to the variation of fuel pressure.

The observation that there was no sudden change in the peaks of the FFID traces during the 1 minute running period of the test suggested that the Leidenfrost temperature of the fuel was not being exceeded, although it might be for longer running at higher load. This however needs further investigation and the concept to be tested over longer periods of engine running.

There were very large differences between the values of peak HC readings taken at the spark plug and those at the cylinder bore. Care was taken not to convert those differences into AFRs of stratification, because of the masking of the cylinder bore probe by the piston. However it is of interest how the AFRs would vary around the cylinder with the targeted injector. It is likely that the ideal of having pure axial swirl with a rich central core is not being fully achieved in practice due to the complexities of air motion within the cylinder. This is explained in the next chapter and investigated by using a novel approach to mount the FFID probe in the cylinder. The method of mounting the FFID probe in the cylinder is also explained and some of the test results obtained are presented as well.

Chapter 9

In-cylinder Air Motion and its Effect on the In-Cylinder HC Concentrations

9.1 Introduction

The control of in-cylinder air motion can be utilized to optimize the combustion process for stability, fuel economy, noise and exhaust emissions without significantly impairing engine performance or engine cost (Boer *et al* (1990)). Controlled in-cylinder air motion may be tumble, swirl or a combination of both. The relative merits of each ordered air motion, and the mechanisms employed to promote its generation, have been discussed in some detail in chapter 1 but, to summarize, an ordered air motion can cause an increase in the small-scale turbulence levels in the cylinder around the time of ignition. This provides the potential for enhancing the early stages of combustion (thus causing a reduction in the delay angle) and also the main combustion period. Such fast burn systems have a greater tolerance to dilute mixtures, either present as a consequence of introducing EGR (internal and external) into the cylinder, or from utilizing lean air/fuel mixtures (Stone *et al* (1993)).

9.2 Zetec Port and Cylinder Head Geometry

The port and cylinder head geometry of the Zetec engine is such that there is a natural tendency to establish a tumbling motion within the cylinder. The Zetec cylinder head has a siamesed inlet port with a bifurcation into a dual inlet port just downstream of the standard injector location. The approach angle of the ports is set to establish the tumbling motion inside the cylinder, and this is helped by the valve guide boss profile (Boer *et al* (1990). In addition a shroud is incorporated into the cylinder head around the portion of the valve seat closest to the cylinder bore. Work carried out by Omori *et al* (1991) found that valve shrouding could be used to eliminate the intake flow on the cylinder bore side under the intake valves thereby enhancing the flow over the top of the valves and the overall tumbling motion (figure 9.1).

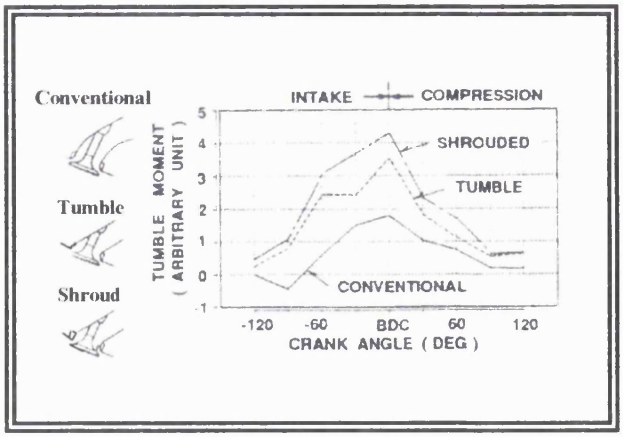

Figure 9.1: Tumbling moment in relation to crank degrees for different port designs [Omori *et al* (1991)]

The Zetec cylinder head has a 18.5° degree pent roof form. The shape of the cylinder head is significant in maintaining the tumbling motion until late in the compression stoke, rather than playing a part in the promotion of tumble. Measurements made by Boer *et al* (1990) on a Ricardo Hydra engine with a similar bore, stroke and compression ratio to that of the Zetec engine found that, for differing shaped cylinder heads, the peak turbulence intensities were similar provided that the angle of entry of the flow was the same. Those geometries that provided a natural shape for a vortical motion achieved their peak turbulence intensities slightly later in the compression stroke and tended to have lower turbulence intensities during the later stages of intake and the early stages of compression. Piston design can also help maintain tumble, but the Zetec engine does not employ any special piston design (chapter 1, section 1.10.1.2) as it uses a simple flat-topped piston.

9.3 The Modified Zetec Cylinder Head

A strong axial swirling motion was required in the cylinder so that a rich central core could be maintained around the spark plug and a leaner swirling mixture around the outside. It was thought that this could be achieved by creating axial swirl rather than tumble within the cylinder. The Zetec cylinder head was modified by sealing a brass plug into the right-hand inlet port (viewed from the inlet manifold side) downstream of the bifurcation. In this manner both inlet valves could be actuated but the fuel and air were forced to enter the combustion chamber via the left-hand inlet valve only (plates 9.1 a

and b). Blocking the right hand inlet port prevented puddling of the fuel beneath this inlet valve. It is envisaged that the principle could be applied in a production engine by having a butterfly valve situated in the right-hand port, which would be closed at part load conditions to allow a stratified charge to be established.

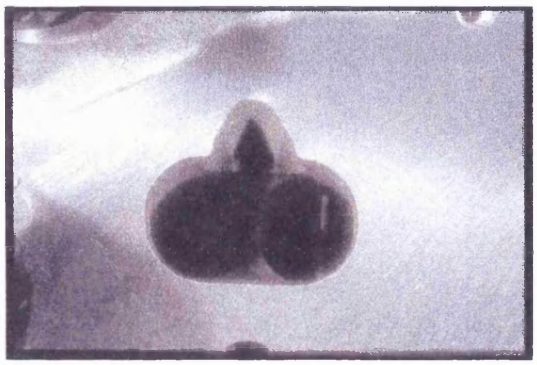

Plate 9.1 a: The conventional Zetec cylinder head inlet port entry geometry

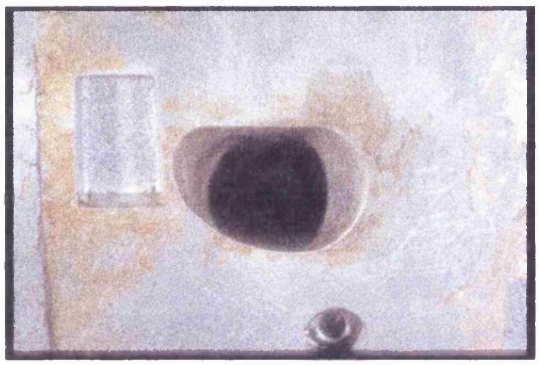

Plate 9.1 b: The modified Zetec cylinder head inlet port entry geometry

Port or valve deactivation combined with a cylinder head and port geometry designed to promote tumble is likely to produce an air motion that is a combination of axial swirl and tumble. Stone *et al* (1993) carried out steady-flow tests that investigated the tumble ratio with both valves opened, and then with the lift of each inlet valve reduced to 1 mm in turn. With both valves opened negligible axial swirl was induced in the cylinder and the air motion was one of tumble. A tumble ratio of 0.45 was obtained based on the Ricardo definition of swirl (Appendix 1). Disabling the right hand valve increased both the barrel and axial swirl to 0.85 and 1.40, respectively. These values were reduced slightly when the left hand valve was disabled. Baker (1995) reported similar findings for the Zetec engine, with valve deactivation producing higher levels of tumble within the cylinder than actuation of both inlet valves. This increase in tumble ratio was expected as a deactivating valve has the effect of doubling the velocity through the active valve with a consequent effect on charge momentum. Again the tumble ratio was greater when the right hand inlet valve was deactivated as opposed to the left.

The combination of axial swirl and tumble can be considered as a single swirling motion (Furuno *et al* (1995)) whose axis is inclined to the cylinder axis. Stone *et al* (1991)

quoted a swirl axis inclination angle of 62.0 degrees when the right hand valve lift is reduced to 1 mm. The small opening of the right hand valve was to allow clearing of any fuel tending to puddle upstream of the valve. It did have the penalty of decreasing the axial swirl by 43 % and tumble by 46 % compared with values for the deactivated port. It is thought that the fuel puddling in the deactivated port would not be a problem with the targeted injector concept, as the pencil-jet of fuel is so specifically directed down the active jet.

Returning to the topic of inclination of swirl axis, Baker suggests tentatively that, at low valve lifts, the predominant air motion is one of axial swirl rather than tumble because the air enters the cylinder at a shallow angle, whereas at the higher valve lifts, the predominant air motion is tumble as a consequence of a significant increase in the angle of entry of the air. This theory is in good agreement with Omori *et al* (1991) who state that the angle the air enters the cylinder is important in determining the resultant air motion. This would suggest that the swirl inclination angle varies with valve lift.

9.4 FFID In-Cylinder HC Concentrations

Although no measurements of the air motion on the engine were taken, a technique was developed whereby the consequences of the air motion could be determined in terms of how fuel vapour was being transported around the cylinder. The Cambustion FFID (chapter 7) was used as before to investigate the HC concentrations but a novel mounting method allowed readings to be taken at a far wider range of positions. The results from the two-probe FFID testing reported in the previous chapter showed that there was a significant difference in HC concentration between the spark plug and the cylinder bore probes. It was not clear whether the stratification was in the axial or radial directions, because the two probes were displaced from each other in both axial and radial senses. The purpose of developing a new mounting method was to determine more about the pattern of the stratification effect.

Use was made of the elongated piston to allow a FFID probe to be mounted through a

hole in the piston cap. The probe remained stationary, thus sampling at a fixed point, whilst the piston oscillated around it. The piston cap was designed in two sections (figure 9.2). The first section screwed onto the piston and comprised of a number of holes through which the probe could be inserted. The second section fitted on top and was held in place by eight screws. This second section had three holes machined into it, A, B and C. During testing a maximum of two probes could be used and the remaining hole/s were blocked. By rotating the top section relative to the bottom section of the piston cap, it was possible to sample at 3 different radii and 8 different radial orientations. In addition, there was complete freedom in where the probe/s could be situated in terms of axial position.

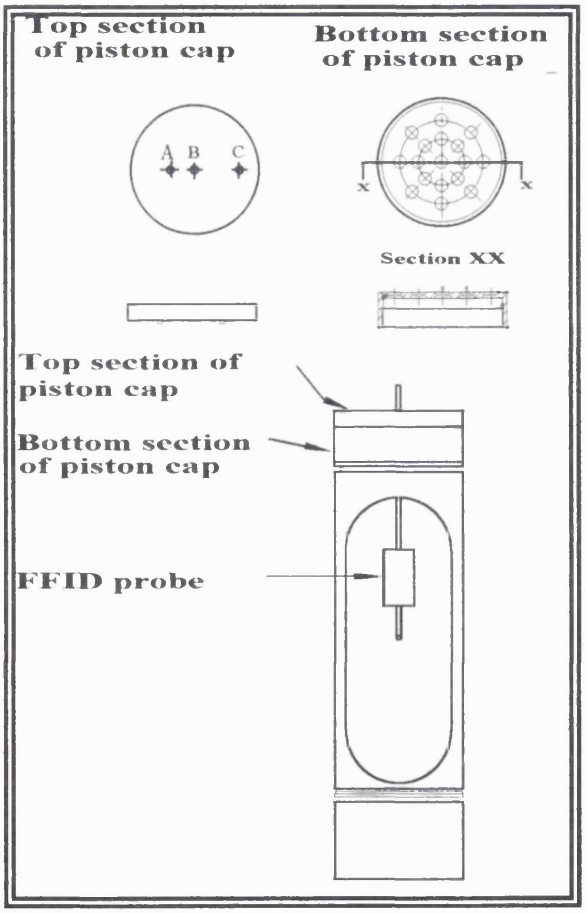

Figure 9.2: Through piston HC measurements

Guides were screwed into the base of the piston cap to ensure that the probes did not leave the cap as the piston approached its BDC position. PEEK seals were fitted at the bottom of the guides to minimize gas leakage. The piston cap was designed so that the probe positions could be altered without having to remove the cylinder head or any other

part of the engine. This facilitated mapping of HC concentrations around the combustion chamber. The FFID probe was located at distances of 5 mm and 15 mm beneath the TDC position of the piston crown in the centre of the combustion chamber and also at a distance of 15 mm beneath TDC at 4 other locations in the combustion chamber (figure 9.3). The engine was fired for periods of 1 minute. Injection started at 135° ATDC for the open-valve injection timing tests. The tip of the probe was reassembled with high temperature solder to help improve its lifetime as it would be sampling within the hot combustion gases.

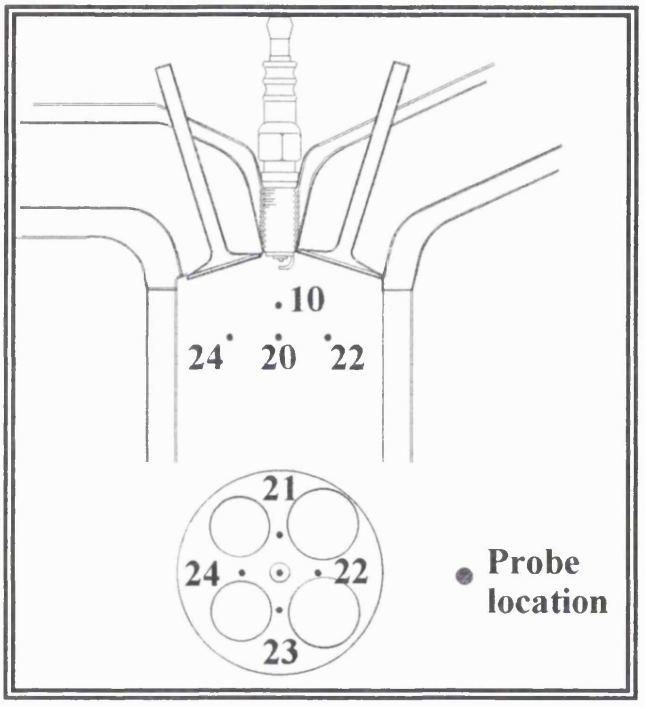

Figure 9.3: The location of the in-cylinder FFID probes

The results for the idle condition are tabulated in table 9.1. The probes situated 5 mm and 15 mm beneath TDC were covered by the piston for approximately 10° and 30° either side of TDC. As such the results are expressed in terms of the percentage difference between the results obtained at the spark plug 30° BTDC and those obtained at the other locations in the combustion chamber for the same crank angle. Thus, for open-valve injection, the HC concentration at position 10 (figure 9.3), was 8 % less than that obtained at the spark plug for the same conditions, and for closed-valve injection it was 3 % greater; these values refer to the differences at 30° BTDC which was shortly before ignition occurred.

Location of FFID probe **	HC concentration % difference from spark plug position	
	Open-Valve Injection*	Closed-Valve Injection
Position 10	- 8	+ 3
Position 20	- 11	- 3.3
Position 21	- 17	+ 2.7
Position 22	-7	- 5
Position 23	+ 8	- 5
Position 24	+5	- 1

*** Injection starts 135° ATDC, ** Refer to figure 9.3 for the relative positions**

Table 9.1: Through-piston FFID results expressed as a percentage of the average value obtained at the spark plug, idle condition

9.5 Concluding Comments

A novel method of mounting FFID probes for in-cylinder sampling has been developed which allows measurement of HC concentration at a range of different positions. However, time constraints have limited the range of readings that have been recorded. The results did indicate that the mixture is reasonably homogeneous (maximum variation of + 3.3% to -5.0 %) for closed-valve injection. These readings were relative to the value taken by the spark plug and all were taken at 30° BTDC. It is likely that the homogeneity would have improved if it had been possible to make the comparison closer to TDC, and also it is almost certain that further improvement would be obtained with a warmer engine. The variation for an open-valve injection timing of 135° ATDC start of injection was considerably greater (+ 8% to -17%), thus indicating significant stratification. The pattern of variation was not consistent with having pure axial swirl containing a rich central core, thus giving weight to the argument that a more complex air motion was present.

Chapter 10

Objectives, Conclusions, Claims for Originality and Future Work

10.1 Objectives

There were two objectives for the research work. The first was to obtain an understanding of the behaviour of liquid fuel within the cylinder for a particular design of current spark ignition engine, namely the Ford Zetec engine. The sponsors of the project were simultaneously commissioning work elsewhere on the same type of engine to measure the emissions characteristics of the engine with different types of injectors. It was hoped that the measurements of liquid fuel behaviour within the cylinder would help to explain emissions results. The second objective was to investigate how the fuel presentation to the cylinder might be improved to make it suitable for the ultra-low engine emission requirements of the year 2000.

10.2 Conclusions

10.2.1 Objective 1 a: Conclusions from the High-Speed Cine Work

A single-cylinder optical version of the Zetec engine was available for the research and a series of visualisation tests investigating three different injector designs, (namely the Bosch four-hole, Nippon Denso twin spray air-assist and the Bosch twin-spray), injection timings (from open-valve injection to closed-valve injection) and engine speeds (idle and 1500 rpm road load condition) were carried out by viewing the combustion chamber through an optical piston. The results were recorded using a high-speed cine camera linked to a copper-vapour laser which provided the necessary illumination of the combustion chamber.

It was observed that for all of the injectors the majority of the liquid fuel impacted on top of the piston. Similar results were obtained regardless of the types of injector, injection timing and engine speed. It was thought that this was because, for the current design of Zetec engine, the injectors were targeted at the port floor and therefore it was likely that the fuel was swept into the cylinder on the side of the inlet valves near the cylinder bore

and carried downwards towards the piston. It was concluded that the targeting of the injector was an important parameter in the resultant fuel entry characteristics.

10.2.2 Objective 1 b: Conclusions from Cylinder Bore Wetting Rig and CCD Camera Testing

The view of the through-piston high-speed cine camera testing was limited to the central 85% of the piston crown, and so it could not be seen whether any fuel impacted on the cylinder wall behind the inlet valves or whether the fuel was carried away from the cylinder bore. A pulsating-flow test rig was arranged to suck off any fuel that impacted on the cylinder bore but no fuel was collected. Visual observation was made by positioning an endoscope through the spark plug hole and it was observed that the fuel travelled vertically downwards away from the cylinder bore. A further series of tests was performed, this time on the optically-accessed engine. Windows were positioned in the cylinder bore so a camera could be focused at various planes across the cylinder bore. The results were recorded using CCD cameras coupled to a spark-flash unit. These tests confirmed that the fuel did travel vertically downwards away from the cylinder bore and impact on the piston. A minimal amount of fuel appeared to travel over the inlet valves as well, probably impacting on the cylinder bore close to the exhaust valves. The overall conclusions of this part of the work were that the path of the fuel within the cylinder was not greatly affected by the type of injector, or by even the timing of the injector. It was thought that the impaction of the fuel on the piston crown was more satisfactory than having impaction either on the cylinder bore or on the combustion chamber roof. Emission testing performed elsewhere showed insensitivity to type of injector which correlated well with the observations reported from this work. In fact, any differences that there were from the emissions testing were attributed to different amounts of fuel being stored on the port walls under transient conditions.

10.2.3 Objective 2: Conclusions from High-Speed Cine Work with the Targeted Injector Arrangement

Having observed the behaviour of liquid fuel within the cylinder with the current design of engine, the next objective was to investigate how the presentation of the fuel might be changed for future engines. One of the conclusions from the literature survey was that

stratified charge engines could bring about simultaneous reductions in fuel consumption and emissions of pollutants. After discussion with the industrial sponsors, it was agreed that the next phase of work should investigate the feasibility of producing a stratified-charge engine by repositioning the injector such that its fuel spray would be deflected off an open inlet valve towards the spark-plug, with the second port deactivated.

A prerequisite for this approach was that the injector should be changed from a conical-spray to a pencil-jet injector. Having defined a suitable position for the injector, further high-speed cine work was carried out comparing open-valve injection to closed-valve injection. This comparison was significant because closed-valve injection would tend to produce a homogeneous charge, whilst open-valve injection should produce a stratified charge. The high-speed cine work showed that most of the fuel impacted around the spark plug for the open-valve injection timings, particularly so at the higher engine speed. A smaller proportion of the fuel was seen to travel across the spark plug and impact either on the exhaust valve or on the cylinder bore. The amount of fuel passing the spark plug decreased with late injection timings, but if the injection timing was so late then not all of the fuel had the time to enter into the cylinder during the cycle in which it was injected. In contrast the closed-valve injection timing produced a cloud of fine droplets that travelled across the combustion chamber and a number of larger droplets around the inlet valve for the 1500 rpm road load condition. The conclusions from this part of the investigation were that the targeted injector arrangement was operating generally as intended, with the majority of the fuel being deposited near the spark plug if an appropriate injection timing was used. It was hoped that the fuel would evaporate from the surface into the air stream which would be exhibiting axial swirl. The fuel vapour would then form a rich core around the spark plug.

10.2.4 Objective 3: Conclusions from FFID Tests for the Targeted Injector, Stages I and II

A Cambustion Fast Flame Ionisation Detector (FFID) was used initially to measure the hydrocarbon concentration at two points in the combustion chamber. The first FFID probe was situated by the spark plug and the second FFID probe directly across from the centre line of the fuel injector in the cylinder bore on the exhaust side.

Measurements from each probe were recorded simultaneously and could be referenced to crank angle. The levels of unburnt hydrocarbons measured by the probes could be related to local air/fuel ratios. The testing investigated the effects of varying injection timing, fuel pressure and injector orientation, with closed-valve injection timings being compared to open-valve injection timings. It was assumed that the mixture within the cylinder would be mainly homogeneous at the time of sparking for closed-valve injection. Measurements from the probe near to the spark-plug indicated a mixture that was approximately 3 AFRs richer at idle for the optimum open-valve injection timing of 135° ATDC than for closed-valve injection. The corresponding difference was 6 AFRs at the 1500 rpm road load condition. The stratifying effect was even greater when making comparisons between the results at the spark plug and those at the cylinder bore, although it should be noted that the probe at the cylinder bore was covered by the piston for 22.5° either side of TDC so care must be taken when interpreting these results.

One possible inaccuracy in estimating the pre-flame HC concentration, was that the fuel local to the probe may not all have evaporated. This was investigated by performing so called skip-firing tests in which a single mis-fire was induced. It was found that not all of the fuel had evaporated, but the relative change between the disabled cycle and the preceding cycles was similar for open and closed -valve injection. Therefore comparisons were valid even if the absolute values of the AFR were not.

The injector was displaced slightly (1°-2°) from its optimum orientation, and it was found that this significantly reduced the stratifying effect. Thus, the arrangement would be sensitive to the production tolerances. Further testing indicated a lack of sensitivity to changes in fuel pressure.

The second stage of FFID testing, involved the resiting of the FFID probes at various locations in the cylinder bore so as to build up more of a contour map as to how the AFR varied around the combustion chamber. The probes were positioned through the piston which was elongated in design to provide optical access. The results indicated that the

fuel distribution prior to ignition was more complex than the simple model of having a rich central core around the spark plug with lean mixture elsewhere. Time constraints meant that it was not possible to construct a full contour map, but indications were that this through-piston HC measurement would be a very useful technique in developing stratified-charge engines.

10.3 Novel Aspects of the Work

There were several novel aspects to the research work and these are listed below.

1) The investigation of the behaviour of liquid fuel in the combustion chamber for a particular design of current spark ignition engine, namely the Ford Zetec engine.
To the best knowledge of the author, no other in-cylinder visualisation work has been carried out on the Zetec engine with a range of injectors. The characteristic feature of this engine is the majority of the fuel was found to impact on the piston, a characteristic that has not been reported for testing performed on other designs of engine.

2) The use of a low-power illumination system (spark-flash unit) to take images inside the combustion chamber.
In-cylinder visualisation techniques tend to require expensive illumination systems. The work carried out in the current research has sought to find an alternative less expensive means to illuminate the in-cylinder areas of interest. Initial tests were performed using the established technique of having illumination provided by a copper vapour laser. This was extremely effective but the copper-vapour laser costs in the region of £80 000. In contrast the spark flash unit provided the necessary illumination for the second set of visualisation tests and it costs in the region of £6000. However, it can only be used in a back illumination arrangement, and it requires careful setting of the CCD cameras.

3) Deflection of a pencil-jet fuel column by an open inlet valve in the direction of the spark plug to obtain a stratified mixture inside the combustion chamber.
The idea was first proposed by the Ford Motor Company, but the author was responsible for organising the first working arrangement. This required the development of a new

technique (impaction plates) to locate a suitable position for the injector.

4) Simultaneous use of two FFID probes inside the cylinder close to the combustion chamber surfaces, followed by a novel through-piston arrangement for mounting the probes.

In particular the use of a static through piston mounting of FFID probes has not been attempted before. Considerable effort was put into the design so that the probe position could be moved without taking the engine apart. This technique offers promise in that it can develop time-varying maps of how the AFR changes around the cylinder prior to combustion

10.4 Future Work

The obvious area for future work is to run emission and fuel consumption test on a full multi-cylinder version of this concept. In fact, the project sponsors have commissioned UCL to provide a prototype cylinder head for testing elsewhere. The design work for this head was performed by Dr M. Miller, as it was thought that involving the \author would detract from her PhD studies. The head was designed by Dr Miller, based on design parameters laid down by the author. It has been manufactured and is awaiting testing elsewhere. This testing would quantify what reductions in emissions levels and fuel consumption were possible through the adoption of this concept to run the engine at high dilution levels. The results would determine whether the concept had sufficient promise further development. Some issues would remain for resolving if the approach did show promise:

(1) whether the deflection of the fuel in the direction of the spark plug would cause plug wetting problems. Experience with the single-cylinder engine suggested that this would not be a problem, but extensive further testing would be required.

(ii) whether the behaviour of the deflected fuel jet will change when the engine is fully warm. This might occur if the Leidenfrost temperature for gasoline is exceeded by the surface of the inlet valve.

(iii) whether deposits would build up on the intake valve after extended engine running.

It is likely that deposits would affect the behaviour of the deflected fuel jet. However, it is thought that the continuous washing of the valve by fresh gasoline would prevent the formation of deposits.

(iv) what strategy to adopt for the full load operation of an engine fitted with this concept. It would be obvious to use a closed-valve injection timing in order to obtain a more homogeneous charge. The normally deactivated port would be opened to allow maximum utilisation of air, but this would only flow air as all the fuel would be passing down the other inlet port. It is thought that this would not cause a problem because in-cylinder mixing would be extensive at full load conditions, leading to a homogenous charge. Jackson *et al* claim no loss in air utilisation at full load on their CCVS engine (chapter 1, section 1.10.5.2) in which the fuel supply is also limited to a single port at full load.

It has been assumed so far that this concept would be linked to running the engine at a lean AFR. However, problems are being experienced with lean operating catalysts in that they are very intolerant of current levels of sulphur in gasoline. An alternative approach would be to use exhaust gas as the diluent, so that the engine could be run at stoichiometric to enable the application of proven TWC technology. The problem here would be to introduce the exhaust gas into the active port in such a way that it enters the cylinder and swirls around its periphery, leaving the fuel /air mixture in the vicinity of the spark plug. This would obviously require extensive development work.

References

Adamczky A A, Kaiser E W, Lavoie G A, (**1983**), "A Combustion Bomb Study of Hydrocarbon Emissions from Engine Crevices", Combustion Science Technology, Vol. 33, pp 261-277

Al-Roub, Farrell P V, Senda J, (**1996**), "Near Wall Interaction in Spray Impingement", SAE 960863

Anand W J D, Roe G E, (**1974**), "Gas Flow in the Internal Combustion Engine", Foulis, Yeovil

Anon. (**1997**), Automotive Engineer

Anon. (**1994**), "Emissions 2000-European Exhaust Emissions Regulations 1992 to 2000", Ford Motor Company UK

Baker T G, (**1995**), "Port Throttles Applied to a High Performance 4-valve S.I. Engine", Ph.D Thesis, Dept. of Mechanical Engineering University College London

Baker T G, Nightingale C J E, (**1996**), "Port Throttling and Port De-activation Applied to a 4-Valve SI Engine" SAE 960587

Benjamin S F, (**1993**), "Prediction of Barrel Swirl and Turbulence in Reciprocating Engines Using a Phenomenological Model", IMechE Publication No. C465/013/93

Boam D J, Finlay I C, Biddulph T W, Ma T, Lee R, Richardson S H, Bloomfield J, Green J A, Wallace S, Woods W A, Brown P, (**1992**), "The sources of Unburnt Hydrocarbon Emissions From Spark Ignition Engines During Cold Starts and Warm-up, IMechE Publication No. C448/064/92

Boer de C D, Johns R J R, Grigg D W, Train B M, Denbratt I, Linna J R, (**1990**), "Refinement with Performance and Economy for Four-Valve Automotive Engines", C394/053/90

Boyle R J, Boam D J, Finlay I C, (**1993**), "Cold Start Performance of an Automotive Engine Using Prevaporised Gasoline", SAE930710

Brown C N, Ladomatos N, (**1991**), 'The Effects of Mixture Preparation and trapped residuals on the performance of a spark-ignition engine with air-shrouded port injectors, at low load and low speed', Proc. Instn Mech Engrs, Vol 205, pp 17-30

Cambustion Ltd, **(1995)**, HFR400 User Manual, V2.1, Cambridge, UK

Chen G, Aggarwai S K, **(1996)**, 'Unsteady Multiphase Intake Flow in a Port-Injected Gasoline Engine', SAE 960074

Crawford J G, Wallace J S, **(1996)**, 'Validation Tests for a Fast Response Flame Ionisation Detector for In-Cylinder Sampling Near the Spark Plug', SAE 961201

Duckworth R F, Barker L, (**1996**), "A Comparative Study of Variable Camshaft Phasing and Port Throttling for Performance and Emissions", SAE 960580

Dwyer H A, Sanders B R, **(1984)**, "Detailed Computation of Unsteady Droplet Dynamics", 20th International Symposium on Combustion, The Combustion Institute, pp. 1743-1749

Dwyer H A, Nirschl H, Kerschl P, Denk V, **(1994)**, "Heat, Mass and Momentum Transfer about Arbitrary Groups of Particles", 25th International Symposium on Combustion, The Combustion Institute, pp. 389-395

Endres H, Schulte H, Krebs R, (**1990**), "Combustion System Development Trends for Multi-valve Gasoline Engines", SAE 900652

Ereaut P R, (**1988**), "Laser Schlieren Measurements of Flames in a Production SI Engine", Experimental Methods in Engine Research Development, IMechE Seminar 9/10 May 1988

European Patent, **(1993)**, Publication Number 0 558 081A

Ferguson, C R, **(1986)**, Internal Combustion Engines-Applied Thermosciences", Wiley, New York

Finlay I C, Boam D J, Bingham J F, Clark T A, (**1990**), "Fast Response FID Measurement of Unburned Hydrocarbons in the Exhaust Port of a Firing Engine", SAE 902165

Fox J W, Min K D, Cheng W K, Heywood J B, **(1992)**, "Mixture preparation in a SI Engine during Starting and Warm-up", SAE 922170

Fry M D, Nightingale C J E, **(1994)**, "Use of high-speed photography to study in-cylinder mixture preparation on a four-valve SI engine", Proc. of IMechE, IMechE HQ, 22 March 1994

Fry M D, **(1994)**, "Optimisation of Mixture Preparation in an SI Engine", Ph.D. Thesis, Department of Mechanical Engineering, University College London

Furuno S, Iguchi S, Iguchi K, Inone K, **(1990)**, "The Effects of 'Inclination of

Swirl Axis' on Turbulence Characteristics in a 4-valve lean burn engine with SCV", SAE 902139

Galliot F, Cheng W K, Cheng C, Sztenderowicz Heywood J B, Collings N, **(1990)**, 'In-Cylinder Measurements of Residual Gas Concentration in a Spark Ignition Engine', SAE 900485

Goldsmith R, **(1990)**, "Passenger Car Exhaust Emissions: Parts 1-3", Mechanical Incorporated Engineer October 1989

Gulder O M, Wong J K S, **(1984)**, "Spheroidal Evaporation and Ignition of Fuel Droplets on a Hot Surface", 20th International Symposium on Combustion, The Combustion Institute, pp. 1751-1760

Hardalupas Y, Taylor A M K P, Whitelaw J H, Ishii K, Miyano H, Urata Y, **(1995)**, "Influence of Injection Timing on In-Cylinder Fuel Distribution in a Honda VTEC-E Engine", SAE 950507

Hardalupas Y, Okamoto S, Taylor A M K P, Whitelaw J H, **(1992)**, "Application of a Phase Doppler Anemometer to a Spray Impinging on a Disc" SAE 920507

Heimrich M J, Albu S, Osborn J, **(1991)**, "Electrically-Heated Catalyst System Conversion on Two Current-Technology Vehicles", SAE910612

Heywood J B **(1988)**, "Internal Combustion Engine Fundamentals", McGraw-Hill International ISBN 0-07-100499-8 1988

Horie K, Nishizawa K, Ogawa T, Akazaki S, Miura K, **(1992)**, "The Development of a High Fuel Economy and High Performance Four-Valve Lean Burn Engine", SAE 920455

Hu Z, Vafidis C, Whitelaw J H, Chapman J, Head R A, **(1992)**, "Correlation Between In-Cylinder Flow, Performance and Emissions Characteristics of a Rover Pentroof Four Valve Engine", IMechE C448/026/92

Hymas G J, Grigulis V J, Brown P G, Woods W A, **(1992)**, "Post Flame Release of Hydrocarbons in a Spark Ignition Engine", C448/033/92

In-Young O, Hee-Sok A, Woo-Jik L, Woo-Tae K, Sim-soo P, Dae-Un L, **(1993)**, "Development of HMC Axially Stratified Lean Combustion Engine", SAE 930879

Ishibashi Y, Asai M, **(1996)**, "Improving the Exhaust Emissions of Two-Stroke

Engines by Applying Activated Radical Combustion", SAE960742

Jackson N S, Stokes J, Lake T H, Sapsford S M, Heikal M, Denbratt I, (**1996**), "Understanding the CCVS Stratified EGR Combustion System", SAE 960837

Kaiser E W, Adamczyk A A, Lavoie G A, (**1981**), "The Effect of Oil Layers on the HC Emissions generated During Closed Vessel Combustion", 18th Symposium on Combustion, The Combustion Institute

Kelly-Zion P L, Young de C E, Peters J E, White R A, (**1995**), "In-Cylinder Fuel Drop Size and Wall Impingement Measurements", SAE 952480

Khaliglhi B, (**1990**), "Intake Generated Swirl and Tumbling Motions in a 4 Valve Engine with Various Intake Configurations Flow Visulisation and Particle Tracking Velocimetry" SAE 900059

Kiyota Y, Akishino K, Ando H, (**1992**), "Concept of Lean Combustion by Barrel-Stratification", SAE 920678

Kuwahara K, Watanabe T, Takemura J, Omori S, Kume T, Ando H, (**1994**), "Optimization of In-Cylinder Flow and Mixing for a Center-Spark Four-Valve Engine Employing the Concept of Barrel Stratification", SAE 940986

Kume T, Iwamoto Y, Iida K, Murakami M, Akishino K, Ando H (**1996**), Combustion Control Technologies for Direct Injection SI Engines", SAE 960600

Kuwahara K, Watanabe T, Takemura J, Omori S, Kume T, Ando H, (**1994**), "Optimization of In-Cylinder Flow and Mixing for a Center-Spark Four-Valve Engine Employing the Concept of Barrel Stratification", SAE 940986

LabVIEW User Manual, (**1990**), National Instruments Corporation, Part Number 320349-01

Ladommatos N, Rose D, (**1995**), 'Monitoring the Mixture Strength in the Cylinders of a Port-Injected Gasoline Engine During Transient Operation', Inst. Mech. Engrs, Vol. 209, pp 127 - 134

Leone T G, Christenson E J, Stein R A, (**1996**), "Comparison of Variable Camshaft Timing Strategies at Part Load", SAE 960584

Lipson C, Sheth N J, (**1973**), 'Statistical Design and Analysis of Engineering Experiments', McGraw-Hill, Inc.

Lindsey R, Thomas A, Woodworth J A, Zeschmann E G, (**1971**), "Influence of Homogeneous Charge on the Exhaust Emissions of Hydrocarbons, Carbon

Monoxide, and Nitric Oxide from a Multicylinder Engine", SAE 710588

Matthes W R, Mc Gill R N, (**1976**), "Effects of the Degree of Fuel Atomization on Single-Cylinder Engine Performance", SAE760117

Miller M J, Nightingale C J E, Williams P A, (**1991**), "Measurement of Spark Ignition Engine Mixture Preparation and Assessment of its Effects on Engine Performance", IMechE Publication No. C433/022/91

Milton B, (**1995**), "Thermodynamics. Combustion and Engines", First Edition, Chapman and Hall, ISBN 0 412 53840 7

Min K, Cheng W K, Heywood J B, (**1994**), "The Effects of Crevices on the Engine-Out Hydrocarbon Emissions in SI Engines", SAE 940306

Misumi M, Thring R H, Ariga S, (**1990**), "An Experimental Study of a Low-Pressure Direct-Injection Stratified-Charge Engine Concept", SAE 900653

Murley L, (1993), "NCSA Handbook", Publisher NCSA, ISBN 090 3474 352

Nakamura N, Nomura K, Suzuki M, (**1987**), "Key Factors of Fuel Injection System to Draw Out Good Response In 4-Valve Engine" SAE 870126

Namazian M, Hansen S, Lyford-Pike E, Sanchez-Barsse, Heywood J, Rife J, (**1980**), "Schlieren Visualisation of the Flow and Density Fields in the Cylinder of an SI Engine", SAE800044

Namazian M, Heywood J B, (**1980**), "Flow in the Piston-Cylinder-Ring Crevices of a Spark Ignition Engine: Effect on Hydrocarbon Emissions, Efficiency, Efficiency and Power", SAE 820088

Nelson R A, (**1986**), "Mechanisms of Quenching Surfaces", Handbook of Heat and Mass Transfer, Volume 1: Heat Transfer Operations, Section II: Industrial Operations and Design, pp. 1103-1153, Editor: Cheremisinoff N P, Publishers: Gulf Publishing Company, (1986), ISBN 0-87201-411-8

Newman C E, Stein R A, Warren CC, Davis G C, (**1989**), "The Effects of Load Control with Port Throttling at Idle-Measurements and Analyses", SAE 890679

Newman O, Foster A, (**1993**), "European Enviromental Statistics Handbook", Manchester Business School, Opublisher Gale Research Internaltional Ltd, ISBN 1 873477 60 80

Ohm I, Hee-Sok A, Woo-Jik L, Woo-Tae K, Sim-soo P, Dae-Un L, (**1993**), "Development of HMC Axially Stratified Lean Combustion Engine",

SAE 930879

Omori S, Iwachido K, Motomochi M, Hirako O, **(1991)**, "Effect of Intake Port Flow Pattern on the In-cylinder Tumbling Air Flow in Multi-Valve SI Engines", SAE 910477

Oxford Lasers Ltd, **(1997)**, Technical Handbook Oxfordshire

Peckham M, Collings N, (**1993**), "Static and 'Flying FID Sampling of In Cylinder Crevice Hydrocarbons",

Plimon A, Werlberger P, Winklhofer E, **(1987)**, "The application of optical methods in the investigation of fuel injection phenomena", SAE 870851

Poole C J, Hancock R J, Cairns D C, (**1992**), "Cosworth MBA Engine", SAE920849

Rogers G F C, **Mayhew Y R**, (**1980**), "Engineering Thermodynamics Work and Heat Transfer", Longman Group Ltd ISBN 0-582-30500-4

Salters D, Williams P A, Greig A, Brehob D, **(1996)**, 'Fuel Spray Characterisation within an Optically Accessed Gasoline Direct-Injection Engine Using a CCD Imaging System", SAE 961149

Schurov S M, Collings N, **(1995)**, 'An Experimental Investiation of Fuel Transport in a Port Injected Engine', SAE 952485

Seabrook J, (**1995**), "Combustion and Emissions Optimisation in a High-Performance S.I. Engine", PhD Thesis, University of London

Shayler P J, Davies M T, Colechin M J F, Scarisbrick A, **(1996)**, "Intake Port Fuel Transport and Emissions: The Influence of Injector Type and Fuel Composition", SAE 961996

Shiga S, Kobayashi K, Kon-No T, Karasawa T, Kurabayashi T, (**1991**), "Effect of Fuel Atomization at a Fuel Supply System on the Lean Burn Characteristics in a Spark-Ignition Engine", SAE 910568

Shin Y, Cheng W K, Heywod J B, (**1994**), "Liquid Gasoline Behaviour in the Engine Cylinder of a SI Engine", SAE 941872

Shin Y, Min K, Cheng W K, **(1995)**, "Visualisation of Mixture Preparation in a Port-Fuel Injection Engine During Engine Warm Up", SAE 952481

Spiegel L, Spicher U, (**1992**), "Mixture Formation and Combustion in a Spark Ignition Engine With Direct Fuel Injection", SAE 920521

Stein R A, Leone T G, Christenson E J, **(1996)**, "Comparison of Variable Camshaft Timing Strategies at Part Load", SAE 960584

Stokes J, Lake T H, Christie M J, Denbratt I, (**1994**), "Improving the Fuel Economy/NOx Emissions Trade-Off for Gasoline Engines with the CCVS System", SAE 940482

Stone C R, Brown A G, Beckworth P, (**1992**), "A Turbulent Combustion Model Used to Insights Into Cycle-by-Cycle Variations In Spark Ignition Engine Combustion", C448/013/92

Stone C R, Carden T R, Podmore I, (**1993**), "Analysis of the Effect of Inlet Valve Disablement on Swirl, Combustion and Emissions in a Spark Ignition Engine", Proc. Inst. Mech. Engrs, Part D, Vol. 207, pp. 295-305, 1993

Stone C R, (**1994**), "An Introduction to Internal Combustion Engines", 2nd Edition Macmillan, ISBN 0-333-55084, 1992

Summers T, Collings N, **(1995)**, "Modelling the Transit Time of a Fast Response Flame Ionisation Detector During In-Cylinder Sampling", SAE 950160

Swindal J C, Dragonetti D P, Hahn R T, Furman P A, Acker W P, (**1995**), "In-Cylinder Homogeniety During Cold-Start Studies with Fluorescent Tracers Simulating Different Fuel Distillation Temperatures", SAE 950106

Takeda K, Shiozawa K, Oishi K, Inoue T, (**1985**), "Toyota Central Injection (Ci), System for Lean Combustion and High Transient Response", SAE 851675

Wentworth J T, (**1971**), "The Piston Crevice Volume Effect on Exhaust Hydrocarbon Emissions", Combustion Science Technology, Vol. 4, pp 97-100

Winklhofer E, Fraidl G K, Plimon A, **(1992)**, 'Monitoring of gasoline fuel distribution in a research engine', Proc. Instn Mech Engrs, Vol 206

Williams P A, Beckwith P, **(1994)**, "Correlation Between the Liquid Fuel Properties, Density, Viscosity and Surface Tension and Drop Sizes Produced by an SI Engine Pintle Type Port Fuel Injector", SAE 941864

Young, W C, **(1989)**, "Roarks Formulas for Stress and Strain", 6th Edition, pp 391-440, McGraw-Hill Publishing, ISBN 0-07-100373-8.

Appendix A

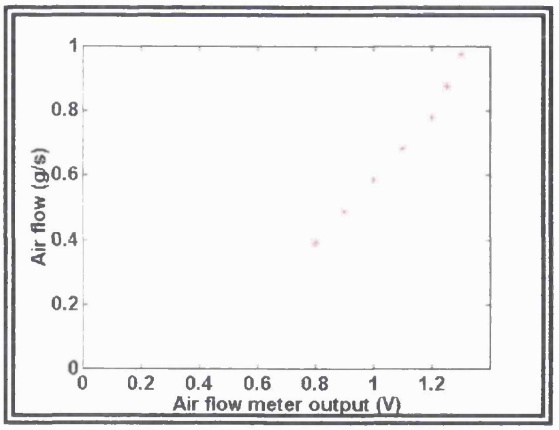

Figure A1: Calibration of the modified Zetec hot wire air flow meter

Laser medium	Copper
Wavelengths (nm)	510.6/578.2
Average power (W) (at optimum repetition rate)	10
Green/yellow ratio (typical)	2:1
Pulse energy (mJ) Max*	2
Pulse to pulse energy stability (% r.m.s)	1
Pulse width (ns)	10 - 40
Peak power (kW)	50
Pulse repetition frequency (kHz) Standard continuous range (kHz) Extended continuous range (kHz) Burst mode operation	 8 - 14 2 - 20 Single shot to 30 kHz
Timing Jitter (ns)	± 2
Beam diameter (mm) nominal	25
Divergence (mrad) Full angle standard cavity Unstable resonator	 4 50% of plane - plane cavity output power within 200 μ radians
Services	
Power consumption (kW)	2.5
Electricity supply	208/220/240V ± 7% 47 - 63 Hz a.c.
Gas supply	99.995% Neon

* Maximum pulse energy obtained at minimum pulse repetition frequency.

Table A1: The specifications of the copper vapour laser Cu10 - A L series (Oxford Lasers Ltd manual)

Appendix B

Droplet sizing techniques

Droplet sizing methods may be considered under three headings, which in turn can be further subdivided. The methods are listed below and some of these together with their advantages and disadvantages will be briefly considered. For a fuller account, refer to the source Lefebvre (1989):

1) **Mechanical**

   Drop collection on slides or in cells

   Molten wax and frozen – drop techniques

   Cascade impactors

2) **Electrical**

   Wicks – Dukler Technique

   Charged wire and hot wire techniques

3) **Optical**

   Imaging – photography, holography

   Non imaging – single particle counters, light scattering, Malvern particle analyzer

Lefebvre (1989)

Mechanical Droplet Sizing Techniques

The frozen drop technique involves the fuel spray penetrating into a bath of alcohol maintained at the temperature of dry ice. On entering, the individual droplets solidify and a measure can be made of their diameters through, for example by, passing them through sieves of known size. The molten wax technique is a variation on the frozen droplet technique, whereby molten wax is passed through the injector nozzle into a bath of water. The droplets solidify on contact with the water. Such a method is feasible because the wax when heated to an appropriate temperature above its melting temperature has a similar viscosity and density to some liquid fuels (Williams 1976). It is important to ensure that the particular fuel used does have a similar surface tension and viscosity as the molten wax. Again, the droplets may be measured by sieving them. It was initially thought that the frozen drop technique method might be applicable for the current application as the bath could be divided into segments, and would allow knowledge to be obtained on the fuel spray distribution and also on the droplet size distribution in relation

to the fuel spray distribution simultaneously. However, it was thought that the complexity of mounting a bath on to the end of the inlet valve would not feasible. In addition, with a coarse spray, the largest droplets were likely to disintegrate on entering the liquid bath and so a true measurement of droplet size distribution would be difficult to obtain. The situation could have been improved by using a liquid that had a low viscosity and surface tension (Lefebvre (1989)).

An alternative mechanical droplet sizing technique is to position a glass slide such that the fuel spray impinges on it. The glass slide is coated with either a layer of Vaseline, magnesium oxide or oil, and the impacting spray would leave indentations on the coating. The size of the indentation, (which may be measure with the aid of a microscope), can be related to the droplet diameter by applying a correction factor which allows for the fact that the size of the droplet changes on impaction. The disadvantage of such a method is that a volume of less than 1% of the spray can be allowed to impact on the slide. Multiple impactions are therefore avoided and true droplet sizes can be obtained (Williams (1976)). Measurement of the indentations is a laborious process.

Electrical Droplet Sizing Techniques

The electrical methods employed in droplet sizing techniques detect and analyse electronic pulses produced by droplets (Lefebvre (1976)). The Wicks – Duckler technique involves placing a probe, that has two needles, in the spray. A potential difference is applied across the needles and the droplets that pass between them completes the electric circuit and a pulse is emitted for each droplet. By varying the spacing of the probes, and counting the number of pulses for each spacing, gives an indication of the spatial distribution of droplets over a specific area. There are several inherent disadvantages of such a method however. The primary one is that the system needs to be very sensitive to avoid ignoring the pulses that are below the noise threshold level.

Optical Droplet Sizing Techniques

Photographic techniques such as the use of high speed cine or CCD camera technology have been previously described (chapter 4) and won't be considered further here. An

alternative optical approach is the use of the Malvern analyser. This comprises of a 2 mW helium neon laser of wavelength 632.8 nm and a receiver unit. The spray that passes through the beam causes the beam to diffract and the distribution of the diffracted beam is measured at the receiver. The deflected spray pattern may be related to concentration of droplet sizes within a particular band.

Appendix C

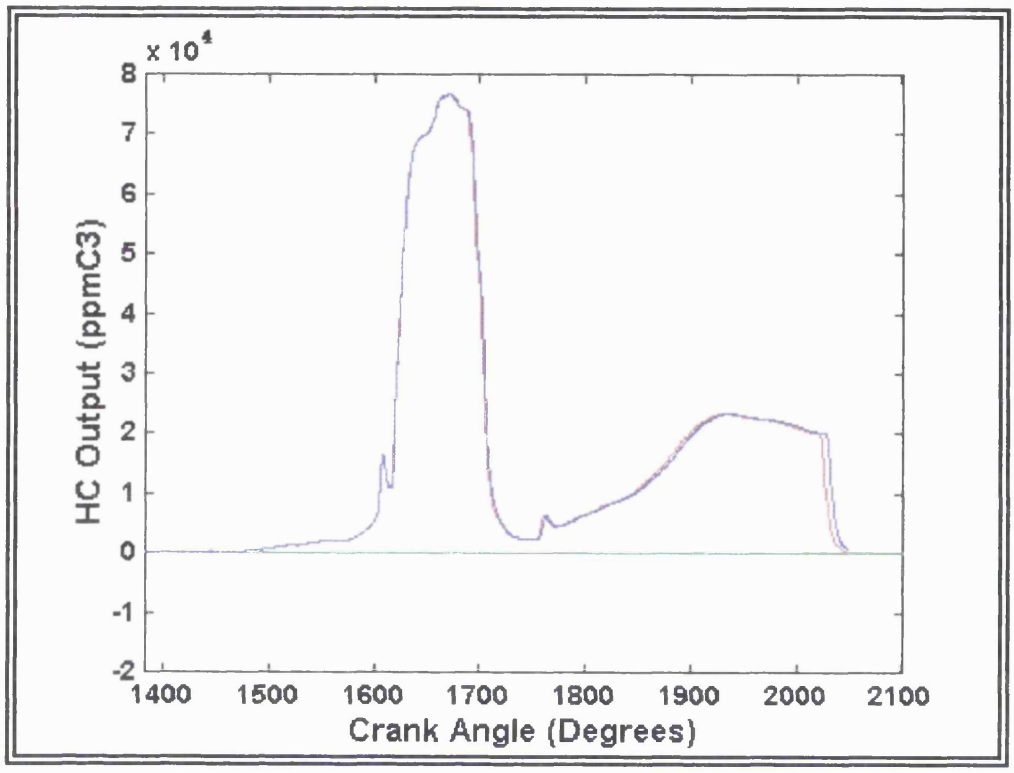

Figure C1: Comparison of raw data and curve fitted data

The above figure shows the comparison of raw data (red curve) with the curve fitted data for open-valve injection, sweep 2, cycle number 2. Both traces are almost identical with only slight differences towards the end of the cycle.